



HAL
open science

3-D reconstruction of the micro-scale mechanical state of the abdominal aortic aneurysm wall

Venkat Siva Radha Krishna Ayyalasomayajula

► **To cite this version:**

Venkat Siva Radha Krishna Ayyalasomayajula. 3-D reconstruction of the micro-scale mechanical state of the abdominal aortic aneurysm wall. Other. Université de Lyon, 2020. English. NNT : 2020LYSEM007 . tel-03461294

HAL Id: tel-03461294

<https://theses.hal.science/tel-03461294>

Submitted on 1 Dec 2021

HAL is a multi-disciplinary open access archive for the deposit and dissemination of scientific research documents, whether they are published or not. The documents may come from teaching and research institutions in France or abroad, or from public or private research centers.

L'archive ouverte pluridisciplinaire **HAL**, est destinée au dépôt et à la diffusion de documents scientifiques de niveau recherche, publiés ou non, émanant des établissements d'enseignement et de recherche français ou étrangers, des laboratoires publics ou privés.



N° d'ordre NNT: 2020LYSEM007

THÈSE de DOCTORAT DE L'UNIVERSITÉ DE LYON
opérée au sein de
École des Mines de Saint-Étienne

École Doctorale N° 488
(Sciences, Ingénierie, Santé)

Spécialité de doctorat: Mécanique et ingénierie
Discipline: Mécanique et Ingénierie

Soutenue publiquement le 11/02/2020, par:
Venkat AYYALASOMAYAJULA

3-D reconstruction of micro-scale mechanical state of the abdominal aortic aneurysm wall

Devant le jury composé de:

HAN, Woo-Suck	Professeur	Mines Saint Etienne	Président du jury
TILLIER, Yannick	Enseignant Chercheur	Mines Paris Tech	Rapporteur
BAILLY, Lucie	Chargé de recherche CNRS	Univ Grenoble Alpes	Rapporteur
LE FLOC'H, Simon	Maître de conférences	Univ of Montpellier	Examineur
ROHAN, Pierre-Yves	Maître de conférences	Arts et Métiers ParisTech	Examineur
PIERRAT, Baptiste	Ingénieur de recherche	Mines Saint Etienne	Co-encadrant de thèse
BADEL, Pierre	Professeur	Mines Saint Etienne	Directeur de thèse

Spécialités doctorales
 SCIENCES ET GENIE DES MATERIAUX
 MECANIQUE ET INGENIERIE
 GENIE DES PROCEDES
 SCIENCES DE LA TERRE
 SCIENCES ET GENIE DE L'ENVIRONNEMENT

Responsables :
 K. Wolski Directeur de recherche
 S. Drapier, professeur
 F. Gruy, Maître de recherche
 B. Guy, Directeur de recherche
 D. Graillot, Directeur de recherche

Spécialités doctorales
 MATHEMATIQUES APPLIQUEES
 INFORMATIQUE
 SCIENCES DES IMAGES ET DES FORMES
 GENIE INDUSTRIEL
 MICROELECTRONIQUE

Responsables
 O. Roustant, Maître-assistant
 O. Boissier, Professeur
 JC. Pinoli, Professeur
 N. Absi, Maître de recherche
 Ph. Lalevée, Professeur

EMSE : Enseignants-chercheurs et chercheurs autorisés à diriger des thèses de doctorat (titulaires d'un doctorat d'État ou d'une HDR)

ABSI	Nabil	MR	Génie industriel	CMP
AUGUSTO	Vincent	CR	Image, Vision, Signal	CIS
AVRIL	Stéphane	PR2	Mécanique et ingénierie	CIS
BADEL	Pierre	MA(MDC)	Mécanique et ingénierie	CIS
BALBO	Flavien	PR2	Informatique	FAYOL
BASSEREAU	Jean-François	PR	Sciences et génie des matériaux	SMS
BATTON-HUBERT	Mireille	PR2	Sciences et génie de l'environnement	FAYOL
BEIGBEDER	Michel	MA(MDC)	Informatique	FAYOL
BLAYAC	Sylvain	MA(MDC)	Microélectronique	CMP
BOISSIER	Olivier	PR1	Informatique	FAYOL
BONNEFOY	Olivier	PR	Génie des Procédés	SPIN
BORBELY	Andras	MR(DR2)	Sciences et génie des matériaux	SMS
BOUCHER	Xavier	PR2	Génie Industriel	FAYOL
BRODHAG	Christian	DR	Sciences et génie de l'environnement	FAYOL
BRUCHON	Julien	MA(MDC)	Mécanique et ingénierie	SMS
CAMEIRAO	Ana	MA(MDC)	Génie des Procédés	SPIN
CHRISTIEN	Frédéric	PR	Science et génie des matériaux	SMS
DAUZERE-PERES	Stéphane	PR1	Génie Industriel	CMP
DEBAYLE	Johan	MR	Sciences des Images et des Formes	SPIN
DEGEORGE	Jean-Michel	MA(MDC)	Génie industriel	Fayol
DELAFOSSE	David	PR0	Sciences et génie des matériaux	SMS
DELORME	Xavier	MA(MDC)	Génie industriel	FAYOL
DESRAYAUD	Christophe	PR1	Mécanique et ingénierie	SMS
DJENIZIAN	Thierry	PR	Science et génie des matériaux	CMP
BERGER-DOUCE	Sandrine	PR1	Sciences de gestion	FAYOL
DRAPIER	Sylvain	PR1	Mécanique et ingénierie	SMS
DUTERTRE	Jean-Max	MA(MDC)		CMP
EL MRABET	Nadia	MA(MDC)		CMP
FAUCHEU	Jenny	MA(MDC)	Sciences et génie des matériaux	SMS
FAVERGEON	Loïc	CR	Génie des Procédés	SPIN
FEILLET	Dominique	PR1	Génie Industriel	CMP
FOREST	Valérie	MA(MDC)	Génie des Procédés	CIS
FRACZKIEWICZ	Anna	DR	Sciences et génie des matériaux	SMS
GARCIA	Daniel	MR(DR2)	Sciences de la Terre	SPIN
GAVET	Yann	MA(MDC)	Sciences des Images et des Formes	SPIN
GERINGER	Jean	MA(MDC)	Sciences et génie des matériaux	CIS
GOEURIOT	Dominique	DR	Sciences et génie des matériaux	SMS
GONDRAN	Natacha	MA(MDC)	Sciences et génie de l'environnement	FAYOL
GONZALEZ FELIU	Jesus	MA(MDC)	Sciences économiques	FAYOL
GRAILLOT	Didier	DR	Sciences et génie de l'environnement	SPIN
GROSSEAU	Philippe	DR	Génie des Procédés	SPIN
GRUY	Frédéric	PR1	Génie des Procédés	SPIN
HAN	Woo-Suck	MR	Mécanique et ingénierie	SMS
HERRI	Jean Michel	PR1	Génie des Procédés	SPIN
KERMOUCHE	Guillaume	PR2	Mécanique et Ingénierie	SMS
KLOCKER	Helmut	DR	Sciences et génie des matériaux	SMS
LAFOREST	Valérie	MR(DR2)	Sciences et génie de l'environnement	FAYOL
LERICHE	Rodolphe	CR	Mécanique et ingénierie	FAYOL
MALLIARAS	Georges	PR1	Microélectronique	CMP
MOLIMARD	Jérôme	PR2	Mécanique et ingénierie	CIS
MOUTTE	Jacques	CR	Génie des Procédés	SPIN
NAVARRO	Laurent	CR		CIS
NEUBERT	Gilles			FAYOL
NIKOLOVSKI	Jean-Pierre	Ingénieur de recherche	Mécanique et ingénierie	CMP
NORTIER	Patrice	PR1	Génie des Procédés	SPIN
O CONNOR	Rodney Philip	MA(MDC)	Microélectronique	CMP
PICARD	Gauthier	MA(MDC)	Informatique	FAYOL
PINOLI	Jean Charles	PR0	Sciences des Images et des Formes	SPIN
POURCHEZ	Jérémy	MR	Génie des Procédés	CIS
ROSSY	Agnès	MA(MDC)	Microélectronique	CMP
ROUSTANT	Olivier	MA(MDC)	Mathématiques appliquées	FAYOL
SANAUR	Sébastien	MA(MDC)	Microélectronique	CMP
SERRIS	Eric	IRD		FAYOL
STOLARZ	Jacques	CR	Sciences et génie des matériaux	SMS
TRIA	Assia	Ingénieur de recherche	Microélectronique	CMP
VALDIVIESO	François	PR2	Sciences et génie des matériaux	SMS
VIRICELLE	Jean Paul	DR	Génie des Procédés	SPIN
WOLSKI	Krzysztof	DR	Sciences et génie des matériaux	SMS
XIE	Xiaolan	PR0	Génie industriel	CIS
YUGMA	Gallian	CR	Génie industriel	CMP

Acknowledgements

Ok, here comes the hard part! I say hard because I have never been good at putting words to emotions. But, I will try and here it goes.

PhD is a bumpy, bruised, long and wearisome, yet incredibly enlightening and enriching (both scientifically and personally) journey. Each student has their own assessment of it, and I am especially thankful to have done my thesis in France. *Vive la France.*

Now the time is therefore to thank all those who, in one way or another, contributed to this journey, in a more casual tone of writing. First of all, I would like to apologize in advance for any omissions. So, I hear there is a pecking order to do this? I will try to honour that code. Lets see how much I get right the first time.

I will start the processions from the D-day. I would like to thank Prof. Yannick Tillier and Dr. Lucie Bailly for agreeing to be the rapporteurs for my thesis defense. I appreciate you taking the time to read and critique the manuscript given the short time frame and it being Christmas season. I hope you had enough time to enjoy the holidays as well ;-). In addition I also thank you for asking intriguing questions about the thesis, which helped me better prepare for the defense.

Next up we have the two examinateurs, Dr. Simon Le'Floch and Dr. Pierre Yves Rohan, I would like to thank you both for making the defense pleasant with your calm and collected demeanor. You have asked a lot of thought provoking questions some of which we haven't thought about during the time of the thesis. These questions surely will open up new pathways for continuing this research and I thank you all for that. Lastly, I would like to thank you for coming from afar and having to listen to the presentation in the morning.

Prof. Woo Suck-Han, you have been a pleasant last minute addition and I would like to thank you for agreeing to preside over the jury. Your addition has made the defense more fun and you have helped me greatly to calm my nerves. In addition, I would like to thank you also for the time spent during the three+ years of my stay in the lab, to all the discussions about skiing, golfing, New York and what not. I still hope I'd make my golfing debut with you one day. Cheers.

Next, the protocol dictates that I speak about the two most important people of the jury, my precious (evil gollum laughter) supervisors. I will start with Pierre.. When I first came here, I've only experienced hierarchical authority. It took me while to get adjusted to the ease of Prof. Pierre Badel. Honestly, I couldn't have asked for a better supervisor for my thesis, I feel incredibly fortunate to have worked with Pierre. Although the role of a thesis director is highly subjective, the amount of liberty he gave me in exploring the the ideas as well as grounding me when necessary was impeccable. *Thank you for putting*

the confidence in me and allowing me to explore the experimental side of things as well, although that was not our initial agreement. You were always available for any clarifications and discussing problems. For any future students reading this, the best time to approach him is before 8:15 AM (you read that right). Pierre, sorry I couldn't understand a lot of your humor (I still don't). I thank you for all generosity and levelheadedness, with which you have supervised me throughout the thesis.

Humble, honest, straightforward, resourceful, witty, Superman, Sheldon Cooper - these seemingly unrelated words are just a modicum of descriptors that come to my mind when I think of Dr. Baptiste Pierrat. Alongside Pierre, Baptiste co-supervised me during the time of my thesis. Let me explain my reasoning for forming such an image of him. You have a problem with Abaqus? You need help setting up your experiment? You have no idea what's going on with your code (python, c++... its all the same)? You've hit a roadblock and can't think of a way out? The answer to all the above questions is "go see Baptiste!". This was established in our office very quickly. Honestly, over the gazillion amount of questions I've thrown at him I cannot come to think of instances where he couldn't help. Baptiste, thank you for being there anytime and agreeing to see me in my office (sometimes for really dumb questions) most times without even having scheduled a meeting. I've come to enjoy your company at work and otherwise and I will continue to look up to you for inspiration.

At the end, it would be too simple to say that you both nourished me to grow as a person and strengthened my desire to continue in research. I will be taking a lot of irreplaceable memories and research principles with me and I'm eternally grateful to you both for that.

Now, I would like to extend my gratitude to some of the other permanent researchers of the lab, who in one way or another helped/ influenced me.

Nicolas Kurt, thank you for aiding me with the experimental protocols and being patient with my broken french.

Claire, you have helped me greatly in preparing for my defense presentation as well as at key points during my thesis through your questions and suggestions, be it in group meetings or through personal discussions. Also, I thank you for initially improve my literature of collagen.

Jerome, although you were never formally involved in my thesis, I thank you for being on the Jury in my 2nd year follow up and encouraging me with your overall positivity. Also, I appreciate your persistence in making me speak in french.

Stephane, thank you for your brief but relevant remarks during the group meetings, which helped me improve significantly my approach.

I cannot describe how much I despise French bureaucracy. I always dread having to go to the prefecture to get anything done. But, I should thank Francoise for her patience and kindness in helping me deal with all the paperwork (it was not an easy task). Also, I would like to apologize to her as I have not heeded her advice many a time. Likewise, I would also like to thank Amelie, who was responsible for my missions and travel, for her generosity and availability. These two made my life a bit easier in dealing with the bureaucracy.

Now turning the attention to my fellow PhD students and PostDocs whom I have come across my time at the lab, I will start with some chronology.

Tina (Cristina Cavinato), the first person I've befriended at the lab. She was a mentor to me the whole time apart from my two supervisors. I would like to thank her immensely

for being so patient and courteous with me. Your attitude towards work and your jovial nature are a huge inspiration. I hope you are not yet tired of looking at images of collagen fibers under the microscope, even though they often appear stubborn to be understood.

I would also like to extend my gratitude to David, Pierre Chelle, Baptiste Charbonier, Boris, Witold and Fanette for making me feel comfortable in the new environment and acquainting me to the French culture.

Jamal and Solmaz, I would like to thank you both for the good times and especially in exchanging Persian pleasantries. Congratulations on your baby and wish you both the best.

Olfa and Victor, thank you for all the Friday dinners and for the many interesting yet the most absurd and silly conversations. Victor, I will remember the times at the Thunderbird pub with the many local rock concerts. Cheers.

Francesca, thank you for being a good friend and a cool neighbor.

Now lets look at the office I've slogged at for more than three years. One ought to find some interesting characters there.

First, there is Aymeric (theres a Dr. in there somewhere). I get a little teary looking back at all the memories. We've started our PhD journey together and I fail to recollect any protocol we've adhered to more than the morning coffee breaks. Although I do enjoy your company, I have to say going to gym with you was a nightmare. But, it was a pleasure to have gotten back to playing tennis. To all the good times and the down times, thank you for being there and playing the metallic version of Zombie.

Mohsen, oh he is a mystery to me. He can either be annoying or obnoxiously funny, there is no in-between. Thank you Mohsen, for sharing this journey with me. And always remember "Khuda ga**d maare toh koi kuch nahi kar sakhta".

A later addition to our entourage was Basti (Monsieur Eydan), starting his PhD an year after us. Without the shadow of doubt, he is arguably the best person I've met here. An absolute gem of a guy! Basti, thanks for being the motivation to run and keeping fit. Also, thanks for spoiling us with your cakes and cheese. Umm, cant decide what I like you more for! It was an immense pleasure to have met your family and friends, although I was the only one there who doesn't speak French. I am looking forward to running again on the trail with you. Cheers man.

Romain, although not part of our office, started his PhD alongside us. Super chill guy. Thanks for teaching me climbing outdoors and indulging in the philosophy of climbing. If the title of little-finger from GOT ever fit anyone, I'd imaging its you. Just kidding, don't drink and drive too much, lol.

Next we have our neighbors, who, an year later got (read stole) the best office in the building.

Joseph, a timid person at the office, but put one beer in him and he's M. Night Charmalar-malan. Thank you for the climbing lessons, the cheese, and all the good times in general. I used to think I was a foodie until I met Nico. Oh man, can he eat! But honestly, hes also the most hardworking so I guess that makes up for it. Thank you for being a good companion for exploring around New York and all the discussions about Abaqus.

My summer vacations in the last three years wouldn't have been half as fun if not for Joan.

Seriously, thanks for the person who hired him. Joan, you have been a tremendous impact in exploring the Alps and traveling around in general. I rather not say much more. Thank you for joining me on my summer backpacking trips and I'm glad I convinced you to start climbing. The amount of positivity you show towards life and your open-mindedness is quite refreshing.

I would also like to wish good luck to all the other newer additions (not so new anymore, actually), Claudie, Danielle (the tall one), Cyriac, Jules, Zaineb, Sophie, Ozge, Laure, and Salma.

I would like to add a few words of appreciation towards the PostDocs. Danielle, Brooks, Miquel (now a permanent researcher), and Jay (LEGEND), thanks for the fabulous fun times during lunch. Brooks, you need to stop watching Arsenal's games, it's not good for your psyche. Thanks to all of you also for mentoring me directly or indirectly at some point in the thesis. I appreciate your patience with bearing me knocking on your door unannounced and allowing time for discussions about mechanics in general.

Outside of the lab, I was incredibly lucky to have found a group of people who mainly speak English and share many common interests.

Although each of you are special to me I would list you all here by name and spare my thoughts about you for a later moment. I would like to mention in this list of close friends: Oudom, my ex apartment-mate and big-broda; Omar, the kid; Khadim; Kamal, the bigshot; Christian, the gentleman; Dennis, the computer geek; Jose, the robot; Adrien and Sandra; Carlos, el marica; Justine; Venki; Vinicus; Bea; and Kaushik. I thank you all for all the meriendas, the cooking sessions, the sports, the trips we took, the board games, the hikes around Sainte and many more. I'm sure there's a lot in store for the future as well.

Also thank you for helping me organize everything for the day of my defense and letting me feel less stressed about it.

And finally, it is imperative to mention the most important people in my life, my parents. Amma, I know it has been hard for you to accept that you do not get to see me as often for the last 5-6 years. I missed you the most at my defense. You should have listened when I told you to make your passport. Anyway, by breaking the stereotypical barriers and pursuing a scientific career in an orthodox family, you are my first and biggest inspiration to succeed in life. Whatever hurdles I've faced so far in life pale in comparison to yours. Although, we were not very well off, I can't thank you enough for all the sacrifices you've made for me to be in this position. Thank you for being a mentor and encouraging me to pursue science and trusting me with my decisions. I hope I've made you happy. Also, I'm a better cook than you now, just putting it out there.

Nanna, thanks for being my emotional strength and helping me get up on my feet when even I fall. I don't think I could have the positive stimulus to go and pursue everything I did without your emotional support.

Finally, it's been hard writing this sitting at home all day (it's almost been two months now) in the middle of a global pandemic. I hope we get out of this situation soon and that you find this in good condition. With that, to all the people I've mentioned above and to all those that I forgot due these unprecedented times of Covid-19, a big thank you. It wouldn't have been possible without you. Wish you all health and happiness.

Introduction générale

Le corps humain est une structure complexe composée de plusieurs types de cellules, de tissus, d'organes et de systèmes d'organes qui fonctionnent collectivement pour maintenir l'homéostasie (l'état stable des conditions physiques et chimiques internes). Au total, le corps humain est composé de onze systèmes d'organes, dont l'un est le système circulatoire (système cardiovasculaire). Il est responsable de la circulation du sang dans tout le corps à travers son réseau de vaisseaux sanguins. Une déficience de l'un ou l'autre des composants de l'appareil circulatoire est catastrophique et peut entraîner la mort. Les maladies cardiovasculaires sont un terme générique utilisé pour décrire les conditions qui affectent les composantes de l'appareil circulatoire. L'une de ces maladies qui prend de plus en plus d'importance en raison de sa nature complexe est l'anévrisme de l'aorte. Les anévrismes de l'aorte peuvent être identifiés comme un renflement de l'aorte, la plus grande artère du corps humain, qui se développe avec le temps en parallèle d'un affaiblissement progressif de la paroi artérielle. Bien que les causes exactes responsables des anévrismes ne soient pas connues avec précision, de nombreux facteurs de risque ont été identifiés, comme le tabagisme, l'athérosclérose, l'hypertension et la toxicomanie. Les anévrismes aortiques sont importants en raison de leur nature pathologique et du risque associé de rupture totale ou de dissection. La rupture est une rupture soudaine de la paroi aortique qui compromet la circulation sanguine à travers le corps. D'autre part, la dissection peut être identifiée comme une déchirure dans les couches internes de la paroi aortique bloquant également parfois la circulation du sang vers les organes importants du corps et compromettant fortement l'intégrité mécanique du vaisseau. Ces deux circonstances conduisent souvent à la mort du patient sans symptômes significatifs, ce qui leur vaut le surnom de "tueur silencieux". Par conséquent, il est incroyablement difficile de diagnostiquer l'affection sur le plan médical, et encore plus compliqué d'évaluer son risque d'échec. Dans ce contexte, cette thèse explorera les mécanismes impliqués dans les tissus artériels d'un point de vue mécanique afin de mieux comprendre les relations structure-fonction et d'évaluer les mécanismes d'endommagement qui conduisent le tissu à la défaillance.

Afin de faire circuler le sang à travers le corps, les artères ont besoin de maintenir la pression induite par ce flux sanguin. Cela fait de la rupture un phénomène mécanique qui se produit lorsque la paroi artérielle n'est plus en mesure de supporter les contraintes induites. À l'heure actuelle, selon les meilleures pratiques cliniques, le diamètre maximal de l'anévrisme demeure le facteur prédictif le plus fiable du risque de rupture d'anévrisme. Une valeur générale de 5,5 cms est utilisée pour conseiller les patients à subir une chirurgie. Il s'agit d'un paramètre très grossier et il a été démontré qu'il échoue dans plusieurs situations, ce qui indique que de telles solutions simplistes ne sont pas suffisantes pour évaluer les anévrismes.

La recherche persistante dans la quête d'évaluation du risque de rupture d'anévrisme a conduit à des analyses biomécaniques convaincantes du tissu artériel. Ces analyses tentent généralement de reconstituer l'état mécanique du tissu à l'aide de géométries précises et de conditions de chargement *in vivo*. La conclusion communément admise est que les anévrismes échouent à l'emplacement de la contrainte maximale. Cependant, de nombreuses analyses biomécaniques ne tiennent pas compte de la nature hétérogène de la paroi artérielle, en supposant un matériau homogène pour évaluer l'état de contrainte. De plus, des résultats contradictoires ont été rapportés dans le cadre d'études expérimentales et numériques qui remettent en question l'applicabilité de la contrainte maximale comme facteur prédictif.

La paroi artérielle est une structure hiérarchique complexe composée de plusieurs constituants répartis de manière hétérogène sur ses trois couches. L'élastine et le collagène, présents sous forme de fibres à l'échelle microscopique, sont les constituants structurels importants qui aident à maintenir la fonction mécanique du tissu. L'organisation et la répartition locale de ces constituants déterminent leurs propriétés mécaniques, qui varient d'un endroit à l'autre dans les tissus. Bien que la mécanique de la paroi artérielle au niveau tissulaire soit bien comprise, le rôle de ces constituants microstructuraux et leurs interactions dans la détermination de l'état mécanique macroscopique n'est pas définitif. De plus, on sait que la rupture d'anévrisme est un événement localisé, ce qui soulève la question de l'implication de ces constituants microstructuraux dans la détermination de la rupture de l'anévrisme. En gardant ces complications à l'esprit, cette thèse vise à étudier l'hypothèse suivante:

Hypothèse de recherche: *Les mécanismes se produisant à l'échelle des fibres de collagène et d'élastine sont directement responsables de la réponse mécanique macroscopique et de l'échec au niveau tissulaire.*

L'hypothèse a été testée en réalisant les objectifs de recherche suivants :

- Evaluation de la réponse mécanique macroscopique du tissu artériel dans plusieurs scénarios de chargement.
- Quantifier la microstructure du tissu artériel en utilisant la microscopie multiphoton en état déchargé.
- Développement de modèles numériques robustes à micro-échelle du tissu artériel à partir de données d'images de microstructure quantifiées.
- Analyse quantitative de l'état mécanique de la microstructure fibreuse par des simulations numériques à des charges proches de la rupture.
- Identifier des critères basés sur la microstructure pour la défaillance macroscopique, c'est-à-dire la rupture.

- Élaborer des modèles multi-échelles fiables pour relier la mécanique micro-échelle à la défaillance des tissus à l'échelle macro.

En abordant les objectifs ci-dessus, cette thèse est divisée en 6 chapitres, décrits de la manière suivante. Tous les chapitres sont rédigés essentiellement en anglais et accompagnés d'un bref résumé rédigé en français au début.

- Le chapitre 1 examine le contexte clinique et biomécanique sur lequel se fonde l'étude. Une revue détaillée de l'état de l'art pertinent pour la caractérisation mécanique et la modélisation numérique des tissus artériels est présentée.
- Le chapitre 2 explique les protocoles expérimentaux employés dans l'imagerie microstructurale des tissus artériels excisés des artères du lapin, du porc et de l'homme, ainsi que leurs essais mécaniques.
- Le chapitre 3 peut être considéré comme deux parties principales :
 - La première partie du chapitre traite de l'état de l'art des techniques de traitement d'images pertinentes pour extraire la morphologie des fibres de collagène des images SHG. Un algorithme de traçage séquentiel basé sur la théorie des graphes est présenté pour le suivi semi-automatique des fibres de collagène, et les résultats sont comparés avec deux autres techniques existantes.
 - La deuxième partie du chapitre présente les méthodes utilisées pour reconstruire numériquement le réseau de fibres de collagène à partir de paramètres morphologiques extraits d'images SHG (génération de seconde harmonique). Enfin, une méthode permettant d'incorporer explicitement les réseaux de fibres reconstruits dans des modèles éléments finis à micro-échelle est décrite.
- Le chapitre 4 présente l'application des méthodes décrites dans les chapitres 2 et 3 aux artères carotides du lapin. La quantification des relations structure-fonction significatives est présentée avec une évaluation de l'état mécanique des fibres de collagène à des charges supra-physiologiques.
- Le chapitre 5 présente l'application de la méthodologie proposée au tissu anévrysmal humain testé jusqu'à la rupture dans le cadre du protocole de gonflement et aux aortes porcines testées jusqu'à la rupture dans le cadre du protocole de tension uniaxiale. Un modèle d'endommagement discret sur les fibres est proposé comme critère de défaillance basé sur la microstructure.
- Le chapitre 6 présente l'extension de méthodologie de la modélisation à l'échelle microscopique à la modélisation à l'échelle tissulaire, couplant ainsi explicitement les deux échelles. Le même modèle d'endommagement est utilisé dans cette étude pour relier les dommages microscopiques causés par les fibres à la rupture des tissus macroscopiques.

-
- Enfin, une discussion détaillée des principales constatations, lacunes, conclusions et perspectives d'avenir est présentée.
 - Une annexe est jointe à la fin de la thèse afin d'éclairer davantage la méthodologie et les résultats de celle-ci.

Cette recherche s'inscrit dans le cadre du projet quinquennal "AArteMIS", financé par le *European Research Council (ERC)*, *starting grant n° 638804*. Le projet a été réalisé au CIS (Centre Ingénierie et Santé), en particulier le groupe STBio (biomécanique des tissus mous), qui fait partie intégrante de l'École Nationale Supérieure des Mines de Saint-Étienne.

General introduction

The human body is a complex structure composed of several types of cells, tissues, organs, and organ systems that function collectively to maintain the homeostasis (the steady state of internal physical and chemical conditions). In total, the human body is composed of eleven organ systems one of which is the circulatory system (cardiovascular system). It is responsible for circulating blood all over the body through its network of blood vessels. An impairment to any of the components of the circulatory system is catastrophic possibly leading up to death. Cardiovascular disease is an umbrella term used to describe the conditions that effect the components of the circulatory system. One such disease that is of growing prominence due to its complex nature is aortic aneurysm. Aortic aneurysms can be identified as a bulge in the aorta, the largest artery in the human body, that grow over time due to gradual weakening of the arterial wall. Although the exact causes responsible for aneurysms are not precisely known, many risk factors have been identified, such as: smoking, atherosclerosis, hypertension, and drug abuse. Aortic aneurysms are significant because of their nature, and the risks they expose the patient to: rupture and dissection. Rupture is a sudden burst of the aortic wall compromising the blood flow through out the body. On the other hand, dissection can be identified as a tear in the inner layers of the aortic wall also blocking the flow of blood to important organs in the body. Both of these circumstances often lead to death of the patient without any significant symptoms, which gains them the nick name "the silent killer". As a consequence it is incredibly difficult to diagnose the condition medically, and even more complicated to evaluate its risk of failure. In this context, this thesis will explore the mechanisms involved in arterial tissues from a mechanical perspective in order to provide better insights regarding its structure-function relationships, and to evaluate the damage mechanisms that drive the tissue to failure.

In order to circulate blood through out the body the arteries need to sustain the pressure induced by this blood flow. This makes the event of rupture a mechanical phenomena that occurs when the arterial wall is no longer able to sustain the induced mechanical stress. At the moment, according to best clinical practice, the most reliable predictor for risk of aneurysm rupture remains to be its maximum diameter. A general value of 5.5 cms is used in advising the patients for undergoing surgery. This is a very crude parameter and has been shown to fail in several situations thus indicating that such simplistic solutions are not sufficient for evaluating aneurysms.

Persistent research in the quest for evaluating the risk of aneurysm rupture led to compelling biomechanical analyses of the arterial tissue. These analyses typically attempt to reconstruct the mechanical state of the whole aorta using accurate geometries and in-vivo loading conditions. Through this the commonly accepted conclusion is that the aneurysms fail at the location of maximum stress. However, many of the biomechanical analyses do

not consider the heterogeneous nature of the arterial wall, there by assuming a homogeneous material for evaluating the stress-state. Further, contradicting results have been reported through both experimental and computational studies that question the applicability of maximum stress as a predictor.

The arterial wall is a complex hierarchical structure composed of several constituents distributed heterogeneously across its three layers. Of these, elastin and collagen, present in the form of fibers at the micro-scale are the important structural constituents, that help maintain the mechanical function of the tissue. The local organization and distribution of these constituents determines its mechanical properties, varying from location to location in the tissue, making the mechanical response of the tissue vary from location to location on the wall for the same loading profile. Although the mechanics of the arterial wall at the tissue level is understood adequately, the role these micro-structural constituents and their interactions in determining the macroscopic mechanical state is not definitive. Further, it is known that aneurysm rupture is a localized event, which begs the question regarding the involvement of these micro-structural constituents in determining aneurysm rupture. Keeping these complications in mind, this thesis is directed to investigate the following hypothesis:

Research hypothesis: *The mechanisms occurring at the scale of the collagen and elastin fibers are directly responsible for the macroscopic mechanical response and failure at the tissue level.*

The hypothesis was tested through realising the following research objectives:

- Evaluating the macroscopic mechanical response of the arterial tissue in several loading scenarios.
- Quantifying the micro-structure of arterial tissue using multi-photon microscopy at no-load state.
- Developing robust structure based micro-scale numerical models of the arterial tissue through quantified micro-structure image data.
- Quantitatively analyzing the mechanical state of the fibrous micro-structure through numerical simulations at loads close to rupture.
- Identifying micro-structure based criteria for macroscopic failure, i.e., rupture.
- Developing reliable multi-scale models for linking micro-scale mechanics to macro-scale tissue failure.

In addressing the above objectives this thesis is divided into 6 chapters, outlined in the following manner. All the chapters are reported essentially in English along with a short abstract at the beginning written in French.

- Chapter 1 explores the clinical and biomechanical context on which the study is based. A detailed review of the relevant state of the art for mechanical characterization and computational modeling of arterial tissues is presented.
- Chapter 2 explains the employed experimental protocols involved in micro-structural imaging of arterial tissues excised from rabbit, pig, and human arteries as well as their mechanical testing.
- Chapter 3 can be viewed as two main parts:
 - The first part of the chapter discusses the state of the art image processing techniques relevant for extracting collagen fiber morphology from SHG images. A graph theory based sequential tracing algorithm is presented for semi-automatic tracking of collagen fibers, and the results are compared with two other existing techniques.
 - The second part of the chapter presents the utilized methods for numerically reconstructing collagen fiber network based on morphological parameters extracted from SHG (second harmonic generation) images. And finally, a method for explicitly incorporating the reconstructed fiber networks into micro-scale finite-element models is described.
- Chapter 4 presents the application of the methods described in chapters 2 and 3 to rabbit carotid arteries. Quantification of meaningful structure-function relationships is presented along with a mechanical state evaluation of collagen fibers at supra-physiological loads.
- Chapter 5 presents the application of the proposed methodology to human aneurysmal tissue tested until rupture under bulge-inflation protocol and porcine aortas tested until failure under uniaxial tension protocol. A discrete fiber-based damage model is proposed as a micro-structure based failure criterion.
- Chapter 6 presents the extension of the methodology from micro-scale modeling to tissue scale modeling, thus explicitly coupling the two-scales. The same micro-structurally motivated damage model is used in this study to link microscopic fiber damage to macroscopic tissue failure.
- Finally a detailed discussion of the main findings, shortcomings, conclusions, and future prospects is presented.
- An appendix section is affixed at the end to shine more light on the methodology and results of this thesis.

This research is part of the five year project "AArteMIS", funded by the European Research Council (ERC), starting grant no. 638804. The project was carried out at CIS (Centre Ingénierie et Santé), in particular the STBio (soft tissue biomechanics) group; which is an integral part of the university École Nationale Supérieure des Mines de Saint-Étienne.

Contents

Acknowledgements	v
Introduction générale	xi
General introduction	xv
Contents	xix
List of Figures	xxiii
List of Tables	xxvii
1 State of the Art	1
1.1 Résumé du chapitre	2
1.2 Abstract of the chapter	3
1.3 The human cardiovascular system	4
1.4 Aorta	5
1.4.1 Etymology	5
1.4.2 Arterial anatomy	5
1.4.3 Aortic wall structure	7
1.4.4 Collagen:	9
1.5 Vascular disease	11
1.6 Abdominal aortic aneurysm	15
1.6.1 Definitions	15
1.6.2 Physiopathology	16
1.6.3 Symptoms	16
1.6.4 Risk factors	17
1.6.5 Diagnosis	17
1.6.6 Complications	18
1.6.7 Current rupture risk criteria	18
1.6.8 Treatment	18
1.7 Mechanical characteristics of the arterial wall	19
1.7.1 Experimental methods	20
1.7.2 Elasticity and Non-linearity	22
1.7.3 Anisotropy	23
1.7.4 Heterogeneity	24
1.7.5 Viscosity	24
1.7.6 Incompressibility	24
1.7.7 Residual stress	24

1.8	Mechanical models of the arterial wall	25
1.8.1	Phenomenological constitutive models	26
1.8.2	Structural constitutive models	26
1.8.3	Growth and Remodeling models (G&R)	28
1.8.4	Poro-elastic and Visco-elastic models	29
1.8.5	Continuum damage models	29
1.9	Discrete network models	31
1.10	Micro-scale approach for quantifying rupture risk	33
1.10.1	Biomechanical rupture risk parameters	33
1.10.2	The need for micro-scale approach for identifying rupture risk	35
1.11	Overview	35
2	Experimental methods	39
2.1	Résumé du chapitre	40
2.2	Abstract of the chapter	40
2.3	Introduction	42
2.4	Micro-structural imaging	42
2.4.1	Multi-photon microscopy applied to rabbit carotid arteries	43
2.4.2	Multi-photon microscopy applied to human aneurysmal aortas	43
2.4.3	Multi-photon microscopy applied to porcine aortas	44
2.4.4	Optical light microscopy of porcine aorta	48
2.5	Thickness measurement protocol	48
2.6	Mechanical testing of arterial tissues	50
2.6.1	General considerations	50
2.6.2	Uniaxial tensile testing of rabbit carotid arteries	51
2.6.3	Bulge-inflation testing of human aneurysmal aortas	53
2.6.4	Uniaxial tensile testing of porcine aortas	53
2.7	Conclusion of the chapter	57
3	Numerical methods	59
3.1	Résumé du chapitre	60
3.2	Abstract of the chapter	61
3.3	Segmentation of collagen fiber network from SHG images	62
3.3.1	Introduction	62
3.3.2	Methods	64
3.3.3	Results	67
3.3.4	Discussion	67
3.3.5	Conclusion	72
3.4	Extraction of morphological parameters of collagen fiber network from SHG images	73
3.4.1	Orientation	73
3.4.2	Waviness	74
3.4.3	Volume fraction	74
3.5	Numerical network reconstruction	74
3.5.1	Stochastic modeling	74
3.5.2	Inverse random sampling	77
3.5.3	Random walk algorithm	78
3.6	Finite element model	80

3.6.1	Material models	80
3.6.2	Boundary conditions	81
3.6.3	Parameter identification	82
3.7	Conclusion of the chapter	84
4	A computational model for understanding the micro-mechanics of collagen fibre network - applied to rabbit carotid arteries	85
4.1	Résumé du chapitre	86
4.2	Abstract of the chapter	87
4.3	Introduction	89
4.4	Methods	92
4.4.1	Experimental data and analysis	92
4.4.2	Mechanical model	97
4.4.3	Design of experiment approach for model evaluation	99
4.4.4	Identification of model parameters	102
4.5	Results	103
4.5.1	Model Validation	103
4.5.2	Parameter identification from experimental data	103
4.5.3	Sensitivity analysis	106
4.5.4	Morphological changes of the fiber network	107
4.5.5	Analysis of the micro-macro relationship	109
4.6	Discussion	113
4.6.1	Main contributions	113
4.6.2	Comparison with the literature	113
4.6.3	Sensitivity analysis	114
4.6.4	Fiber kinematics	114
4.6.5	Rupture prediction	115
4.6.6	Limitations	116
4.7	Conclusions	117
5	A discrete fiber based damage model for assessing the failure of aortic tissue - applied to human and porcine aortas	119
5.1	Résumé	120
5.2	Abstract	121
5.3	Introduction	122
5.4	Materials and methods	125
5.4.1	Experiments	125
5.4.2	Numerical methods	129
5.5	Results	132
5.5.1	Bulge-inflation	132
5.5.2	Uniaxial tension	132
5.5.3	Fiber kinematics	132
5.6	Discussion	135
5.6.1	Main contributions	135
5.6.2	Collagen rupture strain comparison	138
5.6.3	Correlation between micro-structure and rupture	139
5.6.4	Progressive damage model for collagen fibers	140
5.6.5	Limitations	141

5.6.6	Conclusions	142
6	Extension of the methodology from micro-scale to macro-scale	143
6.1	Résumé du chapitre	143
6.2	Abstract of the chapter	145
6.3	Introduction	146
6.4	Methods	147
6.4.1	Micro-structural imaging	147
6.4.2	Uniaxial testing	148
6.4.3	Multi-scale model	149
6.5	Results	153
6.6	Discussion	154
6.7	Conclusion of the chapter	159
7	General discussion and conclusions	161
7.1	Main findings	162
7.2	Implications for research in arterial biomechanics	163
7.3	Limitations	165
7.4	Future prospects	166
	Conclusion générale	169
	Appendix A	173
	Bibliography	177

List of Figures

1.1	The cardiac cycle	4
1.2	Circulatory vascular system	4
1.3	The aortic arch	6
1.4	Anatomy of the aorta	6
1.5	The layered structure of the arterial wall	7
1.6	Medial lamellar units	8
1.7	Synthesis of collagen	10
1.8	Hierarchical structure of collagen from molecular level to fiber level	11
1.9	Dissection and Atherosclerosis	14
1.10	Aortic aneurysms	16
1.11	Aortic aneurysm treatment	19
1.12	Passive response of arterial wall under uniaxial tension	23
1.13	Different aspects of mechanical characteristics of arterial walls	25
1.14	Neo-Hookean vs Holzapfel hyper-elasticity models	26
1.15	Structural models for collagen fiber representation	33
2.1	Max intensity projection of confocal microscopy image stack of rabbit carotid artery (aligned in diagonal direction).	43
2.2	Microscopic architecture of collagen fibers in human aneurysmal tissue at a) zero pressure and b) 250 mm-Hg.	44
2.3	Schema of imaging zones at which microscopic image stacks were obtained for porcine aortic samples.	45
2.4	Max intensity projection of image stacks acquired at different zones of a porcine sample (aligned circumferentially).	46
2.5	Max intensity projection of image stacks acquired at different zones of a porcine sample (aligned longitudinally).	47
2.6	Adventitial collagen fiber architecture imaged under Optical light microscope at magnifications: a) 4 \times , b) 10 \times	48
2.7	Thickness measurement protocol	49
2.8	The uniaxial tension set up used for testing rabbit carotid arteries.	52
2.9	Schema of the bulge inflation set up used for testing human aneurysmal tissue samples	54
2.10	Sample preparation for uniaxial tensile testing.	55
2.11	Uniaxial testing of porcine samples	56
3.1	Max-intensity projection of an SHG image stack of porcine aorta.	63
3.2	Semi-automatic segmentation of collagen fiber network in NeuronJ	64
3.3	Representative collagen fiber cross-section template	65

3.4	Output of the different segmentation techniques on synthetically generated close to linear fibers	68
3.5	Output of the different segmentation techniques on synthetically generated curvy fibers with significant intersections	69
3.6	Output of the different segmentation techniques on an image stack of porcine tissue at zero pressure	70
3.7	Output of the different segmentation techniques on an image stack of porcine tissue at 200 mm-Hg	71
3.8	Comparison of image processing techniques for extraction of fiber orientations	75
3.9	Illustration of collagen fiber crimp	76
3.10	ScanIp segmentation of collagen fiber network	76
3.11	Quantified probability distributions of collagen fiber morphology	78
3.12	Illustration of a reconstructed fiber	79
3.13	Boundary conditions	81
3.14	Inverse parameter identification	83
4.1	Mechanical behavior of collagen under uniaxial tension	89
4.2	(a-d) Multi-photon microscopy images of adventitial collagen at depths of $25\mu m$, $50\mu m$, $75\mu m$, and $100\mu m$ through the micro-structure	94
4.3	Measured vs identified probability density function for a) orientation of collagen, b) waviness of collagen	96
4.4	Schematic representation of the uniaxial tensile test sample	97
4.5	a) Pore size radii distribution in the micro-structure, b) Schematic representation of the reconstruction algorithm	98
4.6	Boundary conditions used for the uniaxial tension simulations	100
4.7	For sample $n^{\circ}4$ comparison of stress-stretch results from finite element simulations with experimental data	104
4.8	Comparison of results obtained from finite element simulations with experimental data of different arterial samples	105
4.9	Sensitivity indices from linear regression for a) final slope response, b) recruitment stretch response	106
4.10	Sensitivity indices from non-linear regression for a) final slope response, b) recruitment stretch response	107
4.11	a) Comparison of orientation distribution of collagen at initial state in each sample to each sample's maximum stretch state, b) Evolution of average waviness of the collagen network in all samples	108
4.12	Evolution of Non-affinity index with stretch computed for all samples	110
4.13	(1-6) Distribution of axial strain in collagen fibres in each sample computed at a global stress of 1 MPa	111
4.14	(1-6) Distribution of axial stress in collagen fibres in each sample computed at a global stress of 1 MPa	112
4.15	Comparison of computed recruitment stretch for collagen in each sample to theoretical estimates	115
4.16	Bar chart of computed values of strain based failure probability of collagen in all the samples	116
4.17	Comparison of collagen network behavior with and without the inclusion of polar angle	118

5.1	Max intensity projection of Multi-photon microscopy image stacks of adventitial collagen of a) healthy porcine sample, b) human aneurysmal sample	126
5.2	Sample preparation. a) Aortic arch of a porcine sample, b) 5 cm cylindrical sections excised from the aorta, c) Schematic representation of cut dog-bone samples for uniaxial testing.	128
5.3	Tensile response of a single collagen fiber.	130
5.4	Applied boundary conditions for a) uniaxial simulations, b) biaxial simulations	130
5.5	Considered window for micro-structural imaging and numerical network reconstruction on the human aneurysmal samples	131
5.6	Comparison of experimental and simulation responses for human aneurysmal samples.	134
5.7	Percentage of fibers broken in each human aneurysmal sample at the point of tissue rupture.	135
5.8	Comparison of experimental and simulation stress-stretch responses for healthy porcine samples	136
5.9	Percentage of fibers broken in each healthy porcine sample at the point of tissue rupture.	136
5.10	Comparison of collagen fiber orientation at supra-physiological pressure state between experiment and simulation. Blue line indicates the orientation distribution obtained from confocal image stacks, red histograms indicate the fiber composition in the reconstructed network at the given load state.	137
5.11	Identified values of collagen fiber rupture strain through inverse method for a) bulge-inflation samples, b) uniaxial samples.	138
5.12	Pearson's correlation between orientation index and recorded tissue strength for a) bulge-inflation samples, b) uniaxial samples	139
5.13	Pearson's correlation between collagen fiber waviness and recorded tissue strength for a) bulge-inflation samples, b) uniaxial samples	140
5.14	Comparison of brittle damage model vs progressive damage on a sample network.	141
6.1	Multi-photon image stacks of a circumferential sample	148
6.2	Multi-photon image stacks of a longitudinal sample	149
6.3	Schematic representation of the multi-scale model	151
6.4	Bi-linear elastic material model for collagen	152
6.5	Embedded element model	153
6.6	Comparison of multi-scale vs embedded element model's mechanical response	155
6.7	Strain distribution in collagen fibers	156
6.8	Comparison of percentage of broken fibers at failure	157
6.9	Representation of ruptured collagen fibers	158

List of Tables

1.1	Material properties of collagen at molecular level	12
1.2	Material properties of collagen at fibril level	12
1.3	Material properties of collagen at fiber level	13
1.4	Function of different arteries in the human body.	15
4.1	Range of input parameters	101
4.2	Optimal parameter set for sample $n^{\circ}4$	104
4.3	Optimal parameter set for samples 1, 2, 3, 5, and 6	105
5.1	Geometrical parameters of uniaxial samples	127
5.2	Identified constitutive parameters of human samples tested under bulge-inflation.	133
5.3	Identified constitutive parameters of porcine samples under uniaxial tension.	133
6.1	Comparison of identified collagen structural and failure parameter for multi-scale and embedded element models.	154

We can judge our progress by the courage of our questions and the depth of our answers, our willingness to embrace what is true rather than what feels good.

Carl Sagan

Chapter 1

State of the Art

Contents of the chapter

1.1	Résumé du chapitre	2
1.2	Abstract of the chapter	3
1.3	The human cardiovascular system	4
1.4	Aorta	5
1.4.1	Etymology	5
1.4.2	Arterial anatomy	5
1.4.3	Aortic wall structure	7
1.4.3.1	Tunica intima	7
1.4.3.2	Tunica media	8
1.4.3.3	Tunica adventitia.	8
1.4.4	Collagen:.	9
1.4.4.1	Synthesis:.	9
1.4.4.2	Hierarchy:	10
1.4.4.3	Mechanical properties:.	11
1.5	Vascular disease	11
1.6	Abdominal aortic aneurysm	15
1.6.1	Definitions	15
1.6.2	Physiopathology	16
1.6.3	Symptoms	16
1.6.4	Risk factors.	17
1.6.5	Diagnosis	17
1.6.6	Complications.	18
1.6.7	Current rupture risk criteria	18
1.6.8	Treatment	18

1.7	Mechanical characteristics of the arterial wall	19
1.7.1	Experimental methods	20
1.7.1.1	In vivo experiments	20
1.7.1.2	In vitro experiments	20
1.7.2	Elasticity and Non-linearity	22
1.7.2.1	Active behavior	22
1.7.2.2	Passive behavior	22
1.7.3	Anisotropy	23
1.7.4	Heterogeneity	24
1.7.5	Viscosity	24
1.7.6	Incompressibility.	24
1.7.7	Residual stress	24
1.8	Mechanical models of the arterial wall	25
1.8.1	Phenomenological constitutive models	26
1.8.2	Structural constitutive models	26
1.8.3	Growth and Remodeling models (G&R)	28
1.8.3.1	Kinematic growth models	28
1.8.3.2	Constrained mixture models	28
1.8.3.3	Hybrid models	28
1.8.4	Poro-elastic and Visco-elastic models.	29
1.8.5	Continuum damage models	29
1.8.5.1	Damage to isotropic component:.	29
1.8.5.2	Damage to anisotropic component:.	30
1.9	Discrete network models	31
1.10	Micro-scale approach for quantifying rupture risk.	33
1.10.1	Biomechanical rupture risk parameters	33
1.10.1.1	Wall stress analysis	33
1.10.1.2	Wall strain analysis	34
1.10.1.3	Rupture risk.	34
1.10.2	The need for micro-scale approach for identifying rupture risk	35
1.11	Overview	35

1.1 Résumé du chapitre

Les artères sont les vaisseaux sanguins qui fournissent le sang aux organes et tissus du corps, dont les propriétés mécaniques sont des déterminants importants de la physiologie circulatoire dans la santé et la maladie. L'anévrisme de l'aorte est une maladie affectant le tissu artériel qui, si elle n'est pas reconnue, entraîne une morbidité et une mortalité importantes. Une meilleure connaissance du comportement mécanique de ces tissus, en particulier dans des conditions mettant la vie en danger, est importante pour l'évaluation de la maladie. Actuellement, les connaissances sur les déterminants microscopiques tels que le réseau fibreux de l'élastine et du collagène, dont le contenu et l'organisation influencent la réponse mécanique du tissu, sont limitées. C'est pourquoi la présente thèse s'engage à combler cette lacune.

Dans ce chapitre, un bref aperçu de l'anatomie, de la physiologie et de l'histologie des artères est présenté, suivi d'un aperçu des maladies aortiques courantes. Ensuite, un aperçu des propriétés biomécaniques des artères et de leurs constituants microstructuraux ainsi qu'une analyse documentaire de modèles mécaniques pour étudier le comportement des artères sont présentés. Enfin, un examen des critères de risque existants pour prédire la rupture de l'anévrisme ainsi que leurs limites est présenté.

1.2 Abstract of the chapter

Arteries are the blood vessels which supply blood to organs and tissues of the body, whose mechanical properties are important determinants of circulatory physiology in health and disease. Aortic aneurysm is a disease affecting the arterial tissue, which if unrecognized result in significant morbidity and mortality. A better knowledge of the mechanical behavior of these tissues especially in life threatening conditions is important for the assessment of the disease. Currently, there is limited knowledge on the microscopic determinants such as the fibrous network of elastin and collagen, whose content and organization influences the tissue's mechanical response. Hence this thesis is committed to addressing this gap, especially in the case of large vessels like the aorta.

In this chapter, a brief overview of the anatomy, physiology and histology of the arteries is provided, followed by an overview of common aortic diseases. Next, an overview of biomechanical properties of the arteries and their micro-structural constituents along with a literature review of mechanical models to study the behavior of arteries is presented. Finally, a review of existing risk criteria for predicting aneurysm rupture along with their limitations is presented.

1.3 The human cardiovascular system

The cardiovascular system consists of blood, the heart (central pump), and a large number of blood and lymphatic vessels [Fowler et al.,]. The heart is a complex muscle, slightly asymmetrical in geometry, consisting of two pumps that control the flow of blood to and from all parts of the body. The network of blood vessels forming the circulatory system include: arteries, the vessels carrying oxygen rich blood to all parts of the body; veins, the vessels carrying deoxygenated blood from all parts of the body to the heart.

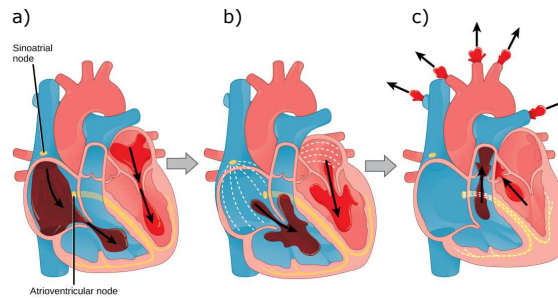


FIGURE 1.1 – The cardiac cycle[Fowler et al.,].

In brief, the heart is composed of four chambers, two atria and two ventricles as shown in figure 1.1. The right atrium receives deoxygenated blood from all parts of the body during systemic circulation through the major veins; the superior vena cava and the inferior vena cava. The superior vena cava drains blood from the head and from the smaller veins that come from the arms, whereas the inferior vena cava drains blood from the lower organs and the legs [Haschek et al.,]. The deoxygenated blood is then passed into the right ventricle through the tricuspid valve, which prevents the back flow of blood. Once filled, the right ventricle contracts to pump blood to the lungs for re-oxygenation. The left atrium receives this oxygen rich blood from the lungs and passes it through the bicuspid valve to the left ventricle where the blood is pumped into the aorta, which is the major artery in the body to be recirculated to the rest of the body through several minor arteries [Entman et al., 2019].

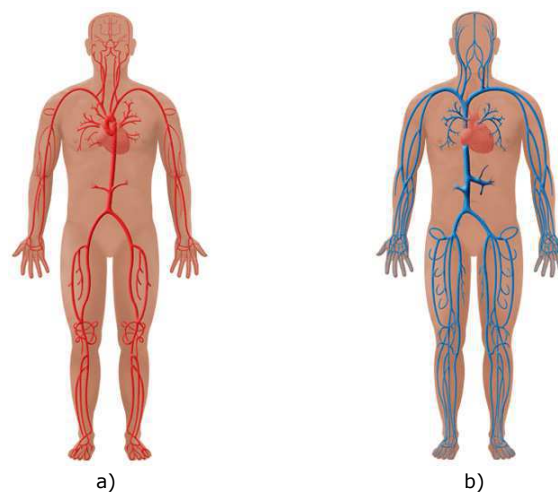


FIGURE 1.2 – The vascular system including the heart, a) arteries, and b) veins [Hopkins,].

1.4 Aorta

1.4.1 Etymology

The word aorta is derived from the ancient greek word 'aorte', originating from the verb aorteo, the lengthened form of aeiro, meaning "to lift/ to rise" [Antoniou et al., 2011]. The origin of the term stems from the gross anatomic morphology of the continuation of the aorta from the heart, illustrating that the aorta extends out from the heart.

It is widely believed that the word aorta had its etymological origins from the medical term "artery". Artery derives from the greek word 'aeirein', which is a combination of the two words 'aer' (air) and 'terein' (to keep) [Stamatakos, 1953]. Aorta was considered to be a windpipe as it appeared empty in corpses, resulting in Hippocrates using the word to mean airways [Stehbens, 1958].

1.4.2 Arterial anatomy

In a closed circulatory system, large arteries become an important component of proper cardiac function by serving as elastic reservoirs, enabling the arterial tree to undergo large volume changes with little changes in pressure. The aorta is the largest artery in vertebrates including humans, that helps sustain the blood pressure due to their elasticity. It supplies oxygenated blood from the heart to the rest of the body. With a total length of little more than a foot, a normal diameter of about 20 mm to 30 mm, and an average thickness of 2 mm, the aorta is not only the largest but also the thickest blood vessel in the body [Tseders and Purinya, 1976, Itani et al., 2002, Humprey, 2002]. It arises from the left ventricle of the heart at the aortic valve, coils to the right, behind the pulmonary trunk, as the ascending aorta (pars ascendens aorte). From this point it coils back, crossing the hilum of the left lung, the bifurcation of the pulmonary trunk, and the left pulmonary artery; thus creating the aortic arch. This second portion of the aorta, the aortic arch, bifurcates into three major arteries:

1. The left brachiocephalic trunk
2. The left common carotid artery
3. The left subclavian artery

The brachiocephalic trunk provides blood to the right arm and right side of the head, including the brain. The left common carotid artery supplies blood of the left side of the head including the brain. Finally, the left subclavian artery carries blood to the left arm [Natsis et al., 2009].

At the level of the 4th thoracic vertebra, the aorta descends initially on the left side of the vertebral column, and then in front of it as the descending thoracic aorta (pars descendens aorte). The aorta penetrates the diaphragm through the aortic hiatus, and after passing through the aortic hiatus of the diaphragm, the aorta is called the abdominal aorta (pars abdominalis aortae). In front of the 4th lumbar vertebra, at the level of the umbilicus, the abdominal aorta divides at the aortic bifurcation (bifurcatio aortae) into the right and left common iliac arteries. Both the left and the right common iliac arteries emanate into one branch into the pelvis, the internal iliac artery and one branch to the leg, the external iliac artery. The final unpaired continuation of the aorta is a remnant of a tail artery, the middle sacral artery [Netter and Colacino, 1989, Leonhardt et al., 1993].

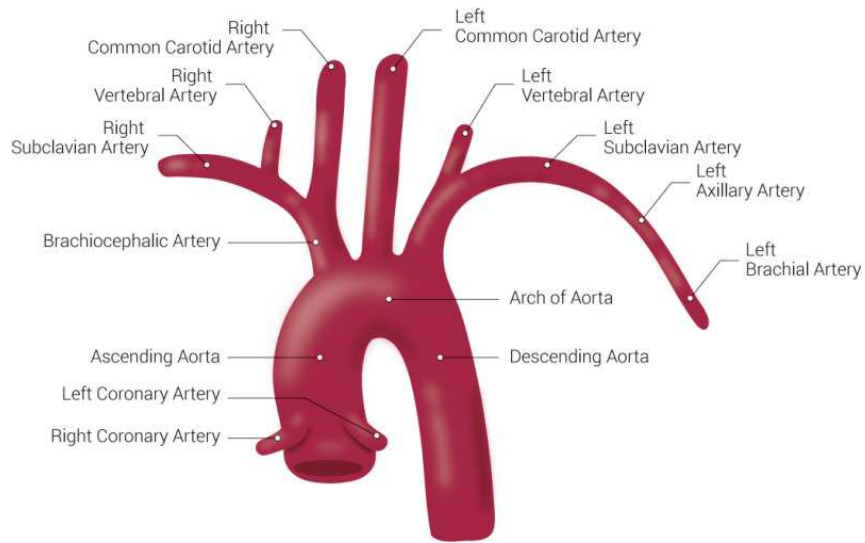


FIGURE 1.3 – The aortic arch [Kelley and Ashurst, 2019].

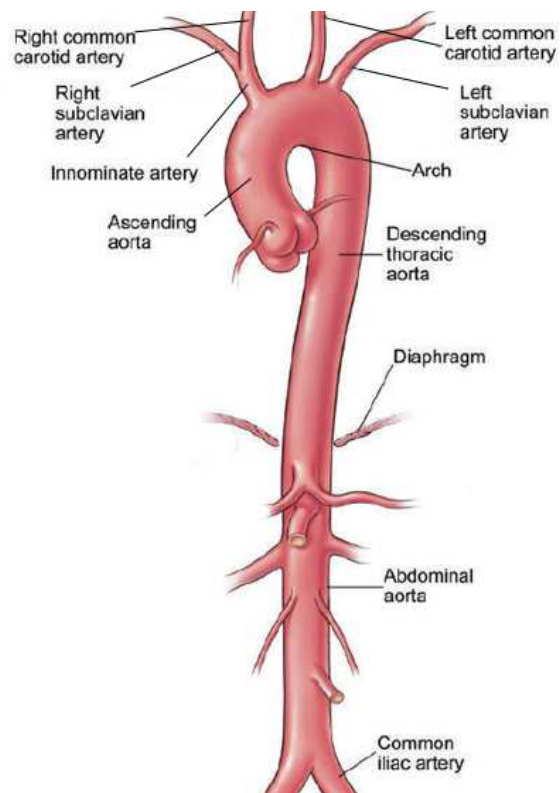


FIGURE 1.4 – The anatomy of the aorta [Cleveland,].

1.4.3 Aortic wall structure

The arterial wall is a complex structure with its micro-structure varying with location along the vascular tree, age, species, local adaptations, and disease. The aorta; regardless of its varying micro-structure is composed of three distinct concentric layers along its thickness, also called tunicae, which is the latin word for a coating/ membrane. All the arterial walls are composed of connective tissue structures with cells and matrix fibers arranged in these three tunicae: the tunica intima, the tunica media, and the tunica adventitia.

1.4.3.1 Tunica intima

The tunica intima is the innermost and thinnest of the arterial wall layers, with an average thickness of about $100 - 200\mu\text{m}$ [Khanafar et al., 2011, Humprey, 2002]. It consists of a single layer of $0.2 - 0.5\mu\text{m}$ thick endothelial cells, which act as a semi-selective biological boundary between the vessel lumen and surrounding tissue, controlling the passage of materials and the transit of white blood cells into and out of the bloodstream [Risau and Flamme, 1995, Suri et al., 1996]. The endothelial cell layer is held on to a $1\mu\text{m}$ thick basal lamina which mostly contains collagen and ground substances [Gerrity and Cliff, 1972, Davis, 1993]. In the aorta and some large muscular arteries including the coronary arteries, it also consists of a sub-endothelial layer constituted of connective tissue and some axially oriented smooth muscle cells. The intima is separated from the tunica media by a layer of elastic tissue known as the internal elastic lamina, which forms the outer most part of the tunica intima. This layer of elastic fibers (thickness of $70 - 100\text{nm}$), is undulated in immersion-fixed histological preparations, but straighten when intraluminal pressure is maintained at normal levels during fixation. The normal intima has negligible structural role because it is very thin. However, intimal hyperplasia or other conditions can increase its mechanical contribution [Labrosse, 2007]. Nonetheless, the intimal layer is significant for its role as a non-clotting interface with blood and its ability to produce elastin.

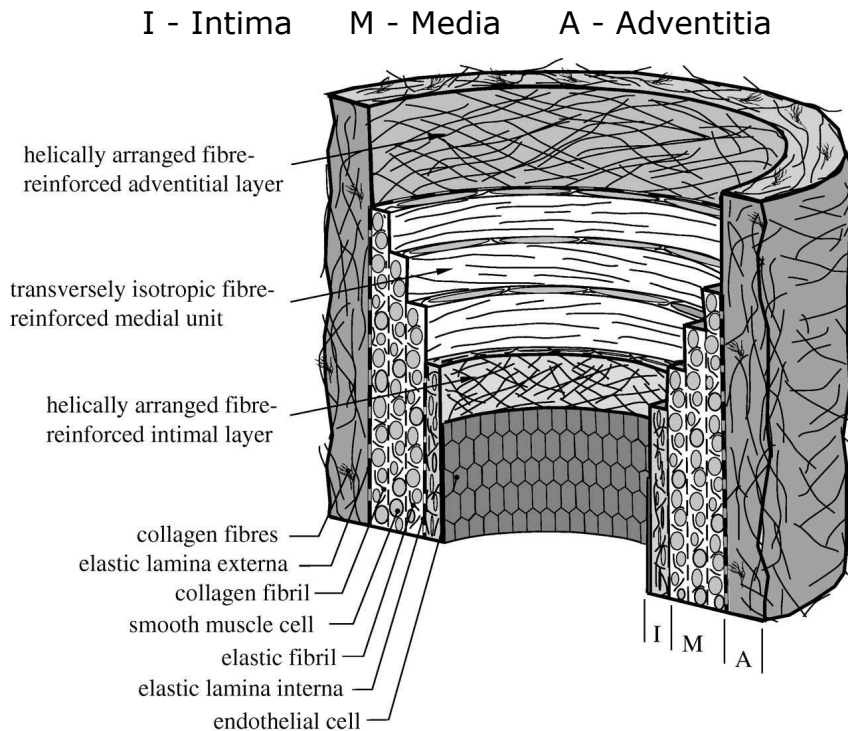


FIGURE 1.5 – The layered structure of the arterial wall [Gasser et al., 2006a].

1.4.3.2 Tunica media

The tunica media is the thickest layer of the arterial wall (thickness of $1000 - 1500\mu m$), starting at the internal elastic lamina which lines the intima and extending up to the external elastic lamina that lines the adventitia [Wong et al., 1993, Khanafer et al., 2011]. The external elastic lamina is much less prominent as it is less clearly marked in muscular arteries and does not exist in cerebral arteries. The medial layer is constituted principally of smooth muscle cells, elastic fibers, and collagen fibers. The classification of arteries into elastic or muscular type is based on the amount of these cellular and fibrous components found in the media. In elastic arteries, elastin and collagen fiber bundles are abundant in the media and the adventitia; where as in muscular arteries smooth muscle cells are the predominant component along with few connective tissue fibers [Levy and Tedgui, 1999]. In elastic arteries such as the aorta, the mechanical function of the medial layer is attributed to the interconnections of its structural components, called as the elastic lamellar units or musculo-elastic fascicles, which can be identified as concentric patterns of fibrous elastin and smooth muscle cells [Clark and Glagov, 1985, Wolinsky and Glagov, 1967a]. The number of these lamellar units in a given artery depends on the diameter of the artery. For instance, in humans there are about 40 – 60 units in the healthy aorta, 20 units in the rabbit, and 8 units in the rat thoracic aorta. The number of these lamellar units further decreases with the distance from the heart. Each unit can in turn be seen as a layer of smooth muscle cells (thickness of $5 - 15\mu m$) separated by a $3\mu m$ thick fenestrated sheets of elastic fibers. Woven in between these elastin sheets are bundles of collagen fibers [Labrosse, 2007]. The predominant orientation of these elastin and collagen fibers in the medial layer is circumferential, which consequently makes it stiffer in that direction [Farand et al., 2007].

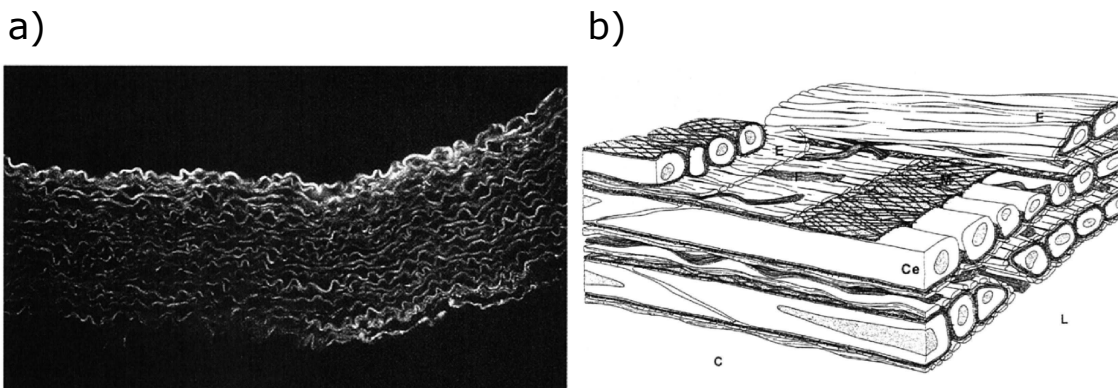


FIGURE 1.6 – a) Lamellar unit structure of the aorta in basal state with lumen at the top and adventitia at the bottom [Levy and Tedgui, 1999], b) schema of a single medial lamellar unit; E: elastin, Ce: smooth muscle cells, F: collagen fiber bundles [Clark and Glagov, 1979].

1.4.3.3 Tunica adventitia

Lastly, the tunica adventitia is the outermost layer of the vessel wall, making up to 20 % of the wall's thickness ($400\mu m$) in elastic arteries and considerably more in the muscular arteries. It can be identified in large arteries as the region exterior to the external elastic lamina, while the outer limit is often difficult to determine as it is usually contiguous with the perivascular connective tissue [Levy and Tedgui, 2007]. In the aorta the adventitia

is primarily made up of a dense network of collagen fibers interspersed with fibroblasts, fibrocytes, few elastic fibers, nerves, and vasa vasorum. The collagen fibers are arranged in thick intertwined bundles oriented in 2 – 4 principle directions with heterogeneous dispersions, and they are undulated in their basal state. The relatively high content of collagen in the adventitia along with its unique organizational structure helps the arterial wall in carrying the load at extremely high pressures. That is, it primarily serves as a protective sheath, similar to the epicardium of the heart [Humphrey, 2002, Burton, 1954]. The vasa vasorum and nerves are also important components with the former providing the vessel's own blood supply and nutrition; the latter contributing to the regulation of medial smooth muscle function. Studies have shown that in arteries with less than 29 medial lamellar units vasa vasorum is absent with a sub-intimal avasculature zone enabling filtration is adequate for medial nutrition. Apart from providing structural stability to the vessel wall, the adventitia is shown to be a unique injury restricting component of the vessel wall [Stenmark et al., 2006, Schulze-Bauer et al., 2002] through its micro-structural components and their interactions. The importance of collagen is detailed in the next sections.

1.4.4 Collagen:

Collagen is a protein that is ubiquitous in all organisms. In most of these organisms collagen is marked distinctly in several tissues and organs. In the human body collagen is the most abundant protein constituting of about 25 – 35% of total protein. It is found in the form of fibers providing the structural integrity to tendons, skin, and other soft tissues [Miller and Gay, 1982].

1.4.4.1 Synthesis:

Collagen is a fibrous structural protein made up of three polypeptide chains (α – *chains*) with atleast one domain in the triple helix conformation. Repeating triplets of Gly-Xaa-Yaa, a high concentration of proline, alanine, and lysine residues with non-collagenous domains at their terminal ends form up the central collagen domain [Van der Rest and Garrone, 1991, Vuorio and De Crombrughe, 1990]. Four different categories of collagen can be identified in the human body based on their structural properties [Díez, 2007]:

1. Fibrillar - Type I, III, V
2. Sheet-forming - Type IV, VIII
3. Fibril associated - Type XV, XVIII, XIX
4. Microfibrillar - Type VI

In general the arterial collagen content and distribution varies highly with the position in the body, age, sex, and species [Grant, 1967, Berillis, 2013]. Collagen found in the vascular tree are mainly of type I and type III, which form up to 80 – 90% of the overall content, the rest of which includes type IV, V, VI, and VIII [Fratzl, 2008]. Even though type I and type III are the predominant ones present, their ratio varies with location on the aorta [Menashi et al., 1987].

Smooth muscle cells control the synthesis of collagen in the intimal and medial layers of the aorta where as in the adventitia it is synthesized by fibroblasts [Fitzsimmons and Shanahan, 2002]. In the first step, the secreted procollagen molecules have their non-collagenous domains removed by synthetic proteinases, leaving the collagen triple helices aggregate in

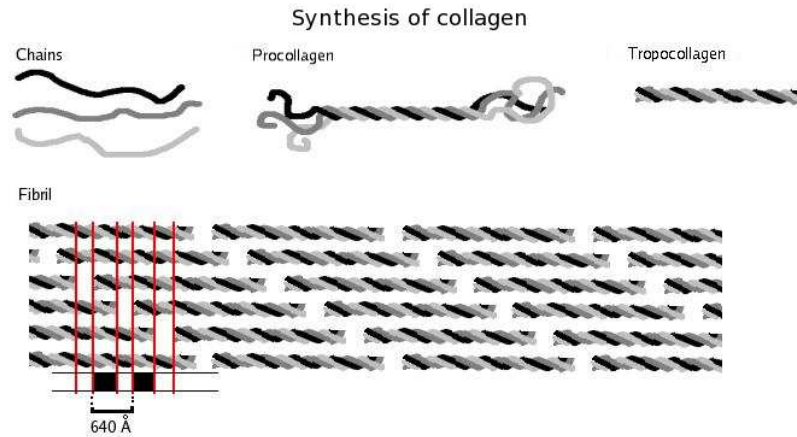


FIGURE 1.7 – Formation of a collagen fibrils from the peptide chains, by successive polymerizations [Solitchka,].

quarter-staggered fibrils. During the subsequent steps, inter and intra-molecular covalent cross-links are formed which increases their tensile strength gradually. At the end of this step, what is left is known as tropocollagen. The final step in the synthesis of fibrillar collagen is marked by lysyl oxidase, an enzyme that helps in the synthesis of collagen fibrils [Molnar et al., 2003, Lucero and Kagan, 2006]. It is responsible for the production of aldehyde groups that eventually undergo covalent bonds between tropocollagen molecules forming collagen fibrils. From this point entropy is an important factor that steams the self assembly of collagen fibrils.

1.4.4.2 Hierarchy:

More often than not collagenous tissues are organized into hierarchical structures, starting from the triple helical collagen molecule [Aladin et al., 2010, Orgel et al., 2006, Currey, 2006]. Tropocollagen molecules have a characteristic length of about $300nm$ and a diameter of about $1.5nm$. Electron micro-graph studies reveal that this structure has an observable periodicity known as the D-band, where $D = 67nm$, with the overall length of the molecule measuring $4.46 D$. The gap between two adjacent collagen molecules is known as the "gap region" measuring about $0.54 D$ or $36nm$. Scaling up from the molecular level, collagen fibrils are formed by bundling of clusters of collagen molecules, with each cluster containing atleast 5 molecules. Collagen fibrils tend to have a diameter of about $100 - 500nm$ and length up to a few microns [Gautieri et al., 2011]. At the next level of hierarchy we have collagen fibers, which are essentially a group of collagen fibrils bound together in a proteoglycan matrix. Within a single fiber; fibrils arrange themselves longitudinally, forming spirals, cross-plys, and even weaves [Orgel et al., 2006]. Collagen fibers have a diameter in the range of $1 - 20\mu m$ and a length in the range of a few millimeters [Carlisle et al., 2010a, Sherman et al., 2015a]. In soft tissues such as the tendon, skin, and the aorta, this hierarchical organization continues where several fibers bind together to form fiber bundles with a diameter of a few hundred microns, which in some cases form secondary fiber bundles so on and so forth [Kannus, 2000, Fratzl et al., 1998].

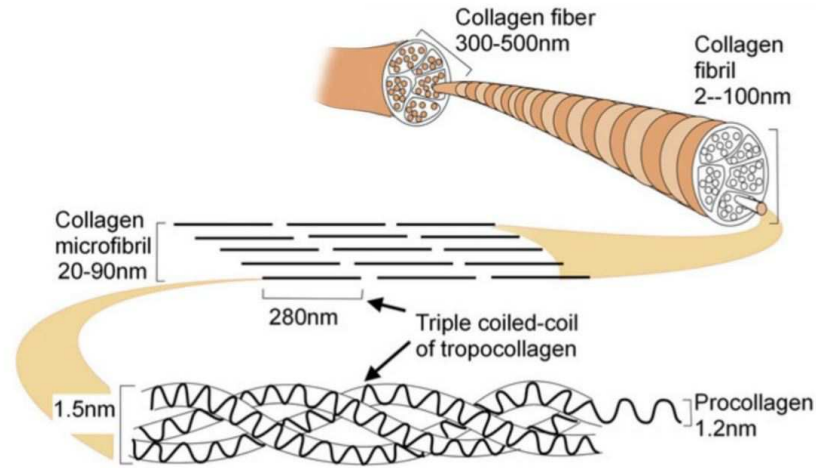


FIGURE 1.8 – Hierarchical structure of collagen from molecular level to fiber level [Scarr, 2011].

1.4.4.3 Mechanical properties:

Determining how collagen based structures confer mechanical strength to soft tissues mandates an understanding of the mechanics at different hierarchical levels explained above. Previous studies have demonstrated that the mechanical strain is distributed over several hierarchical levels [Gupta et al., 2004, Gupta et al., 2005, Gupta et al., 2006]. Based on these observations it has also been concluded that the stiffness varies significantly across different scales. Significant efforts have been made in the recent years focused on quantifying the mechanical properties of collagen using experimental, theoretical, and computational approaches. A review of these works and their measured outcome of collagen stiffness is presented in the table 1.1.

In this work we are primarily interested in the mechanical properties of collagen at the fiber level, which will be discussed herein. Throughout the literature, a limited number of experimental investigations exist which aim at measuring the mechanical properties of collagen at the micro-scale. Reported values of young's modulus of collagen fibers varies from as low as $50MPa$ to as high as $500MPa$ [Aifantis et al., 2011a, Dutov et al., 2016b, Kato et al., 1989a, Morgan, 1960]. This is due to tests being conducted on fibers from different tissues, where differences like shape, mineralization, and degree of crosslinking effect the mechanical response. The stiffness of the collagen fibers decreases significantly with increase in fibril number and is directly proportional to the fourth power of the diameter [Ottani et al., 2001]. Finally, with regard to the failure properties, the subdivision into multiple parallel fibrils does not have significant effect. The ultimate tensile strength of collagen fibers is in the range of $50 - 200MPa$ [Fung, 2013], which makes them suitable to withstand high tensile stresses and simultaneously endow the extracellular matrix with a high compliance [Wainwright et al., 1982].

1.5 Vascular disease

In this section we present the commonly occurring conditions that impair the functionality of the cardiovascular system. Vascular disease can be defined as any abnormal condition of the blood vessels (arteries and veins). Since the vascular system is so complex and far reaching, diseases outside the heart can present themselves anywhere in many different

Hierarchical level	Diameter	Method	Elastic modulus	Ref
Molecular	-	Brillouin light scattering	5.1 GPa	[Cusack and Miller, 1979]
	-	Brillouin light scattering	3 GPa	[Hofmann et al., 1984]
	-	Estimate from persistent length	4.1 GPa	[Nestler et al., 1983]
	-	Atomistic modeling	4 GPa	[Gautieri et al., 2009]
	-	Atomistic modeling	4.8 GPa	[Lorenzo and Caffarena, 2005]
	-	Atomistic modeling	2.4 GPa	[Vesentini et al., 2005]
	-	Coarse grain modeling	4 GPa	[Gautieri et al., 2010]

TABLE 1.1 – Material properties of collagen at molecular level

Hierarchical level	Diameter	Method	Elastic modulus	Ref
Fibril	50 – 200 nm	Atomic force microscopy	5 – 11.5 GPa	[Wenger et al., 2007]
	187 – 305 nm	Atomic force microscopy	1 – 3.9 GPa	[Yang et al., 2008b]
	100 – 600 nm	Atomic force microscopy	1.3 – 7.8 GPa	[Yang et al., 2008a]
	≈ 36 nm	MEMS	≈ 12 GPa	[Eppell et al., 2005]
	150 – 470 nm	MEMS	0.86 GPa	[Shen et al., 2008]
	–	X-ray diffraction	1 GPa	[Gupta et al., 2004]
	–	X-ray diffraction	0.44 GPa	[Sasaki and Odajima, 1996]
	302 ± 126 nm	Atomic force microscopy	2.82 GPa	[Carlisle et al., 2010a]
	–	Mesoscale modeling	4.4 – 38 GPa	[Buehler, 2006, Buehler, 2008]
	–	Atomistic modeling	0.3 – 1.2 GPa	[Gautieri et al., 2011]

TABLE 1.2 – Material properties of collagen at fibril level

Hierarchical level	Diameter	Method	Elastic modulus	Ref
Fiber and bundle	300 μm	Micro-tensile test	216 \pm 68 MPa	[Yamamoto et al., 1999]
	250 μm	Uniaxial tensile testing	498 \pm 44 MPa	[Pins et al., 1997]
	280 μm	Uniaxial tensile testing	280 \pm 115 MPa	[Ming-Che et al., 1994]
	\approx 20 μm	Uniaxial tensile testing	548 \pm 15 MPa	[Morein et al., 1978]
	50 – 100 μm	Uniaxial tensile testing	478 \pm 179 MPa	[Kato et al., 1989a]
	\approx 7 μm	Atomic force microscopy	63 \pm 4 MPa	[Aifantis et al., 2011a]
	125 mm	Uniaxial tensile testing	50 – 250 MPa	[Gentleman et al., 2003]
	\approx 200 μm	Uniaxial tensile testing	960 – 1570 MPa	[Haut, 1986]
	20 – 40 μm	Uniaxial tensile testing	223 \pm 94 MPa	[Law et al., 1989]

TABLE 1.3 – Material properties of collagen at fiber level

forms. Vascular disease often occurs along with other diseases like diabetes or heart disease. Vascular disease often occurs where the blood flow tends to be turbulent, for instance when the flow changes direction abruptly in the arteries. The table 1.2 briefly describes these areas and their associated risks. They can be very severe with many of them causing disability and death. In this section, a brief overview of predominant vascular diseases is presented; with the exception being aortic aneurysms, which will be discussed in detail in the forthcoming sections. They are as follows:

- **Aortic aneurysm:** A dilatation or a bulge of the aorta caused by progressive weakening of the aortic wall.
- **Aortic dissection:** Aortic dissection is a catastrophic condition caused when there is a tear in the inner layer of the aortic wall, which then gradually peels away from the next layer creating two channels for blood flow. This often results in significant decrease in blood flow to various organs and tissues eventually leading to loss of consciousness or death. It is a very serious, life threatening condition that warrants immediate medical attention.
- **Atherosclerosis:** This is a vascular disease caused by build up of plaque in the inner lining of arteries restricting the blood flow to some specific organ or region in the body. Although exact causes are still unknown, inflammation in the intimal layer is often associated to the development of the disease.

Peripheral artery disease (PAD): Resulting from atherosclerosis this condition is prevalent in the peripheral arteries serving the legs, stomach, arms, and the head.

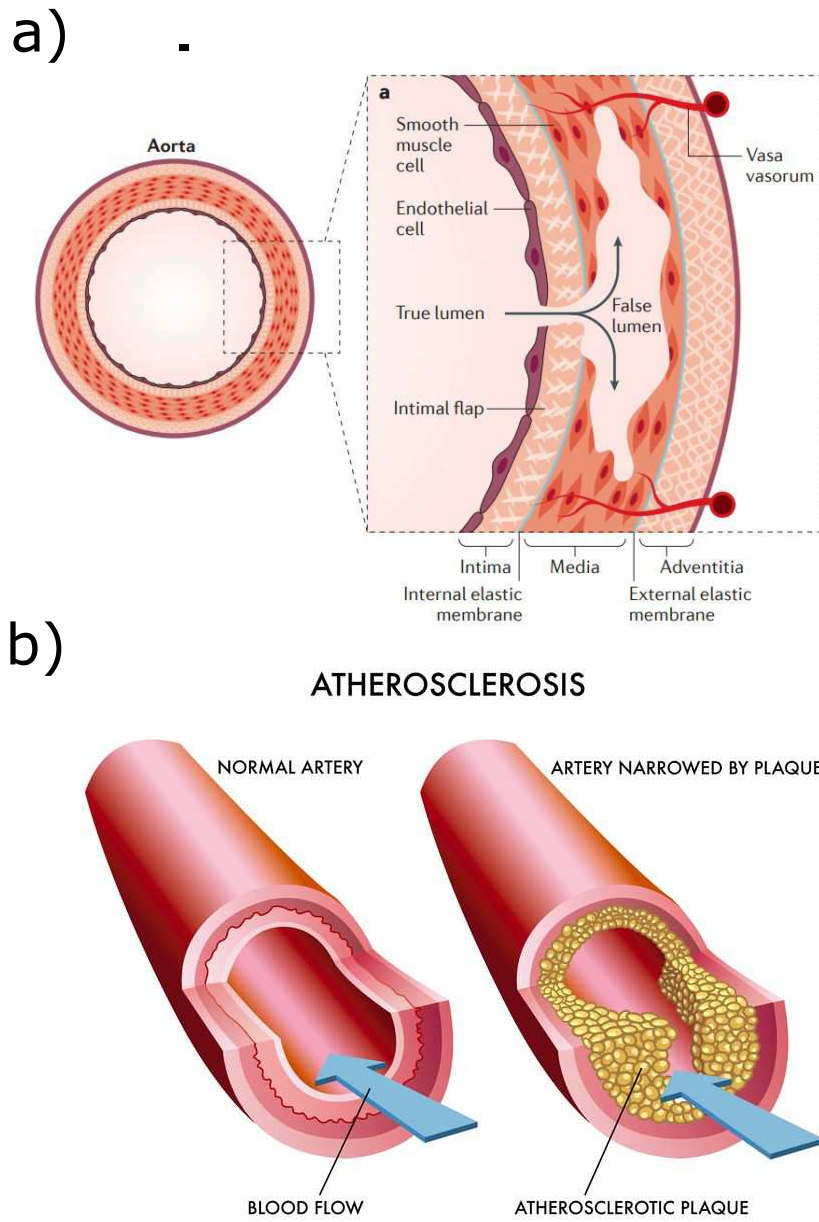


FIGURE 1.9 – a) Dissection [Nienaber et al., 2016], b) Atherosclerosis [Atlantic,].

People with PAD typically have cramps in the hips, thighs, or calves that alleviates with rest.

Carotid artery disease (CAD): Similar to the PAD, CAD is also caused by atherosclerosis. The carotid arteries supply blood from the heart to head and brain. When the blood supply to the brain is compromised, it results in either damage (ischemia) or death (infarction) of the brain cells. Damage to the brain can be permanent if the brain is deprived of blood for three to six hours.

- **Hypertension:** High blood pressure (HBP) or hypertension is a persistent abnormal elevation of the pressure within the arteries. The heart's rhythmic pumping causes the upper systolic pressure (normal ≈ 120 mm-Hg) and the lower diastolic pressure (normal ≈ 80 mm-Hg). Four common stages of hypertension are identified:
 1. Prehypertension: 120/80 to 139/89
 2. Mild hypertension: 140/90 to 159/99
 3. Moderate hypertension: 160/100 to 179/109
 4. Severe hypertension: 180/110 or higher

High blood pressure needs to be treated (immediately) when in the prehypertension stage as it leads to kidney failure, heart attacks, heart failure, stroke, and blindness.

Artery type	Function	Consequence
Arch branches	blood supply to the brain	stroke
Coronary arteries	blood supply to heart	heart attack
Iliac arteries	hips and legs	claudication
Renal arteries	blood supply to kidneys	hypertension, kidney failure

TABLE 1.4 – Function of different arteries in the human body.

1.6 Abdominal aortic aneurysm

In this thesis we are mainly concerned with abdominal aortic aneurysm, which is a focal dilation of the descending aorta. The rupture of an aortic aneurysm is a mechanical event that occurs when the stress exceeds local tissue strength. At present there is still a lot of gap in understanding the mechanical phenomena leading up to aneurysm rupture signifying its importance. This section presents an clinical overview of the condition and discusses the current rupture risk assessment methods.

1.6.1 Definitions

Aortic aneurysm is diagnosed when the maximal external diameter of the aorta is either greater than $40mm$ or exceeds the diameter of the adjacent aorta by atleast $5mm$ [Morris and Wood, 2000, Wanhainen et al., 2008, Steinberg and Stein, 1966]. One further, and possibly more practical definition is 'a focal dilation of an artery resulting in an increase in the diameter of more than or equal to 50 % of the ordinary diameter [Sterpetti et al., 1987, Johnston et al., 1991, Collin et al., 1988].

Aneurysms could be further classified based on their anatomical shape into fusiform and saccular aneurysms. Fusiform aneurysm can be identified as a symmetrical bulge along radial direction of the aortic wall, and is the most common type. Saccular aneurysms involve the dilatation of a localized area of the arterial wall.

1.6.2 Physiopathology

Aortic aneurysm is a very complex condition which exhibits dynamic physiopathological process rather than a static pathological problem [Nordon et al., 2011]. In this context, several biological processes and risk factors have been identified that contribute to AAA pathogenesis. At the histological level some easily identifiable signs include inflammation, smooth muscle cell apoptosis, extracellular matrix degradation, and oxidative stress [Boddy et al., 2008, Kuivaniemi et al., 2012]. Although auto-immunity is also believed to be responsible towards aneurysm development and progression, the exact order of pathological events and their contribution is not yet clearly understood [Golledge and Norman, 2010]. Recent investigations involving molecular level micro-array based mRNA analysis concluded that the results were different for healthy and diseased aortic tissues. At the micro-scale disorganized distribution of collagen fibers along with fragmented network of elastin fibers were reported [Pasta et al., 2016, Phillippi et al., 2014]. In addition, commonly reported changes in micro-structure include decreased content of elastin, deposition of proteoglycans and collagen [Iliopoulos et al., 2009, Tang et al., 2005].

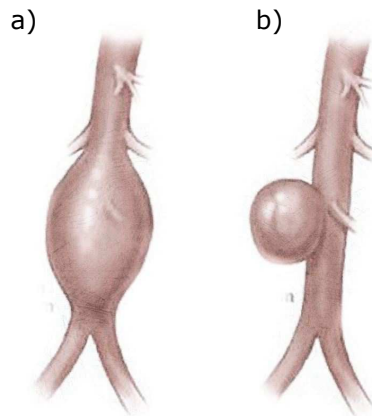


FIGURE 1.10 – a) A fusiform abdominal aortic aneurysm, b) saccular abdominal aortic aneurysm.

1.6.3 Symptoms

Most people with aortic aneurysms do not have any symptoms, which makes them difficult to detect. They often grow gradually and symptoms may occur when the aneurysm gets bigger and puts pressure on surrounding organs. Some of the most common symptoms include: belly pain or discomfort, chest pain, pain in the lower back, or flank. Other symptoms include hoarseness, cough, fever, and weight loss. If an aneurysm is ruptured,

it causes sudden, severe pain in the chest, an extreme drop in blood pressure, and signs of shock. If not attended to immediately it can quickly lead to death.

1.6.4 Risk factors

Although the exact reasons for aneurysm development are still not completely known, several risk factors have been identified. A few significant ones are listed here:

1. **Age:** Aortic aneurysms are rarely seen before the age of 55 years, beyond which point the prevalence increases gradually with age.
2. **Smoking:** Blanchard et al [Blanchard et al., 2000] demonstrated that prolonged cigarette smoking is a major risk factor associated with aortic aneurysms.
3. **Male sex:** Blanchard et al [Blanchard et al., 2000] also confirmed that aortic aneurysms are more common in men than in women, with an odds ratio of 2.68. On the contrary, women have a higher risk of rupture compared to men [Sweeting et al., 2012, Brown and Powell, 1999]; reasons for which might include weaker wall strength and relatively higher rate of aneurysm growth [Larsson et al., 2011].
4. **Connective tissue diseases:** There are two main connective tissue diseases that result in an increased risk of aneurysm formation:
 - **Ehlers-Danlos syndrome:** It is a rare, inherited connective tissue disorder, which stems from an irregularity in type III collagen. Ehlers-Danlos syndrome is comprised of 10 different sub types, of which only type IV is associated with vascular disease, which include 4% of all cases [Oka et al., 2001].
 - **Marfan syndrome:** It is a connective tissue disease, resulting from a defect in the fibrillin gene [Hewett et al., 1994]. Furthermore, patients affected by marfan syndrome exhibit elastin deficiency and a reduction in cross linking density [Perejda et al., 1985]. This could lead to enlargement of aortic wall diameter, subsequently resulting in aneurysms [Fonck et al., 2007].
5. **Atherosclerosis:** For a number of years, atherosclerosis has been regarded as one of the major causes of aortic aneurysms by clinicians. The reason for this belief is that aneurysms demonstrate features like calcification, ulceration, and lipid deposition which are also evident in atherosclerosis. And as the saying goes 'correlation does not imply causation', credible evidence is still needed to implicate that atherosclerosis as the cause for aneurysms.

1.6.5 Diagnosis

Diagnosing an aortic aneurysm is a difficult task because often there are no symptoms, with most cases it only getting recognized post rupture. Many aneurysms are found as a by product during routine medical tests. Early diagnosis is imperative for managing the condition. The larger the aneurysm, or the faster it grows, the more likely it is to rupture. If an aortic aneurysm is suspected, the physician may order the following tests:

1. **Chest x-ray:** A very small amount of radiation is used to produce an image of the structures of the chest. It is often used to diagnose lung and cardiac diseases.

2. **Ultrasound:** Ultrasound Elastography has been highlighted in recent years for non-invasive estimation of tissue mechanical properties. It recognizes the changes in tissue stiffness, through which it is able to provide useful quantitative and qualitative data for diagnostic purposes [Sigrist et al., 2017].
3. **Computed tomography (CT) scan:** A CT scanner sends X-ray beams through the body and recognize different levels of density and tissues inside a solid organ, and can yield detailed information about the body by constructing cross-sectional images. Regardless of its advantages, in younger patients the cumulative radiation dose from follow-up examinations could be harmful for the patient [Fred, 2004].
4. **Magnetic resonance imaging (MRI):** A test that produces high quality pictures of the heart and blood vessels. These are used to evaluate the anatomy and function of the structures of the chest.

1.6.6 Complications

The primary complications involved with aortic aneurysms are a tear in the wall of the aorta (dissection) and rupture, both of which are life-threatening conditions. A ruptured aortic aneurysm can lead to severe internal bleeding. In general, the larger the aneurysm, the greater the risk of rupture.

1.6.7 Current rupture risk criteria

Progressive treatment for treating aortic aneurysms cannot be offered to all patients, and is usually considered when the perceived risk of rupture exceeds the risk of surgical intervention. However, a reliable measure of rupture risk quantification still remains the barrier in clinical decision making [Gasser, 2016]. As per the current standards, aortic aneurysm rupture risk is assessed by largest transverse diameter and its change over time. Clinicians recommend AAA repair if the largest diameter exceeds 5.5cm or if the aneurysm grows more than 10 mm per year [Participants, 1998, Greenhalgh and Powell, 2008]. However, these criteria are very crude as its reported that many aneurysms with diameter less than 5.5cm do rupture [Brown and Powell, 1999], where as aneurysms larger than 5.5cm never rupture [Nicholls et al., 1998, Darling et al., 1977]. Besides these two, many other clinical risk factors have been proposed which include aneurysm shape [Vorp et al., 1998, Hua and Mower, 2001], female sex [DeRubertis et al., 2007, Wilson et al., 2003], mean arterial pressure [Brown and Powell, 1999], thick intraluminal thrombus (ILT) [Kazi et al., 2003], and rapid increase in ILT volume [Stenbaek et al., 2000] . Biomechanical rupture risk assessment is a relatively new field, which will be addressed in latter sections.

1.6.8 Treatment

The treatment of aortic aneurysms remains operative. If untreated, the aneurysm will increase in size and will eventually rupture; unless the patient dies from other causes prior to this event occurring. As discussed in the previous section, the decision to opt for progressive treatment is made by the clinician after an assessment of apparent rupture risk. Two common types of surgery exist for aneurysm repair as seen in the figure 1.11, which are:

1. **Open surgery:** This is the most common yet the most invasive method, meaning the surgeon will probe into your body to do it. In brief, the surgeon replaces the weakened section of the aorta with a graft. The entire procedure may take up to 6 hours. The 30 day mortality rate after open surgery in 2003 was reported to be 4.7% [Greenhalgh and The, 2004].
2. **Endovascular repair (EVAR):** If a patient's anatomical criteria does not allow for an open surgery, the surgeon suggests a endovascular repair. In this procedure, the surgeon inserts a flexible wire frame tailored onto a graft into the aorta, with the help of a catheter. The stent graft self expands once positioned in the aorta and protects the weakened arterial wall. The aneurysm sac is still intact after EVAR unlike in open surgery. The 30 day mortality rate after EVAR was reported to be 1.7% in 2003 [Greenhalgh and The, 2004]. Long-term survival rates were similar for EVAR versus open-surgery with a ratio of 1 and 0.98 for 3.5 and 10 years respectively [Bulder et al., 2019]. Although EVAR proved to be superior with regard to post-operative mortality in the short term, long term results indicate little difference between the two surgical methods [Lederle et al., 2009, Lederle et al., 2012, Sugimoto et al., 2017].

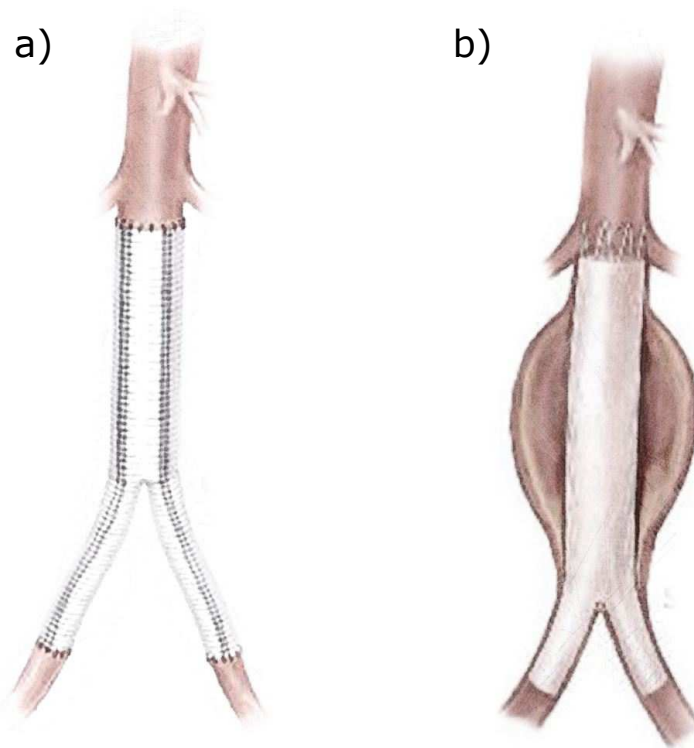


FIGURE 1.11 – Result after a) Open surgery, b)endovascular aortic repair.

1.7 Mechanical characteristics of the arterial wall

In order to better understand the mechanisms of aortic rupture, an accurate description of its mechanics is imperative. In this section a review of the existing insights accumulated through empirical research is presented.

1.7.1 Experimental methods

Numerous studies have been conducted in understanding the mechanical characteristics of the arterial wall. These studies were performed both in clinical and laboratory settings to identify relationships between diameter, compliance, stiffness, and the corresponding pressures, and forces to which the vessel wall is subjected. Further, these experiments are necessary for collecting data with which constitutive equations could be parameterized. A brief overview of the experiments conducted to study the mechanics of the artery is presented herein.

1.7.1.1 In vivo experiments

There are currently limited ways to determine the state of strain or stress of an artery in vivo with respect to its undeformed or unstressed configuration [Vaishnav et al., 1972, Stålhand et al., 2004]. Nonetheless, in vivo studies do yield important information. Studies are performed regularly in the clinical setting using invasive (intravascular ultrasound), and non-invasive (magnetic resonance imaging) imaging methods to study blood pressure, changes to vessel geometry, state of disease, and responses to external stimuli [Draney et al., 2002]. They were used to measure the relative increase in the arterial diameter between diastole and systole allowing one to evaluate the circumferential stiffness. Early studies done on animals used invasive techniques, with calipers patched to the arterial wall and fitted with strain gauges to measure relative circumferential and longitudinal strains. It was consistently reported that the in vivo length of the arteries changes significantly. Extensions induced by blood pressure are usually in the range of 1 – 2% [Labrosse, 2007]. The change in diameter during the cardiac cycle reaches up to 10 – 15% in the pulmonary aorta 6 – 10% in the carotids, and 2 – 5% in the aorta [Humphrey and Rajagopal, 2002]. Darney et al [Draney et al., 2002] reported nonuniform deformations in the thoracic aorta during the cardiac cycle, with a peak average strain of 8 – 11%. For a detailed discussion on the use of clinical studies in evaluating mechanical properties of the aorta, the reader is directed to reviews by Banks [Bank, 1999] and Cameron [Cameron, 1999]. But, in vivo studies are only useful for a comparative analysis of the mechanical behavior of the aorta. They are not used to establish comprehensive material behavior of the arterial wall. This can be only attempted in vitro, which will be discussed in the next section.

1.7.1.2 In vitro experiments

Experimental methods to test the mechanical behavior of soft tissues have evolved over time. Manual experiments have given way to computer controlled experiments, which provide accurate data measurement and a variety of testing conditions. Researchers have recognized that as is the case with other soft tissues, a broad range of loading conditions are required to represent the multi-axial behavior of arterial walls, which include:

1. **Uniaxial testing:** Uniaxial tensile tests are an easy way to study the mechanical response of excised tissues and obtain stress-strain curves. This approach has been followed widely in the literature for comparative studies of different soft tissues [Valenta, 1993]. Such tissues exhibit a non-linear stress-stretch response, with a low modulus regime and a high modulus regime. M. G. Wertheim was among the first researchers to point this out in 1846 [Wertheim, 1847], wherein he performed force-elongation tests on human tissues including arteries, muscles, and tendons. It was not until 1957, that an explanation was provided by Roach and Burton [Roach and

Burton, 1957]. In addition to providing basic information on the mechanical response of the tissue, uniaxial tests also help in understanding the failure properties. They yield interesting data about what level of mechanical stimulus is required to permanently damage the tissue. Values of yield stress and strain, along with ultimate stress and strain are reported in that regard describing tissue failure [Raghavan et al., 1996]. The average ultimate tensile strength of healthy arterial tissues from uniaxial tensile tests is reported to be in the range of $1 - 2MPa$ [Karimi et al., 2013, Mohan and Melvin, 1982]. It has been also reported that the ultimate tensile strength of the arterial tissue is generally higher in the circumferential direction compared to the axial direction [Okamoto et al., 2003, García-Herrera et al., 2012]. Several researchers have also investigated the mechanical responses of diseased and healthy tissues with the help of uniaxial tensile testing. For instance Karimi et al [Karimi et al., 2013] studied the mechanical behavior of atherosclerotic human coronary arteries and reported that the maximum tensile stress was higher in diseased arteries ($2.08 \pm 0.86MPa$) compared to healthy arteries (1.47 ± 0.87). In addition, they have reported that atherosclerotic arteries bear more stress at a similar strain level compared to healthy arteries, meaning that the ultimate tensile strain is higher in healthy arteries. When it comes to aneurysmal aortas, Vorp et al [Vorp et al., 2003] have reported aneurysmal tissues to be much stiffer compared to control samples. Several other researchers reported similar conclusions while comparing the mechanical response of aneurysmal tissue to healthy tissue [Duprey et al., 2010, Duprey et al., 2016, Cavinato et al., 2019]. In contrast, there is no common consensus on the failure properties of aneurysmal tissue in comparison to control specimens, with some reports stating higher ultimate stress in healthy tissue and vice versa [Duprey et al., 2016].

- 2. Biaxial testing:** Biaxial testing machines allow for stretching a piece of tissue in two orthogonal directions at the same time, possibly even with different stretch values in each direction. Although this an improvement over uniaxial tensile tests, the sample is usually stretched in plane, which does not take into account the curvature of the arterial tissue [Okamoto et al., 2002]. Sommer et al [Sommer et al., 2010] conducted a wide range of biaxial tests on healthy carotid arteries which brought into spotlight two important aspects: anisotropy and heterogeneity. Equibiaxial tests on intact arterial tissue showed a stiffer response in the circumferential direction compared to the axial direction, which concur with several other findings [Cavinato et al., 2019]. Similarly, they report different mechanical responses in adventitia and media signifying the heterogeneity of the wall layers. Miroslav et al [Zemanek,] reported the importance of factors like preconditioning, specimen location, and strain rate on the mechanical response of the tissue. It was concluded that while preconditioning is important in uniaxial tensile tests, no preconditioning is necessary for biaxial testing. Similarly, they have reported that the influence of strain rate on the mechanical response under biaxial loading is negligible. In an attempt to study the failure properties of healthy aortas using biaxial testing, Mohan et al [Mohan and Melvin, 1983] reported that the tissues failed consistently in the circumferential direction. In addition, when the strain rate was increased significantly, the failure stress was found to be almost twice the value from quasi-static tests. In aneurysmal tissues, an increase in stiffness and decrease in extensibility were observed in its biaxial biomechanical behavior. The increase in stiffness was observed to be particularly substantial in the

circumferential direction [Vande Geest et al., 2006]. These findings are contentious as other researchers have reported no predominant directional dependence for stiffness [Matsumoto et al., 2009]. In understanding the failure mechanics of aneurysmal tissues Duprey et al [Duprey et al., 2016] reported a rupture mechanism resembling dissection which was never detected in uniaxial tests. In coherence with observations made by Mohan et al, they report that the samples ruptured with a crack perpendicular to the axial direction.

- 3. Others:** In view of the limitations of the uniaxial and biaxial testing protocols, investigators have turned to other sophisticated experimental setups, which allow for accurate and independent control of dilation, extension, and twist of the artery [Humphrey, 2002]. For instance, experiments have been performed for a combination of pressure loading at different axial stretches [Brossollet and Vito, 1996, Dixon et al., 2003, Humphrey et al., 2009, Humphrey, 1995]. Torsional loading experiments were conducted with an aim to study the shear profile for blood vessels [Deng et al., 1994]. Similarly, methods for collecting residual stress data and measurements of the opening angle of the artery were of significant interest [Van Dyke and Hoger, 2002, Chuong and Fung, 1986, Fung, 1967]. Researchers have also looked at the effect of thermal stresses [Kang et al., 1995] and the use of pharmacological agents to differentiate passive and active responses [Armentano et al., 1995].

Experiments have revealed that the arteries are very complex when it comes to their mechanical characteristics. Some of the important aspects are presented briefly in the following sections.

1.7.2 Elasticity and Non-linearity

The elastic response of the arteries can be essentially categorized into active and passive behaviors, which vary with location on the vascular tree, age, species, etc. Both of these responses can be characterized as nonlinear over finite strains and understanding of each in detail is necessary for development of constitutive equations.

1.7.2.1 Active behavior

Under physiological conditions arteries are subjected to an average pressure of 98 mm-Hg and pressure pulsations of about 35 mm-Hg . Although they exhibit minimal changes in axial direction in vivo, the pressure pulsations cause diameter fluctuations of about $8 - 12\%$ [Dobrin, 2011]. Vascular smooth muscle cells are responsible for maintaining the local blood pressure by either contracting or relaxing. This mechanism is responsible for the redistribution of blood within the body. Excessive contraction of smooth muscle cells leads to high blood pressure, while their excessive dilation leads to low blood pressure. Thus, the quantification of the mechanics of this behavior is important for understanding pathophysiology.

1.7.2.2 Passive behavior

Arterial wall is a composite structure of several constituents, whose distributions, orientations, and interconnections give rise to its mechanical properties. Due to this, a distinctive mechanical characteristic of the tissue can be observed in a simple tension test where the initial response is almost flat with relatively large extension followed by rapid stiffening at

higher extensions. This nonlinear response of arterial tissue to mechanical stimulus was first reported by Roy et al, who conducted experiments on excised animal arteries [Roy, 1881]. Further investigations have revealed that the passive response of arteries at low pressures is governed by elastin in the medial layer, whereas the response at high pressure is governed by collagen in the adventitia [Roach and Burton, 1957]. This is because, in the media the elastin and collagen fibers are neatly aligned towards the circumferential direction. In contrast, in the adventitia, which is predominantly collagen, the fibers are disorganized with highly dispersed orientations. To add to that, the fibers are in an undulated configuration in the basal state. Also, the elastic modulus of collagen fibers is much higher compared to elastic fibers, the ratio of which is on the order of 10^3 [Holzapfel, 2001, Metafratzi et al., 2002]. Two interesting phenomena: uncrimping, where the collagen fibers slowly release their crimp; reorientation, where the fibers align towards the loading direction; get the collagen fibers in the adventitia to be recruited to resist the applied load. The resulting response is a "J" shaped curve with three distinctly identifiable regions: toe, heel, and the linear region as depicted in the figure 1.12.

In this work, we are only interested in understanding and modeling the passive mechanical behavior of the arteries in health and disease.

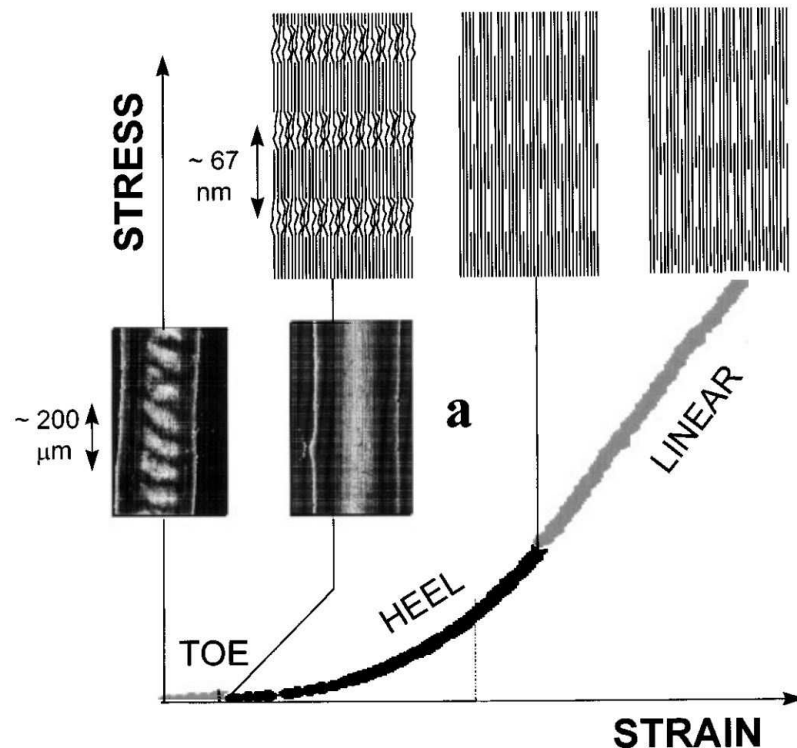


FIGURE 1.12 – Passive response of arterial wall under uniaxial tension [Fratzl et al., 1998]

1.7.3 Anisotropy

Isotropy and anisotropy refer to whether a material's mechanical response is independent of the direction in which the material is loaded. This is of course a manifestation of material symmetry and must be specified with respect to a particular configuration. The organization of the structural components such as elastin and collagen fibers of the arterial wall causes it to be anisotropic. To the best of author's knowledge Patel and Fry [Patel

et al., 1969] were the first to conduct a study on arterial anisotropy, suggesting that the wall is cylindrically orthotropic. Although this is in general agreement, there is quite a debate on the direction of anisotropy, especially in physiological range of deformation [Dobrin, 2011, von Maltzahn et al., 1984]. While the majority of reports suggest that the circumferential direction is stiffer than the axial direction [Weizsacker and Pinto, 1988, Cox, 1975, Cox, 1978], there exist a few published experimental records where it is the opposite [Patel et al., 1969].

1.7.4 Heterogeneity

On the microscopic level, healthy arteries are not homogeneous. The wall is comprised of several constituents, and the distribution of these elements varies from the inner wall to the outer wall, along the vascular tree, from individual to individual. Ultimately, the unknown interaction of the fibrous constituents and their organization dictates the mechanical properties of the extracellular matrix [Fung, 2013]. For instance, the heterogeneity of the arterial wall has been demonstrated by Davis et al [Davis et al., 2016] at the millimeter scale, wherein they captured the heterogeneity at length scales between 1 *mm* to 1 *cm*.

1.7.5 Viscosity

The transmission of energy across the system in arterial tissue is split into two parts: one that can be stored in the tissue and can be retrieved due to elasticity, while the second part is dissipated due to viscosity. The first relevant studies in understanding this behaviour was conducted on examining static and dynamic viscoelastic behavior in dog arteries [Bergel, 1961, Bergel, 1960]. The knowledge of this behavior maybe paramount in understanding the physiological mechanisms of degenerative diseases affecting the arteries.

1.7.6 Incompressibility

Based on histology, the arterial wall can be thought of as a mixture composite structure [Humphrey, 1995], the solid part of which is composed of elastin, collagen, and smooth muscle cells. The arterial wall is considered as a homogenized solid ignoring the fluid transport in and out of the wall. Although arteries are not truly incompressible, they appear to be virtually incompressible under various loading conditions. For instance mechanical testing of the aorta in the range of physiological loading demonstrated that the tissue does not change in volume [Girerd et al., 1992]. Carew et al [Carew et al., 1968] demonstrated incompressibility of the arteries by comparing the evaluated bulk modulus to computed shear modulus by Bergel et al [Bergel, 1961], the ratio of which was on the order of 10^3 .

1.7.7 Residual stress

Residual stress is the stress that exists in a body in the absence of externally applied loads. Fung et al [Fung, 1973] were the first to note that a natural configuration is highly unlikely to exist in soft tissues as they remodel continually and undergo many irreversible processes while continually under loading. This indeed also applies to arteries, in which Bergel [Bergel, 1960] first observed the existence of residual stresses and strains. This phenomena is commonly known as the "unrolling" of the artery, where in a longitudinal cut results in the artery unrolling itself [Vaishnav and Vossoughi, 1983]. Similar findings were recorded by other independent researchers, which have been instrumental in understanding

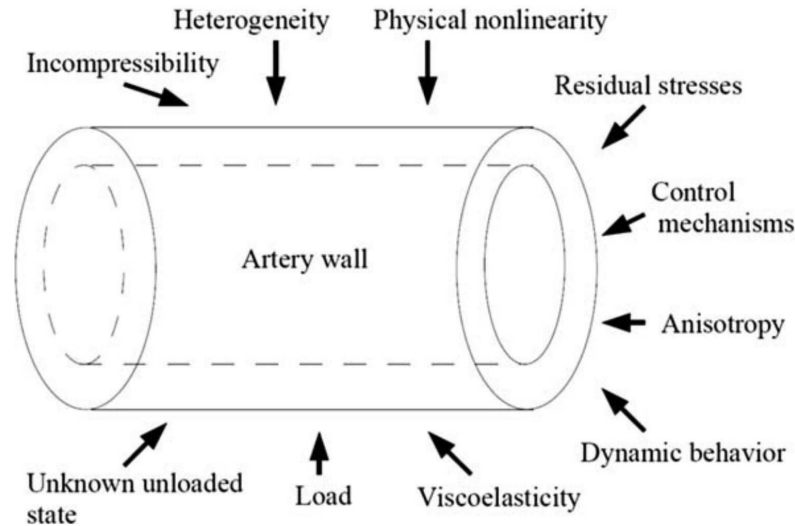


FIGURE 1.13 – Different aspects of mechanical characteristics of arterial walls [Kalita and Schaefer, 2008]

and demonstrating the importance of this phenomena [Fung, 1984, Liu and Fung, 1988, Vlachopoulos et al., 2011].

1.8 Mechanical models of the arterial wall

In physics, elasticity refers to the ability of a material to resist a distorting influence and return to its original configuration when the influence is removed. One such commonly known elastic material is rubber, which exhibits this behavior. A spectra of elastic materials are found in nature, which can be described using mathematical models. The simplest mathematical model used to describe the elastic nature of materials is the Hooke's law, which states that for small deformations, the applied force is directly proportional to the induced displacement. Of course this is an over generalization in the real world with most materials that possess elasticity remaining linearly elastic only up to very small deformations. The elastic behavior of materials at large deformations therefore needs more complex mathematical descriptors, some of which include hyper-elasticity and hypo-elasticity. In the context of this thesis, hyper-elasticity is the most relevant descriptor for the complex mechanical behavior of the arterial wall. Briefly, it uses a scalar valued function to equate the strain energy density of a material to the deformation gradient. The stress-strain relationship is derived from the defined strain energy density function. A comparison of two existing incompressible hyper-elastic material models, namely the Neo-Hookean material model and the Holzapfel hyper-elastic model [Holzapfel et al., 2000] is shown in figure. As discussed in the previous section, the passive mechanical response of the arterial wall is nonlinear, thus complicating mathematical descriptors of the stress-strain relationship. Due to this reason, the stress at any given stretch/strain cannot be computed with a single constant, but requires a set of constants. Since its not possible to duplicate the whole range of in vivo loading conditions experimentally, these mathematical descriptors of the mechanical behavior are required to extrapolate existing experimental results. This in turn aids in measuring stresses in vivo by measuring the strain non-invasively, which can be further used to predict vessel wall stability. A plethora of models exist for studying the arterial wall mechanics, which include phenomenological models (pseudo-elastic), struc-

Nonlinear material models

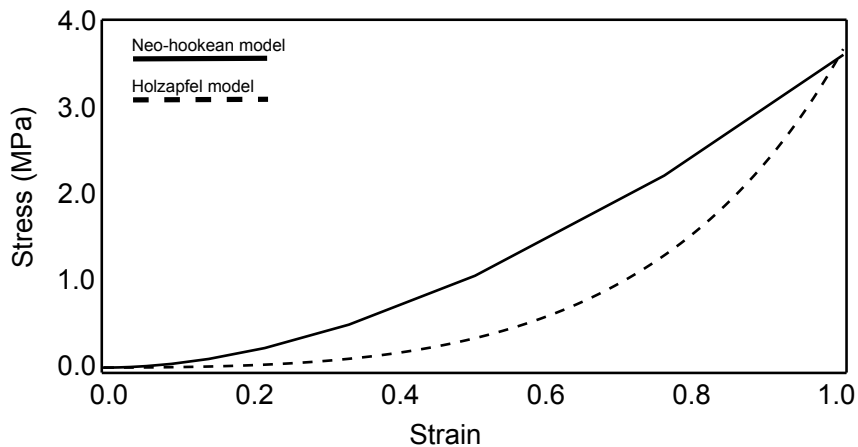


FIGURE 1.14 – Comparison of Neo-hookean vs Holzapfel hyper-elasticity models

tural models, poro-elastic or viscoelastic models, and discrete network models. Each of these category of models will be presented briefly herein.

1.8.1 Phenomenological constitutive models

Phenomenological models use mathematical functions of the form exponential, logarithmic, or polynomial with a set of unknown coefficients to describe the strain energy density of arterial tissues. Patel and Vaishnav [Patel and Vaishnav, 1972] pioneered the work by proposing a seven-parameter polynomial model. Fung et al conceived a four parameter exponential model observing repeatable loading and unloading response in arterial tissue [Fung et al., 1979]. Following their four parameter exponential model, Chuong and Fung [Chuong and Fung, 1983a] introduced a seven parameter exponential function. But it has been shown that the four parameter exponential model has limited capability in capturing the anisotropic properties of the tissue. A four parameter logarithmic model was introduced by Takamizawa, which also suffered from the same limitation as the four parameter exponential model. Humphrey compared these commonly used phenomenological models and concluded that the seven parameter exponential is the best available for studying the mechanical behavior of arteries [Wagenseil and Mecham, 2009a]. Several researchers utilized these strain energy density functions to model the mechanical behavior of artery assuming it to be an incompressible thick walled homogeneous material [Vorp et al., 1995, Chaudhry et al., 1997]. Holzapfel et al [Holzapfel and Weizsäcker, 1998] used a four parameter exponential function to model the anisotropic behavior in combination with a neo-hookean strain energy density function to model the isotropic part.

Although phenomenological models predict the behavior of the tissue accurately, they do not account for any structural information. The coefficients identified inversely do not bear any correlation to the structure of the tissue. This leads to difficulties in studying and predicting the behavior of diseased arteries where changes in physiology and pathology directly influence the mechanical behavior [Alford, 2007].

1.8.2 Structural constitutive models

Structural constitutive models are similar to phenomenological models in the sense that they too define a strain energy density function to describe the stress-strain relationship.

The difference being structural constitutive models incorporate morphological information such as fiber orientation and crimp into the constitutive relationships. Lanir developed the first micro-structure motivated three dimensional model for fibrous soft tissues, that directly incorporates fiber orientation [Lanir, 1983a]. The realization that the structural organization of microscopic constituents is different in the media and the adventitia gave rise to separate strain energy densities for each layer [Von Maltzahn et al., 1981]. Holzapfel and Weizsacker instead defined separate strain energy densities for elastin and collagen, with elastin behaving like a linear isotropic material and collagen behaving like a nonlinear anisotropic material [Holzapfel and Weizsäcker, 1998]. Structural models grew into popularity since early 2000 with a number of investigators improving on early models. These can be broadly classified into structural tensor and angular integration approaches. Holzapfel et al [Holzapfel et al., 2000] first introduced the structural tensor approach to take into account the collagen fiber morphology in the arterial wall . The strain energy function is additively split into two parts, isotropic and anisotropic (assuming elastin governs the response in low pressure region). This two term potential is defined in the equation below:

$$\psi(C, a_{01}, a_{02}) = \psi_{iso}(C) + \psi_{aniso}(C, a_{01}, a_{02}) \quad (1.1)$$

where C is the right Cauchy-Green tensor, a_{0i} are two reference direction vectors representing the directions of two families of collagen fibers [Holzapfel et al., 2000]. Although this model does not account for dispersion of collagen fibers, it still remains to be the most utilized model for artery with implementations in commercial finite element software like Abaqus. Later, Gasser et al [Gasser et al., 2006a] generalized this model by extending it to include fiber orientation dispersions. They introduced a generalized structural tensor (GST) H , which takes into account a probability density function in place of a single unit vector for collagen fiber orientations.

$$H = kI + (1 - 3k)a_0 \otimes a_0 \quad (1.2)$$

$$k = \frac{1}{4} \int_0^\pi \rho(\theta) \sin^3 \theta d\theta \quad (1.3)$$

where k is the dispersion parameter which feeds the structural tensor H . A π periodic Von-Mises function is the most commonly used probability distribution to represent the morphology of embedded collagen fibers. As introduced in [Holzapfel et al., 2014a], another approach is to consider the strain energy of single collagen fiber $w(\lambda)$ and integrate (AI) it over the unit sphere to obtain the total strain energy associated with collagen fibers per unit volume as in

$$\psi_f = n \int_S \rho(\theta) w(\lambda) dS \quad (1.4)$$

where $\rho(\theta)$ is the probability density function, n is the number of fibers per unit volume, and λ is the fiber stretch. The probability function allows for the quantification of collagen fiber dispersion in the arterial wall layers. The comparison of the two above mentioned methods was discussed in detail in [Cortes et al., 2010a]. In brief, the angular integration approach requires an integration to be performed on the unit sphere, whereas the structural tensor approach does not need one. It has been also concluded that identification and exclusion of fibers under compression is possible in AI, while it is not straightforward in GST [Melnik et al., 2015, Holzapfel and Ogden, 2015].

A brief overview of existing continuum mechanical models which implement the above approaches is presented. Sacks et al [Sacks, 2003] implemented a two dimensional distribution in the strain energy function based on a beta probability distribution, thereby neglecting the out of plane dispersion of fibers, while a gaussian distribution was used to study biaxial behavior [Driessen et al., 2005]. Several other studies implemented these formulations by incorporating different probability density functions such as: Von Mises distribution [Federico and Gasser, 2010, Agianniotis et al., 2011, Ateshian et al., 2009, Alastrué et al., 2009], and bingham distribution [Gasser et al., 2012a], the latter of which was claimed to be superior to the Von-Mises distribution. The claim was later challenged by Holzapfel et al [Holzapfel et al., 2015a] who implemented a mixture of two Von Mises distributions to model the asymmetric dispersion of collagen fibers in the arterial walls.

1.8.3 Growth and Remodeling models (G&R)

Growth and remodeling in arteries signifies the coordinated ability of arteries to maintain homeostasis, which represents the state of steady internal physical and chemical conditions maintained by living systems, and adapt to mechanobiological changes in their environment. In this context, two main approaches exist, namely, kinematic growth and constrained mixture models, which are essentially two different ways to compute the strain energy density function and mass density.

1.8.3.1 Kinematic growth models

First pioneered by Rodriguez et al [Rodriguez et al., 1994] kinematic growth models conceptualize growth via two deformations: inelastic "growth" deformation gradient and a subsequent elastic "assembly" deformation gradient. The theory requires a constitutive equation for inelastic deformation in addition to elastic constitutive equation, which typically does not include rigid body rotations [Cyron and Humphrey, 2017]. Even though most implementations of this theory are mechanobiologically limited, it still continues to be used widely for its simplicity and computational efficiency [Menzel and Kuhl, 2012, Ambrosi et al., 2011].

1.8.3.2 Constrained mixture models

Motivated by Fung's suggestion to describe growth in terms of mass-stress relations plus the desire to incorporate mechanobiological data, Humphrey et al [Humphrey and Rajagopal, 2002] proposed a constrained mixture model for G&R. Each representative element of the arterial wall is assumed to be a mixture of its structural constituents. Each constituent is assumed to have different turnover rates, allowing different mass increments to be deposited at each time increment [Cyron and Humphrey, 2017]. These models are an improvement over kinematic growth models as they incorporate differential turnover of individual constituents. Yet, they are both computationally expensive and much harder to implement.

1.8.3.3 Hybrid models

To address the limitations of both kinematic growth and constrained mixture models, hybrid models have been proposed to study growth and remodeling in arteries [Eriksson et al., 2014, Watton et al., 2004, Watton et al., 2011, Selimovic et al., 2014]. A temporally homogenized constrained mixture model has been proposed by Cyron et al [Cyron et al., 2016]. This differs from the classical constrained mixture model by performing a temporal

homogenization across all mass increments of one constituent. This method was reported to converge to the same solution as the classical method in the vicinity of a homeostatic state [Cyron et al., 2016, Rajagopal and Srinivasa, 1998].

1.8.4 Poro-elastic and Visco-elastic models

Poro-elastic models consider the artery to be a fluid saturated porous medium. Poro-elastic models include measures of both the solid and fluid components in the kinematic and conservation equations. Simon et al [Simon et al., 1998] conducted experiments of rabbit aortas in the presence and absence of fluid to assess the response. Their model incorporates an incompressible fluid along with an incompressible and isotropic solid. They reported that the model fits accurately to their experiments with minimal error. Other studies which model the poro-elastic behavior of artery assume a transversely isotropic, linear elastic material with an anisotropic axis in the radial direction [Kenyon, 1979, Johnson and Tarbell, 2001]. Although these models present intriguing results, they are not frequently used in solid mechanics studies. Maxwell and Kelvin-Voigt models constitute the simplest of viscoelastic models [Vito and Dixon, 2003]. The Maxwell model represents a damper in series with a spring while the Kelvin-Voigt model represents a damper in parallel with a spring. Due to the nature of strain rate independence in arteries, these models cannot be used to represent their mechanical behavior. To address this limitation, quasi-linear viscoelastic models with an independent time and strain dependent components have been used. Fung et al provide a concise review of these early models [Fung, 2013]. Armentano et al used three Maxwell elements in series to model the viscoelastic behavior, the limitation being the inability to model viscoelastic effects when smooth muscle cells are inactivated [Armentano et al., 1995]. Veress et al introduced a standard nonlinear solid to model viscoelastic behavior of arteries. The model includes a nonlinear spring element in parallel to a Maxwell element [Veress et al., 2000]. The model showed encouraging results when compared with experiments conducted on porcine arteries. Holzapfel et al modified their structural constitutive model to incorporate viscoelastic effects using a 3-D Maxwell model and demonstrated its efficiency to predict viscoelastic behavior by comparing the results to human aorta experiments [Holzapfel et al., 2002]. More recently Suncica et al [Čanić et al., 2006] introduced a linearly visco-elastic cylindrical shell model, which uses a Kelvin-Voigt type visco-elasticity to capture the hysteresis behavior of the arterial stress-strain response. Excellent agreement was observed between the numerical simulation results and experimental measurements.

1.8.5 Continuum damage models

In the arterial wall damage can occur in both elastin and collagen. For this reason, this section is focused on theoretical models of damage to both collagen and elastin. The sources of damage in arterial tissue varies from specimen to specimen, with the main ones including: low cycle fatigue at high loads, high cycle fatigue, biochemical degradation of elastin, etc.

1.8.5.1 Damage to isotropic component:

In order to differentiate the failure of other components of the arterial wall to the failure of internal elastic lamina (IEL), a nonlinear anisotropic constitutive equation was proposed

[Wulandana and Robertson, 2005]. The constitutive equation takes the form

$$W = (1 - d)W_{iso} + W_{aniso} \quad (1.5)$$

with W_{iso} representing the isotropic contribution and W_{aniso} representing the anisotropic contribution of the arterial wall. The parameter d represents the scalar damage parameter incorporating three modes: continuous, discontinuous, and enzymatic damage, the effect of which is represented as $(1 - d) = (1 - d_{continuous} - d_{discontinuous} - d_{enzymatic})$. The range of the scalar damage parameter is zero to one, with one representing a fully damaged material.

1.8.5.2 Damage to anisotropic component:

In order to develop realistic computational tools for studying vascular disease the inclusion of material anisotropy, damage and heterogeneity are required to be included. An anisotropic elasto-plastic material model was developed by Gasser and Holzapfel in order to study dissection during angioplasty [Gasser and Holzapfel, 2002]. The above mentioned damage model was extended to incorporate damage to the anisotropic contribution as well, resulting in

$$W_{iso} = (1 - d_{iso})W_{iso}^0 \quad (1.6)$$

$$W_{aniso} = \sum_{i=1}^2 (1 - d_{aniso}^i)W_{aniso}^0 \quad (1.7)$$

where d_{iso} and D_{aniso} represent scalar damage parameters of elastin and collagen respectively. Holzapfel extended their structural constitutive model to incorporate damage by assuming that damage occurs only in the two families of fibers. Hence, the strain energy function for the matrix material was left unchanged, but the two energy functions for collagen were updated.

$$W_{aniso} = \frac{k_1}{2K_2} \exp[k_2(1 - d)(I_i - 1)^2 - 1] \quad (1.8)$$

They tested three different functions for the evolution of damage (exponential, polynomial, and sigmoidal) and evaluated their applicability by comparing with experimental data. It was concluded that sigmoidal function showed the best fit while exponential and polynomial functions showed good fit in the beginning, they tend to diverge in the final loading stage. Subsequently, Volokh et al [Volokh, 2007] implemented a softening hyperelasticity approach to model the failure of aortic tissue, with energy limiters to describe strain softening. The model showed good predictive capabilities when compared with experimental data. In order to model the irreversible damage in arterial tissues, Gasser introduced an elasto-plastic damage model to model the deformation behavior of collagen fiber [Gasser, 2011]. The state of damage of the collagen fiber is defined by an internal scalar variable d such that

$$S_c = (1 - d)S_c^0 \quad (1.9)$$

where damage variable d represents the loss of stiffness, S_c and S_c^0 represent the damaged and undamaged stress states respectively. The damage variable is represented by an exponential function, coupled with a rate dependent plasticity.

These above damage models for arteries incorporate an isotropic damage variable, where as anisotropic damage to collagen fibers can also be implemented [Li and Robertson, 2013, Li and Robertson, 2009]. Multi-scale models developed by Sachin et al [Shah et al., 2014] to model the prefailure and failure mechanics of ascending thoracic aorta assume a brittle discrete failure of individual collagen fibers. The difference is that they incorporate collagen fiber network directly in their geometry in the form of random Delaunay networks.

1.9 Discrete network models

Discrete network models try to incorporate the geometry of the fibrous micro-structure into the model. Segmenting the fiber network with image processing techniques still remains challenging for complex structures like the arterial wall. Nonetheless this technique has shown great potential in studying other fibrous structures such as the axonal network of the brain [Garimella and Kraft, 2017, Krauss et al., 2012a].

Disordered networks or open-cell spatial structures are ubiquitous in nature and represent the spatial morphology of many micro-structured materials. Some of them include collagen gels, carbon nanotubes, nano-wovens and fibrous scaffolds. The morphology of the deposited fibers in these structures is often random and has a huge impact on the resulting mechanical properties. It is therefore imperative to study the mechanics of such networks. Finite element modeling is often the preferred tool for evaluating the mechanics of random fiber networks. However, apart from the fiber morphology several other considerations are important in determining the mechanics of the network, of which the important ones are listed here:

- Network structure: The set of parameters that characterize the random geometry of the network, such as: fiber density, orientation distribution, density and nature of cross-links, co-ordination number at cross-links, etc.
- Joints type: The nature of cross-links used to model fiber intersections has a major influence on the mechanics of the network. Three types of cross-links can be used to model this behavior. First type includes pin joints, where fibers only carry axial forces with no transfer of bending moments. Second, a rotating joint could be used to model both the transfer of axial forces and bending moments, essentially modeling the fibers as beams. Finally, a welded joint could be used to maintain a constant intersection angle between the fibers.
- Affine nature of fiber kinematics: Affine kinematics assumes that each fiber deforms in accordance with the macroscopic deformation, which means that the local microscopic strain is equivalent to the global macroscopic strain.

Based on these considerations, a large number of deterministic models have been utilized to predict the mechanical response and relate it to microscopic fiber network architecture [Chandran and Barocas, 2006, Lake et al., 2012a, Wang et al., 2000, Spanos and Esteva, 2009a, Zhang et al., 2013, Mauri et al., 2016] for non-biological materials. Random processes like Voronoi tessellation and Delaunay triangulation are used in reconstructing the

fiber network. Such structurally motivated fiber network models have had implications for gaining insight on the effects of inclusions on global structure mechanics [Amoroso et al., 2011], and fabricating better performing tissue surrogates [Moutos et al., 2007, Engelmayr Jr et al., 2008] that could recapitulate native tissue mechanics both in terms of in-plane behavior [Sacks, 2003] and of out-of-plane behavior [Amoroso et al., 2011].

Structural deterministic models utilize idealized fiber geometries and generally lack experimental validation and it can be a limiting factor in model fidelity and utility. There is thus a need to extend present approaches in modeling biological fibrous soft-tissues starting from the level of the fibers. Transmission electron microscopy and second harmonic generation (SHG) imaging are some of the useful techniques in this regard for studying collagen fiber network morphologies in arterial tissues. These studies revealed that the collagen fibers in arterial tissue are highly disorganized and undulated in unloaded configuration. While the segmentation of fiber network in artery still remains elusive, the stochastic nature of it can be studied from micro-structural imaging [Schriebl et al., 2011, Schriebl et al., 2012a, Cavinato et al., 2017]. There exist a limited number of models that use numerically generated discrete fiber networks to study arterial wall behavior. Nonetheless, structural models have been developed to describe the mechanical response of the tissue using discrete collagen fibers at the micro-scale [Diamant et al., 1972, Beskos and Jenkins, 1975, Comninou and Yannas, 1976, Jin and Stanciulescu, 2016a, Thunes et al., 2018, Witzenburg and Barocas, 2016]. In order to represent the wavy nature of collagen fibers, Diamant et al [Diamant et al., 1972] modelled fibers as zig-zag shaped beams as shown in figure 1.15 b. The bending modulus of the beam was used to add stability to the network. In 1976, Comninou and Yannas [Comninou and Yannas, 1976] developed a sinusoidal model for fiber shape as illustrated in figure 1.15 c, which was later simplified by Lanir [Lanir, 1979] in 1978. Beskos and Jenkins [Beskos and Jenkins, 1975] proposed a helical model as shown in figure 1.15 d to incorporate collagen fiber undulations. Jin et al [Jin and Stanciulescu, 2016b] presented a random walk algorithm for reconstructing collagen fiber networks. They utilized a two-fiber family characterized with Von-Mises probability function for this purpose. The waviness of the fibers was modelled using a uniform relative angle with respect to the global orientation. The main limitations of this approach include the absence of any histological investigations on the arterial tissue for extracting fiber orientations and the assumption of affine fiber kinematics. It has been demonstrated that collagen fiber network in the adventitia does not undergo affine deformation [Krasny et al., 2017a, Morin et al., 2018]. Thunes et al [Thunes et al., 2018] developed a computational model of the aortic media using morphology information acquired through multi-photon image analysis of the micro-structure. However, they represented the fibers to be straight as shown in figure 1.15 a, accounting for their undulations implicitly through the constitutive model. Moreover, they assume affine transformation for the underlying fiber kinematics as well. Finally Witzenburg et al [Witzenburg and Barocas, 2016] developed a multi-scale model for studying aortic tissue's failure behavior. They too represented fibers to be straight, accounting for fiber crimp in its constitutive model. Furthermore, the fiber morphology does not correspond to any microscopic investigation limiting the reliability of the model's implications.

To the best of author's knowledge, these are the major current discrete fiber models utilized in investigating the mechanical behavior of arterial tissue. The thesis, in part attempts to address some of the gaps present in the described models and develop anatomically

accurate micro-structure models of the outer most layer of the arterial wall.

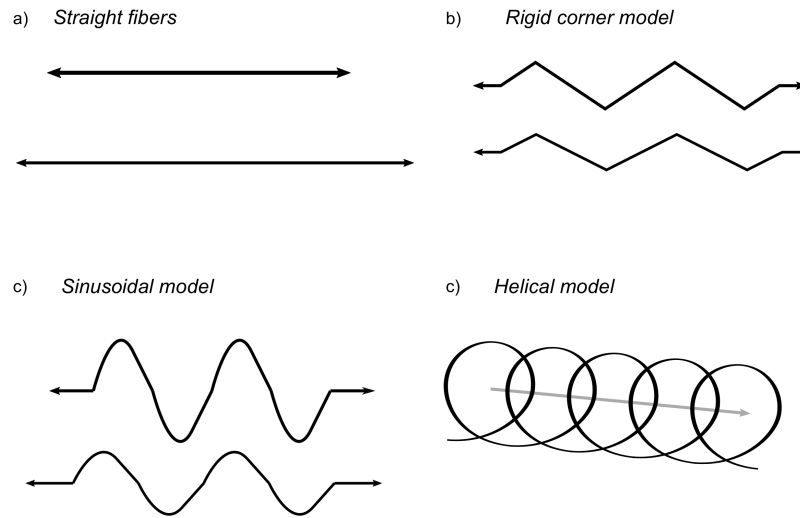


FIGURE 1.15 – Different structural representations of collagen fibers in mechanical models.

1.10 Micro-scale approach for quantifying rupture risk

The microscopic constituents of the arterial wall have a strong influence on its macroscopic mechanical behavior. In case of soft tissue analogs and other fibrous materials, it has been shown through computational modeling that macroscopic failure could also be determined assuming a fiber-scale damage [Hadi and Barocas, 2013, Shah et al., 2014, Hadi et al., 2012]. Hence an investigation of micro-scale failure mechanisms for assessing macro-scale tissue rupture seems compelling. In this section a brief overview of the current biomechanical analysis based rupture criteria are discussed.

1.10.1 Biomechanical rupture risk parameters

1.10.1.1 Wall stress analysis

It is well accepted that the rupture of aneurysmal wall occurs when the mechanical stress is more than the wall strength. In this context, several studies focused on analyzing wall stresses in search of risk criteria for aneurysm rupture and dissection. In order to analyze accurate patient specific wall stresses, the 3 – D geometry including zero-pressure and residual stresses is necessary. Krishnan et al [Krishnan et al., 2015, Mousavi and Avril, 2017], who modeled the zero-pressure configuration concluded that peak principle stresses obtained were greater than the ones obtained using zero stress geometries. Wall stress analysis of aneurysms with bicuspid and tricuspid aortic valves showed a greater wall stress in both circumferential and longitudinal directions in arteries with bicuspid aortic valves [Xuan et al., 2018]. However, wall stress evaluation suffers from unreliability and uncertainty in wall thickness measurement between patients and between measurement methods.

1.10.1.2 Wall strain analysis

Electrocardiograph image data was used to gauge the in-vivo strain in the arterial wall in AATA patients [Pasta et al., 2017]. The results indicated that the aneurysmal ascending aorta is stiffer compared to the healthy one and patients over 55 years old have significantly lower extensibility. In addition, the patient risk (the ratio of in vivo strain to the rupture strain) increased significantly in high systolic blood pressure, old age and higher pressure-strain modulus. Moreover, statistical analysis showed that a strong correlation could be established between pressure-strain modulus and rupture risk in patients with bicuspid aortic valve, suggesting a alternative mechanism of failure.

1.10.1.3 Rupture risk

Owing to the limitations posed by geometric indicators for assessing risk of aneurysm rupture, several studies have been conducted to define a reliable risk parameter using biomechanical analysis. These are based on peak wall stress, peak wall stretch, peak wall rupture index, and probabilistic nature of rupture.

- Rupture risk prediction based on peak wall stress is usually done by taking the ratio of principle Cauchy stress divided by the strength of the tissue [Fillinger et al., 2003, Maier et al., 2010, Heng et al., 2008, Venkatasubramaniam et al., 2004]. Apart from Cauchy stress, Von-Mises stress is often used as a failure criterion to account for spatial variations of the stress-strain state. Another popular stress criterion is the maximum shear stress, which is shown to be not a good choice [Volokh, 2010].
- Similar to peak wall stress, the stretch ratio risk index, which is the ratio of current tissue stretch to stretch at failure. But, this is shown to be unreliable as the critical stretch state changes drastically from uniaxial tension to equibiaxial tension [Volokh, 2010].
- Peak wall rupture risk indices incorporate factors such as gender, thickness of the wall, family history along with peak wall stress in computing the risk parameter [Gasser et al., 2010a, Erhart et al., 2015, Gasser et al., 2014].
- Deterministic models of aortic aneurysms do not take into account factors like local wall thickness and local biomechanical properties. In order to determine a probabilistic rupture risk indicator, Polzer et al assumed a distribution for peak wall stress along the wall geometry based on local thickness distribution [Polzer and Gasser, 2015a]. They concluded that taking into consideration the probabilistic nature of wall thickness and strength could enhance rupture risk assessments.

Although in the recent years modeling assumptions have improved by taking into account zero pressure configurations [De Putter et al., 2007], wall calcifications [O’Leary et al., 2015, Speelman et al., 2007], wall anisotropy [Geest et al., 2008], etc, there are still many limitations to the above mentioned rupture risk criteria. Firstly, the wall thickness in aneurysmal tissues is highly nonuniform and may not show a considerable reduction near rupture site [Raghavan et al., 2011]. Cavinato et al [Cavinato et al., 2019] reported similar findings with their bulge inflation testing of aneurysmal tissues where they observe no correlation between wall thickness and location of rupture. Interestingly, wall thickness may or may not change among ruptured and unruptured aneurysms [Raghavan et al., 2006, Di Martino et al., 2006]. Moreover the wall strength shows significant inter-and

intra-patient variability which introduces uncertainty in computation of above rupture risk indices [Vallabhaneni et al., 2004, Takamizawa and Hayashi, 1987]. Recent investigations by Cavinato et al [Cavinato et al., 2019] have shown that the location of rupture might not correspond to either peak wall stress or peak wall strain.

Evidently, tissue scale mechanical predictors for rupture risk have their limitations. The main problem surrounding this methodology is that there is a lack of knowledge on the intrinsic strength of the tissue, which seemingly is heterogeneous within a tissue and in-between tissues. This is the point at which a micro-structure level investigation could help in the assessment of the risk of aneurysm rupture in a superior way.

1.10.2 The need for micro-scale approach for identifying rupture risk

A lot of studies have been dedicated in incorporating micro-structure for studying the mechanics of the arterial wall. As described in section 1.10 this is done either by including structural properties [Holzapfel et al., 2000, Gasser et al., 2006a] in the constitutive equation or by directly incorporating the geometry [Jin and Stanciulescu, 2016a, Ayyalaso-mayajula et al., 2019]. This helps in establishing and analyzing critical structure-function as the organization of micro-structural components directly effects the mechanical response of the tissue. However, these studies were limited to the elastic response of the tissue and do not attempt to model the yield and failure of the tissue. To fill the gap, damage models have been implemented to replicate the failure response of the tissue [Gasser and Holzapfel, 2002], but the function used to represent damage evolution is generally phenomenological and bears little resemblance to failure mechanisms at the fiber level. On the other hand, the existing rupture risk parameters only take into account the macroscopic criteria such as the peak wall stress or peak wall stretch. It has been shown that these criteria have their limitations [Cavinato et al., 2019] even though they take into consideration local thickness and elastic properties of the wall. They do not take into consideration local morphological heterogeneity introduced by the arrangement of micro-structural constituents. This goes to show that aortic aneurysm rupture is a highly complex event which requires further investigation into the mechanics at different scales (fibers at micro-scale, and cells at meso-scale) to come up with better rupture risk indices.

1.11 Overview

The review of the state of the art presents us with an immense understanding of the complexity surrounding the mechanical behavior of arteries. They are anisotropic, heterogeneous, and highly non-linear in their response. The knowledge of their macroscopic behavior acquired through experimental investigations has been indispensable in gaining insights on initiation and propagation of diseases such as aneurysms. However, arteries are hierarchical structures made up of several micro-structural constituents as revealed by micro-structural imaging [O’Connell et al., 2008]. The organization, content, and interactions control the tissue’s mechanical response, giving rise to its varied local strength. Adding to this information, it has also been reported that a significant micro-structural remodelling takes place in aneurysms compared to healthy tissues [Cavinato et al., 2017, Phillippi et al., 2014]. It has been long hypothesised that these changes in the micro-structural architecture of collagen and elastin are some how responsible for degradation of the tissue. Also,

the event of aneurysm rupture is a localised mechanical event occurring when the stress exceeds the local strength of the tissue, again pointing at the micro-structure for possible explanations. However, currently there is a lack of knowledge in understanding the precise role these micro-structural constituents play in determining the macroscopic mechanical behavior. This thesis aims at shortening this gap by realizing the following aspects:

- ***Characterizing the tissue's mechanical behavior through novel experimental techniques:*** To this aim arterial tissue samples were tested under mechanical testing protocols, such as uniaxial tension and bulge-inflation. In order to better interpret the recorded mechanical response, mechanical testing was coupled with micro-structural imaging using a multi-photon microscope. An assumption was made that adventitial collagen is the crucial component for microscopic investigation in understanding the event of rupture. This was based on the knowledge that the adventitia operates as a protective sheath, preventing the wall from rupture at supra-physiological loads. The experimental protocols followed and the range of tissues tested are presented in chapter 2.
- ***Developing robust micro-structure based numerical models:*** Following the assumption that adventitia is the crucial layer for investigation, a choice was made to develop micro-scale numerical models of the adventitia by explicitly incorporating its collagen fiber network for analysis. The model assumes that the interactions between collagen and the matrix are negligible, enabling the enforcement of non-affine behavior for fiber kinematics. The whole work flow of developing anatomically accurate micro-scale models of the adventitia is presented in chapter 3. This chapter also presents a brief review of existing image processing techniques for generating a direct segmentation of the collagen fiber network from second harmonic generation (SHG) images.
- ***Quantitatively analyze the mechanical stress-strain state of fibrous micro-structure:*** A successful realization of the above two objectives made way for numerical simulations of the micro-scale models emulating the performed macro-scale mechanical tests. Explicitly incorporation the anatomy of the collagen fiber network combined with appropriate modeling assumptions enabled the quantification of collagen fiber mechanical state in the adventitia at loads especially close to rupture. The results of the methodology applied to rabbit carotid arteries is presented in chapter 4. The modeling technique further facilitated the quantification of crucial structure-function relationships in better understanding which micro-structural descriptors have a considerable influence on the macro-scale mechanical response.
- ***Quantification of micro-scale rupture criteria:*** The knowledge of quantitative criteria driving the rupture of aneurysmal tissue at the microscopic scale is expected enhance fundamental understanding and open paths to future clinical applications. For this purpose, a fiber-level damage mechanism was hypothesized as an explanation for tissue's rupture. The applicability of such a model was tested by comparing the experimentally recorded response of human aneurysmal and healthy porcine tissues. The results of the model in predicting tissue's failure is presented in chapter 5.

- ***Macro-scale modeling based on micro-scale evidence:*** Currently, the numerical models by many research groups to study arterial rupture suffer from various validity limits. The structural models as presented in this chapter follow some kind of a homogenization scheme neglecting the local heterogeneities. To address this limitation, an extension of the developed micro-scale model to capture multi-scale mechanics is presented in chapter 6. The model is useful in examining effects such as damage localizations leading up to failure.
- ***Global discussion:*** Finally the results and their implications for future research in the area of vascular mechanics is presented in chapter 7.

Chapter 2

Experimental methods

Contents of the chapter

2.1	Résumé du chapitre	40
2.2	Abstract of the chapter	40
2.3	Introduction	42
2.4	Micro-structural imaging	42
2.4.1	Multi-photon microscopy applied to rabbit carotid arteries	43
2.4.2	Multi-photon microscopy applied to human aneurysmal aortas	43
2.4.3	Multi-photon microscopy applied to porcine aortas	44
2.4.4	Optical light microscopy of porcine aorta	48
2.5	Thickness measurement protocol	48
2.6	Mechanical testing of arterial tissues	50
2.6.1	General considerations	50
2.6.2	Uniaxial tensile testing of rabbit carotid arteries	51
2.6.2.1	Sample preparation	51
2.6.2.2	Preconditioning	52
2.6.2.3	Testing protocol	52
2.6.3	Bulge-inflation testing of human aneurysmal aortas	53
2.6.3.1	Sample preparation	53
2.6.3.2	Preconditioning	53
2.6.3.3	Testing protocol	53
2.6.4	Uniaxial tensile testing of porcine aortas	53
2.6.4.1	Sample preparation	53
2.6.4.2	Preconditioning	54
2.6.4.3	Testing protocol	54

2.1 Résumé du chapitre

Comme nous l'avons vu dans le premier chapitre de la thèse, les artères présentent un comportement mécanique complexe à l'état passif, qui dépend fortement du contenu et de l'organisation des constituants microstructuraux tels que le collagène et l'élastine. Il est donc important de comprendre la relation entre les paramètres microstructuraux et la réponse mécanique des tissus à l'échelle macroscopique. Même s'il existe une bonne compréhension des impacts du collagène sur la réponse mécanique des tissus, les données décrivant les changements dans l'organisation microstructurale du collagène sous chargement sont rares en raison de l'absence d'une méthode simple et fiable pour quantifier cette structure lors des essais mécaniques. Ce chapitre donne un aperçu des études expérimentales réalisées et suivies dans cette thèse. En particulier, les méthodes expérimentales couplant un chargement mécanique et l'imagerie par microscopie multiphotonique sont présentées. Plus précisément, nous avons étudié les changements morphologiques de la microstructure d'artères carotides de lapins et d'aortes porcines et humaines (anévrismes). L'analyse nous a permis de comprendre et de renforcer les relations structure-fonction, en particulier la réorientation et le déploiement des fibres de collagène. L'ensemble de ces données sera utilisé dans la suite du manuscrit pour développer et alimenter les méthodes et modèles proposés, ainsi que pour leur validation. L'imagerie microstructurale et les tests mécaniques effectués sur les artères carotides des lapins ont été réalisés par Witold Krasny [Krasny et al., 2017a], les aortes anévrysmales humaines ont été testées par Cristina Cavinato [Cavinato et al., 2017] et les tests effectués sur les aortes porcines par l'auteur. Les résultats de l'étude réalisée par Witold Krasny ont été utilisés dans le développement et l'évaluation d'un modèle mécanique à micro-échelle pour comprendre le comportement élastique du tissu artériel, dont les résultats sont présentés au chapitre 4. De même, les résultats de l'étude réalisée par Cristina Cavinato et ceux de l'étude réalisée par l'auteur ont servi à évaluer le modèle microscopique développé pour prédire la défaillance du tissu.

2.2 Abstract of the chapter

As we have seen in the first chapter of the thesis, arteries exhibit complex mechanical behaviour in the passive state, which depends strongly on the content and organization of micro-structural components such as collagen and elastin. It is therefore important to understand the relationship between micro-structural parameters and the mechanical response of tissues at the macroscopic scale. Although there is a good understanding of the impacts of collagen on the mechanical response of tissues, data describing changes in the micro-structural organization of collagen under loading are rare due to the lack of a simple and reliable method to quantify this structure during mechanical tests. This chapter provides an overview of the experimental studies carried out and followed in this thesis. In particular, experimental methods combining mechanical loading and multi-photon microscopy imaging are presented. More specifically, we studied morphological changes in the

micro-structure of the carotid arteries of rabbits and porcine and human aorta (aneurysms). The analysis allowed us to understand and strengthen structure-function relationships, in particular the reorientation and uncrimping of fibres. The micro-structural imaging and mechanical testing performed on rabbit carotid arteries were performed by Witold Krasny [Krasny et al., 2017a], human aneurysmal aortas were tested by Cristina Cavinato [Cavinato et al., 2017], and the testing done on porcine aortas were conducted by the author. The outcomes of the study performed by Witold Krasny were used in developing and evaluating a micro-scale mechanical model for understanding the elastic behavior of arterial tissue, the results of which are presented in chapter 4. Similarly, the outcomes of the study performed by Cristina Cavinato and the study performed by the author were used in evaluating the developed micro-scale model in predicting the tissue's failure.

2.3 Introduction

The advancement of measurement and computational techniques makes way for the discovery of new applications that increase the accuracy of characterizing tissue behavior. Even though arteries have been subject to mechanical testing for decades, new insights are still gained through new experimental protocols. One has to overcome many challenges in characterizing the mechanical behavior of soft bio-materials like arterial tissue. These include their highly non-linear stress-strain response, large deformations under loading, heterogeneity, and anisotropy. Thus one has to perform mechanical testing of arterial tissue using different geometries and testing protocols to accurately assess its mechanical behavior. In all cases of experimental testing, it is possible to conduct both destructive and non-destructive testing. In the case of non-destructive testing, the tissue is loaded in such a way that all the changes induced to the tissue are reversible. In contrast, destructive testing protocols deform the tissue irreversibly.

In this chapter, we present the state of the art methods in soft-tissue mechanics that combine micro-structural imaging with specific mechanical testing methods. Firstly, multi-photon microscopy combined with uniaxial testing of rabbit carotid arteries was overseen by Witold Krasny [Krasny et al., 2017a]. Secondly, multi-photon microscopy combined with bulge-inflation testing until rupture of human aneurysmal aortas was handled by Cristina Cavinato [Cavinato et al., 2017]. Finally, multi-photon microscopy combined with uniaxial testing of porcine aortas was conducted by the author.

2.4 Micro-structural imaging

Microscopic investigation of arterial tissues is a decisive tool that can yield valuable information and insight into the mechanisms behind the tissue's mechanical behavior. This is generally achieved in many ways: in the first case the tissue is allowed for microscopy after the desired mechanical testing has been done; in the second case the microscopy imaging is carried out during mechanical testing; whereas in the third case the tissue specimen is imaged before carrying out the desired mechanical testing.

Histological staining has been traditionally used for ages to image particular biological components such as collagen, elastin, and smooth muscle cells. Picro-sirius red staining and Masson's trichrome staining are commonly employed for imaging collagen fibers [Schrieffl et al., 2012a]. These protocols have been used to investigate the kinematics of collagen fibers in the tissue at different load levels. With the advent of more powerful optical imaging techniques such as multi-photon microscopy, microscopic investigations of collagen fiber architecture in arterial tissues could be achieved thanks to second harmonic generation (SHG) without any staining or fixation. Microscopy is useful in understanding the mechanisms of failure in arterial tissue by investigating micro-structure at the failure point.

In this section, a few different microscopy investigation methods that have been used for healthy and aneurysmal arterial tissues are presented.

2.4.1 Multi-photon microscopy applied to rabbit carotid arteries

The microscopy investigation presented here corresponds to the tissue samples tested mechanically in section 2.6.2. To image the elastin and collagen networks of the arterial tissue, a multi-photon microscope (Nikon, A1R MP Plus[®]) of IVTV platform (Engineering and Ageing of Living Tissues Platform ANR-10-EQPX-06-01) was used. As recommended in [Jayyosi et al., 2016] the band pass filters were set to 500 – 550 nm and 400 – 492 nm respectively for collecting auto-fluorescence (elastin) and collagen second harmonic generation signals without any staining or fixation. The excitation wavelength of the scanning laser was set to 870 nm [Hill et al., 2012a]. The acquired images were composed of 1024×1024 pixels, ensuring high-resolution, high-quality images. Similarly, an imaging resolution of $0.5 \mu\text{m}$ was used in all directions, which resulted in an imaging window of $512 \times 512 \mu\text{m}^2$. Depending on the quality of the signal at in-depth focal position, the resulting stacks ranged in 60 – 90 μm in the z-direction. A max-intensity projection of a representative image stack aligned in the diagonal direction is shown in figure 2.1. A scan speed of 0.25 frames per second combined with two frame averaging (meaning that each frame was scanned 2 times the average value was taken) resulted in total acquisition time of approximately 20 – 30 minutes per image stack. Each arterial tissue was imaged on the adventitial side. Each arterial sample was imaged in four different configurations: unloaded, at a uniaxial tensile load of 0.2 N load, at 0.5 N load, and at 0.8 N. Before imaging in each above configurations a period of 10 – 15 minutes was observed so as to stabilize the tissue after initial material creep. This choice was relied on previously conducted analyses, which showed that 10 minutes was sufficient to avoid any important creeping.

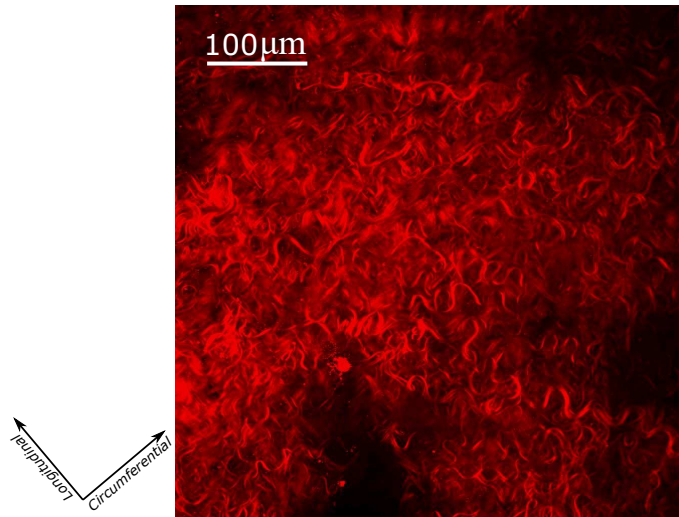


FIGURE 2.1 – Max intensity projection of confocal microscopy image stack of rabbit carotid artery (aligned in diagonal direction).

2.4.2 Multi-photon microscopy applied to human aneurysmal aortas

A different microscopy setup to the one presented in the previous section was used to obtain image stacks of human aneurysmal aortic tissues. This setup has been presented in [Cavinato et al., 2017] and is summarized here. The micro-structural imaging was carried out in conjunction with the bulge-inflation testing. The mechanical testing protocol of the corresponding tissues is presented in section 2.6.3. A LEICA SP2 microscope with a

Ti:sapphire femtosecond laser source and a water immersion objective was used for microstructural imaging. Setting the laser excitation wavelength to 830 nm allowed for collecting the two-photon fluorescence (TPF) and collagen second harmonic generation (SHG) signals through 560 – 700 nm and 375 – 425 nm band pass filters respectively as suggested by other studies[Boulesteix et al., 2006]. The acquired image stacks had an image resolution of 1024×1024 pixels, a 12 bit-dynamic range and a z-step of $1 \mu\text{m}$, with two-frame averaging at each z-step. The imaging window was set to $750 \times 750 \mu\text{m}^2$, with varying scan depths of 100 – 500 μm , which depended on the permeability of the sample to the pulsed laser beam. Each sample was imaged at three different pressure levels: zero pressure, corresponding to the reference configuration; 250 mm-Hg, inducing a wall stress close to diastolic-systolic loading conditions (equivalent to average in-vivo pressure of 120 mm-Hg [Länne et al., 1992]); a third pressure level of 450 mm-Hg corresponding to over-pressurization beyond the physiological range. The collagen fiber architecture in a human aneurysmal tissue at zero pressure and 450 mm-Hg is presented in figure 2.2.

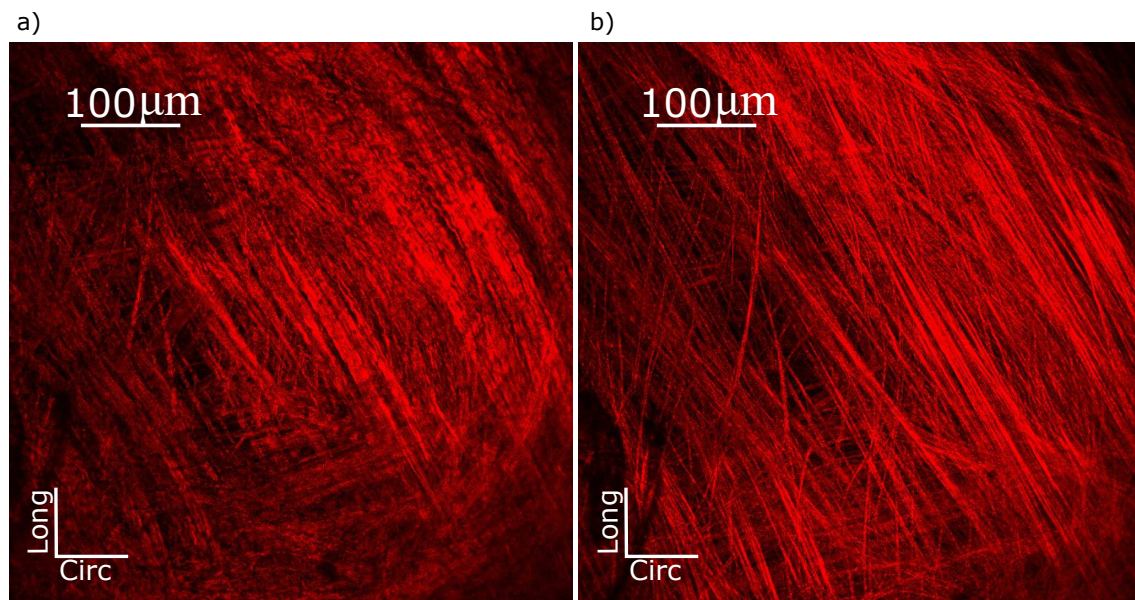


FIGURE 2.2 – Microscopic architecture of collagen fibers in human aneurysmal tissue at a) zero pressure and b) 250 mm-Hg.

2.4.3 Multi-photon microscopy applied to porcine aortas

The following microscopy protocol described here is applied to porcine aortic tissues, before they were subjected to uniaxial mechanical testing until rupture.

Second harmonic generation (SHG) microscopy of collagen fibers was performed with a confocal microscope consisting of a Biorad (MRC 1024) scan head and an Olympus BX50WI upright microscope stand. An 810-nm excitation beam from a mode-locked femtosecond laser delivering up to 3W of power (COHERENT, CHAMALEON VISION II) was focused into the sample using a 20x water-immersion objective of $\text{NA}=1$ (XLUMPLFLN20XW, Olympus). The incident laser intensity was varied by using a rotating half-wave plate and a polarizer in front of the microscope so that the average power delivered at the surface ranged from 10 to 100 mW. The SHG signal was collected in transmission through a 710 nm short-pass filter (Omega-filters Corp) and a 405-nm interference filter by a photo-multiplier

tube. The laser beam scanned the axial-circumferential plane to acquire images of resolution 512×512 pixels with an acquisition time of 0.9 seconds per image. This resulted in an imaging window of $498 \times 498 \mu\text{m}^2$ in the plane. The z-scan (variation of the observation depth) was realized by translation of the motorized objective. An imaging resolution of $1\mu\text{m}$ was set in the z-direction resulting in scans of depths ranging between $60 - 130 \mu\text{m}$.

Each arterial tissue sample underwent four separate scans taken along the length of

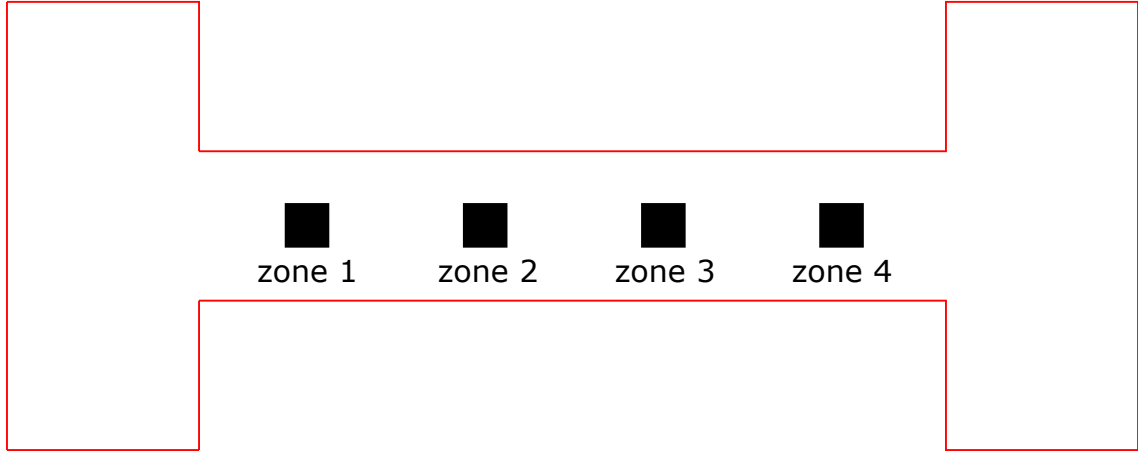


FIGURE 2.3 – Schema of imaging zones at which microscopic image stacks were obtained for porcine aortic samples.

the sample without any overlap regions as shown in figure 2.3. The sample was made sure to remain submerged under water throughout the test. The rationale behind acquiring multiple image stacks of one sample was to obtain a more representative profile of micro-structure organization in the tissue. Figures 2.4 and 2.5 present the architecture of collagen fiber network in the adventitia in circumferential and longitudinal samples respectively. This goes to show that collagen architecture is highly unorganized and changes from point to point in the tissue. Such detailed information enables us to establish a better correlation between tissue's structure and its mechanical response.

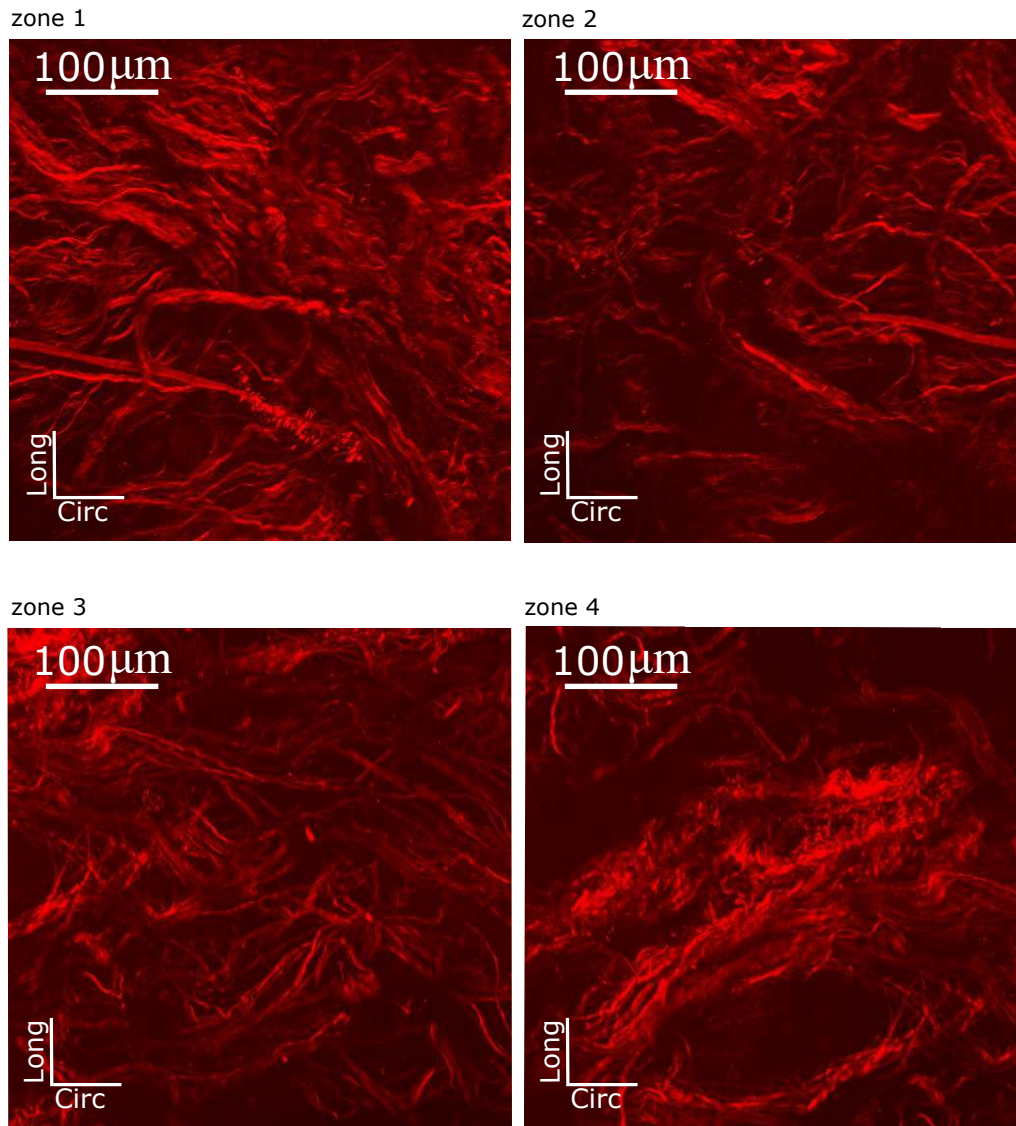


FIGURE 2.4 – Max intensity projection of image stacks acquired at different zones of a porcine sample (aligned circumferentially).

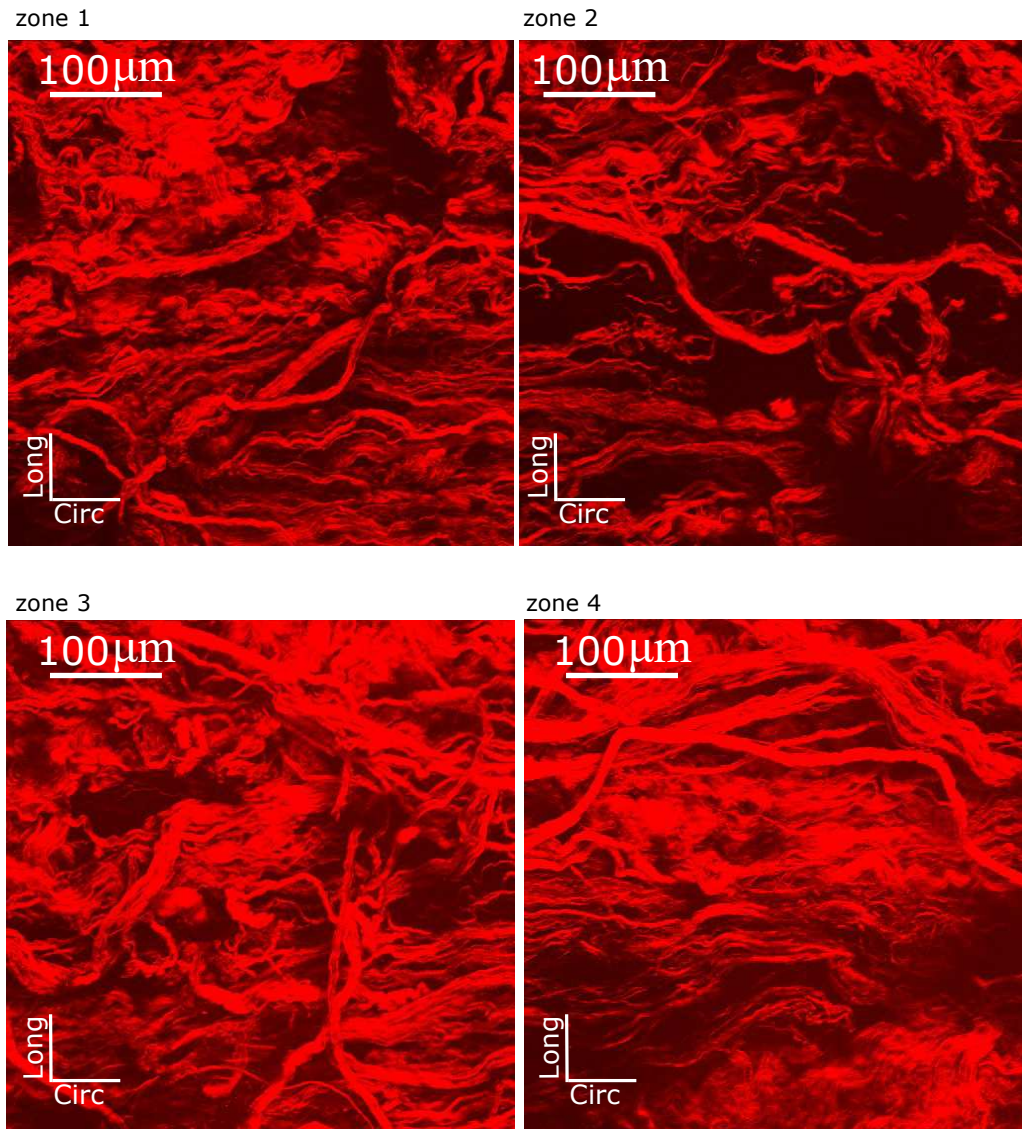


FIGURE 2.5 – Max intensity projection of image stacks acquired at different zones of a porcine sample (aligned longitudinally).

2.4.4 Optical light microscopy of porcine aorta

In this section an easy and straight forward procedure is presented for investigating collagen architecture in arterial tissues for descriptive and statistical purposes.

Healthy porcine aortas were procured from a local butchery within 24 hours of death. The

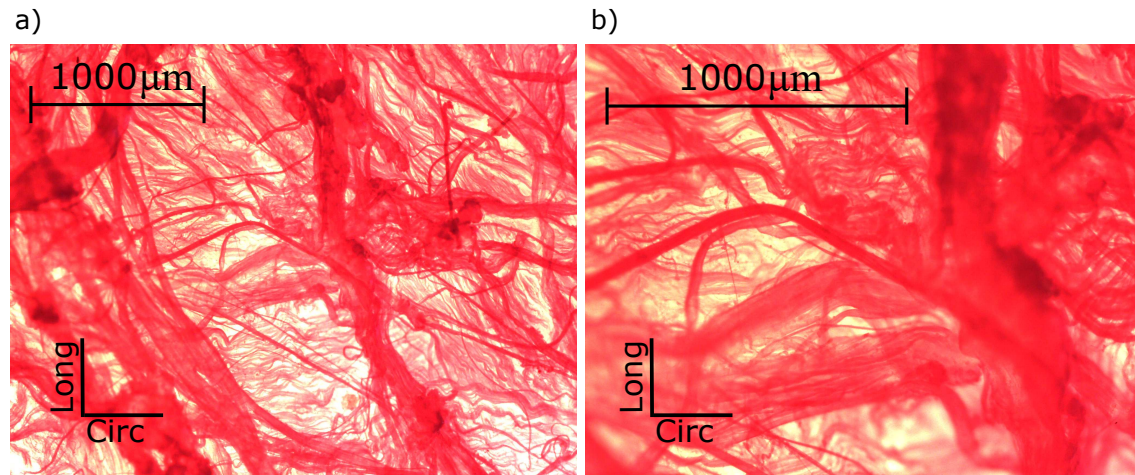


FIGURE 2.6 – Adventitial collagen fiber architecture imaged under Optical light microscope at magnifications: a) 4 \times , b) 10 \times .

aortas were cleaned with ionized water and the connective tissue was carefully removed. Cylindrical portions of the descending zone were cut and stored at -20°C until the day of the experiment.

For optical light microscopy, a fluorescence compatible LEICA DM750 P educational microscope equipped with standard LED illumination was used. The cylindrical samples were unfrozen in ionized water for 15 – 30 mins and cut open longitudinally. The medial layer of the aorta was carefully peeled off resulting in rectangular strips of the adventitia. The prepared samples were stained in picro-sirius red solution for one hour and washed in ionized water. At this point, the prepared samples were placed in-between two glass slides in-order to protect the sample and the objective lens and mounted on to the stage. Images of collagen architecture as shown in figure 2.6 were procured at two different magnifications: 4 \times and 10 \times giving insights into multi-scale (fiber bundles and fibers) organization of collagen fibers in the adventitia.

2.5 Thickness measurement protocol

The thickness measurement device presented in [Cavinato et al., 2019] consisted of two high spatial resolution line laser sensors (optoNCDT 1700BL, Micro-Epsilon Messtechnik GmbH & Co. KG, Germany) facing each other in a horizontal line and a central body midway between the sensors (figure 2.7 a). The central body consisted of a linear translation stage (MFA-PPD, Newport, CA, USA) capable of moving the specimen in the vertical direction. Two PVC supports were used to hold the specimen in between them, which were then attached to the movable translation stage.

Two laser beams in the region of blue light ($\lambda = 405\text{nm}$) were chosen such that soft tissues reflected these wavelengths without significant light absorption and blur, as demon-

strated for skin [Boyer et al., 2013]. These incident laser beams were used to scan the surface of the tissue on either side. The scanner exposure time was 1 ms and the total measurement field was 1280×768 pixels. A program developed in LabVIEW (National Instruments, Austin, USA) was used to record the measured position profiles of both exposed surfaces of the specimen with a vertical step of $50 \mu\text{m}$ and a lateral resolution of $20 \mu\text{m}$. Measurements on each aneurysmal specimen were made two consecutive times over a period of about 3 minutes, and the measurement on porcine aortas (adventitial strips) was made once with a total scan time of about 2 minutes. A custom Matlab[®] program (as schematized in figure 2.7 b) was used to determine the thickness of the tissue. This was done by first mapping the two surfaces on to each other, which allowed for defining a vector normal \vec{n} to the mean surface. Finally, the thickness was computed as the distance between the two surfaces along this normal. Thickness profile of a representative human aneurysmal tissue and a porcine aorta (only the adventitia) are presented in figure 2.7 c and 2.7 d respectively.

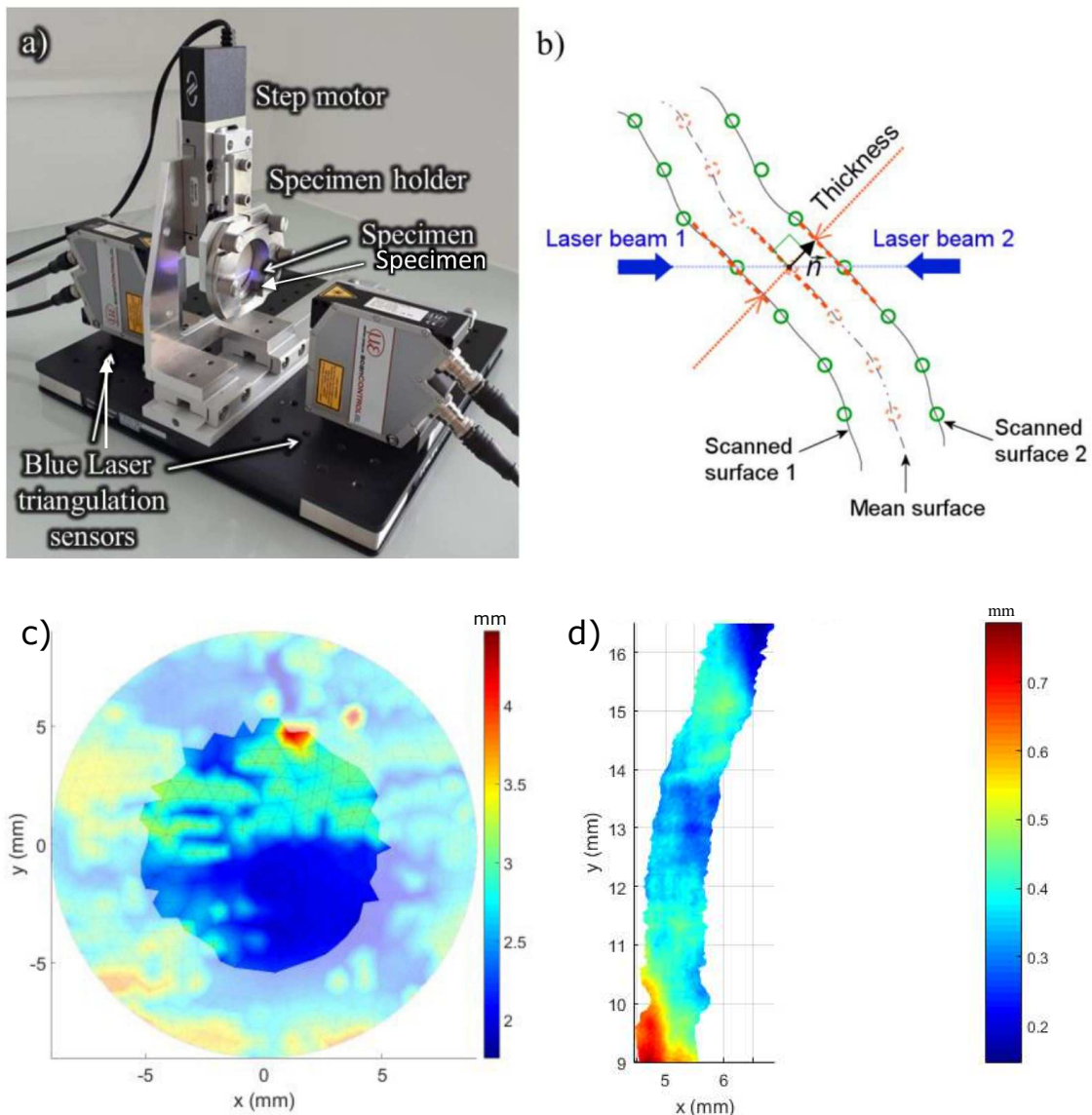


FIGURE 2.7 – a) Thickness measurement device, b) schema of the thickness measurement protocol, c) measured thickness profile of a human aneurysmal tissue [Cavinato et al., 2019], and d) measured thickness profile of the adventitial layer of a porcine tissue.

2.6 Mechanical testing of arterial tissues

This section presents the mechanical testing of arterial tissue under three different protocols: non-destructive testing of rabbit carotid artery in uniaxial tension; destructive testing of human aneurysmal aorta in bulge-inflation; and destructive testing of porcine aorta in uniaxial tension. While the data from bulge-inflation tests increase the ability to model the behavior of vessels under supra-physiological loading conditions [Balzani et al., 2012], the tensile strength data from uniaxial tests can be incorporated to model arterial damage and increase the accuracy of rupture risk prediction models [Pierce et al., 2015, Weisbecker et al., 2012, Geest et al., 2006].

2.6.1 General considerations

- *Storage: In order to minimize the effects of autolysis on aortic tissue in the time between harvesting and testing, the tests should be carried out as soon as possible. But, since immediate testing is not always feasible, various methods of storing the sample have been used and care must be taken in selecting an appropriate method for storage.*

In this context, many studies have investigated the effects of refrigeration on arterial tissue. The effects of long term refrigeration on the mechanical properties of thoracic aorta was investigated by Adham et al [Adham et al., 1996], who concluded that there were no significant changes in tissue stiffness. Contrarily, other studies have shown that refrigeration times of 24 – 48 hours showed a significant decline in tissue’s ultimate stress and stiffness [Stemper et al., 2007a]. In the same study, Stemper et al also showed that freezing the tissue up to 3 months exhibited no significant difference in mechanical behavior as compared to fresh tissue. A similar finding was reported by Ebenstein et al [Ebenstein et al., 2009] where they found no significant difference in the mechanical behavior of fresh and frozen atherosclerotic plaque tissues when subjected to nano-indentation. More recently, O’Leary et al [O’Leary et al., 2014] demonstrated that porcine aortic tissue samples display no significant change in mechanical behavior even after an year of freezing.

Similarly, no consensus has been established on the micro-structural changes occurring in arterial tissues because of freezing [Stemper et al., 2007a, Adham et al., 1996]. In particular, the study conducted by Ramji et al [Venkatasubramanian et al., 2006a] pointed effects of freezing and cryopreservation on the mechanical properties of arteries but it is important to note that no proper conclusion had been drawn. On the other hand, Chow et al [Chow and Zhang, 2011a] investigated the biomechanical changes in aortic tissues induced from freezing. Their results showed contradictory results to the study of Ramji et al regarding the slope of stress-strain curves beyond the toe region. Also contrary was the observation made on recruitment strain of collagen, which was found to increase after freezing the sample. In addition, though these report possible micro-structural changes in the tissue due to freezing, the conclusions were based on observed changes in mechanics rather than microscopic imaging observations.

Thus it is recommended that samples be tested within 24 hours of removal to avoid any mechanical degradation. If samples are unable to be tested within 24 hours of excision, they can be frozen and tested within a year with no significant effect on their mechanical properties.

- *Tissue environment: When testing biological tissues in-vitro, effects characteristic to in-vivo state are usually neglected. But, to replicate the in-vivo environment as proximately as possible, the tissue should be maintained in a bath of physiological solution such as a phosphate saline buffer or Krebs-Ringer solution and tested at a temperature of 37° C [García-Herrera et al., 2012, Iliopoulos et al., 2009, Pham et al., 2013]. Fung reported that allowing the tissue to dry resulted in an increase in tissue stiffness [Fung, 1967], thereby indicating that the tissue should be kept moist. Also, as it has been shown that arterial tissue response varies with temperature [Guinea et al., 2005, Humphrey, 2003], it is preferable to test the samples at physiological temperature.*
- *Preconditioning: In order to characterize the mechanical response of arterial samples, it is important to account for the existence of a transient mechanical response: after a long term resting of the tissue (absence of externally applied load), its mechanical response exhibits an important but transient hysteresis which is reduced after several load cycles. This is usually got rid of by performing several preconditioning cycles. Preconditioning is conducted by subjecting the sample to a series of loading-unloading cycles, over which the sample demonstrates a change in stress-strain response. After a series of cycles, the stress-stretch response becomes repeatable. Although this is a necessary step before mechanically testing vascular tissue [Humphrey and Epstein, 2002], there is no common consensus on the maximum stretch or number of cycles for preconditioning. The preconditioning protocol should be as similar to the testing protocol as possible in terms of maximum strain level and rate so as to not influence the test data with inconsistent loading patterns. Similarly during biaxial preconditioning, the ratio between axial stretches should be kept consistent with intended test ratios. Where a maximum strain level is not feasible, such as when testing the tissue until failure, the maximum preconditioning strain level should mimic physiological conditions, at the same strain rate intended for testing. A wide range in the number of pre-conditioning cycles have been reported in the literature, but to ensure repeatability, 5 – 10 cycles should be conducted on the sample prior to testing, as this is sufficient to generate repeatable data [Choudhury et al., 2009, Okamoto et al., 2002].*

2.6.2 Uniaxial tensile testing of rabbit carotid arteries

The experiments outlined in this section were performed by another PhD student of the group and were used for validating the numerical models. More information on this regard can be found at [Krasny et al., 2017a].

2.6.2.1 Sample preparation

Carotid arteries ($n = 7$) excised from healthy male New Zealand white rabbits were used in this study. Immediately after the excision, the arteries were frozen at -20° C until the day of the experiment. On the day of experimental testing, the arteries were unfrozen in a bath of phosphate-buffered saline ($10\times$ PBS, pH 7.1), at an ambient temperature of 24° C. Cylindrical portions of length $10mm$ were excised from the arteries, which were cut open longitudinally resulting in rectangular samples of width $\approx 5mm$. Dog-bone shaped samples [Hill et al., 2012a] aligned in three different directions (circumferential, longitudinal, diagonal) were excised from the rectangular strips. These prepared samples were dedicated to mechanical testing coupled with multi-photon microscopy.

2.6.2.2 Preconditioning

In order to limit the hysteresis in the stress-strain response of the arterial tissue, each mechanically tested sample underwent 10 cycles of triangular quasi-static preconditioning.

2.6.2.3 Testing protocol

A screw-driven high precision tensile machine (Deben[®] Micro-test tensile/compression stage) was used for uniaxial tensile tests (figure 2.8 d). The load cell capacity was 150 N with the signal providing a 0.01 N precision and satisfactory stability. The sample was stretched by moving the two heads of the tensile device in opposite directions. The displacement and force response were recorded at each step. Prior to the test, sample clamping was achieved with utmost care so as to not induce any pre-strain or pre-stress. A displacement control loading was applied at a rate of $0.5 \text{ mm} \cdot \text{min}^{-1}$ (as suggested by Hill et al [Hill et al., 2012a]) until a fixed target tensile force equal to 1 N was achieved. It was ensured that the sample remained immersed in PBS at a constant ambient temperature of 24°C through out the test. The computation of reference cross-sectional area A_0 (at zero load, after preconditioning) was achieved through the measurement of width and thickness of each sample with a digital caliper. From this the first Piola-Kirchhoff (engineering) stress $\sigma_{pk} = \frac{F}{A_0}$, where F is the measured tensile force. The stretch was computed from the actual and reference inter-clamp length of the strip (respectively l and l_0) as: $\lambda = \frac{l}{l_0}$. The reference length of the strip was defined as the inter-clamp length of the strip after preconditioning. The whole schema of the experimental protocol is presented in figure 2.8.

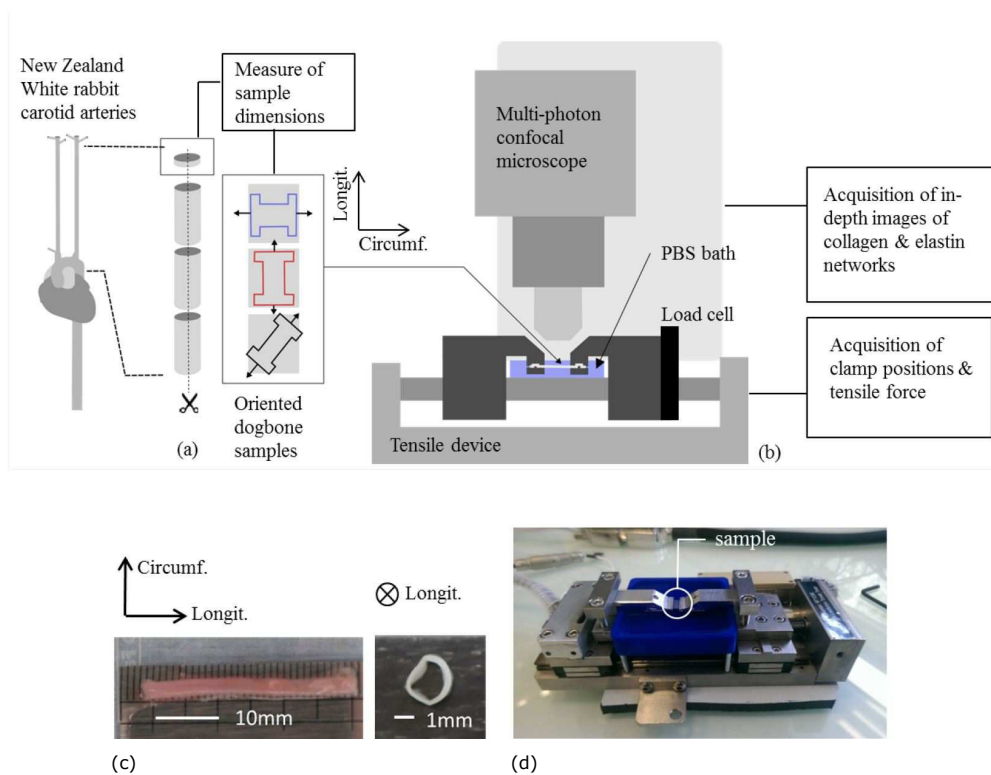


FIGURE 2.8 – The uniaxial tension set up used for testing rabbit carotid arteries[Krasny et al., 2017a].

2.6.3 Bulge-inflation testing of human aneurysmal aortas

The experiments outlined in this section were performed by another PhD student of the group and were used for validating the numerical models. More information on this regard can be found at [Cavinato et al., 2017].

2.6.3.1 Sample preparation

Unruptured human ascending thoracic aortic aneurysms (ATAA) (patients = 19, specimens = 20) were collected from patients undergoing elective surgery to replace the segment with a graft. Within 12 hours of procuring the tissue samples, they were cleaned and the surrounding connective tissue was removed carefully. Prior to dissection the external diameter of the aortas were measured on the CT scan. The aortas were cut open along the longitudinal direction resulting in near rectangular planar strips. Square samples of length 45 mm were excised with edges aligned towards circumferential and longitudinal directions. The collections and the experiments on the specimens were done in accordance with a protocol approved by the Institutional Review Board of the University Hospital Center of Saint Etienne. The thickness profile of the samples were computed as described in section 2.5. Once the samples were prepared, they were placed in PBS and refrigerated at 4°C for a maximum time period of 12 hours.

2.6.3.2 Preconditioning

A preconditioning program was first performed through five loading-unloading cycles up to 50 mm Hg at the same inflation rate.

2.6.3.3 Testing protocol

Two 30-mm-inner-diameter PVC supports were used to clamp the sample. Once the thickness measurement was done the sample was mounted on to the inflation device as depicted in figure 2.9. An automatic water pumping system (WPI[®], NE-501 Multi-Phaser) was used to perform the inflation of the samples, and a custom program was developed in Lab-VIEW to control the injected volume at a constant rate. A transducer (Omega[®]) was used to simultaneously note down the pressure values. Samples were mounted with the adventitial surface pointing outwards (AOUT). The water pumping system was used to pressurize the hermetic cavity formed between the specimen and the inflation system at a rate of 10 ml/min uninterrupted, until the tissue ruptured. Pressure levels of 250 mm-Hg and 450 mm-Hg were chosen to capture image stacks of micro-structure as described in 2.4.2. These specific values were chosen for the purposes of evaluating a wall stress state close to diastolic-systolic conditions (120 mm-Hg) and a second state beyond the physiological range.

2.6.4 Uniaxial tensile testing of porcine aortas

The experiments outlined in this section were performed by the author of the thesis.

2.6.4.1 Sample preparation

Healthy porcine aortas in whole were procured from a local butchery within 24 hours of death. Once in the lab, the aortas were cleansed with ionized water and the surrounding connective tissue was carefully removed. Cylindrical segments of lengths 5 cms were excised

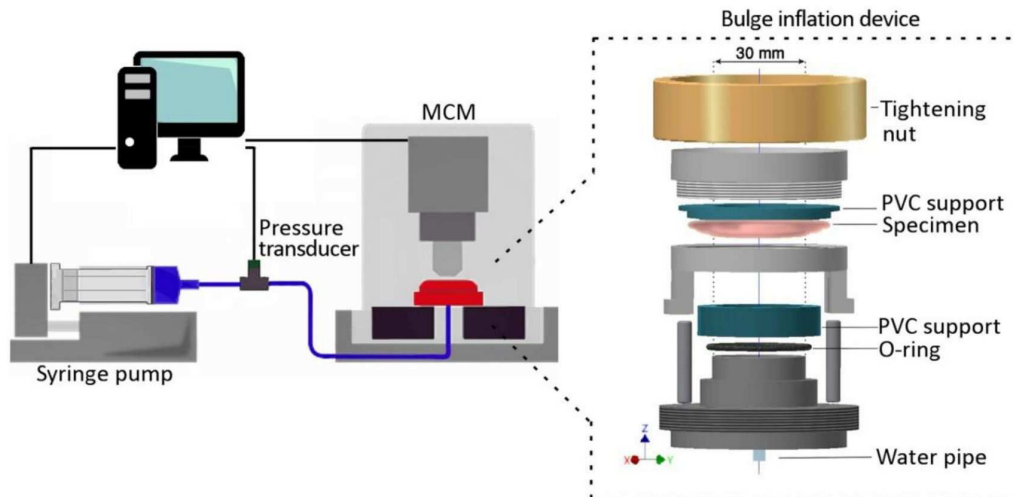


FIGURE 2.9 – Schema of the bulge inflation set up used for testing human aneurysmal tissue samples[Cavinato et al., 2017].

around the descending portion of the aorta and cut open longitudinally. This resulted in rectangular samples of length 5 cms and width 3 – 4 cms (figure 2.10 c). The medial layer of the aorta was carefully peeled off from each excised sample resulting in adventitial strips. These resulting adventitial strips were frozen at -20° C until the day of the experimental testing.

On the day of the experiment the frozen adventitial samples excised from healthy porcine aortas were unfrozen in ionized water. Dog-bone shaped specimens were cut in both circumferential and longitudinal alignments for mechanical testing. The thickness profile of each specimen was measured as per the protocol described in section 2.5.

2.6.4.2 Preconditioning

Each tested sample followed a preconditioning protocol, where 5 cycles of a triangular load profile of up to 30% strain and unloading was applied.

2.6.4.3 Testing protocol

The mechanical testing was conducted using a screw driven high precision tensile machine (Newport[®], tension-compression stage) with a load cell capacity of 22 N. The load cell was integrated to an IPM650 panel mount for digital display of load cell readings. Each sample was carefully mounted on to the testing machine and clamped at the ends with the help of sandpaper so as to prevent slipping. It was also ensured that the sample was submerged under water for the entirety of the test. Ensuring a zero-strain state in the initial configuration before preconditioning was achieved by maximally constraining and controlling sample and clamp positions, upon fixation (figure 2.10 d). The zero-stress initial configuration was achieved by resetting to 0 the load cell offset before mounting each sample, and by verifying the unchanged force readout after mounting the sample. This verification gave an a posteriori check that the fixation did not induce any pre-stress of the sample larger than the force threshold being detected by the sensor (i.e. 0.02 N, which corresponds to 30 kPa according to our sample’s mean cross-sectional area). A dis-

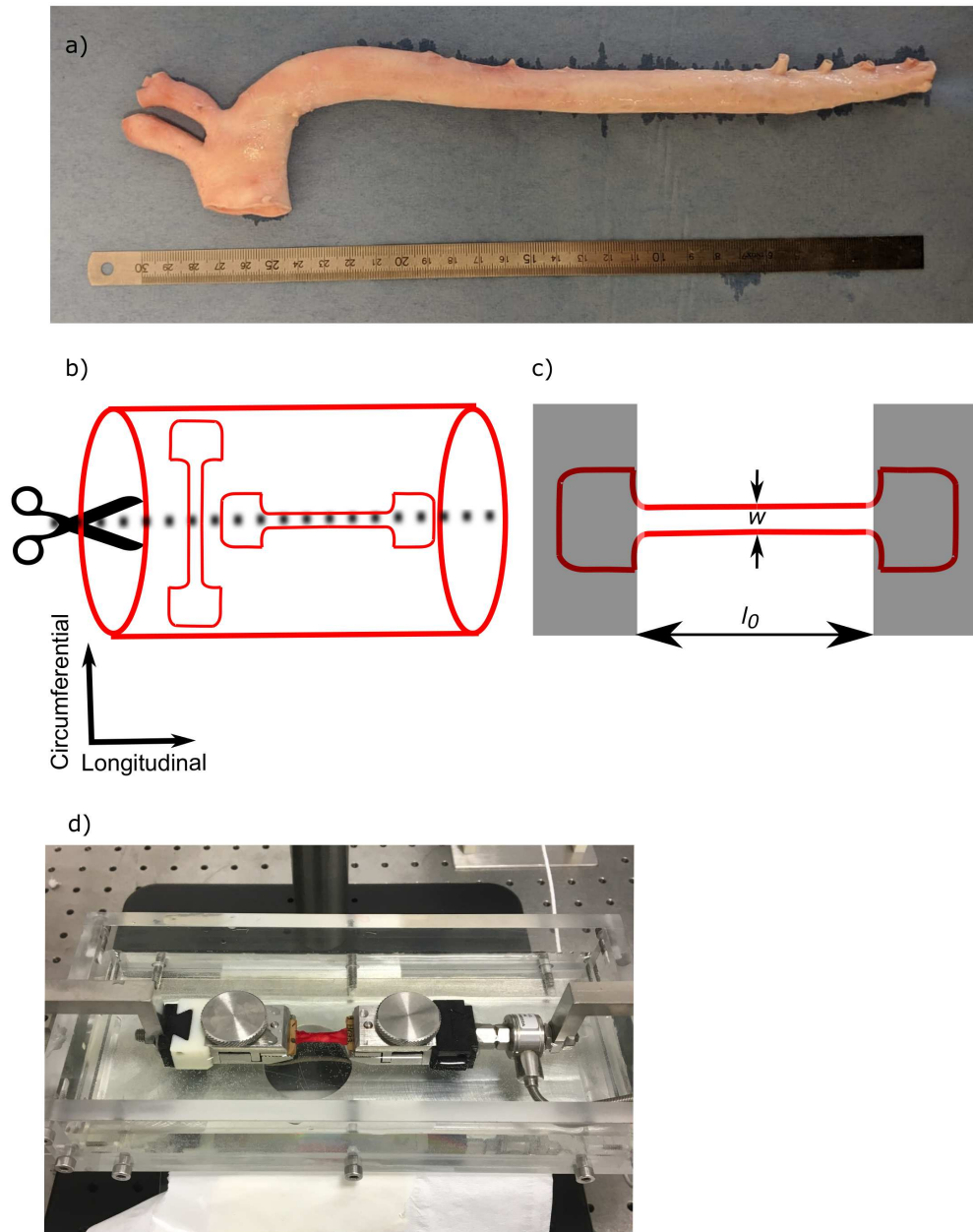


FIGURE 2.10 – a) Whole porcine aorta used for mechanical testing, b) schema of prepared dog-bone samples, c) sample after preconditioning with the length of the sample taken as the inter-clamp length, d) uniaxial tension set up used for testing porcine aortic tissue samples

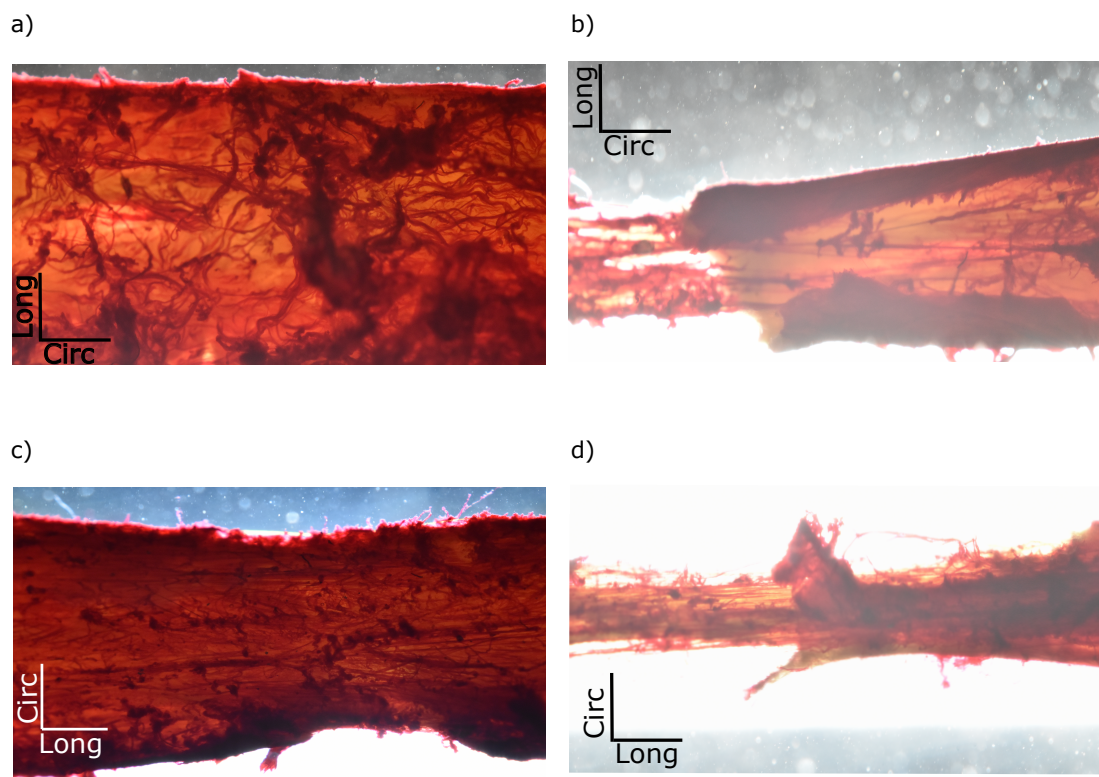


FIGURE 2.11 – a) Circumferential sample at load-free state, b) Circumferential sample at close to failure under uniaxial tension, c) Longitudinal sample at load-free state, d) Longitudinal sample at close to failure under uniaxial tension

placement control loading was applied to each sample at a rate of 2 mm.min^{-1} until failure.

The above mentioned zero stress and zero strain conditions are related to the initial configuration before preconditioning. It was decided not to account for any residual strain from preconditioning when plotting the stress-strain curves of the samples. After preconditioning, three measurements of the sample length and width in the unloaded configuration were recorded using a caliper and averaged. This measured sample width in conjunction with the mapped thickness profile of the sample allowed for the computation of the reference cross-sectional area A_0 (at zero load, after preconditioning). From this, the first Piola-Kirchoff stress was computed as: $\sigma_{pk} = \frac{F}{A_0}$, where F is the measured tensile force. The knowledge of initial inter-clamp length allowed for the computation of stretch as: $\lambda = \frac{l}{l_0}$, where l and l_0 are current and initial inter-clamp lengths respectively.

A Nikon 5600 digital camera was used to image the sample through out the test at each intermediate loading state. The set-up was aimed at imaging the fibers and capture their reorientation with progressive tensile load. To achieve this the samples were stained with Picrosirius red for 30 mins prior to mechanical testing. The recorded images for a circumferential and a longitudinal sample at their initial configuration and close to failure is presented in figure 2.11.

2.7 Conclusion of the chapter

In this chapter we presented the entire workflow of the experimental techniques used to study the mechanical behavior of arteries and assess its relationship to the micro-structural organization of collagen. The experimental results of rabbit carotid samples [Krasny et al., 2017a] and human aneurysmal samples [Cavinato et al., 2017, Cavinato et al., 2019] have been previously published. These results showed that the organization of organization of collagen in arterial walls is random, showing significant difference between species, tissue type, and the location investigated in the tissue. The mechanical testing results reinforced the highly anisotropic and non-linear response of arteries. Furthermore, combining micro-structural imaging with mechanical testing showed that the underlying fiber kinematics follow non-affine transformation. Porcine tensile testing experiments were performed specifically for the purpose of the present PhD work. Specific experimental data, including details of samples and specific results, will be presented in relevant sections. All this information, combined with knowledge of micro-structure organization, led to the development and analysis of fiber level numerical models including damage mechanisms. These models were used to understand, describe and quantify the tissue's mechanical response and failure in relationship with its structure, as presented in chapters 4 and 5.

The one thing that doesn't abide by majority rule is a person's conscience.

Harper Lee

Chapter 3

Numerical methods

Contents of the chapter

3.1	Résumé du chapitre	60
3.2	Abstract of the chapter	61
3.3	Segmentation of collagen fiber network from SHG images	62
3.3.1	Introduction	62
3.3.2	Methods	64
3.3.2.1	Method I: CT-Fire	64
3.3.2.2	Method II: Sequential tracing algorithm	65
3.3.2.3	Minimal path based approach: ScanIp	67
3.3.3	Results	67
3.3.4	Discussion	67
3.3.5	Conclusion	72
3.4	Extraction of morphological parameters of collagen fiber network from SHG images	73
3.4.1	Orientation	73
3.4.1.1	CT-Fire	73
3.4.1.2	OrientationJ.	73
3.4.1.3	Fast Fourier Transform based methods	73
3.4.1.4	Comparison	74
3.4.2	Waviness	74
3.4.3	Volume fraction	74
3.5	Numerical network reconstruction	74
3.5.1	Stochastic modeling	74
3.5.1.1	Orientation	77
3.5.1.2	Waviness	77

3.5.2	Inverse random sampling	77
3.5.2.1	Mixed Von-Mises distribution	77
3.5.2.2	Beta distribution	78
3.5.3	Random walk algorithm	78
3.5.3.1	Assumptions	79
3.5.3.2	Algorithm	80
3.6	Finite element model	80
3.6.1	Material models	80
3.6.2	Boundary conditions	81
3.6.3	Parameter identification	82
3.7	Conclusion of the chapter	84

3.1 Résumé du chapitre

Les composants extracellulaires du tissu artériel sont assemblés en une structure hiérarchique complexe propre au type, à l'emplacement et à l'espèce du tissu. La mécanique de ces tissus est régie par des mécanismes se produisant à l'échelle de ces unités structurales (microstructure). Plus précisément, les forces appliquées à l'échelle du tissu sont transférées à la microstructure et à la matrice extracellulaire, dont l'organisation et le contenu définissent la réponse du tissu. Dans ce chapitre, nous présentons les outils numériques utilisés dans ce travail pour évaluer la morphologie des fibres de collagène à partir de piles d'images SHG de la couche externe de la paroi artérielle, l'adventitia. D'après les illustrations présentées au chapitre 2, il est évident que les fibres de collagène sont soumises à une distribution d'orientation et sont ondulées dans leur configuration sans charge, deux critères importants qui donnent lieu à une réponse mécanique non linéaire à l'échelle du tissu. Dans la première partie du chapitre, nous évaluons quelques outils numériques existants et proposons une nouvelle technique pour segmenter les fibres de collagène des piles d'images SHG. Les résultats de cette segmentation étant peu satisfaisants, nous avons choisi de procéder à l'extraction de paramètres morphologiques des piles d'images pour une reconstruction fiable du réseau. Enfin, nous présentons l'approche numérique micro-macro développée pour utiliser ces réseaux reconstruits dans des simulations de chargement mécanique jusqu'à rupture

3.2 Abstract of the chapter

The extracellular components of the arterial tissue are assembled into a complex hierarchical structure specific to tissue type, location, and species. Mechanics of such tissues are governed by mechanisms occurring at the scale of these structural units (micro-scale). More precisely, the forces applied at the tissue scale are transferred to the micro-structure and extracellular matrix, whose organization and content define the response of the tissue. In this chapter we present the numerical tools utilized in this work in assessing the morphology of the collagen fibers from SHG image stacks acquired from the outermost layer of the arterial wall, the adventitia. From the illustrations presented in chapter 2, it is evident that collagen fibers are randomly oriented to some degree and undulated in their load free configuration, two important criteria that give rise to a non-linear mechanical response at the tissue scale. In the first part of the chapter, we evaluate some existing numerical tools and propose one for segmenting collagen fibers from SHG image stacks. Based on the objectionable results obtained in this section, we shift our focus to extracting morphological parameters from the image stacks for a reliable reconstruction of the network. And finally, the method for utilizing the reconstructed network for numerical analysis is presented.

3.3 Segmentation of collagen fiber network from SHG images

3.3.1 Introduction

Arteries are prominent organs in the human body that require reliable mechanical models for a better understanding of several cardiovascular diseases such as atherosclerosis, balloon angiopathy, and aneurysms. Medical treatment could be improved using numerical simulations based on realistic and efficient mechanobiological models. In this regard, structure based models that are either statistical [Engelmayr and Sacks, 2006, Courtney et al., 2006], or deterministic [Chandran and Barocas, 2006, Wang et al., 2000] need as input a detailed description of concentration and morphological arrangement of collagen fibers (being a primary component of the extracellular matrix) in the arterial tissue. Random fiber networks such as the ones that occur naturally in arteries have been extensively investigated in the last decades [Wilhelm and Frey, 2003, Heussinger et al., 2007, Head et al., 2003]. The conclusion was that the micro-structure influences the mechanics of the network. The length scale and diameter of the collagen fibers vary from tissue to tissue and have an influence alongside their organization [Wu et al., 2003]. Guido et al [Guido and Tranquillo, 1993] demonstrated that cell migration could be explained by collagen fiber reorganization, possibly providing an explanation for tissue-repair mechanisms. Because of this, we and other researchers are interested in quantifying the morphology of collagen fibers in the arterial tissue through automatic and semi-automatic segmentation and skeletonization of collagen fibers from second harmonic generation (SHG) image stacks.

Microscopic observation of collagen fibers has always been a great challenge. Virchow et al pioneered the work by determining the orientation of collagen fibers in the cornea using light microscopy [Virchow, 1910]. Polarized light microscopy could be used in characterizing collagen fibers [Sweat et al., 1964] and was applied to obtain quantitative information of collagen in cornea, sclera [Newton et al., 1995], and other tissues [Dickey et al., 1998]. However, it fails in providing a 3-D profile of the tissue. Much of this work is based on multi-photon microscopy (MPM), in particular second harmonic generation imaging to capture high-resolution, high-contrast images of collagen in the tissue (described in chapter 2). SHG imaging has been extensively used for investigating collagen fiber architecture soft-tissues [Brown et al., 2003, Williams et al., 2005, Zoumi et al., 2002]. SHG imaging enables greater penetration depths compared to the above mentioned imaging techniques of up to $300 \mu\text{m}$ with a highest resolution of 10 nm in plane and 800 nm in the z-direction [Smith et al., 1986] making it one of the leading techniques for visualizing collagen fibers in 3-D structures.

The complexity of collagen fiber organization in arterial tissue as seen in figure 3.1 makes segmentation of individual fibers very difficult. A number of segmentation algorithms have been presented in the context of fibrous networks which include: sequential tracing [Al-Kofahi et al., 2002], skeletonization [Cohen et al., 1994, He et al., 2003], minimal cost path [Meijering et al., 2003], and active contour [Vasilkoski and Stepanyants, 2009]. Sequential tracing methods require the user to define or identify a list of seed points. At each identified seed point in the image, the local hessian matrix is computed which is used in searching the next point along the tangential direction provided by the hessian. Instead, edge detectors could also be used to extract the information for guided traversal. One of the common pitfalls for sequential tracing is that it suffers from discontinuities thereby producing fragmented networks. Skeletonization refers to the process of trimming the

foreground regions in a binary image to the extent of ensuring connectivity of the original region while clearing most of the original foreground pixels. Introduced by Cohen et al [Cohen et al., 1994] for tracing neuronal anatomy, it was improved by He et al [He et al., 2003] by combining an automatic method with semi-automatic and manual tracing. The unordered set of skeleton points were used to generate a graph-theoretic representation of the neuronal anatomy. Skeletonization-based methods are however sensitive to the quality of segmentation and often require additional post-processing. Minimal path based tracing approaches define a cost or energy function based on the image features that needs to be optimized. For implementing a minimal approach, the image needs to be first binarized and skeletonized thereby creating a cluster of points. A graph can then be constructed using a geodesic metric function such as the one proposed by Peng et al [Peng et al., 2010]. Once a graph is constructed, the center-line can then be estimated by solving the shortest path problem [Dijkstra, 1959] on the graph. Fast marching algorithms constitute another

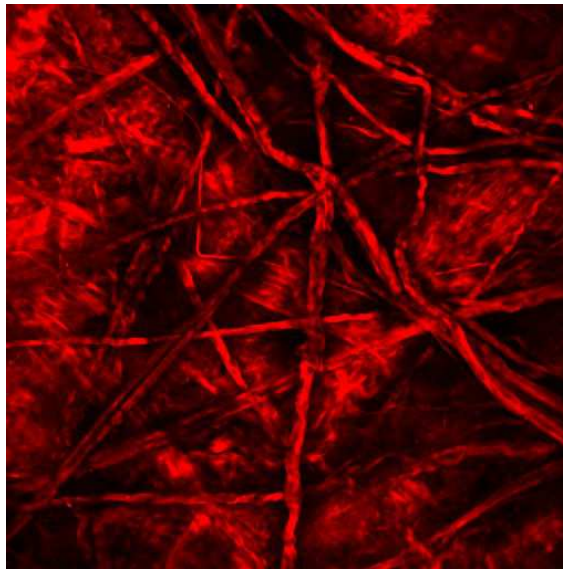


FIGURE 3.1 – Max-intensity projection of an SHG image stack of porcine aorta.

class of minimal path based techniques for tracking tubular structures in images [Cohen and Kimmel, 1997, Benmansour and Cohen, 2011]. Similar to Dijkstra’s method, it requires the user to specify two end points of a branch to be tracked. Using gradient descent the minimal path is tracked by sliding between the two points on the arrival time surface. A common limitation of this approach is that the tracked path might not represent the center-line of tubular structures.

Active contour algorithms characterize the tubular structures in an image with lines and edges. The solution for the center-line is obtained by minimizing an energy function (defined implicitly in shape and explicitly in the image). Active contour (snake) models are unable to segment blurred boundaries and are computationally expensive for processing large 3-d image stacks [Xiong et al., 2006].

Many of the algorithms listed here have been implemented in available software. For instance, NeuronJ [Meijering et al., 2003], a plugin in ImageJ, can accurately extract the center-lines of the line structures in the z-projected 2D image, requiring that users manually select the starting and ending points. Other similar software include Reconstruct, and Imaris. Reconstruct and Imaris are semi-automatic and rely on a lot of manual input from the user making them cumbersome to use on large 3-D SHG image stacks. A semi-automatic tracing was conducted on the reported image stack in figure 3.1, the result

is shown in figure 3.2. The result shows that while possible to track straight fibers, it gets complicated when there are fiber intersections and highly curvy fibers, limiting the usability of this software. Some of the recurring methods used for SHG collagen analysis

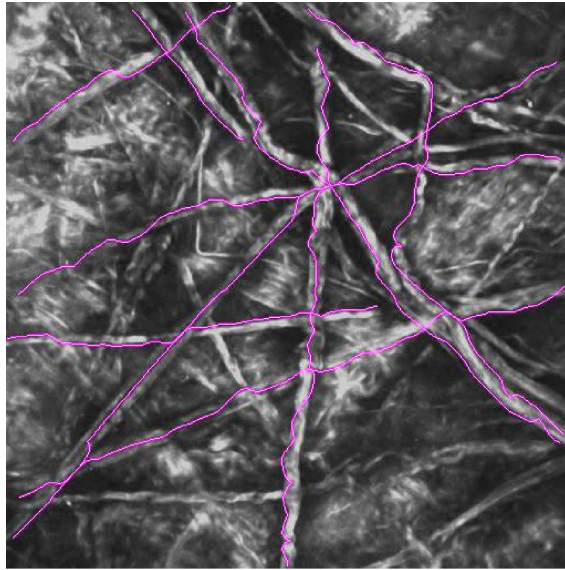


FIGURE 3.2 – Fibers traced semi-automatically with NeuronJ are superposed on the image stack. Pink lines represent the traced fibers, the grey patches in the image represent collagen.

include transform or filter based methods such as Fourier transform (FFT) [Falzon et al., 2008], Hough transform [Bayan et al., 2009], frangi algorithm [Koch et al., 2014] curvelet transform [Pehlke et al., 2014], and the gradient technique suggested by Altendorf et al [Altendorf et al., 2012]. These methods often fail in representing accurate information about fiber connectivity and intersections [D’Amore et al., 2010a]. Automated fiber tracking and extraction methods have been presented [Wu et al., 2003, Stein et al., 2008] enabling objectivity and speed of the analysis that are difficult to achieve through semi-automatic analyses. In this work we present a preliminary evaluation of a graph-theory based sequential tracing algorithm for SHG images of collagen in arterial tissue and compare it to a more established method like CT-FIRE.

3.3.2 Methods

This section covers the details of three fiber segmentation algorithms used in this study. The algorithms mentioned here were evaluated on four different image stacks: two synthetic stacks manually created by the author, and two SHG image stacks acquired on porcine arterial tissues.

3.3.2.1 Method I: CT-Fire

Curvelet filter: The curvelet transform (CT) is used for an optimal representation of directional objects with edges. It was originally developed by Starck et al [Starck et al., 2002] to overcome the limitation of highlighting lines and edges. The acquired SHG image stacks were pre-processed by treating with a denoising filter, based on the CT. The use of curvelet transform in quantifying collagen information in SHG images has been previously reported [Pehlke et al., 2014, Bredfeldt et al., 2014].

Fire algorithm: The FIRE algorithm used for extraction of individual collagen fibers is briefly described here. Interested readers are directed to [Stein et al., 2008]. It describes the fiber network as a set of n vertices and paths p , with each path representing a fiber identified by a vector of k vertex identifiers ($p^i = \{n_1^i, n_2^i, \dots, n_k^i\}$). A gaussian filter is used to smooth the image prior to binarizing it with an appropriate intensity threshold. This step ensures that the selected foreground pixels represent potential fibers. After binarization, the euclidean distance map is computed for each binarized pixel. The identification of nucleation points is facilitated based on the computed euclidean distance map. The fibers are then traced along the identified nucleation points based on the fiber trajectory. A post-processing step is then ensued to remove short dangling fibers, and link closely associated fibers. The CT-Fire algorithm is implemented in Matlab[®] with a few parameters to be defined by the user.

3.3.2.2 Method II: Sequential tracing algorithm

Template matching: Template matching is used in identifying specific components in a large image stack. This has been reported for line networks such as actin filaments and microtubuli [Krauss et al., 2012a]. This is justified with the realization that the intersection of a line segment with a plane is an ellipse. An example of a representative template for scanning collagen fiber cross-sections is shown in figure 3.3.

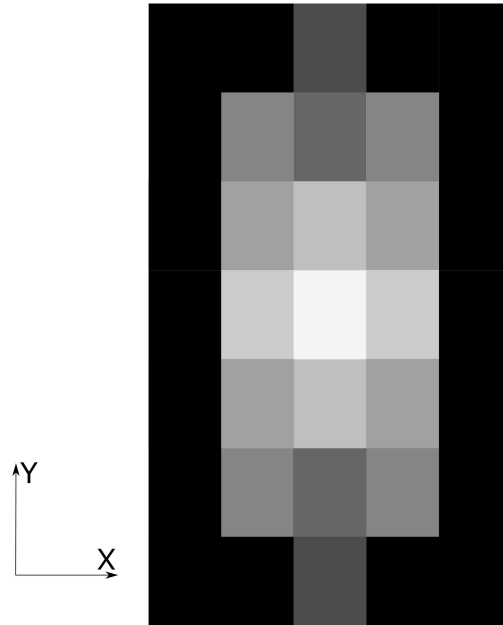


FIGURE 3.3 – An example of a 2-D template for scanning SHG image stacks.

A template matching algorithm is applied to the SHG image stack as a pre-processing step. The end result of this step is a binarized and skeletonized image stack. A more

detailed description of the algorithm can be found in [Krauss et al., 2012a]. Briefly, the algorithm first automatically generates a template for each scan direction (x,y, and z) through a trial and error process. This is done by randomly choosing a large number of 2-D sections ($\approx 10^5$) and perform a weighted average. The weight of each 2-D section is proportional to the intensity of the central pixel, ensuring that there is a fiber at the center. This results in a template with a typical cross-section of bright pixels in the center surrounded by a dark border. Once a template has been chosen for each scan direction, it is used for detecting sections of fibers in the search plane. For instance, assume a scan in the z-direction, with an identified template of size $T_x \times T_y$ with search sections in the X-Y plane of the same size. In this case, the template and the search section are represented as a vector with $T_x \times T_y$ components. Euclidean distance is used as the measure to quantify the mismatch between the template and the search section by defining a distance threshold. If the distance exceeds the defined threshold, the central pixel of the search section is flagged to 0. A bunch of pixels are identified in this manner corresponding to fiber cross-section. The pixel corresponding to the local minima of mismatch within this group of pixels are set to 1 and the rest are set to 0. A similar process is repeated for scan in y and z directions. A logical OR operation is performed at the end these individual scans, yielding the final result.

*Fiber trajectory:*The end result analysing the SHG image stacks with template matching is a cluster of points belonging to the center-line of fibres. In order to trace the fiber path from the identified points, the trajectory of the fiber needs to be known. OrientationJ, a plugin in ImageJ is used for this purpose. Structure tensor, which is a matrix of partial derivatives of the image is computed for each pixel. Structure tensors represent information related to partial derivative of the image: for a 2-D image this is represented as a 2×2 matrix. It is useful for evaluating gradient or edge information in an image. Once the structure tensor is computed for a region of interest, the local orientation is then computed as the direction corresponding to the largest eigen vector of the tensor. A gaussian window is used along with two other thresholding parameters (coherency and energy), which evaluate the isotropic nature of the pixel's neighborhood. The orientation values are weighted by the coherency values (ranging between 0 – 1) so that elongated structures are given priority in a local neighborhood. Hence, a minimum coherency of 15 % and a minimum of energy of 3 % are used in this study [Cavinato et al., 2017]. Using this approach, the local fiber orientations are collected at each pixel of the SHG image stack. It was assumed that the radial angle of the fibers is negligible and hence the orientations were collected only in the axial-circumferential plane.

*Reconstruction:*A custom matlab script was used to reconstruct the center-lines of fibers by combining the results of the above two steps. The algorithm used for tracing the fibers is as follows:

1. A 3-D array of size corresponding to the size of the SHG image stack is defined. The voxels identified as part of fiber center-line are given a value 1 (nucleation point) and the remaining elements are assigned a value of 0.
2. Each element of the 3-D array with a value of 1 is assigned a boolean value to assess whether it has been already traced. An initial boolean value of false is assigned to all, indicating none of them have been traced yet.
3. The array is scanned from the top left corner of the image iteratively. Once a nucleation point is reached, the array is probed for a nearby nucleation point in a direction defined by the identified local orientation at that voxel. The radius of the probe is

manually defined through an iterative process to minimize too many disconnected regions.

4. The tracing is carried out either until no nucleation point is found or when the boundary is reached. All the traced points are stored in a separate 2-D array, with each row indicating the vertices of an identified fiber.
5. the scan is stopped when all the points have been traced to a fiber.

3.3.2.3 Minimal path based approach: ScanIp

A fast-marching algorithm was used in ScanIP[®] for segmenting the collagen fibers in SHG image stacks. The images were subjected to pre-processing for denoising and removing spurious artifacts. In order to implement the fast marching algorithm, the user needs to provide a set of seed points from which the contour will expand. The seed points were chosen manually in order to optimize the chance of segmenting complex objects and to minimize the time needed for the front to visit the whole image. This was also advantageous for reducing the amount of leaks and branches when unnecessary. For instance, it was observed that when segmenting elongated objects such as the fibers, placing several seed points along the axis was the best strategy. The density of the seed points was significantly higher in case of fiber intersections in order to achieve a desirable quality of segmentation.

3.3.3 Results

For a preliminary evaluation of the three methods, two synthetic image stacks were created manually in ImageJ. Figures 4 and 5 show that for the synthetic image stacks, the presented methods evaluate the fiber morphology satisfactorily. In the first case where the fibers were mostly linear and do not have many intersections, all but the sequential tracing algorithm display an accurate representation of the network. On the other hand, in the second case where the fibers were wavy and have significantly more intersections, both CT-Fire and sequential tracing fail to recognize significant portions of the network.

Two SHG image stacks of descending porcine aorta were also tested with the above mentioned fiber segmentation techniques. Figures 6 and 7 present the segmentation results for the same. Comparison of the three techniques reveals that while CT-Fire has difficulty tracing fibers in high noisy regions giving rise to many erroneous fiber tracks. Contrarily, the segmentation technique implemented in ScanIP[®] and the sequential tracing technique showed many truncated fiber tracks and completely missed some bright fibrous regions.

3.3.4 Discussion

In this study we present a qualitative comparison of three different techniques for segmentation of collagen fibers from SHG image stacks of arterial tissue. A proper segmentation of such networks facilitates the analysis of fiber morphological features such as fiber lengths, density, curvature, and orientation. The knowledge of these parameters is important in studying the role of micro-structural constituents in the mechanics of the tissue. Automated quantification of these patterns has the potential to generate more reliable and reproducible results compared to manual quantification methods.

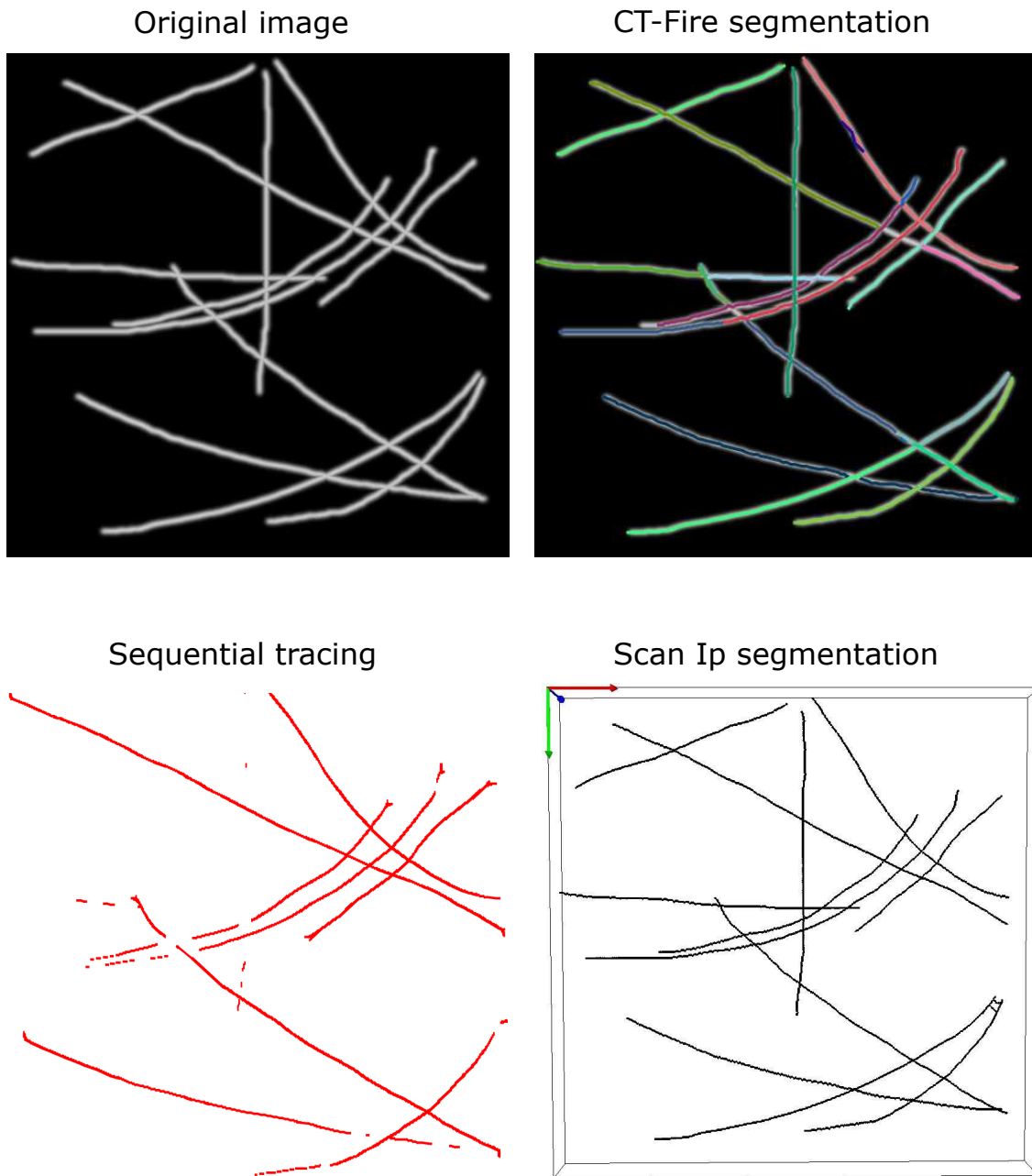


FIGURE 3.4 – Output of the different segmentation techniques on synthetically generated close to linear fibers.

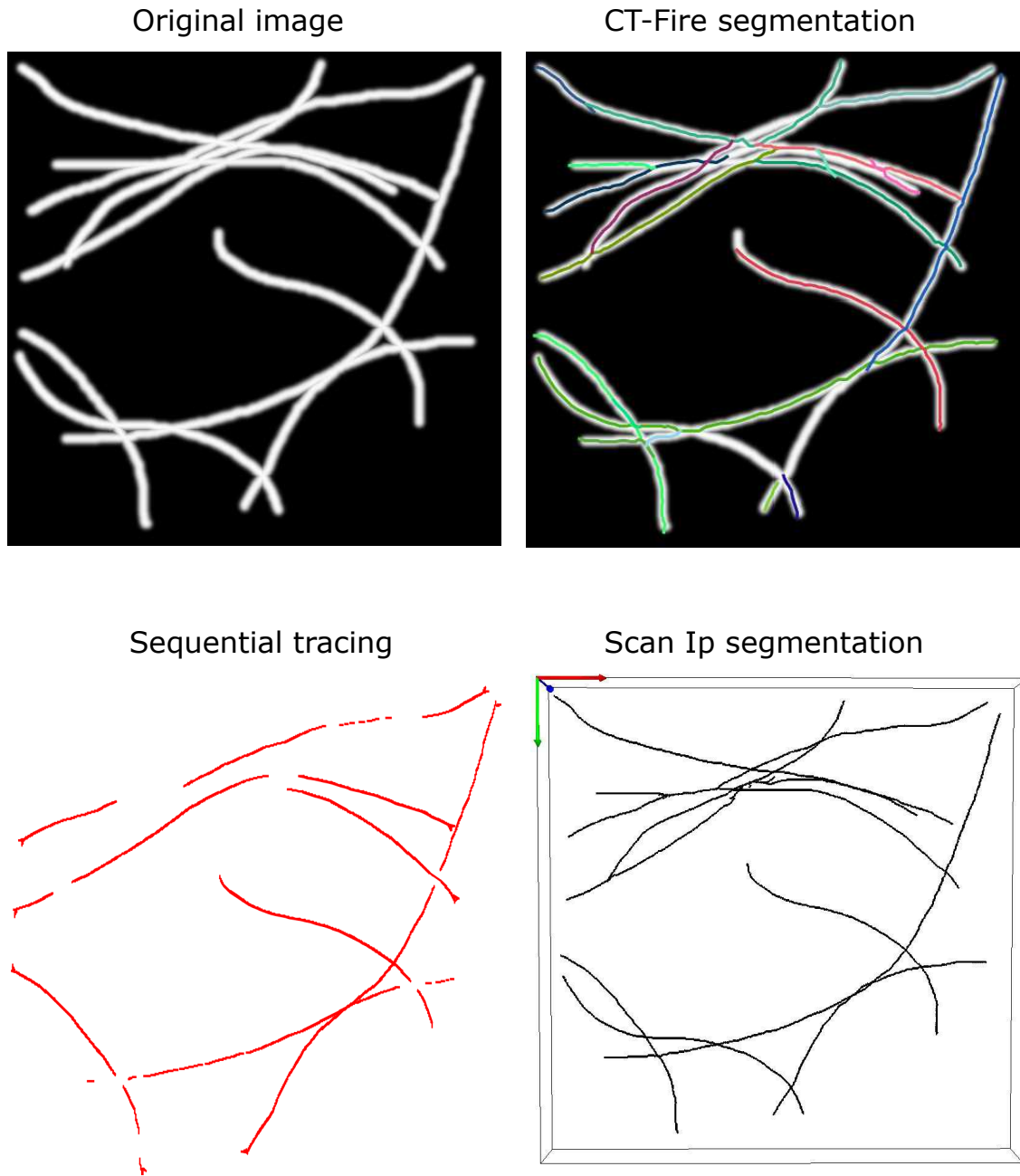


FIGURE 3.5 – Output of the different segmentation techniques on synthetically generated curvy fibers with significant intersections.

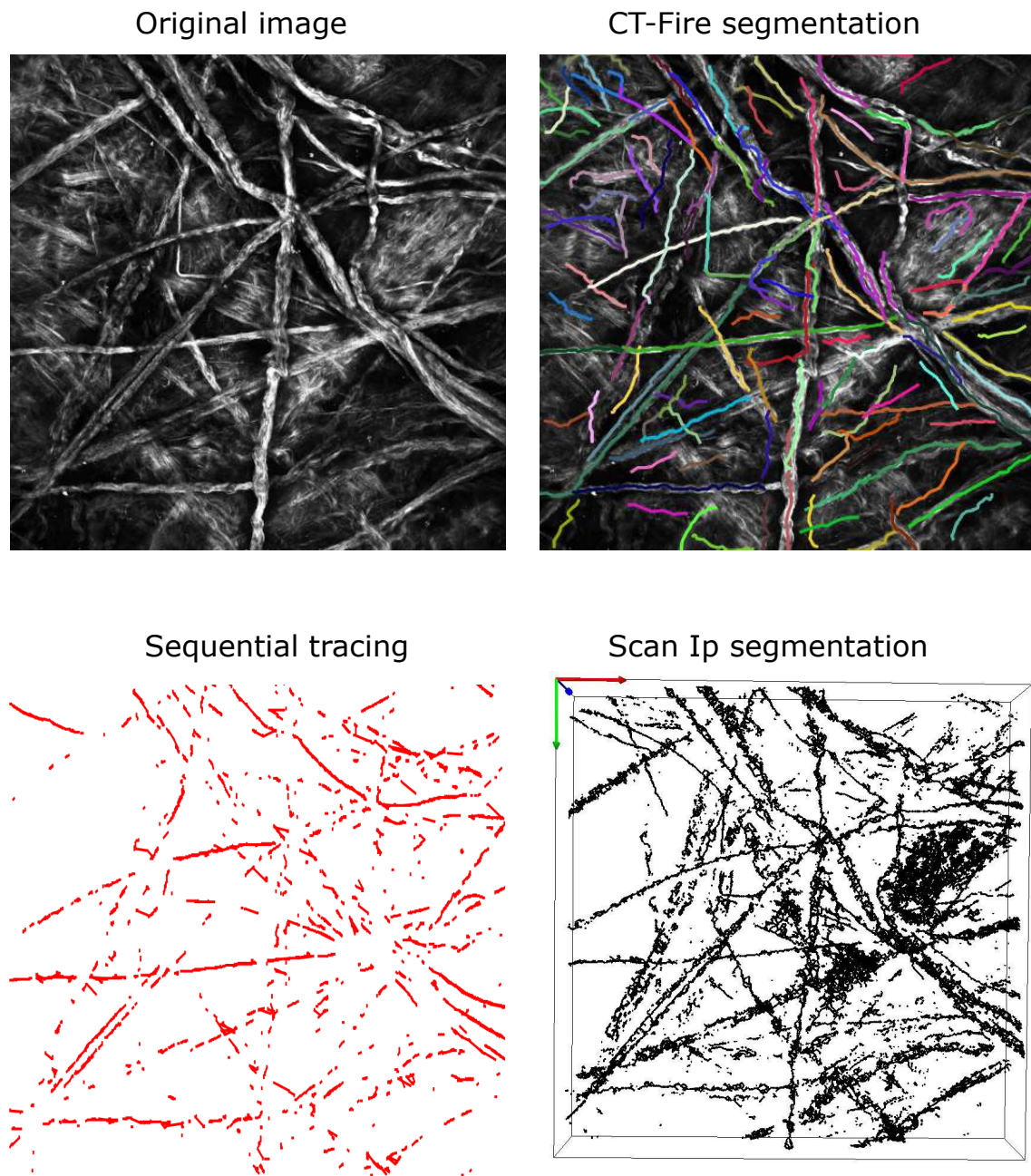
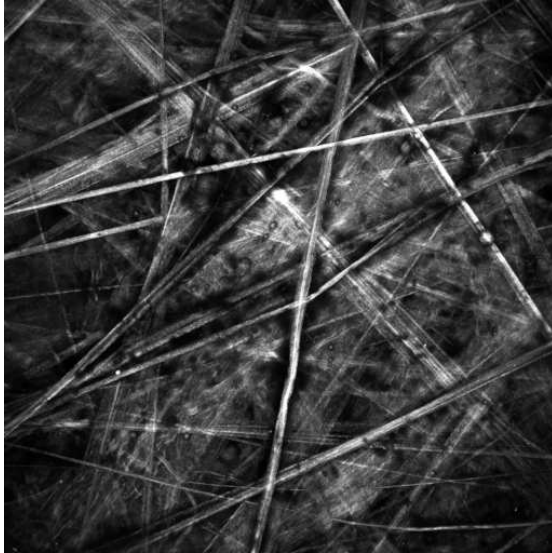


FIGURE 3.6 – Output of the different segmentation techniques on an image stack of porcine tissue at zero pressure.

Original image



CT-Fire segmentation



Sequential tracing



Scan Ip segmentation

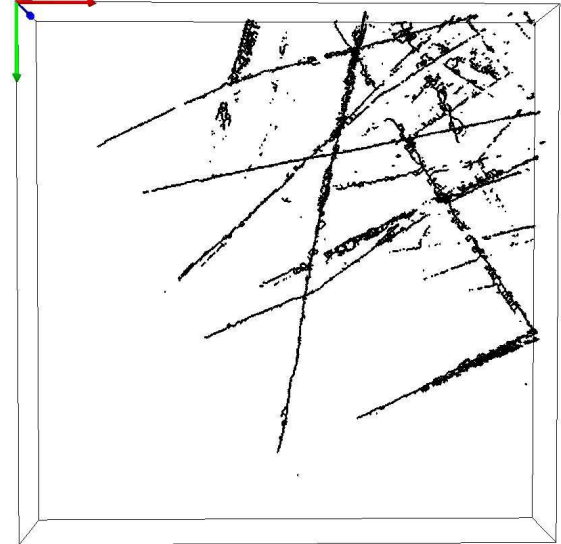


FIGURE 3.7 – Output of the different segmentation techniques on an image stack of porcine tissue at 200 mm-Hg.

The first method described in this study was used to quantify collagen morphologies in breast cancer patients [Bredfeldt et al., 2014]. The algorithm was an extension of the FIRE [Stein et al., 2008] algorithm to overcome the obstacle of extracting fibers in densely packed images. The results shown in figures 6 and 7 suggest that the application of CT (curvelet transform filter) generally improved the fiber extraction. Even though the algorithm performed well in fiber networks with low cross-link densities, it was not suitable in crossing or cross-linked fibers, extremely curvy fibers, or fibers with gaps. Another limitation of this method is that the fiber tracing is limited to 2-D images. Given the result of the CT-Fire algorithm, it could be used to quantify the fiber morphology (length, orientation, and width). This will be discussed briefly in section 3.4

The second method presented here combines three different algorithms (template matching, OrientationJ, and sequential tracing). Although the method has not been tested on a wide range of SHG image stacks, a few remarks could still be made. The reconstruction is sensitive to the skeletonization result (density of identified nucleation points) and thus retains some intrinsic limitations of the template matching algorithm. From preliminary observations, the template matching algorithm produces a satisfactory skeletonization for networks with tubular structures of homogeneous cross-sections, thereby failing with networks with many intersections and high noise. Since the template is built automatically by weighing several sampled templates, for an isotropic orientation distribution, many fibers are discarded as seen in figures 3.4, 3.5, 3.6, and 3.7 (for instance the y-z direction template in figure 3.4). The local orientation at each voxel used in this study was limited to the axial-circumferential direction. In order to trace the fiber in 3-D the out of plane orientation ($< 10^\circ$) was assumed by the user. This choice enhanced the probability of finding the next point since the seed points resulting from template matching were in 3-D. A 3-D assessment of voxel wise gradient would be better suited for the reconstruction process, which was not explored in this work.

The final method presented here was based on the image-processing toolbox of ScanIP[®]. A fast-marching method with manually chosen seed points was used to segment the fibers. The SHG image stacks were pre-processed to reduce the noise. The segmented fibers were skeletonized using a skeletonization algorithm. The main objective for implementing this method was to import the end result as an input for finite element analysis. The skeletonized network as seen in figures 6 and 7 suggested that this was not feasible. However, the end result was used to extract other information like volume fraction, which is discussed in section 3.4.3.

3.3.5 Conclusion

This study presents some preliminary investigation of three algorithms for segmenting collagen fibers from SHG image stacks. Although CT-Fire and ScanIp[®] were already established, a new algorithm based on sequential tracing technique was presented here. The algorithm's capability to automatically identify and quantify the fiber network topology was limited and ideally works only for tubular structures with a homogeneous cross-section distribution and with networks with low fiber intersections. The method however shows some affirmation and needs further research in overcoming its limitations.

3.4 Extraction of morphological parameters of collagen fiber network from SHG images

An anatomically accurate description of the collagen fiber network in arterial tissue is useful for developing powerful numerical tools that provides a mechanical description of the tissue. The result of direct segmentation of collagen from SHG image stacks as shown in section 3.3 was not adequate for achieving this purpose. But, the SHG images still withhold a lot of meaningful information that could be used to generate numerical models in an inverse manner. In this section we outline the three such important parameters that characterize collagen fiber morphology in arterial tissue: orientation, waviness, and volume-fraction; and provide reliable tools for extracting and quantifying this information with the aim of subsequently reconstructing high similarity networks (see section 3.5).

3.4.1 Orientation

The current section focuses on quantifying collagen fiber orientations based on fiber extraction methods explained in section 3.3 and other transform or filter-based image processing techniques. Fiber angle was defined as the angle with respect to the circumferential direction, ranging from -90° to 90° .

3.4.1.1 CT-Fire

Individual fiber extraction was performed in CT-FIRE V2 Beta and CurveAlign V4.0 Beta [Liu et al., 2017]. 8-bit images were imported into the program where they were subjected to a curvelet transform (CT) followed by fiber extraction using the FIRE algorithm. The extracted fibers from the above step were subjected to post-processing using CurveAlign, another custom built fiber network analysis software developed at the laboratory for optical and computational instrumentation (LOCI), for analyzing and quantifying the fiber morphology.

3.4.1.2 OrientationJ

OrientationJ was used to estimate the in plane orientation of collagen fibers as detailed in section 3.3.2.2. The local neighborhood for the evaluation of the structural tensor was set to 3 pixels, from which the local fiber orientation was computed. The end result of this a weighted histogram of orientations was computed for each image of the SHG stack. The representative orientation density of the stack was taken to be the average value of all the images.

3.4.1.3 Fast Fourier Transform based methods

The classical 2-D discrete Fourier transform (FFT) was performed on each image of the SHG image stack. Prior to the application of the FFT, the images were subjected to pre-processing routine to remove edge artifacts. A Hanning window function, which reduces the contrast of the image from the center towards the edges was used for this purpose [Polzer and Gasser, 2015a]. Further, the images were rotated by 90° in order to obtain the original orientation of the fibres. The resulting amplitude spectrum function was amplified by powering it with a factor greater than 1. This process enabled the enhancement of high

values while suppressing low values. An Optimal value 3 – 5 was chosen for this powering factor as reported in earlier investigations [Polzer and Gasser, 2015a]. A 1° wedge-filter was used to extract the fiber orientations by summing up the amplitudes in each wedge. This resulted in a discrete distribution of amplitudes which was used to compute the orientation histogram.

3.4.1.4 Comparison

The SHG image stacks of 6 human aneurysmal tissues, and 6 healthy porcine tissues acquired prior to mechanical testing were used in this study. A description of the sample preparation and imaging protocols is presented in Chapter 2. The comparison of image processing methods in quantifying the fiber orientations is shown in figure 3.8 for a representative stack. It demonstrates that all three methods could be used to quantify fiber orientation reliably leading to a similar orientation distribution.

3.4.2 Waviness

Collagen fibers are crimped in their initial configuration, meaning that they do not contribute to the load bearing of the tissue until a certain pressure state. This phenomenon combined with their high tensile stiffness as compared to other ECM components makes the adventitia the protective sheath of the arterial walls. The crimp parameter used in this work was extracted manually on the SHG images and is similar to the one reported in [Rezakhaniha and Agianniotis, 2012] for confocal laser scanning microscopy of the adventitia. The following definition was used in order to quantify it:

$$W = \frac{l_s}{l_c} \quad (3.1)$$

where l_s and l_c represent the end to end length and length along the curve of the fiber respectively. A schematic representation of a wavy fiber is shown in figure 3.9 a. The crimp parameter is bounded by 0 on the lower limit and by 1 on the upper limit. A value of 1 indicates a straight fiber whereas values less than 1 indicate a curvy fiber (crimp increases as the parameter value decreases). l_s and l_c were quantified using the measure tool in ImageJ on manually traced fiber segments as shown in figure 3.9 b.

3.4.3 Volume fraction

The content of collagen fibers in the arterial tissue was estimated using the segmentation technique described in 2.3.2.3. The fast marching based minimal path algorithm resulted in collagen segmented from the SHG image stack. Before running the skeletonization algorithm, the amount of voxels in the segmented stack were noted down. Collagen volume fraction was then defined as the ratio of segmented voxels (V_S) to total number of voxels (V_T). Figure 3.10 a and 3.10 b represent the original image stack and its segmentation output respectively.

3.5 Numerical network reconstruction

3.5.1 Stochastic modeling

The quantified collagen fiber morphology data are fitted to relevant probability distribution functions as described in the following subsections.

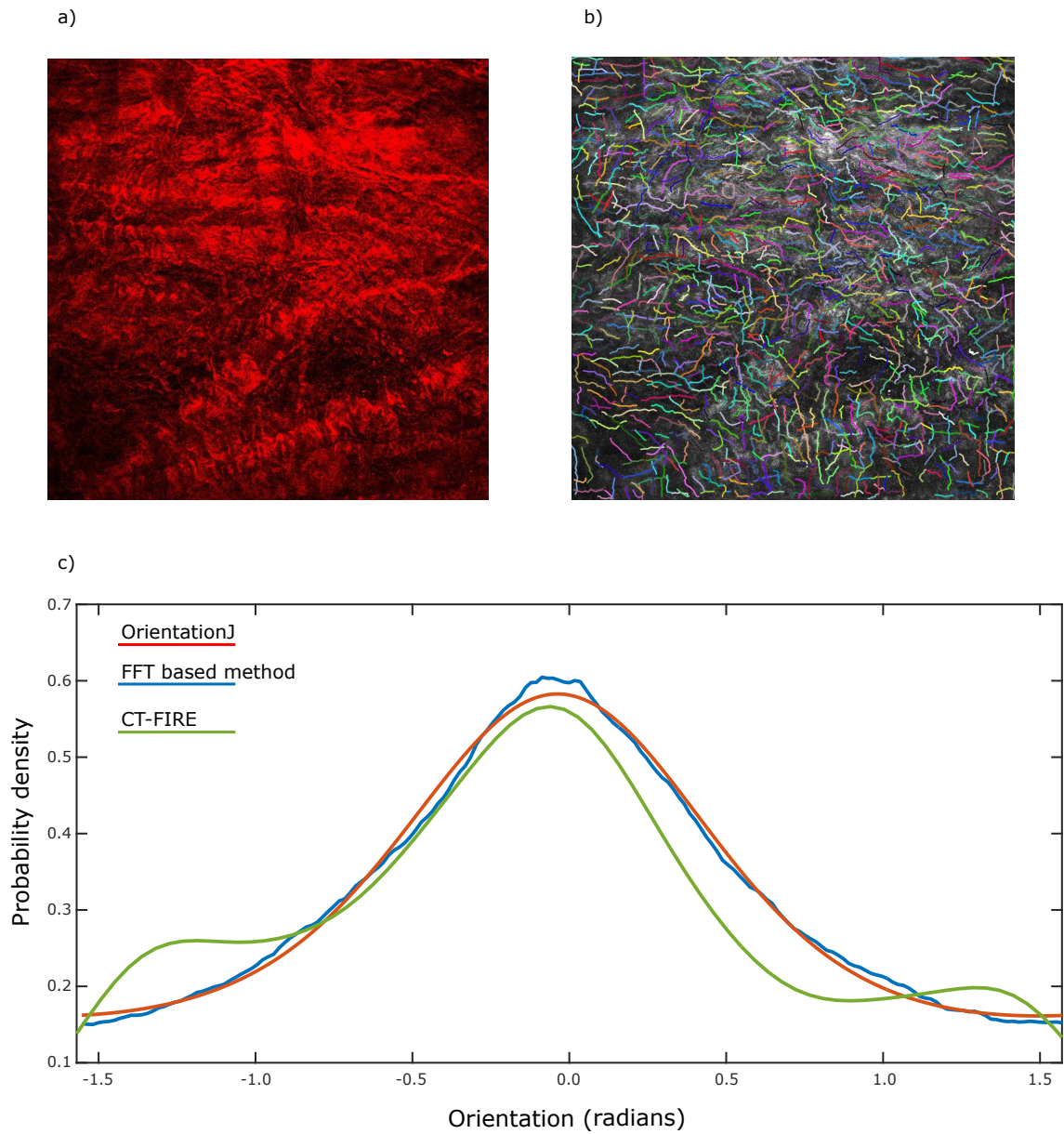


FIGURE 3.8 – a) Max-intensity projection of an SHG image stack acquired on human aneurysmal tissue, b) The fibers traced through CT-FIRE algorithm for post-processing, c) Comparison of quantified orientation distributions through the three presented techniques.

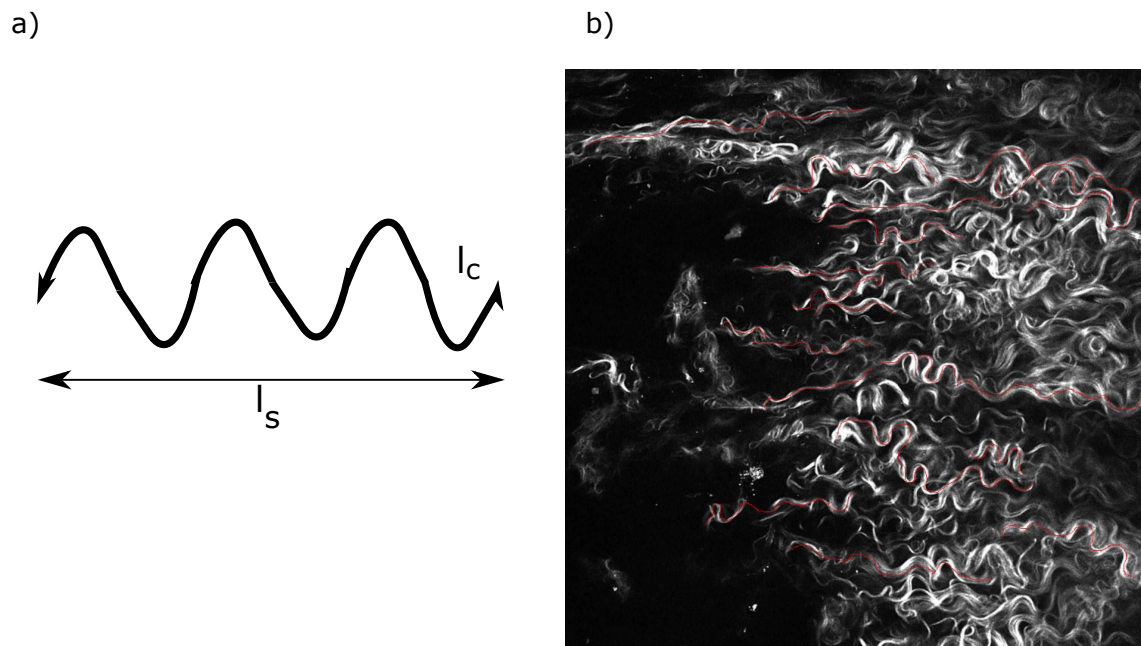


FIGURE 3.9 – a) An illustration of a crimped collagen fiber, b) An example of measured waviness values on an SHG image with measured traces represented in red overlaid on the grey scale image.

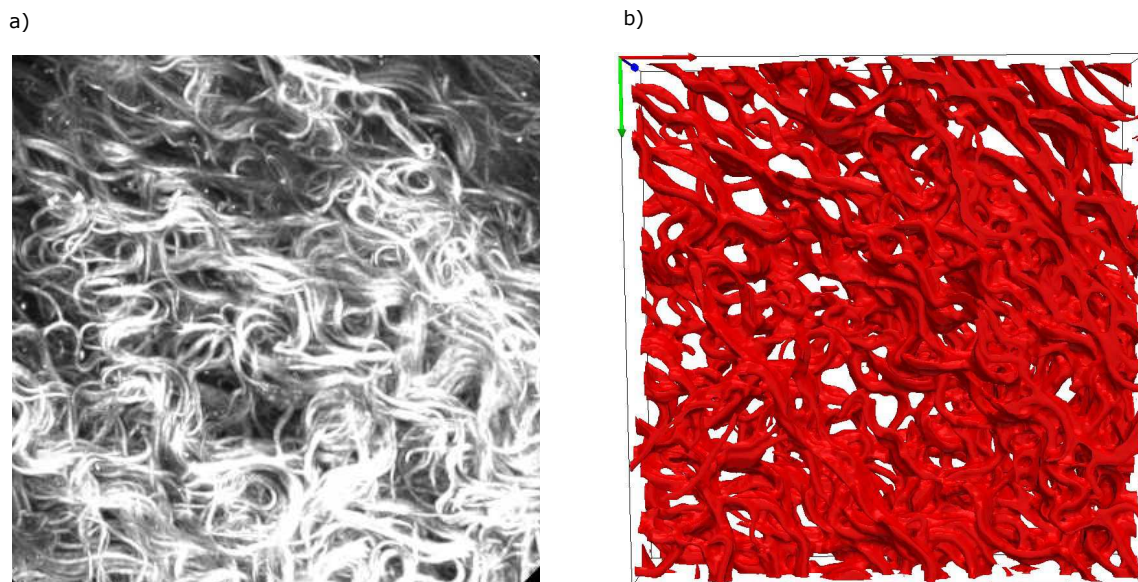


FIGURE 3.10 – a) Max intensity projection of an image stack acquired on rabbit carotid artery, b) Output of 3-D segmentation on the image stack using a minimal path based approach in ScanIP.

3.5.1.1 Orientation

Recognizing the presence of two distinct families from the fiber orientation data, a mixture of two Von-Mises functions was used to represent the orientation distribution. A pi -periodic Von-Mises probability density function is defined in equation 2.2:

$$f(\theta|\mu, k) = \frac{e^{k \cdot \cos 2(\theta - \mu)}}{\pi I_0(k)} \quad (3.2)$$

$$I_0(k) = \frac{1}{\pi} \int_0^\pi e^{k \cos \theta} d\theta \quad (3.3)$$

where μ and k are the mean orientation and concentration parameters (a measure of standard deviation). $I_0(k)$ is a zero order Bessel function of type I, which acts as a normalization parameter such that $\int_0^\pi f(\theta|\mu, k) d\theta = 1$. The two family representation of the probability distribution can be defined as:

$$f(\theta|\mu_1, \mu_2, k_1, k_2, p) = p \frac{e^{k_1 \cos 2(\theta - \mu_1)}}{\pi I_0(k_1)} + (1 - p) \frac{e^{k_2 \cos 2(\theta - \mu_2)}}{\pi I_0(k_2)} \quad (3.4)$$

where the subscript 1 represents the first family and the the subscript 2 represents the second family. The parameter $0 < p < 1$ was used to characterize the weight of each fiber family. A constrained optimization was performed in Matlab[®] in order to identify the five parameters of the orientation distribution.

3.5.1.2 Waviness

The measured collagen crimp was characterized by a Beta probability distribution. The choice was made as the Beta probability function is defined on the domain $[0, 1]$, and is parametrized by two shape parameters α and β , which accommodate for skewness in the distribution. The Beta probability distribution is defined as:

$$f(W, \alpha, \beta) = C(\alpha, \beta) W^{\alpha-1} W^{\beta-1} \quad (3.5)$$

$$C = \frac{1}{\int_0^1 t^{\alpha-1} (1-t)^{\beta-1} dt} \quad (3.6)$$

where C is the normalizing constant.

3.5.2 Inverse random sampling

Inverse random sampling is a method for simulating random data sets from any given probability distribution. In order to perform inverse random sampling, an analytical solution needs to exist for the inverse of the cumulative distribution function.

3.5.2.1 Mixed Von-Mises distribution

Since an analytical solution does not exist for the inverse of the cumulative distribution function for the Von-Mises distribution, the usual straightforward method cannot be used. Here, an acceptance rejection algorithm was implemented in Matlab[®] as described in [Hornik and Grün, 2014, Gatto, 2008]:

1. Define $g(\theta) = k_1 \cos 2(\theta - \mu_1) + k_2 \cos 2(\theta - \mu_2)$ and determine $m = \sup_{\theta \in [0, \pi]} g(\theta)$.

2. Generate u from a uniform distribution over $(0, \pi)$, and v from a uniform distribution over $(0, 1)$.
3. Check $v \leq g(u)$. If true, then accept u as a Von-Mises pseudo-random number else reject and go back go step 2.
4. Repeat until desired sample size is reached.

An example of the inverse random sampling for orientations and waviness is presented in figure 3.11.

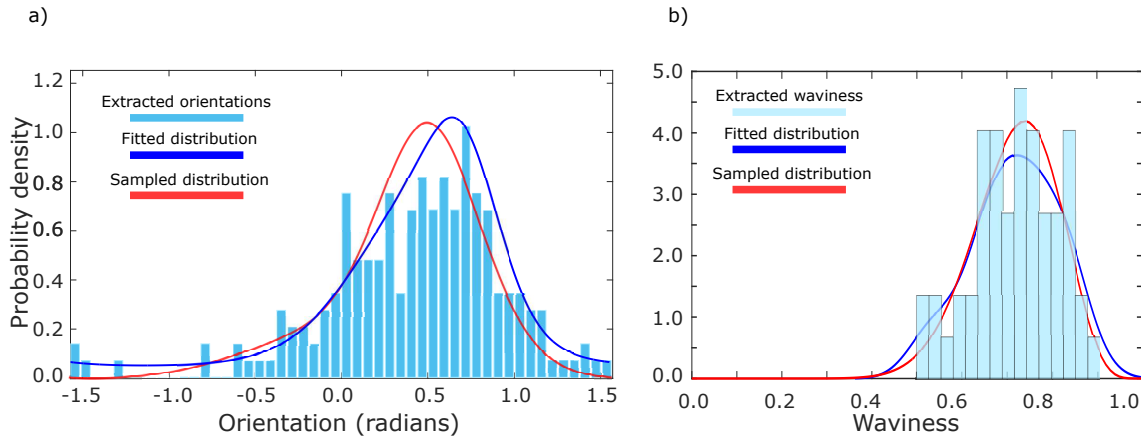


FIGURE 3.11 – Measured, quantified, and sampled probability distributions for fiber morphology.

3.5.2.2 Beta distribution

The cumulative distribution (CDF) for the Beta probability distribution is defined as $B(x, \alpha, \beta)/B(\alpha, \beta)$, where $B(x, \alpha, \beta)$ is an incomplete beta function as defined in equation 2.7.

$$B(x, \alpha, \beta) = \int_0^x t^{\alpha-1}(1-t)^{\beta-1} dt \quad (3.7)$$

Since an inverse function exists for the cumulative distribution function, inverse random sampling procedure is straightforward for the beta distribution as described in the algorithm below:

1. Generate uniform samples of a number u between 0 and 1, which represents the probability.
2. Identify the largest value x in the domain for which the $CDF(x) \leq u$, such that $CDF^{-1}(u) = x$.
3. Accept the value of x as the beta-distribution pseudo random number.

3.5.3 Random walk algorithm

A random walk algorithm was implemented here to numerically generate the collagen fiber network of the adventitia for finite element simulation purposes. The input data required for a successful implementation of this algorithm are: fiber global orientations, fiber local orientations (which can be computed from the measured waviness), and fiber volume fraction. With this information, the model is generated under the following assumptions:

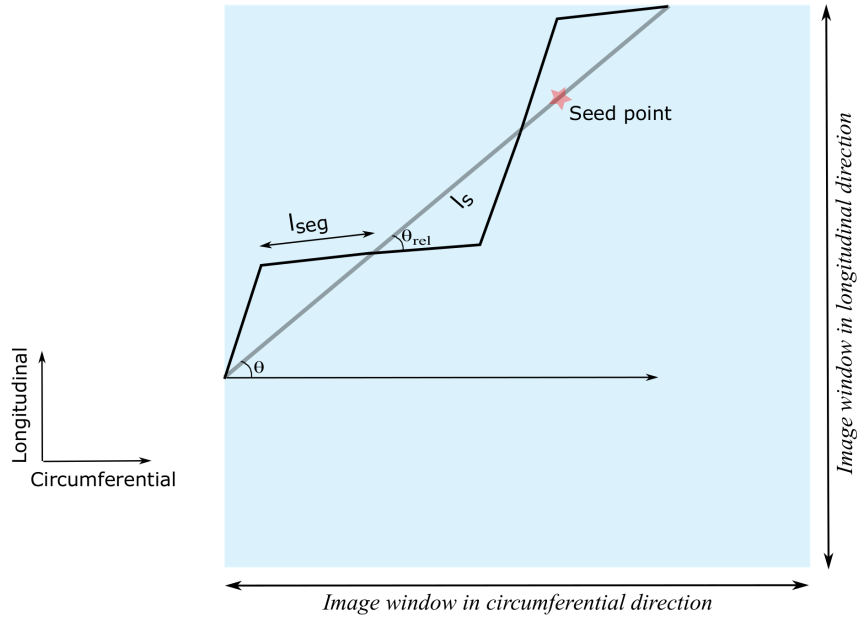


FIGURE 3.12 – A schematic representation of the fiber reconstruction process.

3.5.3.1 Assumptions

1. Each fiber is modelled as a piece-wise linear curve, made up of a fixed number of segments N_{seg} of lengths l_{seg} .
2. The number of segments for each fiber is assumed to be constant. If this value could not be measured from the images, a constant value of 50 was taken to be representative. This generates different wavelengths for each fiber, yet still in the experimentally identified range.[Koch et al., 2014].
3. Each fiber is characterized by a global orientation (θ), extracted and quantified from SHG image stacks of the tissue.
4. Fibers are assumed to be crimped in the initial state, with the parameter defined in 2.5.1.2. It is assumed to follow a beta distribution and is extracted from the image stacks. In cases where it was not feasible to quantify it from images, an inverse identification method is used. The most probable value (mode) is used for all fibers.
5. The polar (out-of-plane) orientation of the fibers is assumed to be negligible.
6. The length of each fiber is assumed to be much greater than the region of interest. Hence every fiber has its ends intersect with the boundary.
7. All fibers are assumed to have a circular cross-section of uniform diameter ($10 \mu m$).
8. The fiber network is modelled as an entangled network, hence there are no cross-links between fibers. Friction between the fibers are thus assumed to be negligible.
9. Interactions between the matrix and the fibres is assumed to be negligible and their stresses are considered to be additive. Thus the mechanics of the model is determined by the constitutive behavior of the fibers.

3.5.3.2 Algorithm

Following the stated assumptions, the fiber network is regenerated using the following algorithm. A schematic of the numerical reconstruction is shown in figure 3.12.

1. Define a 3-D volume according to the size of the SHG image stack.
2. Sample seed point in the selected volume using a uniform distribution.
3. Sample global fiber angle (θ) from the identified mixture Von-Mises distribution.
4. Trace the fiber ends (fiber intersections with the volume), using the seed point and the global fiber orientation. Fiber start and end points and fiber end to end length (l_s) are thus known.
5. The length of each fiber segment can be computed as $l_{seg} = \frac{l_s}{N_{seg}W}$, where W is the waviness of the fiber.
6. From the starting point the fiber can be propagated along the global direction with length segments of l_{seg} and a relative angle of $\theta_{rel} = \cos^{-1}(W)$.
7. The fiber is added to the network. Check if the volume exceeds the desired volume fraction. If yes, stop. If not, repeat steps 2 to 6.

3.6 Finite element model

A choice was made to incorporate the generated collagen fiber network explicitly into a finite element model. This choice relied on ease of implementation of such a model, plus the scope for enhancing the complexity of the model in future iterations to include fiber interactions, cross-links, and possibly other micro-structural components such as elastin fibers to model the whole wall instead of merely modeling the adventitia.

A custom matlab[®] script was used to generate input files for finite element analysis in Abaqus[®] v6.14. The matrix was modelled as a 3-D solid with C3D8H elements (Simulia, 2014). Collagen fibers were modelled as beams with B31H elements (Simulia 2014).

3.6.1 Material models

- An isotropic, in-compressible neo-hookean material with a single material parameter was used for the matrix.
- An isotropic, linear elastic material was used for collagen. This application of this material model is presented in chapter 4, in investigating the mechanical response of rabbit carotid arteries.
- The isotropic linear elastic material model presented above was extended to model brittle damage in collagen (based on fiber strain $\epsilon_{rupture}$). An isotropic, scalar damage parameter was defined to model this behavior. A custom user subroutine was written for this purpose. The application of this material model is presented in chapter 5, in investigating the mechanical response of human aneurysmal and healthy porcine arteries.

- The brittle damage model for collagen was extended to model progressive damage purely for comparison purposes. The scalar damage parameter was activated upon initiation (strain based ε_{init}) and increased until rupture ($\varepsilon_{rupture}$) as $D = 1 - \frac{\varepsilon_{rupture} - \varepsilon}{\varepsilon_{rupture} - \varepsilon_{init}}$. The Young's modulus of collagen was degraded according to the recorded damage parameter as $E_{collagen}^* = (1 - D)E_{collagen}$.

3.6.2 Boundary conditions

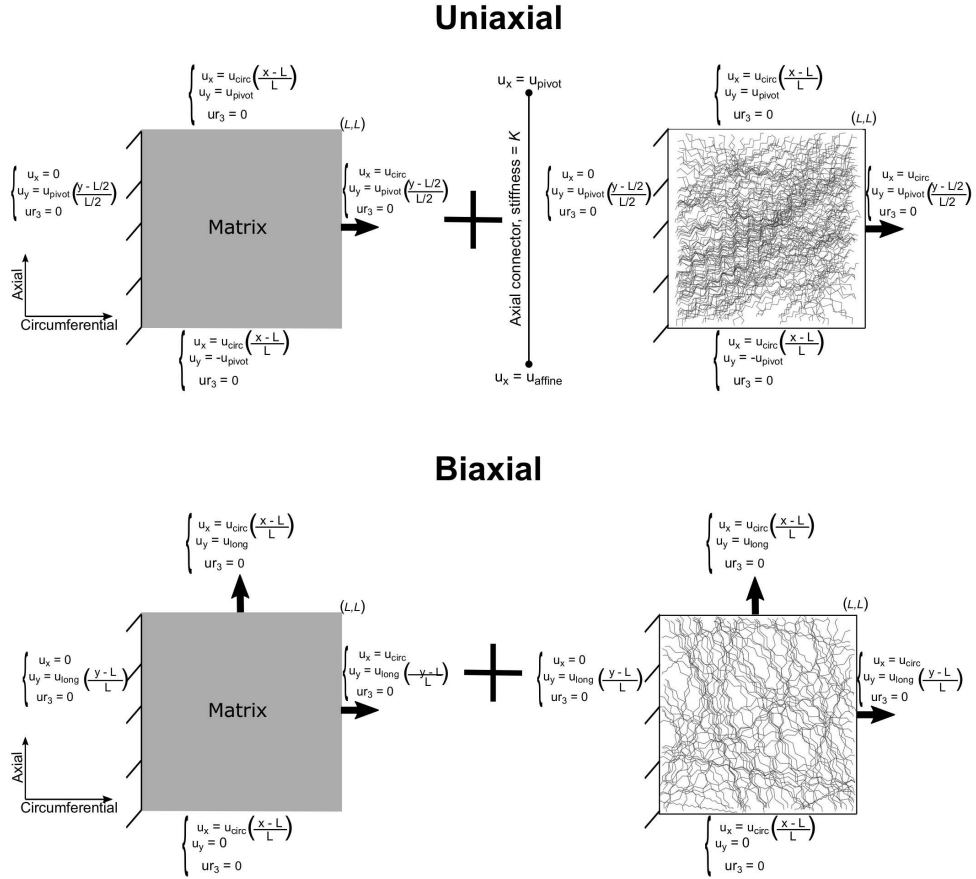


FIGURE 3.13 – Boundary conditions imposed on the generated finite element model for simulating uniaxial and biaxial tension.

- *Uniaxial*: The boundary conditions applied for uniaxial simulations were chosen in order to allow non-affine transformation of the fiber network. A schematic of the applied boundary conditions is shown in figure 3.13 a. Here we define four boundary faces: $circ_{pos}$, $circ_{neg}$, $long_{pos}$, $long_{neg}$; two in circumferential and two in longitudinal directions respectively. All nodes of the fibers intersecting a face were grouped into a node-set. For instance, we can focus here on the tensile testing in circumferential direction. The desired tensile stretch was achieved by displacing nodes on $circ_{pos}$ face while restraining the nodes on $circ_{neg}$ face. The transverse deformation of the network was controlled using a spring-like connector element. One node of the connector was given a longitudinal displacement according to the affine transformation while coupling the other end to the y-displacement values of the nodes on $long_{pos}$, $long_{neg}$ faces. The tensile stiffness of this connector element controlled the

transverse displacement of the network. A relatively high stiffness represents affine kinematics for the fiber network while lower values represent increasingly non-affine behavior.

- *Biaxial*: In the case of biaxial simulations, a tensile displacement was applied to two orthogonal surfaces: *circ_{pos}* and *long_{pos}*, while restraining the other two surfaces. For each biaxial simulation the amplitude of displacements was derived from experiments and was not equal in circumferential and longitudinal directions. The schema of the applied boundary conditions is shown in figure 3.13 b.

3.6.3 Parameter identification

The following parameters characterize the mechanical response of the model:

- Neo-hookean material parameter for the matrix
- Elastic modulus of collagen
- Axial stiffness of the connector
- Collagen fiber waviness
- Collagen fiber content in the adventitia
- Collagen fiber orientation distribution
- Collagen fiber failure strain

In the case of prediction the elastic behavior of the tissue, the model takes into account six parameters: matrix material parameter, elastic modulus of collagen, stiffness of the connector, collagen crimp, volume fraction, orientation of collagen. In case of predicting the tissue's failure behavior, an additional parameter for collagen fiber failure strain was used. The geometric parameters can be identified from SHG image stacks as demonstrated in section 3.4. Constitutive parameters for arterial tissue and collagen fibers have been widely reported but exhibit a wide range of values. Consequently these parameters and in some cases, the geometric parameters were identified in an inverse manner. The strategy used in this work is explained below and schematically shown in figure 3.14 c.

Response surface: An n -dimensional gridded data interpolant was built in Matlab[®], with n representing the number of parameters to be identified. For this purpose, each unknown parameter was identified with a reported minimum and maximum values from the literature. Each parameter was then uniformly sampled from its identified domain. The principle of this technique was to partition space of n parameters into $\prod_{i=1}^n k_i$, where k_i represents the number of sampled values for i^{th} parameter. This process resulted in $\prod_{i=1}^n k_i$ parameter sets, with each set containing exactly one sampled value of each parameter. For instance, if three parameters: Young's modulus of collagen, neo-hookean material parameter, and volume fraction were to be identified; each with three sampled values, this results in 27 simulations as shown in figure 3.14 a and 3.14 b. For each simulation, the stress-stretch response was recorded in order to build a response surface for the whole parameter domain.

Constrained optimization: A cost function representative of R-Square was built in Matlab[®] based on the experimental and recorded stress-stretch responses. This function was subjected to a constrained optimization loop using genetic algorithm, a part of

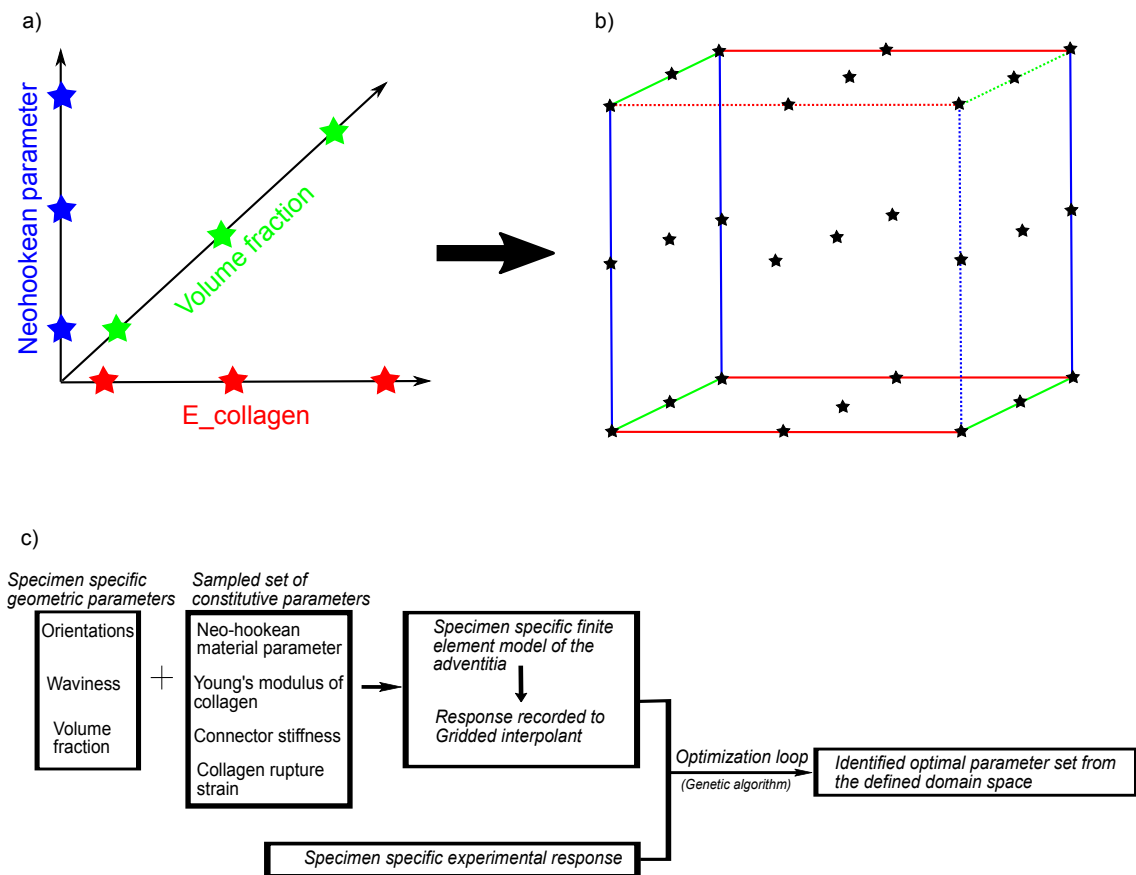


FIGURE 3.14 – A graphical illustration of the optimization algorithm for inverse identification of model parameters.

the optimization toolbox in Matlab[®]. For a complete parameter set identification, an input of 7200 simulations were used in the optimization procedure. In order to reduce the complexity of the parameters, the orientation distribution parametrized using just the standard deviation with two fiber families having mean orientations of 40° and -40° . On the other hand, for samples whose morphology was quantified, the material parameters were identified using an input of approximately 200 simulations per sample. The bounds of the unknown parameters were applied as constraints to the objective function. R-square was chosen to be a reliable estimator for parameter identification. Multiple runs of the genetic algorithm were run in order to ensure a global optimization. The averaged identified parameter set corresponding to maximum R-Square value was accepted as the optimal value. Each simulation had a run time of approximately 20 – 30 minutes where as each sample had about 200 evaluations during the optimization loop. The originality of this approach is the use of the response surface to estimate the stress-stretch curve for a set of parameters, instead of running new simulations. This dramatically cuts down the identification time.

3.7 Conclusion of the chapter

In this chapter we present viable methods for analyzing SHG image stacks of arterial tissue and using that data for developing reliable numerical models. More precisely, the first part of this chapter deals with segmenting collagen fibers from the image stacks. The aim of this operation was to incorporate the segmented fiber network explicitly in a finite element model. Our preliminary analysis in testing different algorithms shows that an accurate 3-D segmentation of collagen fiber architecture is achievable at the moment. The limitations of the methods were pronounced especially when dealing with images that have high noise. In order to overcome this obstacle, the second part of this chapter presents reliable tools for numerically regenerating collagen fiber networks based on morphological parameters estimated from SHG images. Such numerical models could act as a tool in understanding the bio-mechanical behavior of arterial tissue in health and disease. The potency and predictive capabilities of the model are demonstrated in chapters 4 and 5.

Look up at the stars and not down at your feet. Try to make sense of what you see, and wonder about what makes the universe exist. Be curious.

Stephen Hawking.

Chapter 4

A computational model for understanding the micro-mechanics of collagen fibre network - applied to rabbit carotid arteries

Contents of the chapter

4.1	Résumé du chapitre	86
4.2	Abstract of the chapter	87
4.3	Introduction	89
4.4	Methods	92
4.4.1	Experimental data and analysis	92
4.4.1.1	Image acquisition	93
4.4.1.2	Image processing	93
4.4.1.3	Mechanical testing	96
4.4.2	Mechanical model	97
4.4.2.1	Assumptions	97
4.4.2.2	Numerical network reconstruction	97
4.4.2.3	Finite element model	99
4.4.2.4	Boundary conditions	99
4.4.3	Design of experiment approach for model evaluation	99
4.4.3.1	Input parameters	100
4.4.3.2	Responses	101
4.4.3.3	Linear and non-linear regression for sensitivity analysis	102

4.4.4	Identification of model parameters	102
4.4.4.1	Validation on sample $n^{\circ}4$	102
4.4.4.2	Identification of model parameters on other samples	103
4.5	Results	103
4.5.1	Model Validation	103
4.5.2	Parameter identification from experimental data	103
4.5.3	Sensitivity analysis	106
4.5.3.1	Linear model	106
4.5.3.2	Non-linear model	106
4.5.4	Morphological changes of the fiber network	107
4.5.4.1	Reorientation	107
4.5.4.2	Straightening	108
4.5.4.3	Non-affine behavior	108
4.5.5	Analysis of the micro-macro relationship	109
4.6	Discussion	113
4.6.1	Main contributions	113
4.6.2	Comparison with the literature	113
4.6.3	Sensitivity analysis	114
4.6.4	Fiber kinematics	114
4.6.5	Rupture prediction	115
4.6.6	Limitations	116
4.7	Conclusions	117

4.1 Résumé du chapitre

L'anévrisme de l'aorte abdominale est une maladie cardiovasculaire répandue avec des taux de mortalité élevés. La réponse mécanique de la paroi artérielle repose sur le comportement organisationnel et structurel de ses composantes micro-structurales, de sorte qu'une compréhension détaillée de la réponse mécanique microscopique des couches de la paroi artérielle à des charges allant jusqu'à la rupture est nécessaire pour améliorer les techniques de diagnostic, et éventuellement les traitements. Suivant la notion commune que l'adventice est la barrière ultime aux charges proches de la rupture, dans la présente étude, un modèle d'éléments finis du réseau de collagène de l'adventice a été développé pour étudier l'état mécanique au niveau des fibres sous charge uniaxiale. Des piles d'images du tissu adventiciel de la carotide de lapin au repos et sous tension uniaxiale obtenues par microscopie multi-photonique ont été utilisées dans cette étude, ainsi que les courbes force-déplacement obtenues lors d'expériences publiées précédemment. Des paramètres morphologiques tels que la distribution de l'orientation des fibres, l'ondulation et la fraction volumique ont été extraits pour un échantillon des piles d'images multi-photons. Une approche d'échantillonnage aléatoire inverse combinée à un algorithme de *random walk* a été utilisée pour reconstruire le réseau de collagène pour la simulation numérique. Le modèle a ensuite été validé à l'aide de courbes expérimentales allongement-contraintes. Le modèle montre la capacité des fibres de collagène à se désordonner et à se réorienter dans le sens de la charge. Ces résultats montrent en outre qu'en cas d'allongement important, le réseau de collagène se comporte d'une manière non affine, ce qui a été quantifié pour

chaque échantillon. Une étude complète des paramètres pour comprendre la relation entre les paramètres structurels et leur influence sur le comportement mécanique est présentée. Dans le cadre de cette étude, le modèle a été utilisé pour conclure à d'importantes relations structure-fonction qui contrôlent la réponse mécanique. Nos résultats montrent également qu'à des charges proches de la rupture, la probabilité de rupture au niveau de la fibre est de 2,5 %. Les incertitudes des indicateurs de risque de rupture habituellement utilisés et la nature stochastique de l'événement de rupture, combinées à une connaissance limitée des déterminants microscopiques, motivent l'élaboration d'une telle analyse. De plus, cette étude fera avancer l'étude du couplage des mécanismes microscopiques à la rupture de l'artère dans son ensemble.

Cette méthode de reconstruction numérique de l'état mécanique à micro-échelle a d'abord été évaluée par rapport à des expériences menées sur les artères carotides de lapins, et a été publiée dans le journal of *Biomechanics and Modeling in Mechanobiology* (doi : <https://doi.org/10.1007/s10237-019-01161-1>)

4.2 Abstract of the chapter

Abdominal Aortic Aneurysm is a prevalent cardiovascular disease with high mortality rates. The mechanical response of the arterial wall relies on the organizational and structural behavior of its micro-structural components, thus a detailed understanding of the microscopic mechanical response of the arterial wall layers at loads ranging up to rupture is necessary to improve diagnostic techniques, and possibly, treatments. Following the common notion that adventitia is the ultimate barrier at loads close to rupture, in the present study, a finite element model of adventitial collagen network was developed to study the mechanical state at the fiber level under uniaxial loading. Image stacks of the rabbit carotid adventitial tissue at rest and under uniaxial tension obtained using multi-photon microscopy were used in this study, as well as the force-displacement curves obtained from previously published experiments. Morphological parameters like fiber orientation distribution, waviness, and volume fraction were extracted for one sample from the confocal image stacks. An inverse random sampling approach combined with a random walk algorithm was employed to reconstruct the collagen network for numerical simulation. The model was then verified using experimental stress-stretch curves. The model shows the remarkable capacity of collagen fibers to uncrimp and reorient in the loading direction. These results further show that at high stretches, collagen network behaves in a highly non-affine manner, which was quantified for each sample. A comprehensive parameter study to understand the relationship between structural parameters and their influence on mechanical behavior is presented. Through this study, the model was used to conclude important structure-function relationships that control the mechanical response. Our results also show that at loads close to rupture, the probability of failure occurring at the fiber level is up to 2%. Uncertainties in usually employed rupture risk indicators and the stochastic nature of the event of rupture combined with limited knowledge on the microscopic determinants motivate the development of such an analysis. Moreover, this study will advance the study of coupling microscopic mechanisms to rupture of the artery as a whole.

This method of numerical reconstruction of the micro-scale mechanical state was first evaluated against experiments conducted on rabbit carotid arteries, and was published in

the journal of Biomechanics and Modeling in Mechanobiology (doi: <https://doi.org/10.1007/s10237-019-01161-1>)

4.3 Introduction

Aortic aneurysm can be identified as a focal dilation of the blood vessel in comparison to the normal, healthy artery [MBBS et al., 2011, Humphrey and Holzapfel, 2012a]. Aortic aneurysms are found to fail in two ways: dissection and rupture, mechanical phenomena that occur when the wall stress exceeds the local strength of the artery [Humphrey and Taylor, 2008a]. This fatal condition has been reported to have a mortality rate of up to 85% in western countries [Erhart et al., 2014, Robert et al., 2017]. Maximum vessel diameter and diameter increase rate are the clinical indicators used for decision making. Peak wall stress is also an indicator often promoted for predicting rupture [Marini et al., 2012b, Gasser et al., 2010b]. However various cases have been recorded where the above indicators fail to predict aortic rupture. This might be due to the fact that these indicators are based on the macroscopic mechanical state of the tissue and do not take into consideration the mechanics at the micro-level, and the local strength of the tissue. Hence, in order to better understand the mechanical phenomena responsible for rupture, an accurate description of the mechanical response at the level of the micro-structure is needed. Structurally accurate computational models of arterial wall layers are still an improving aspect of arterial mechanics and any step forward would be very significant.

The current paper focuses on the tunica adventitia, which is the outermost layer of the arterial wall. The adventitia primarily consists of a dense network of collagen type-I fibers, a small amount of elastin fibers, fibroblasts, nerves, vasa vasorum, and connective tissue [He and Roach, 1994]. The collagen fibers in the adventitia tend to have a complex organizational structure with highly dispersed orientations, and undulations in their unloaded configuration [Smith et al., 1981]. In contrast, the fibers in the tunica media, the middle layer, are less undulated and highly aligned towards the circumferential direction [Wolinsky and Glagov, 1967b]. The distribution and organization of collagen in the adventitia gives the layer its unique structural integrity. The adventitia serves various functions like anchoring the wall to the surrounding tissue, supplying necessary nutrients and oxygen through vasa vasorum, and synthesizing collagen through fibroblasts. But, the main function of the adventitia is to protect the arterial wall from over-distention and rupture, i.e. is to act as a protective sheath at loads beyond physiological pressure [Humphrey, 2002]. This is facilitated by the fact that the elastic modulus of collagen fibers is much higher than that of elastin [Oxlund and Andreassen, , Viidik et al.,]. As the pressure increases, collagen fibers in the adventitia get straightened and become stiff to carry the load. Hence, the overall tissue mechanical response is highly dependent on the microscopic structural organization of collagen as illustrated in figure 4.1.

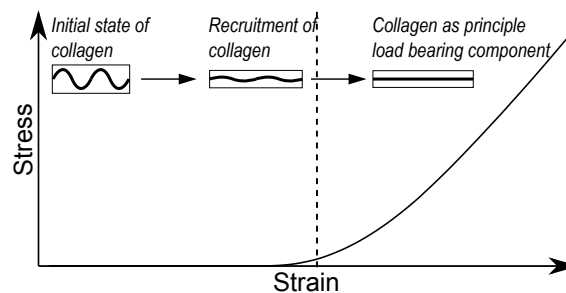


FIGURE 4.1 – Mechanical behavior of collagen under uniaxial tension

Numerical models provide an alternate means to study the evolution of abdominal aortic aneurysm and understand rupture as they are non-invasive and time efficient. Initial ad-

vances in developing a computational model for the arterial wall gave rise to the realization that, due to the non-linear, anisotropic stress-strain behavior, mathematical descriptions in the form of exponential, polynomial or logarithmic functions are needed to extrapolate the experimental results to full range of in-vivo loading conditions [Wagenseil and Mecham, 2009b]. This type of modeling technique where a strain-energy density function is deployed to compute stresses is called phenomenological modeling. Phenomenological models vary in terms of their choice of strain-energy density function and the number of parameters. These parameters are later fit using non-linear regression methods with a comparison to experimental data. Some of the widely used phenomenological models include: seven-parameter polynomial [Vaishnav et al., 1973], four-parameter logarithmic model [Takamizawa and Hayashi, 1988], four-or seven-parameter exponential models [Chuong and Fung, 1983b]. Humphrey made a detailed comparative study of the strain energy functions proposed in above-mentioned literature [Humphrey, 1999]. Although phenomenological models predict the behavior of the tissue accurately they do not account for any structural information. This leads to difficulties in studying and predicting the behavior of diseased arteries where changes in physiology and pathology directly influence the mechanical behavior [Alford et al., 2008].

On the other hand, structurally-motivated constitutive models incorporate the contributions of individual micro-structural components in the strain energy density function [Zulliger and Stergiopoulos, 2007a]. A number of researchers investigated structural constitutive models, which can be broadly classified into two categories – the angular integration approach and the structural tensor approach [Gasser et al., 2006b]. Improving on their existing physiological exponential model [Holzapfel and Weizsäcker, 1998] used for predicting the behavior of arterial walls in the physiological pressure range, Holzapfel et al. proposed a structural model for individual layers of the arterial wall. Two structural tensors each representing a family of collagen fibers are used to model the anisotropic behavior of collagen. Collagen is assumed to be embedded as parallel fibers within each family, which is limited by the fact that collagen is dispersed in the arterial wall and does not maintain a fixed orientation at no distention state. A generalized structure tensor was introduced by Gasser et al. to address the above limitation [Gasser et al., 2012b]. More recently, based on their experimental findings, a bi-variate Von-Mises distribution to define the structural tensor was implemented in [Polzer et al., 2013]. Angular integration approaches, on the other hand, utilize a probability distribution for the fibers to be incorporated directly into the strain energy potential [Gasser et al., 2006b, Holzapfel et al., 2014b]. In [Alastrué et al., 2010], a Bingham distribution for collagen was used to statistically model the mechanical response of the arterial wall within the angular integration framework. A detailed study made in [Holzapfel et al., 2015b] and [Cortes et al., 2010b] to evaluate these two approaches concluded that both approaches yield significantly different results at high fiber dispersion and for different loading conditions. Although these formulations are straightforward and offer significant computational advantages, the parameters are often derived using an inverse approach rather than a histology study, like in purely phenomenological approaches. In addition, the structural organization arising from crimp is not directly considered from such analysis.

Another important structural aspect of fibrous tissues is the presence of waviness and the phenomenon of fiber recruitment. A few of the existing micro-structural constitutive models assume a wave shape for the collagen crimp and incorporate it at either the fibril or molecular level. Lanir pioneered this work [Lanir, 1979, Lanir, 1983b] by laying out the theoretical framework for modeling collagen fiber as a two-dimensional wave, with statis-

tical distributions for either the wave shape or crimp behavior. This work was followed by the idea of modeling collagen crimp as a stochastic parameter [Cacho et al., 2007] and motivated further works which adopted it for constitutive modeling of various fibrous soft tissues [Zulliger and Stergiopoulos, 2007a, Hurschler et al., 1997]. Assuming a wave-like structure for the shape of crimped collagen fibers was also considered for discrete models by introducing kinematic linkages between small straight fiber segments [Stouffer et al., 1985, Kastelic et al., 1980, Diamant et al., 1972]. Owing to the ambiguity in observing the shape of collagen crimp from experiments, Beskos et al [Beskos and Jenkins, 1975] proposed a cylindrical helix to represent it and derived a constitutive model based on this assumption. Being the first to model the collagen crimp as a smooth 3-D wave, the model was riddled with limitations, one of which was the assumption of fiber in-extensibility resulting in an infinite stiffness at full extension. Several authors extended the model by modifying the fiber response with simple [Freed and Doehring, 2005] or more refined assumption like that of beam deformation [Grytz and Meschke, 2009]. These models were shown to be capable to reproduce stress-stretch responses of fibrous tissues in uniaxial tension, but their outputs in terms of micro-structural geometry were not completely in agreement with experimental observations. In this context, the advantage of a discrete numerical model would be to consider the kinematics of fibers at a local and individual level, thus enabling non-affine transformation, and possible local interactions. Multi-scale homogenization method constitutes another class of models to be mentioned. They incorporate collagen crimp at either the fibrillar level or the fiber level also as a function of strain [Marino and Vairo, 2014, Bianchi et al., 2016]. In the framework of arterial mechanics, these models have provided novel insights in various scenarios, especially in rupture prediction, however, they often assume an average value of the constitutive parameter for the whole wall, thus neglecting local heterogeneities. Discrete models are suitable to address this limitation and motivated the presented work.

Another way of studying micro-mechanics of homogeneous fibrous networks is to incorporate the network geometry into the model. One approach for incorporating structural information of the fiber network can be achieved through image processing, in which the desired network is segmented from the images and skeletonized [Krauss et al., 2012b]. Instead, numerically generated random fiber networks have been instrumental in studying the mechanics of large network models like collagen gels, carbon nanotubes, polymer networks, etc. [D’Amore et al., 2010b, Spanos and Esteva, 2009b, Lake et al., 2012b, Zhang et al., 2012]. The mechanical behavior of human amnion was modeled and predicted using a discrete network model by ensuring geometric and stiffness percolation [Mauri et al., 2016, Bircher et al., 2017]. Commonly used methods like Voronoi tessellations, Delaunay triangulations and other tessellations resulting from similar construction principles are not ideal for studying complex structures such as the adventitia. This is due to the fact that even though the structural arrangement of fibers in the adventitia is random, it can be identified by a stochastic process with proper geometrical implications. This is necessary as the mechanical response of the structure is highly sensitive to the microscopic arrangements of the fibers. More recently, random walk algorithms have been used to model fiber networks in fibrous bio-materials and arterial wall layers [Jin and Stanciulescu, 2016c]. Although the approach presented by Jin et al. in [Jin and Stanciulescu, 2016c] utilized morphological parameters like orientation and waviness to describe the fiber network, the model fails to address some important aspects related to morphology and kinematics. Firstly, the assumption of realizing the collagen network to be made up of two families of fibers with identical mean orientations about the axis with an equal percentage of fibers in both fam-

ilies for adventitia. Upon investigation of several second harmonic generation microscopy image stacks of adventitia, we observed that this is not the case where sometimes even the presence of two families of fibers is indistinguishable. Secondly, the assumption that the underlying kinematics of the fibers follow an affine transformation is perhaps inaccurate. Random fiber networks such as collagen in the adventitia are shown to not necessarily undergo affine kinematics [Krasny et al., 2017b, Chandran, 2005]. These factors pose some important questions to be addressed, which motivated us in developing a discrete model generated based on experimentally-measured orientation distributions, and including features to enable and control non-affinity of the network’s transformation, similar to the previous works [Mauri et al., 2016]

Hence, the main objective of this paper is to bridge the gap by combining the above mentioned numerical reconstruction methods with a thorough histological analysis and stochastic quantification of the micro-structure, with the aim to study the micro-scale mechanical state of such fibrous tissues. The interactions between neighboring fibers, and between fibers and the ground matrix are not included in the model. The possible contribution of the matrix on the mechanical response of the tissue is in the form of hydrostatic pressure developing with stretch [Lanir, 1979]. The assumption to exclude any interactions between the ground matrix and fibers was shown to be a valid one by some studies [HARKNESS and HARKNESS, 1959, Daly, 1969]. The present study was based on experimental data previously obtained on rabbit carotid arteries using multi-photon confocal microscopy and uniaxial tension testing [Krasny et al., 2017b]. Herein, we hypothesized that the parameters which influence the passive mechanics of the adventitial fiber network are: orientation, waviness, volume fraction, diameter and elastic modulus of the fibers. Note that the study was limited to the mechanics of the collagen network in the adventitia – most relevant in studying extreme loading scenarios – neglecting the effects of other micro-structural components. This choice lied onto the common hypothesis that at high loads beyond physiological pressure levels, collagen acts as the principal load-bearing component in the arterial wall. Through thorough histological analysis, the morphological parameters were quantified for one sample. Next, discrete network modeling was implemented for reconstructing the collagen fiber network which was further used as an input for numerical (Finite Element, FE) simulations of uniaxial tension tests. A constrained optimization problem was defined to identify constitutive (and morphological, if missing) parameters for various samples. After finding a good agreement for the macroscopic mechanical behavior, the microscopic mechanical state was quantified and analyzed. Finally, an extensive sensitivity analysis was performed to establish the relationship between (i) the selected mechanical outputs and (ii) each of the governing constitutive/morphological parameters, thus providing insight to discuss structure-to-mechanics relationships in adventitial tissue. A brief discussion on the non-affine nature of fiber kinematics is provided based on the obtained results. And finally, utilizing the result of the mechanical state of the fibers at various load levels, a possible probabilistic tool for understanding the onset of rupture is presented.

4.4 Methods

4.4.1 Experimental data and analysis

All the data that were used to develop and validate the finite element model were acquired from experiments on carotid arteries from male New Zealand White rabbits which were

previously published [Krasny et al., 2017b]. Briefly, the initial pre-stretch condition of the excised samples was assessed by measuring in vivo and ex vivo lengths promptly after harvesting. The excised samples were frozen until the day of the experiment at -20°C and then unfrozen in a phosphate-buffered saline solution at an ambient temperature of 24°C . It should be noted that the mechanical tests were conducted at a temperature less than the one in-vivo, which might possibly stiffen the arterial wall [Zemanek and Michal,]. Also, it was evident from the literature that freezing the arteries also induces mechanical and structural changes, but there is no consensus as to what kind of histological changes happen [Stemper et al., 2007b, Venkatasubramanian et al., 2006b, Chow and Zhang, 2011b]. A better understanding of these changes requires a more in-depth examination, perhaps with the aid of better imaging techniques, which was not carried out during the experimental study. However, all the samples were stored and tested under similar conditions. Cylindrical sections of length 10 mm were cut out from the arteries and cut open along the longitudinal axis to form rectangular sections of approximately 5mm width. In the present study, the following data from these experiments were used: multi-photon microscopy imaging in the initial no-load state, and the mechanical testing curves (uniaxial tests in in-plane circumferential, axial, and diagonal directions).

4.4.1.1 Image acquisition

Multi-photon microscopy images of the arterial specimens at zero load state were acquired with a Nikon A1R MP plus microscope. The excitation wavelength was set to 870 nm for optimal adjustment of auto-fluorescence and second-harmonic generation (SHG) signals. Microscopic images of the tissue were obtained, with the adventitial side facing the objective of the microscope (see Fig. 2). The images were acquired at an imaging resolution of $0.5\ \mu\text{m}$ in each direction with an imaging window of $512 \times 512\ \mu\text{m}^2$. The depth of the scan, which depended on the quality of the signal in response to the pulsed laser beam, varied in the range of 60-90 μm . The total acquisition time for each stack with a scan speed of 2 frames per second, with two-frame averaging, took about 20-30 minutes.

4.4.1.2 Image processing

In order to develop a structurally accurate FE model of the adventitia, it is pivotal to study histology, to identify morphological parameters which define the structure, and to quantify those using reasonable stochastic formulations. Hence, the image stacks representing the collagen (SHG signal) were analyzed to extract relevant quantitative information regarding orientation, waviness, volume fraction, and diameter of this fibrous component.

The global orientation of a collagen fiber can be quantified with two parameters, polar angle ϕ , which is the angle with respect to the axial-radial plane, and azimuthal angle θ , which is the angle in the circumferential plane. Previous studies [Humphrey, 2002, Wagenseil and Mecham, 2009b] showed that the orientation of collagen fibers in the axial-radial direction is negligible. Subsequently, we only focused on extracting the orientation of fibers in the axial-circumferential plane. The images were analyzed using an FFT analysis, which was previously utilized in studying the global orientation of collagen in the arterial wall [Polzer et al., 2013, Polzer and Gasser, 2015b]. A total of 10 slices through a depth of 100 microns were analyzed and the measured azimuthal angles θ were averaged for all analyzed sections to obtain the orientation of collagen. The orientation distribution of fibers in the micro-structure was then fit using a finite mixture of Von-Mises distributions given by equations 1 and 2, in order to later generate a numerical network by inverse

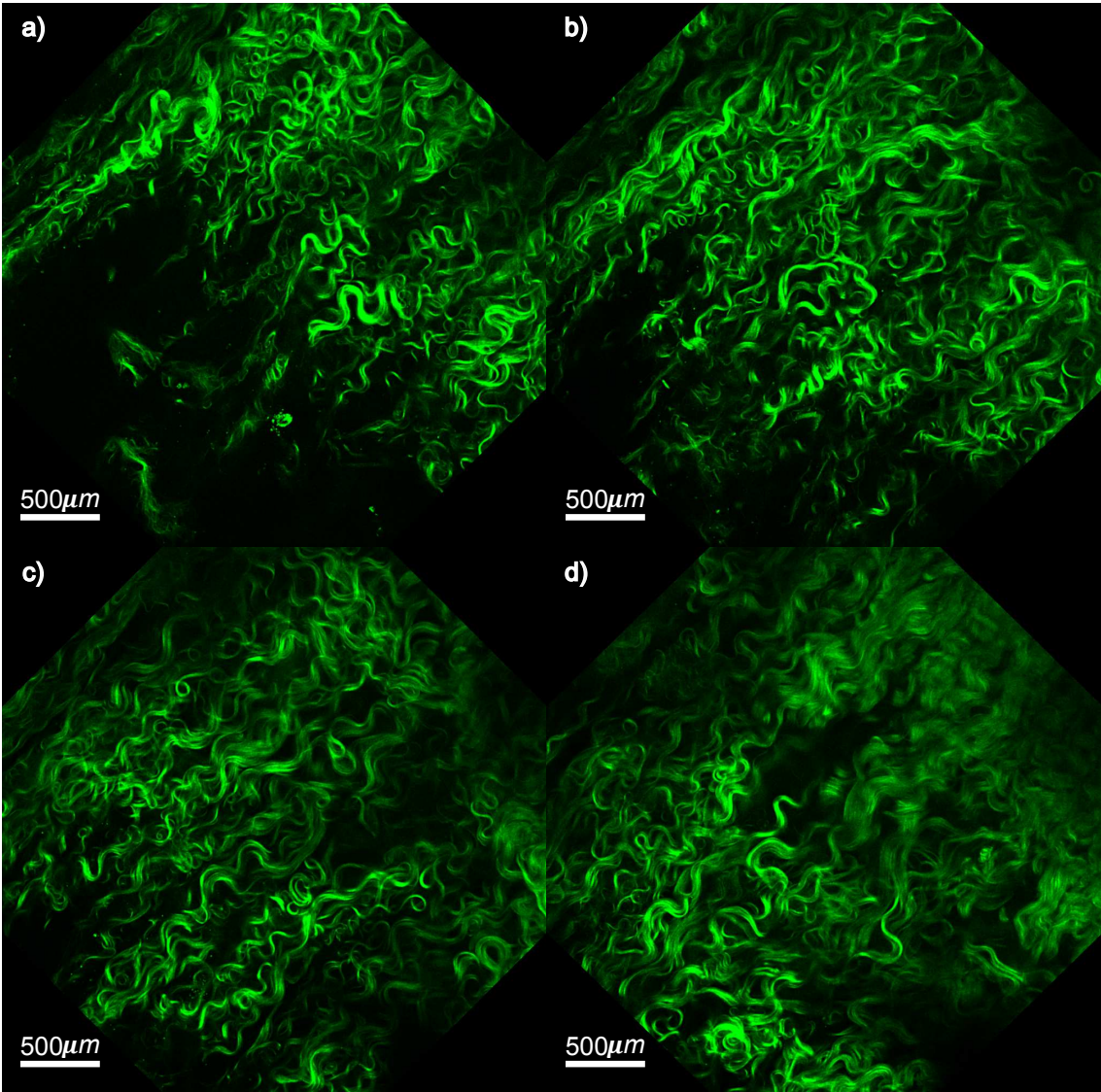


FIGURE 4.2 – (a-d) Multi-photon microscopy images of adventitial collagen at depths of $25\mu m$, $50\mu m$, $75\mu m$, and $100\mu m$ through the micro-structure

random sampling.

$$f(\theta|\mu_1, \mu_2, k_1, k_2, p) = p \frac{e^{k_1 \cos 2(\theta - \mu_1)}}{\pi I_0(k_1)} + (1 - p) \frac{e^{k_2 \cos 2(\theta - \mu_2)}}{\pi I_0(k_2)} \quad (4.1)$$

$$I_0(k) = \frac{1}{\pi} \int_0^\pi e^{k \cos \theta} d\theta \quad (4.2)$$

where k_1 and k_2 are the concentration parameters defining the dispersion of each family of fibres, μ_1 and μ_2 are the mean orientation angles, and $0 < p < 1$ is assigned to define the weight of each distribution. Finally, $I_0(k_1)$ and $I_0(k_2)$ are zero order Bessel functions of type I given by equation 2, which act as a normalization parameter such that:

$$\int_0^\pi f(\theta|\mu_1, \mu_2, k_1, k_2, p) d\theta = 1 \quad (4.3)$$

If k is small, the distribution tends to be uniform, whereas for very high values of k the distribution assumes a Dirac-delta function. As the value of k increases, the distribution approaches a Gaussian distribution with mean μ and variance $\frac{1}{k}$. Von-Mises distribution is π -periodic such that $f(\theta) = f(\theta + \pi)$. By varying the mean and concentration parameters, the above function can represent a wide range of collagen organizations, which can be used in modeling collagen networks in these tissues.

Collagen fiber waviness defines the initial crimp in the model and partially controls the strain at which collagen is recruited under loading, therefore it is significant in network reconstruction. For this reason, all the images of the stack were analyzed semi-automatically to obtain fiber characteristics such as end-to-end length (l_s), and crimped length (l_c). These parameters were measured using ImageJ tracing and measuring tools, which was also demonstrated by Rezakhaniha et al. [Rezakhaniha et al., 2012] using NeuronJ, an ImageJ plugin for neurite tracing and analysis. The waviness of a collagen fiber is then defined by equation 4.

$$W = \frac{l_s}{l_c} \quad (4.4)$$

As the above equation suggests, W has a lower bound of 0 and an upper bound of 1. The higher the value of W , the straighter the fiber is. A value of 1 indicates that the fiber is not undulated. A beta distribution was used to characterize waviness distribution in the imaged sample. It consists of a continuous probability density function defined by equation 5, where α and β are shape parameters, and $C(\alpha, \beta)$ is the normalizing constant. Maximum likelihood estimation was used to obtain the parameters of orientation and waviness distributions.

$$f(W, \alpha, \beta) = C(\alpha, \beta) W^{\alpha-1} (1-W)^{\beta-1} \quad (4.5)$$

The result of using a finite mixture of Von-Mises distributions is illustrated in figure 4.3a. The resulting parameters from the identification process were $\mu_1 = -38.7^\circ$, $k_1 = 8.32$ and $\mu_2 = 40.7^\circ$, $k_2 = 10.03$, and $p = 0.31$. Similarly, the resulting probability density function for waviness with $\alpha = 15.78$ and $\beta = 6.21$ from the fitting process is illustrated in figure 4.3b.

To estimate the amount of collagen in the micro-structure, a semi-automatic segmentation analysis was conducted in ScanIp[®], a core image processing platform of the commercial software Simpleware[®]. As a first step, the images obtained from confocal microscopy

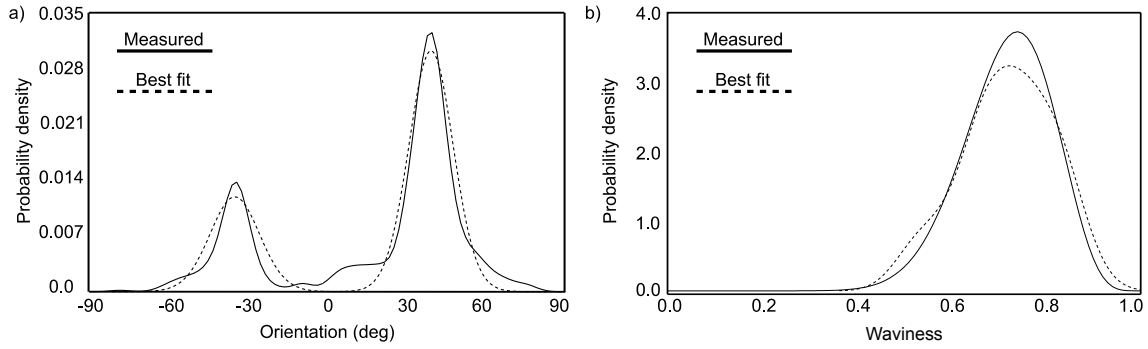


FIGURE 4.3 – Measured vs identified probability density function for a) orientation of collagen, b) waviness of collagen

are pre-processed in order to enhance the contrast of the fibers and diminish the background. The main segmentation step was realized with utilizing an array of path-finding algorithms (shape detection, fast marching, geodesic active contours, etc). Seed points were defined manually by the user to track the fibers in the image stack following which the segmentation was achieved by solving a global optimization function specific to each algorithm used, which is based on the energy. Even though the segmented network could not be used to run a full-scale finite element analysis, it was used to approximately estimate the collagen content. An average value of 8 semi-automatic segmentations was taken as the representative volume fraction of collagen. This was done by taking the ratio of segmented volume to envelope volume, which yielded a volume fraction of $36.4 \pm 2.57\%$. The obtained value of volume fraction is in accordance with the reported values in the literature [Chen et al., 2016a, Chen et al., 2011].

4.4.1.3 Mechanical testing

As mentioned in the above section, harvested arteries were used to perform uniaxial tension tests in three in-plane directions: circumferential, axial, and diagonal [Krasny et al., 2017b]. For this purpose, the samples were cut into a dog-bone shape. The cross-sectional area of the resulting strips was measured to be about $0.5 \pm 0.1 \text{ mm}^2$. A high precision tensile machine (Deben[®] Microtest tensile/ compression stage) with a load cell capacity of 150N and a precision of 0.01N was used for the uniaxial tensile tests. Before conducting the test, each sample was subjected to quasi-static triangular preconditioning. Following this step, the width of the tissue in the unloaded configuration was recorded four times and averaged. Uniaxial tension was then carried out at a controlled displacement until a target tensile force of 1N was reached. The force measured at every loading state allowed the computation of first Piola-Kirchoff stress $\sigma = \frac{F}{A_0}$, where F is the force at a given displacement and A_0 is the initial cross-section area. The stretch was measured based on the inter-clamp lengths measured at the initial state, which serves as the reference configuration, and at a given load [Krasny et al., 2017b]. For a more detailed understanding of the uncertainties arising from the experimental protocols, we direct the reader to [Krasny et al., 2017b]. The obtained stress-stretch curves will be later used to identify model parameters and further validation.

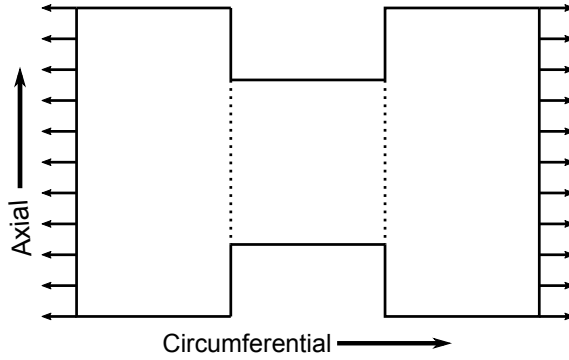


FIGURE 4.4 – Schematic representation of the uniaxial tensile test sample

4.4.2 Mechanical model

4.4.2.1 Assumptions

The following assumptions were taken into account in building and analyzing the mechanics of the model:

1. Each fiber was assumed to be a sinusoidal curve; made up of segments of length l_{seg} , whose direction of propagation is defined by a global orientation θ and local orientation θ_{rel} .
2. For each fiber, the global mean orientation was defined by the finite mixture of Von-Mises distributions given by equation 1.
3. The waviness of the fibre W was introduced by θ_{rel} such that $W = \cos(\theta_{rel})$.
4. The polar angle of the fibers, which is the angle out of the axial-circumferential plane was assumed to be negligible for the reconstruction.
5. Every fiber was assumed to have its ends intersect the boundaries of the defined volume, such that no fiber lies dangling inside the volume. This assumption stems from the observations made on the micro-structure of the adventitia under the confocal microscope of different arterial tissues. It was noted that the length scale of a collagen fiber is much larger than the field of view employed for this study, which is $500\mu m$.
6. For global orientations of each sample, a similar probability density function with constant mean orientations and varying standard deviation was used to generate the network.
7. All the fibers were assumed to have the same diameter, instead of a distribution.
8. For the mechanics, only the collagen fiber network was simulated and analyzed. On the other hand, mechanical tests were performed on the whole tissue

4.4.2.2 Numerical network reconstruction

Motivated by the work of Jin et al [Jin and Stanciulescu, 2016c] and Mauri et al [Mauri et al., 2016], we defined the collagen fiber network as a discrete line network with each fiber represented as a worm-like chain, with a uniform diameter of $10\mu m$ [Carlisle et al., 2010b, Sherman et al., 2015b] for each fiber. This assumption was supported following

a pore size analysis conducted on image stacks using a template matching algorithm as described by Krauss et al [Krauss et al., 2012b]. The radius was taken to be the most probable value from the distribution of radius of fibers inside the tissue as shown in figure 4.5 a. This enforced more support to the scale at which the mechanics of the collagen network are being studied. In this respect, a distinction can be made between the fibril and fiber scales based on the recorded diameter values [Ushiki, 2002]. It was also observed that at initial state some fibers tend to coalesce into bundles, which later separate upon application of load.

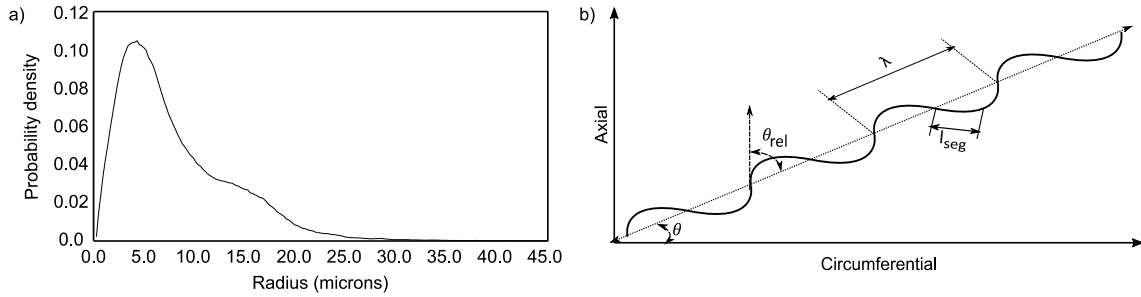


FIGURE 4.5 – a) Pore size radii distribution in the micro-structure, b) Schematic representation of the reconstruction algorithm

The steps followed in reconstructing the collagen network were as follows:

1. A 3-D volume of $500\mu m \times 500\mu m \times 100\mu m$ was specified to simulate the samples.
2. A uniform random distribution was used to specify the initial seed points of the fibers.
3. The orientation of each fibre $\theta \in (0, \pi)$ was inverse sampled from its defined probability density function (eq. (1)).
4. The waviness of the fiber W was inversely sampled from its defined probability density function (eq. (4)).
5. The angle of each line segment relative to the fiber's mean orientation, θ_{rel} , was computed based on the fiber waviness.
6. The fiber was propagated with segments of length l_{seg} , which is the average wavelength measured from images, in opposite directions from the initial seed point until both ends meet the boundary of the volume.
7. Steps 2-6 were repeated until the desired fiber volume fraction was achieved.

A schematic of the above-mentioned fiber parameters is shown in figure 4.5 b. The polar angle of the fiber was assumed to be insignificant and hence not considered in the reconstruction process. The parameter θ_{rel} captures the waviness of fiber in the network. For sample $n^{\circ}4$, the morphological parameters identified directly from the images were used as input, whereas for other samples an inverse approach based on the tensile stress-stretch response was used to identify modulus of collagen, axial connector stiffness, volume fraction, waviness, and orientation. This has been done for two reasons: the image stacks were only available for the first four samples, and the quality of the images for the other samples at no-distention state was adjudged to be insufficient to extract any meaningful morphological information.

4.4.2.3 Finite element model

The collagen fiber network obtained from the above reconstruction process was then used as an input for FE analysis. A custom script in Matlab[®] was used to generate an input file to be imported to Abaqus[®]. It has been well documented that a pin-jointed random fiber network is stable for a coordination number of at least 4 at each joint [Picu, 2011b]. As this is not the case with the generated network, which has a coordination number of 2 at each joint, the fiber segments were modeled using 3-D beam elements in the input file generation process. In order to simulate an equivalent truss-like behavior, the ratio of axial stiffness to bending stiffness for the beams was adjusted by reducing the radius from $5\mu\text{m}$ to $0.1\mu\text{m}$ and increasing the elastic modulus proportionally, thus keeping the axial stiffness constant. The reconstructed network was meshed with 11000 B31H beam elements with the material behavior of each collagen fiber defined as incompressible and linearly elastic.

4.4.2.4 Boundary conditions

The boundary conditions imposed on the model in order to simulate the uniaxial tension experiments are shown in figure 4.6. Node sets for each face where the fibers intersect with the boundaries were created. The desired axial stretch is achieved by displacing all the nodes on one axially symmetric surface, by a value u_{circ} , while restraining the other end. To induce the effect of apparent Poisson's ratio of the sample on the network, an axial connector was introduced and coupled to the transverse displacement degree of freedom of all boundary nodes. One node of the axial connector element was displaced in the traction direction according to the affine kinematics assumption while the other node (called pivot) was free (hence only transverse displacement possible). The stiffness of the axial connector was varied to control the displacement of the pivot. This pivot was then coupled with boundary nodes of the network to control their transverse displacement. Equation constraints were used to couple each node of the circumferentially-symmetric boundary surfaces to the pivot as $u_y = \pm u_{pivot}$. Similarly, a user-defined constraint was defined to couple each node on the axially-symmetric boundary surfaces to the pivot as $u_y = (\frac{y-\frac{L}{2}}{\frac{L}{2}}) u_{pivot}$. The transverse deformation of the network was then controlled by the axial connector stiffness, a parameter of the present model. Static analyses were performed using the Abaqus Standard solver. A displacement $u_{circ} = 500\ \mu\text{m}$ (i.e a stretch of 2) was applied in the traction direction. The main output of the simulations was the force vs. stretch curve. The response was then used to compute the first Piola-Kirchoff stress $\sigma = \frac{F}{A_0}$, where F is the tensile force computed as the sum of individual fiber reaction forces (projected along the traction direction) at the elongation boundary and A_0 is the initial cross-section area.

4.4.3 Design of experiment approach for model evaluation

A reduced model of the previously presented model was constructed for two purposes. First, it was employed in an inverse identification approach to accelerate the identification of missing input parameters of samples exhibiting insufficient image quality. Second, the reduced model was used in a sensitivity analysis of the mechanical response to the main model parameters (see section below).

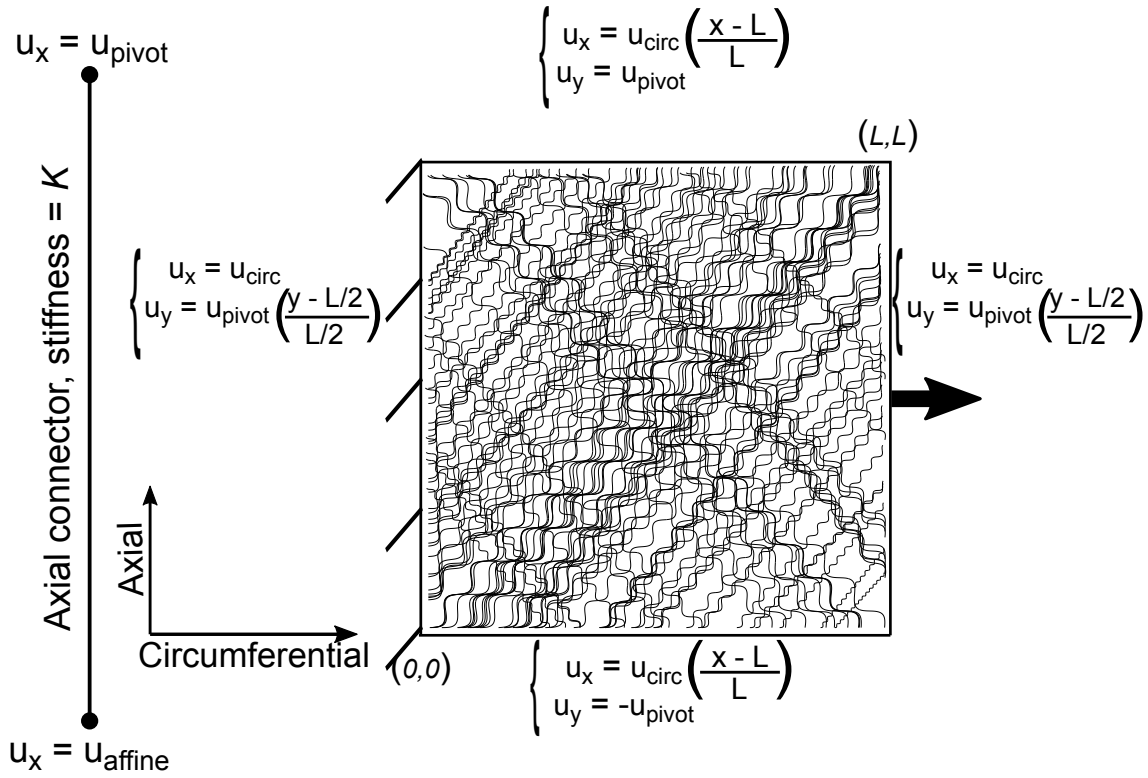


FIGURE 4.6 – Boundary conditions used for the uniaxial tension simulations

4.4.3.1 Input parameters

To build this reduced model, it was important to know the meaningful range of each parameter to be identified. All the parameters and their range of values used in constructing the reduced model are presented in table 1. The modulus of collagen employed in this model was taken from previously reported experimental data [Aifantis et al., 2011b, Dutov et al., 2016c, Kato et al., 1989b]. About 20 simulations with varying stiffness values for the axial connector were run, following which the bounds of stiffness values for the axial connector element were chosen such that the lower bound value represented a free pivot and the upper bound value asymptotically approached affine kinematics behavior. A similar literature study helped in choosing the bounds for collagen content in the adventitia and initial collagen waviness. Following the choice of bounds for each input parameter, a uniform sampling method was employed to sample input points in all dimensions of the parameter space. The principle of this technique is to partition space of m parameters into $\prod_{i=1}^m n_i$ parts, where n_i is the number of intervals the i^{th} input parameter range is divided into. Then $\prod_{i=1}^m n_i$ sets of m dimensions were created such that each set contains exactly one partition of each parameter.

A total of 7200 simulations were performed for extracting the uniaxial response and micro-scale mechanics of networks generated by varying the parameters presented in table 1. For the purpose of avoiding over-complexification, the mean fiber orientations and weight of individual distributions were not varied from the values extracted from the image stacks. Only the standard deviation was varied but assumed to be the same for both families. The standard deviation for a given Von-Mises distribution can be computed using the equation $\sigma^2 = 1 - \frac{I_1(k)}{I_0(k)}$, where k is the concentration parameter as described in section 4.4.1.2. This allowed reducing the number of parameters to be varied for orientation distribution to one in place of five and yet be able to simulate a wide range of initial network configurations.

Parameter List		
Parameter	Lower bound	Upper bound
Collagen modulus	60 MPa	300 MPa
Axial connector stiffness	$0.05 Nm^{-1}$	$20 Nm^{-1}$
Volume fraction	20%	40%
Waviness (μ)	0.67	0.83
Orientation (σ)	2.5°	10°

TABLE 4.1 – Range of input parameters

The resulting stress-stretch data from each simulation were fed to a six-dimensional gridded interpolant in Matlab[®]. The first dimension of the grid corresponded to a macroscopic stretch value, while the other five dimensions correspond to the input parameters. This helps in extracting the stress-stretch response of any configuration of parameters defined within the bounds of the input parameters.

4.4.3.2 Responses

The overall response of the micro-structure depends on the parameters used to construct the model, which are shown in table 1. In order to study the influence of varying these model parameters on the global response of the micro-structure, two independent responses of the model were specifically chosen: the final slope, and the recruitment stretch of the stress-stretch curve. The final slope response was chosen such that it is indicative of the macroscopic stress of the network. This implies that higher the final slope of the network, higher will be the global stiffness of the network. Thus the index is helpful in identifying the various possible combinations of constitutive and morphological parameters which result in stresses leading up to rupture. On the other hand, collagen recruitment is a stiffening mechanism observed in the arterial wall and other collagenous tissues and marks the onset of collagen being the principle load-bearing component. The recruitment stretch response was chosen in order to quantify the mechanical behavior of collagen in the network. There is not a lot of information in the literature as to what factors influence the recruitment of collagen. The commonly accepted notion is that the waviness of the fibers controls collagen recruitment [Hansen et al., 2002]. Thus the evaluation of this response is used to quantify the effect of other parameters on collagen recruitment.

Final slope: The final slope was computed as the slope of the stress-stretch curve comprising the final 10 % of the stretch. This index, unit of MPa, was computed for all the 7200 simulations and the result was stored as a vector $s_{final} = \{s_1, s_2, \dots, s_{7200}\}$.

Recruitment stretch: The recruitment stretch of a collagen network can be defined as the global stretch at which collagen starts to act as the major load-bearing component. The recruitment stretch was computed, in this study, as the global stretch at which the rate of change of slope was found to be the highest in the stress-stretch curve. The index for recruitment stretch is unit-less. Like for the final slope, the index was computed for all the 7200 simulations and the result was stored as a vector $\lambda_{recruitment} = \{\lambda_1, \lambda_2, \dots, \lambda_{7200}\}$

4.4.3.3 Linear and non-linear regression for sensitivity analysis

5-dimensional response surfaces s_f and ϵ_r respectively represent the final slope and recruitment stretch indices as a function of the 5-dimensional input parameter matrix (X) described by equation 6:

$$\begin{aligned} s_{final} &= s_f\{X\} + c_s \\ \lambda_{recruitment} &= \lambda_r\{X\} + c_\lambda \end{aligned} \quad (4.6)$$

where c_s and c_e are the residuals obtained during the fitting process. Each of the response surfaces was fit using regression analyses, which were performed in Matlab[®] using the in-built regression models. First, a linear regression with 5 linear terms and 1 constant term was fitted to study the global influence of each input parameter on each of the chosen indices. Then a quadratic regression with 5 linear terms, 14 quadratic terms and 1 constant term was fitted to study the interactions between input parameters for each response. Practically, each of the regression analyses utilized the whole parameter space of the reduced model. Since all parameters have different units, they were normalized on a scale of 0 to 1, where 0 corresponds to the lower bound and 1 corresponds to the upper bound of the parameter.

In order to assess the accuracy of the fitted models, two different statistical methods were used. The Root Mean Squared Error (RMSE) value and the R-Squared value were calculated for both linear and quadratic regressions. Finally, in order to assess the meaningfulness of each predicted regression coefficient, the p-value was used. Using this information, regression coefficients with an insignificant p-value ($p - value > 0.05$) were neglected and the regression analyses were performed again.

4.4.4 Identification of model parameters

The 6-D gridded interpolation function was used as a reduced model in order to speed up the identification process of the missing parameters including collagen modulus, axial connector stiffness, volume fraction, waviness, and orientation for each sample.

4.4.4.1 Validation on sample n^o4

Through a morphological analysis, we were able to extract the morphological parameters required to build the model for sample n^o4 , hence leaving us with only collagen modulus and axial connector stiffness to be identified. Using the experimental stress-stretch data, it was possible to uniquely identify these two parameters which optimize the predictive capability of the model to represent the measured behavior of the micro-structure. To do so, the geometry of the micro-structure of sample n^o4 was built following the algorithm described in section 4.4.2.2; and a genetic algorithm (MathWorks, 2015), which takes into account the initial population data for the gridded interpolants, and their input parameters as specified in table 1 was used in Matlab[®] to perform a constrained optimization. An r-squared function given by the equation below was used as the objective function to minimize the error between experimental and model force vs. stretch curves. In the equation below, n represents the number of data points where stress-stretch data was collected from the experiments. Corresponding values of stress-stretch data were computed from the gridded interpolant in order to complete the equation below. The r-square function was defined in a negative sense owing to the global minimization procedure adapted in the genetic algorithm. The constraints for the above function were given in the form of bounds for the input parameters. For the morphology parameters, the values were fixed to the extracted

data, whereas for the constitutive parameters, bounds were assigned as defined in table 1. A sufficient number of independent runs were performed in order to obtain a global minimum. Finally, once an optimal set of constitutive parameters was obtained, the model was compared with experimental data for validation.

$$R - Square = \frac{\sum_{i=1}^n (Experiment(i) - Interpolant(i))^2}{\sum_{i=1}^n (Experiment(i) - mean(Experiment))^2} - 1 \quad (4.7)$$

4.4.4.2 Identification of model parameters on other samples

Unlike for sample n^o4 , for the other 5 samples the complete input parameter set (i.e. morphological + constitutive) was inversely identified from experimental data. As described earlier, a genetic algorithm with the objective function resembling an r-squared function was used to perform the constrained optimization. In this case, the constraints were applied in the form of bounds for all parameters as defined in table 1. A series of independent runs were performed to ensure a global minimization.

4.5 Results

In order to demonstrate the predictive capability of the proposed model, the computational results obtained from the simulations were compared to experimental data of six samples of rabbit carotid arteries under uniaxial tension (previously published in [Krasny et al., 2017b]). It is interesting to note that the uniaxial tension tests were performed on the whole tissue, while the reconstructed micro-structure represents only the adventitial layer. This was done due to the fact that the depth to which confocal microscopy images could be obtained with reasonable quality was limited. This often times resulted in image stacks representing a thickness of less than $200\mu m$, while the tissue is much thicker than that. To overcome this limitation, comparisons were made on stress data, assuming homogeneous stress through the sample thickness. Also, it is interesting to note that comparisons were made beyond a high stretch value, where collagen is usually considered to be the principle load-bearing component.

4.5.1 Model Validation

First, we present the model parameters corresponding to sample n^o4 in the table below, for which only the modulus of collagen and axial connector stiffness were identified. The comparison between experimental data and the numerical response of the model is presented in figure 4.7. Note that since we are interested in the mechanical response of the collagen fiber network as opposed to the whole tissue, the relevance of comparison mainly lies in the recruitment stretch value and beyond that point, where the simulation results demonstrated an accurate prediction of the mechanical response. In this case, an r-squared value of 0.968 was obtained, which confirmed the fitting accuracy.

4.5.2 Parameter identification from experimental data

The methodology described above was applied to 5 other samples previously tested experimentally to obtain their optimum input parameter set. The parameters obtained from multiple runs of the genetic algorithm for each sample are presented in the table 3. It can

Collagen modulus	Axial connector stiffness	Volume fraction	Waviness	Orientation (σ)
297 MPa	0.955 Nm^{-1}	37.1%	0.80	3.55°

TABLE 4.2 – Optimal parameter set for sample $n^{\circ}4$

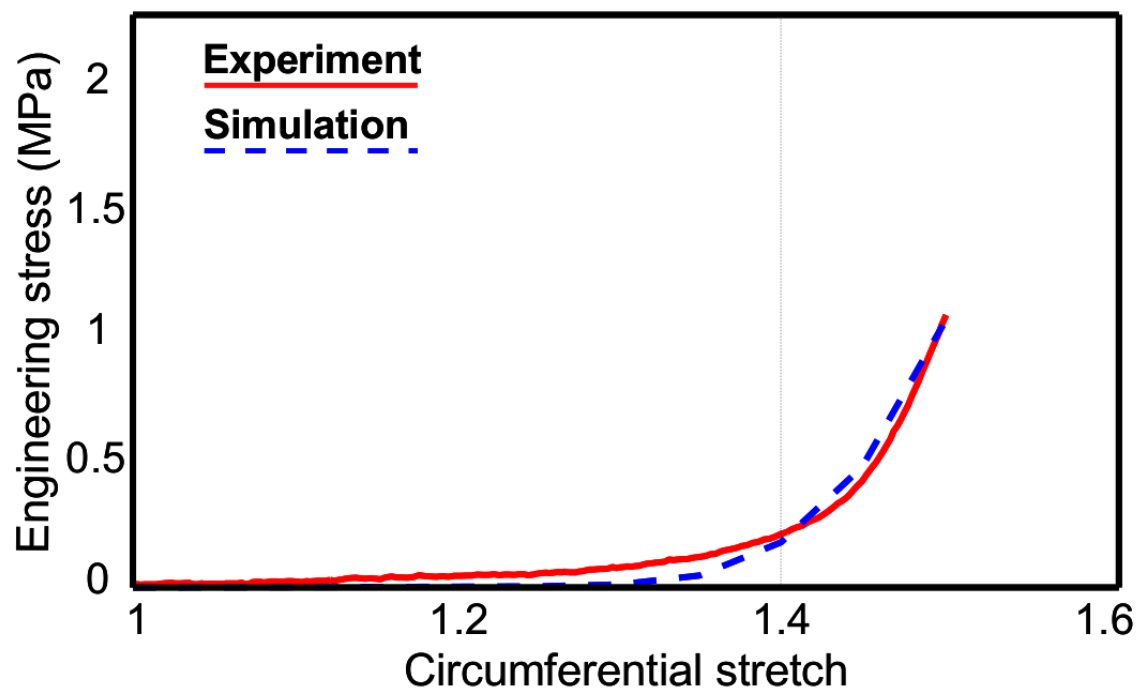


FIGURE 4.7 – For sample $n^{\circ}4$ comparison of stress-stretch results from finite element simulations with experimental data

Sample	Collagen modulus	Axial connector stiffness	Volume fraction	Waviness	Std deviation of orientation
1	163.34 MPa	1.78 Nm^{-1}	29.03%	0.757	5.21°
2	283.86 MPa	3.81 Nm^{-1}	28.53%	0.793	4.33°
3	80.64 MPa	1.06 Nm^{-1}	31.98%	0.746	5.86°
5	194.6 MPa	4.4 Nm^{-1}	36.80%	0.769	3.98°
6	70.45 MPa	1.39 Nm^{-1}	29.35%	0.757	6.16°

TABLE 4.3 – Optimal parameter set for samples 1, 2, 3, 5, and 6

be seen that all the parameters lie in their respective range without reaching range limits. The comparison between experimental data and the simulation results for these samples is shown in figure 4.8. In each case, an r-squared value above 0.9 was obtained, with a minimum obtained value of 0.92 for n^o3 . Note that the insignificant contribution of fibres to the global stress until the point of recruitment can be explained by the uncrimping process they undergo as the sample stretches. This aspect is addressed later in section 4.5.4.

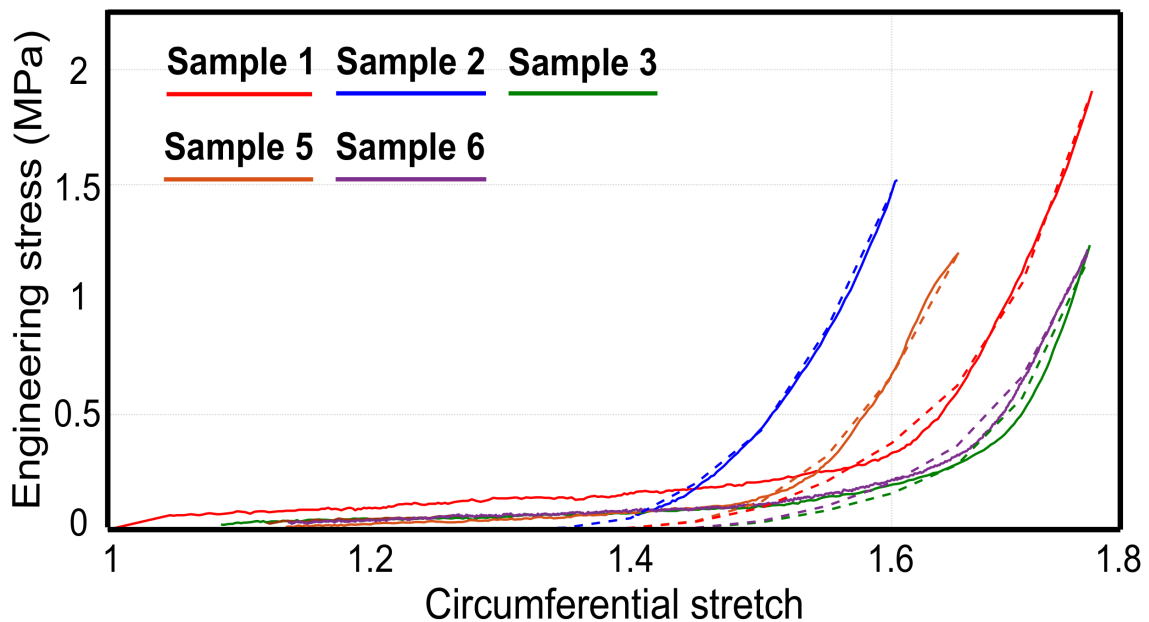


FIGURE 4.8 – Comparison of results obtained from finite element simulations with experimental data of different arterial samples

4.5.3 Sensitivity analysis

4.5.3.1 Linear model

A linear regression model with 6 terms was identified to study the linear effect of each parameter on the overall response. The linear regression model with 6 terms exhibited an RMSE value of 0.246 MPa, an r-squared value of 0.94 for final slope and an RMSE value of 0.0328, an r-squared value of 0.92 for recruitment stretch. The computed sensitivity coefficients for each output are presented in figure 4.9. The value of a coefficient signifies the amount of influence the corresponding parameter has on the response. For instance, in evaluating the sensitivity on the final slope, it was observed that modulus of collagen has the most influence. By increasing its value on the normalized scale from 0 to 1 (i.e. 60 MPa to 300 MPa) the final slope of the response increases by 7.15 MPa. On the other hand, the initial waviness in the network exhibited the most negative influence on the final slope of the response. A sensitivity coefficient of -1.92 MPa signifies that by increasing the initial waviness in the network from 0 to 1 (i.e. 1.2 to 1.45 straightness), the final slope reduces 1.92 MPa. The most influential parameter for recruitment of collagen was the initial waviness in collagen. By increasing its value from 0 to 1 on the normalized scale, stretch at which collagen is supposed to be recruited increased by 0.19. While collagen modulus, volume fraction, and orientation variance had almost no influence on collagen recruitment; axial connector stiffness displayed a slight negative influence with a sensitivity coefficient of -0.028.

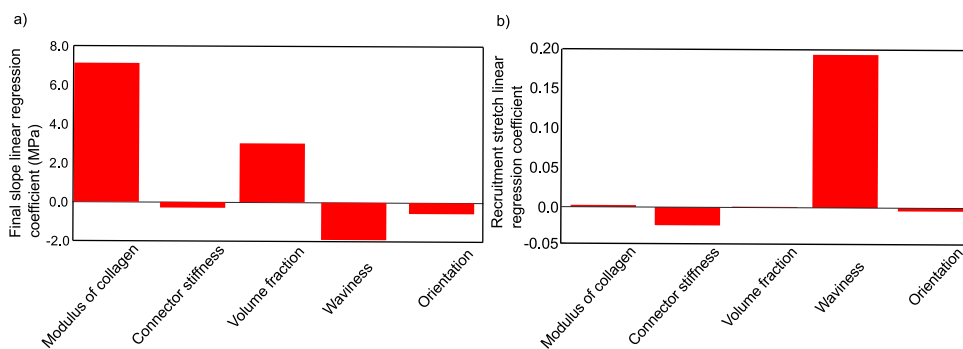


FIGURE 4.9 – Sensitivity indices from linear regression for a) final slope response, b) recruitment stretch response

4.5.3.2 Non-linear model

A non-linear regression model with 20 terms was also built to analyze the non-linear effects and interactions between parameters. An initial analysis revealed some parameters which

did not have any significance on the output (p -value > 0.05). Following this, the analysis was repeated with 18 terms for final slope and 13 terms for recruitment stretch. The non-linear regression model with 6 terms exhibited an RMSE value of 0.0889 MPa, an r-squared value of 0.992 for final slope and an RMSE value of 0.312, an r-squared value of 0.902 for recruitment stretch. The non-linear contribution of individual parameters and their interactions are presented in figure 4.10, from which they can be interpreted according to the intensity of the color plot. The coefficient values which were found to be insignificant (p -value > 0.05) are displayed in black. The quadratic terms corresponding to each parameter revealed that none of them exhibit a strong non-linear response w.r.t. both final slope and recruitment stretch. Waviness exhibited the most non-linear behavior in both cases. For the final slope response, modulus of collagen with volume fraction, and modulus of collagen with waviness exhibited significant interactions. The interaction between modulus of collagen and waviness was found to be negative, which is reasonable as they have a reciprocal influence on it. For the recruitment stretch, the interaction between collagen modulus and every other parameter was found to have very little significance, whereas axial connector stiffness and waviness showed the most interaction.

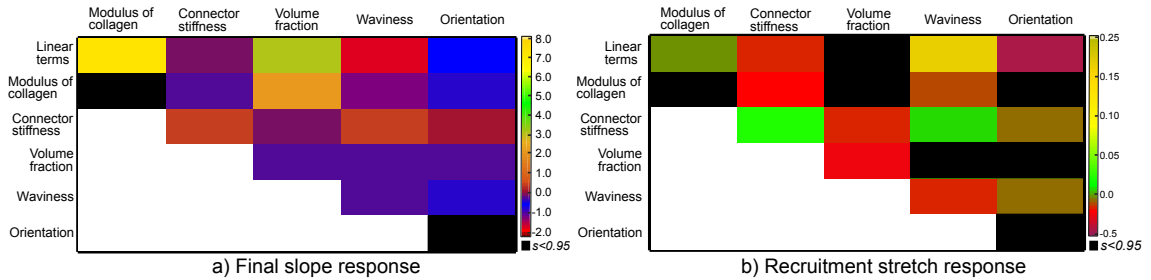


FIGURE 4.10 – Sensitivity indices from non-linear regression for a) final slope response, b) recruitment stretch response

4.5.4 Morphological changes of the fiber network

4.5.4.1 Reorientation

The mechanics of the model collagen network is completely determined by the constitutive behavior of the fibers, their waviness and orientation, and the network density. It has been well documented in the experimental literature that collagen fibers gradually reorient towards the load direction [Niestrawska et al., 2016, Krasny et al., 2017b]. To understand this behavior, the evolution of the orientation distribution of fibers was studied at various stages of loading. The orientation distribution of collagen in its initial configuration and at a maximum stretch of each sample is presented in figure 4.11 a. The analysis of fiber angles in their final configuration suggested that fibers preferred orienting themselves close to the traction direction. The dispersion of fibers was also observed to reduce as fibers tend to align towards the loading direction. The initially preferred orientations of collagen fibers with respect to the circumferential direction in all samples were approximately 40° and -40° . As the samples were stretched uniaxially in the circumferential direction, the preferred orientations changed to approximately 18° and -18° respectively. The amount of reorientation in each sample was dictated by its transverse stiffness and global stretch. This was computed as the average of percentage reorientation of all fibers in a sample. At a given global stretch, the sample identified with least axial connector stiffness underwent most reorientation. For instance, at a global stretch of 2.0 in the simulations; sample

$n^{\circ}4$ underwent the maximum reorientation of about 85.63% followed by sample $n^{\circ}3$ with 85.14%, sample $n^{\circ}6$ with 77.89%, sample $n^{\circ}1$ with 72.81%, sample $n^{\circ}2$ with 72.05%, and sample $n^{\circ}5$ with 70.62%. Nevertheless, at their respective maximum global stretches of 1.75 and 1.52 in the experiments, sample $n^{\circ}3$ underwent a maximum reorientation of about 67.45%, and sample $n^{\circ}4$ a reorientation of about 46.33 %, signifying that the axial connector stiffness bore lesser influence on the amount of reorientation as compared to the global stretch.

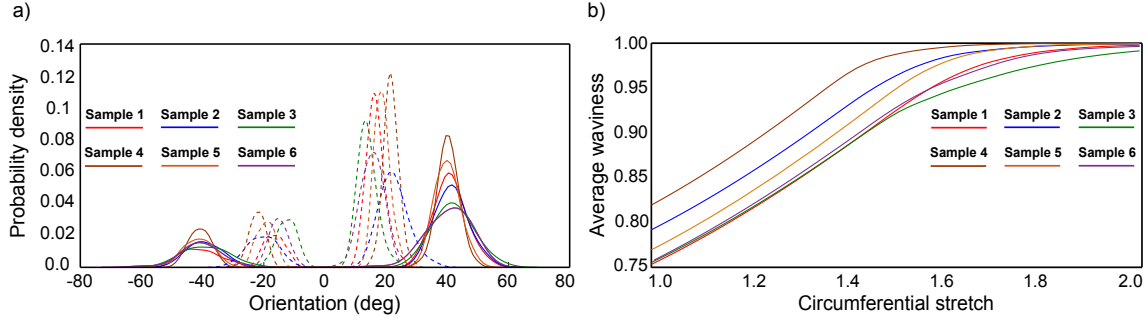


FIGURE 4.11 – a) Comparison of orientation distribution of collagen at initial state in each sample to each sample's maximum stretch state, b) Evolution of average waviness of the collagen network in all samples

4.5.4.2 Straightening

Collagen fibers which were undulated in their initial state underwent a straightening process as the load increased. It can be seen from figure 4.11 b that the average waviness in the network almost reaches 1 at high stretches. It was observed that, for some samples, even at high loads the collagen fibers remained slightly crimped. This might be due to a high initial average waviness combined with the amount of transverse displacement induced by the pivot governing transverse response. For two samples with approximately equal initial waviness, the amount of reorientation had a direct impact on the final average waviness in the model. For instance, sample $n^{\circ}3$ and sample $n^{\circ}6$ had identical initial waviness of about 0.752, which resulted in 0.984 and 0.996 respectively. In the above scenario, sample $n^{\circ}3$ had to undergo a reorientation of 85.14% whereas sample $n^{\circ}6$ underwent a re-orientation of about 77.89% signifying that the straightening process for a fiber undergoing higher reorientation is slower than for a fiber undergoing lesser reorientation.

4.5.4.3 Non-affine behavior

The morphological rearrangement of collagen also determines the apparent non-affine nature of the network deformation. A random fiber network with low network density and a high ratio of axial to bending stiffness are more compliant with non-affine behavior [Picu, 2011b]. To this effect, the computed collagen fiber displacements were used to study the apparent non-affinity in the network using a strain-based metric defined in equation 8.

$$NA(r) = \|(E - E_{affine})^2\| \quad (4.8)$$

where $E = \epsilon_1 1, \epsilon_2 2, \epsilon_1 2, \omega_1 2$ is a vector containing the strain and rotation components, E_{affine} is the corresponding affine vector. The length scale at which these strain values were probed is defined by r , which was chosen to be l_{seg} , the distance between the

crosslinks. To understand the evolution of non-affine behavior of these networks, the obtained non-affinity value was plotted against far-field stretch and reported in figure 4.12. The amount of non-affinity computed using the above method showed a clear tendency that samples with low transverse stiffness exhibited a higher non-affine behavior as compared to samples with high transverse stiffness. This can be observed to be the case from the figure where sample 4 exhibited the highest non-affinity of almost 16%, and sample 5 exhibited the lowest of about 2.5%. The reason for such a drastic difference between the highest and lowest is that for sample 5 the identified transverse stiffness corresponded to a near affine behavior. The amount of non-affinity in the network can be quantitatively analyzed at various stages of loading, which revealed a similar evolution trend in all samples. The initial phase was characterized by low non-affine values with a very gradual increase when increasing global stretch. Beyond this, the non-affinity increased considerably when increasing global stretch. The point of separation between these two phases was observed to be the recruitment stretch of collagen.

4.5.5 Analysis of the micro-macro relationship

The model was further used to analyze the micro-level mechanical state of each sample at stretches corresponding to average peak wall stress at rupture. This kind of analysis facilitates the investigation of physical quantities that are not (yet) accessible through experiments. A value of 1 MPa, representative of peak wall stress at rupture was taken from literature [Gasser et al., 2010b, Fillinger et al., 2002] and a simulation was run again for each model in order in to reach that stress value and study the corresponding mechanical state of the fiber network.

The microscopic strain distribution in fibers for each sample at this macroscopic stress of 1 MPa is shown in figure 4.13. It is possible to observe from the histograms that majority of the fibers in each sample underwent an axial strain of less than 5%. Samples 1, 3, and 6 exhibited axial strains of more than 10% in several fibers. It is possibly a result of high macroscopic stretch required for each of these samples to achieve stress of 1 MPa. It should also be observed that these three samples were identified with relatively lower values of collagen modulus and higher values of initial collagen waviness. From the sensitivity analysis conducted, it was found that these two parameters bear the most influence on the final slope response. Samples 2, 4, and 5, which were identified with high collagen modulus and low initial waviness, had all fibers with an axial stretch less than 10%. Thus it can be concluded that axial strain in individual collagen fibers at a given macroscopic stretch depends indirectly on their elastic modulus and initial crimp.

A similar analysis of the microscopic stress distribution of fibers at macroscopic stress of 1 MPa is shown in figure 4.14. It can be noticed that even though samples 3 and 6 have been identified with a relatively low elastic modulus, the fibers exhibit high-stress values. This is possibly due to the fact that they exhibit high axial strains in fibers as noted in figure 4.13. Although it might be imperative to conclude interesting remarks about fiber rupture based on these stress values, the heterogeneity in the material constitutive parameters should be noted. There is not enough data in the literature to facilitate such an analysis. Hence, only strain distributions were used as will be described in section 4.6.5.

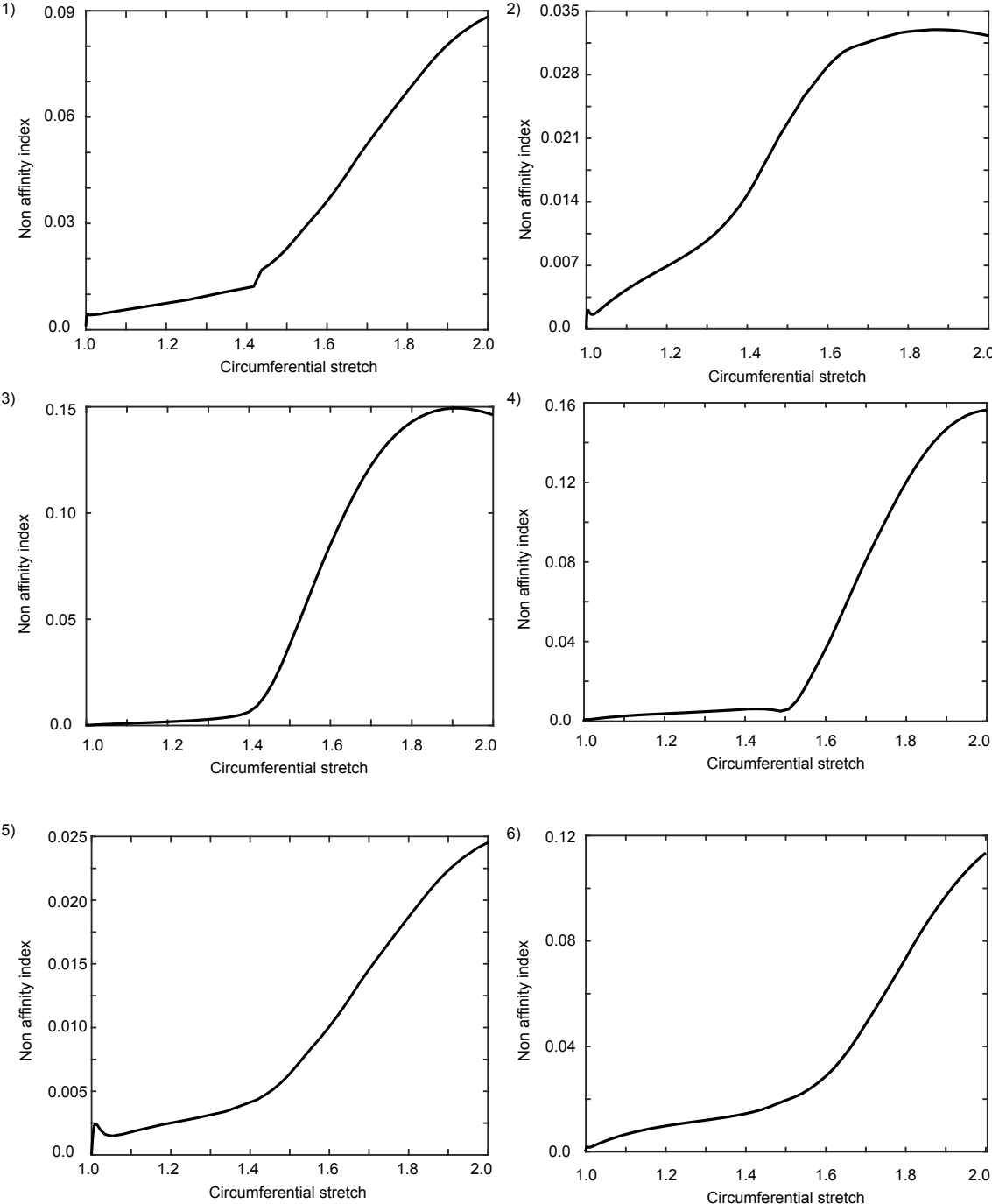


FIGURE 4.12 – Evolution of Non-affinity index with stretch computed for all samples

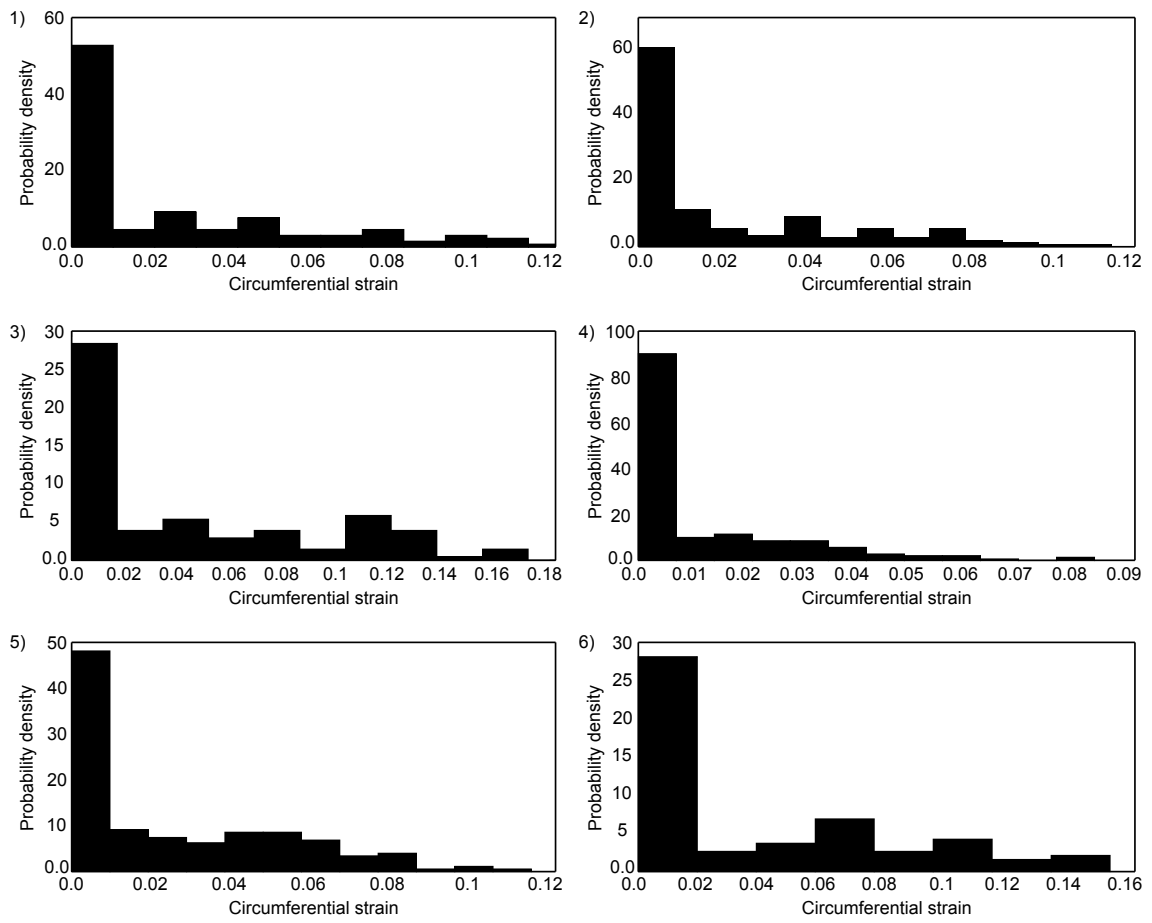


FIGURE 4.13 – (1-6) Distribution of axial strain in collagen fibres in each sample computed at a global stress of 1 MPa

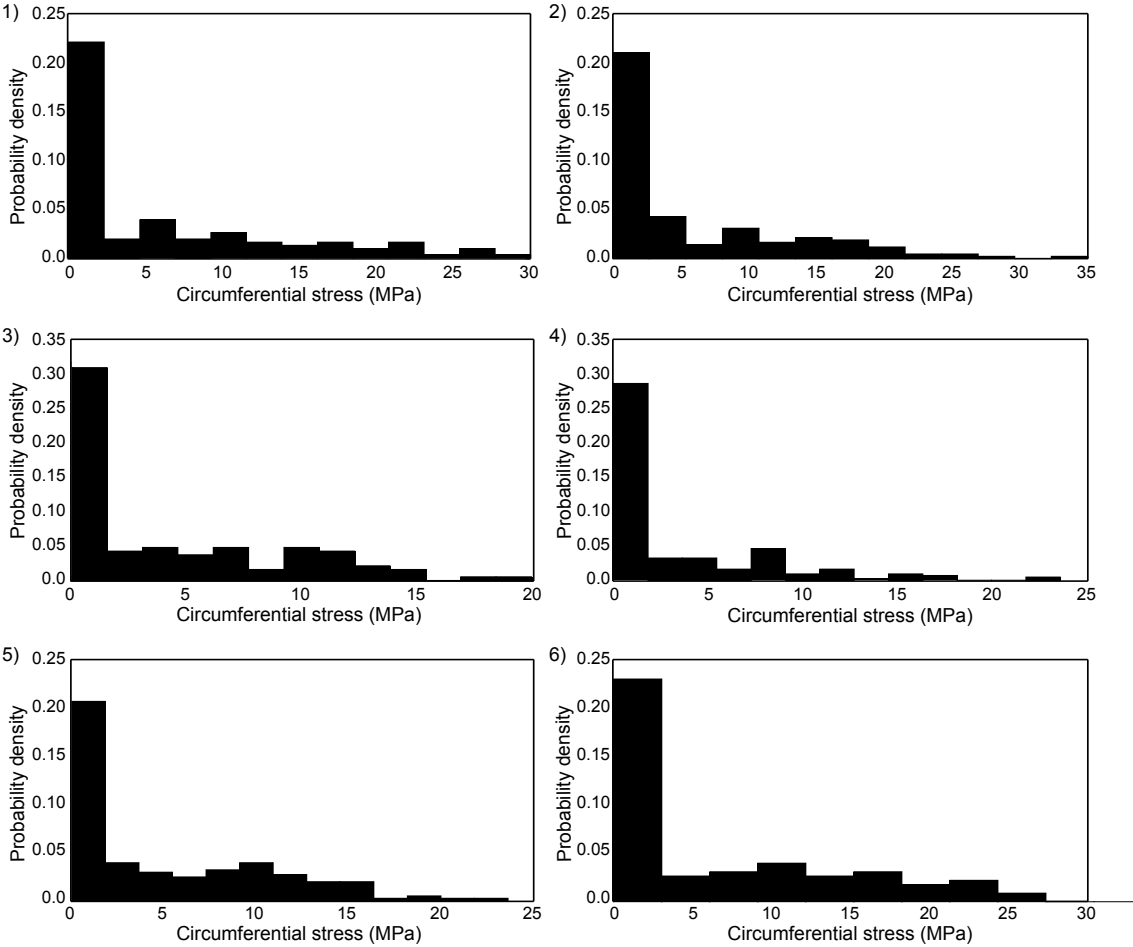


FIGURE 4.14 – (1-6) Distribution of axial stress in collagen fibres in each sample computed at a global stress of 1 MPa

4.6 Discussion

4.6.1 Main contributions

In this paper, a discrete random network model of the tunica adventitia built from experimental data is presented, to capture the mechanical behavior at the scale of the fibrous micro-structure. Computing and analyzing the mechanical phenomena occurring at the scale of the micro-structure has been a focused area in arterial mechanics. Histomechanical constitutive models are used widely to distribute macroscopic stress to various micro-structural components and correlate macroscopic loading to microscopic component responses. Previous attempts at developing an anatomically representative finite element model for arterial wall layers did not investigate the morphology but rather relied on inversely identifying the morphological parameters. With the method specified here, morphological analysis was made to study the distribution of collagen fiber orientations, waviness, diameter and their volume fraction in the tissue. The proposed model is anatomically based, as it incorporates this information by employing an inverse random sampling approach. Recently it has been realized that macro-scale rupture occurs at locations of localized strain concentration, which interestingly was in contradiction to the notion that rupture occurs at the location of maximum stress [Romo et al., 2014a]. While it is possible to investigate the mechanical behavior of individual arterial wall layers with analytical models, it is interesting to develop a micro-scale finite element model of the adventitia to study microscopic mechanical phenomena responsible for the risk of rupture. The main objective of this work was to introduce a method that can be readily implemented with necessary image processing and FE analysis tools.

The histology based reconstruction presented in this paper is general in the sense that it can be applicable to many stochastic fibrous micro-structures. The orientation of fibers is one of the two important parameters required for the reconstruction. The presence of two distinct families of fibers was evident from the microscopy images. Hence the orientation distribution of collagen in the network obtained through an FFT analysis was later fit to a mixture of Von-Mises distributions (with each distribution representing a family of fibers). Also, it was observed from the analysis of the images that the number of fibers in each family was not the same as it was normally believed to be. To this effect, a weighting parameter p was introduced to take into account the contribution of each family of fibers. The model also takes initial waviness of collagen into consideration which was fit to a beta probability distribution. The initial waviness of collagen coupled with dispersed orientations controls the highly non-linear mechanical response of the network. To reconstruct a numerical network which represents the actual collagen network as accurately as possible the diameter and content of collagen were also extracted from the image stacks, which had not been previously considered. The entire workflow of this forward approach of reconstructing numerical network from morphology data was conducted on a sample $n^{\circ}4$.

4.6.2 Comparison with the literature

To ensure fast applicability of the method on a wide range of experimental data from other samples, a reduced model was constructed using constitutive and morphological parameters as inputs. Constrained optimization was then conducted to inversely identify the parameters of all samples from which obtaining morphological data was not feasible due to image quality. The data from uniaxial tensile tests were used in that case. All the identified parameters (see Table 2) fell in an acceptable range of values reported in the

literature [Rezakhaniha et al., 2012, Chen et al., 2011, Sherman et al., 2015b, Chandran, 2005, Schriebl et al., 2012b]. Since we were mainly interested in studying the behavior of collagen in the adventitia, the response of the network prior to the point of collagen recruitment was not taken into consideration. The capability of this modeling method was demonstrated by comparing the numerical simulation result in experimental data (Fig. 7, 8). The satisfying agreement with experimental data demonstrated the capability of the model to predict the macroscopic response of the tissue at high strains for a wide range of micro-structural arrangements.

4.6.3 Sensitivity analysis

Following the comparison of numerical results with experimental data, a comprehensive parameter sensitivity analysis was conducted to establish meaningful relationships between individual model parameters and macroscopic mechanical response determinants. The responses studied include the stretch at which collagen is recruited and the stiffness of the tissue following collagen recruitment. Linear regression model for the final slope response revealed that axial connector stiffness and orientation dispersion had negligible impact compared to those of collagen modulus, waviness and volume fraction. As previously shown in [Gizzi et al., 2014, Chen and Kassab, 2016] it was observed here that collagen waviness had a negative influence on the final slope response. Regarding the recruitment stretch, collagen waviness was found to be the main influencing parameter. This aspect was also briefly studied from 3-D rendered MPM images [Hill et al., 2012b], where it was found to bear a direct relationship. This finding is in line with the present linear regression coefficient predicting an increase in recruitment stretch with an increase in collagen waviness. A comparative study conducted by Holzapfel et al [Holzapfel and Ogden, 2017] showed that collagen fiber dispersion effects the macro-scale mechanical response significantly. However, it is to be noted that the range of dispersions considered in their study is much higher than what we explore with our model. In any case, a quantitative comparison of the explored sensitivity indices could not be made at this moment. Although the linear regression helped to understand the overall effect each parameter exhibited on each response, the non-linear regression model was found to be a more accurate representation in both cases with lesser RMSE and higher r-squared values. However, it did not highlight any remarkable combined effect.

4.6.4 Fiber kinematics

The kinematical reorganization of collagen fibers under load was emulated by the model as shown in figure 4.11 and is in coherence with previous investigations. The amount of transverse deformation combined with the increasing tension the fiber network has to bear dictated the amount of reorientation in collagen fibers. A review on the mechanics of random networks of various densities in [Picu, 2011b] suggested that collagen fiber reorientation is explained by non-affine kinematics. We always observed that collagen reorientation predicted by the model was greater than the affine prediction. It was also computed that the average error in reorientation prediction made by an affine assumption was $22.65\% \pm 6.02\%$, which is in agreement to the average value of 25% reported from experimental investigation [Krasny et al., 2017b]. As the load increased, collagen fibers also underwent a straightening process which combined with reorientation to control their recruitment. It was observed that the average waviness in the network did not reach 1 meaning not all fibers were straightened at the end of loading. To understand the recruitment phenomena,

a mathematical foundation for fibril recruitment in tendons was developed by Bevan et al [Bevan et al., 2018], based on which they estimated average critical recruitment waviness in arteries as 0.996. For further analysis, for each sample, collagen recruitment stretch was computed as the global stretch at which the rate of curvature change was found to be the highest. As can be seen from figure 4.15, recruitment of collagen is in a comparable range of the average experimental value. It was also noted that the rate of straightening reduced significantly beyond the point of recruitment stretch. This result confirms that the macroscopic notion of recruitment stretch defined from macroscopic stretch-strain curves [Bevan et al., 2018, Hill et al., 2012b] is closely related to the microscopic, fiber-level, recruitment stretch which could be investigated thanks to the present model.

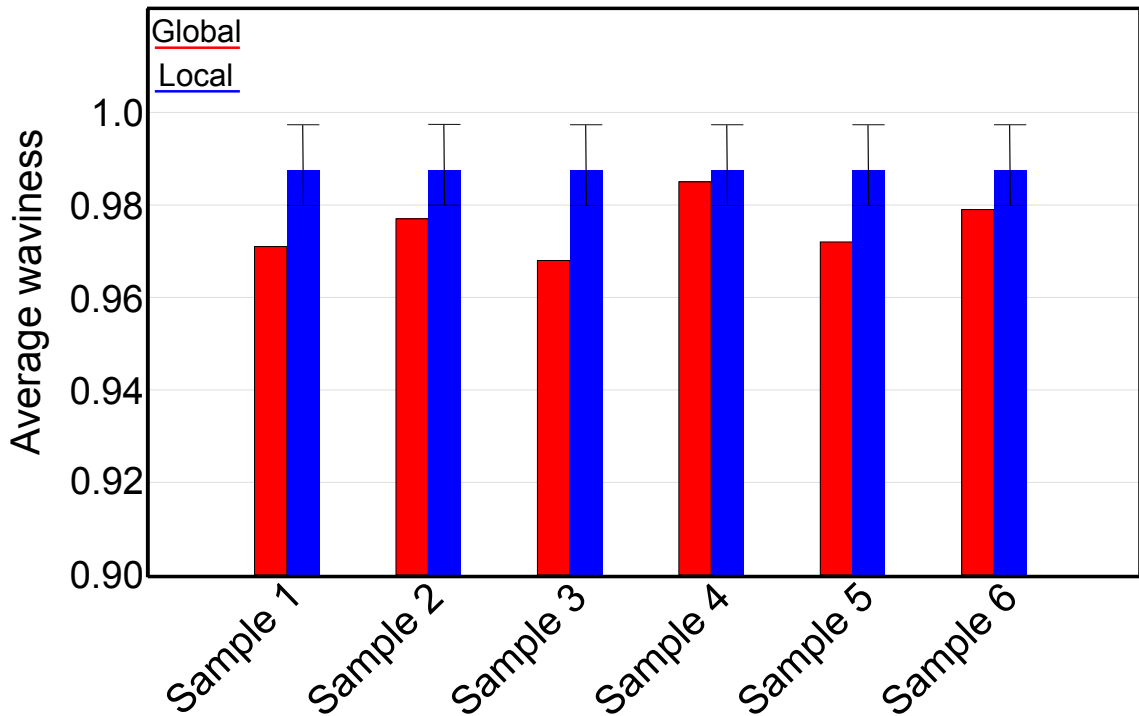


FIGURE 4.15 – Comparison of computed recruitment stretch for collagen in each sample to theoretical estimates

4.6.5 Rupture prediction

The study of the macroscopic mechanical response of arterial wall layers is well documented in the literature with the use of phenomenological and structural constitutive models [Chuong and Fung, 1983b, Raghavan et al., 2000]. While these models accurately predict the mechanical behavior of the tissue, they do not provide any insight into the phenomena occurring at the microstructure level. To this effect, the proposed model was used to investigate the microscopic strain and stress distributions in individual fibers constituting the network. This was used to study the mechanical state of collagen fibers at a macroscopic stress level corresponding to rupture. Interestingly, this analysis indicated that fibers approaching their tensile limit were closely oriented towards the circumferential direction in comparison to their mean orientation at that loading level. Following that, for each sample, the strain distributions at load corresponding to rupture were analyzed and fit to a probability density distribution. This could be used to compute the probability of finding a fiber in any given range of tensile stress/strain, and hence estimating a

rupture probability index. Indeed, it was noted that for some samples a small percentage of fibers approached their tensile limit. Their probability is quantified and presented in figure 4.16. It was noted that for a sample $n^{\circ}3$, which was subjected to maximum stretch the probability was found to be the highest. From this, we can hypothesize that damage initiation would possibly occur at a local level before propagating towards macroscopic rupture. By utilizing this information, the model could serve as a probabilistic tool for predicting rupture based on the morphological information of the micro-structure. As current experimental data do not include the necessary information for quantifying rupture, one of the main perspectives of the present study would be to gather experimental data at loading conditions reaching rupture. This data would be then fed to the model in order to quantify meaningful rupture criteria based on structure-function relationships.

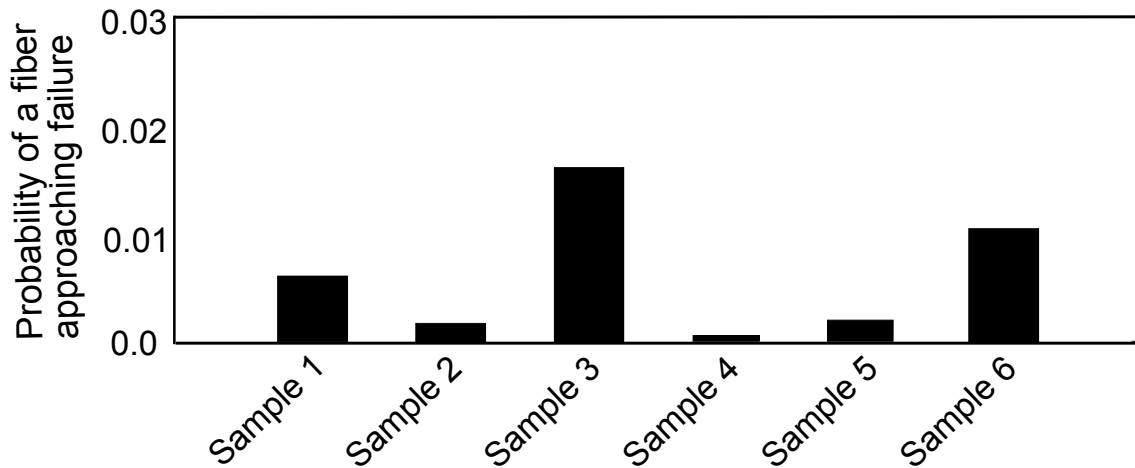


FIGURE 4.16 – Bar chart of computed values of strain based failure probability of collagen in all the samples

4.6.6 Limitations

The model presented in the study is not without limitations, which can be discussed as below:

1. We recall, first, that the study was limited to the mechanics of collagen network in the adventitia as the effects of the connective tissue and other micro-structural components were not considered. This choice lied onto the common hypothesis that at high loads beyond physiological pressure levels, collagen acts as the principal load-bearing component in the arterial wall.
2. Physical interactions between the fibers and the ground matrix was not considered in the current model. This was rather modeled phenomenologically using a connector element which is kinematically linked to the boundary edges of the model, thus controlling the overall non-affine behavior of the network and enabling compressibility in the collagen network.
3. Interactions between individual fibers are not considered in this model assuming that their effect would be of a lesser order compared to tension effect in the overall response to uniaxial tension.
4. In the presented model, collagen fibers were assumed to be oriented mostly in the axial-circumferential plane. Hence, the orientation distribution obtained from image

stacks only corresponded to the azimuthal angle, neglecting the effect of a polar angle like in many studies in the literature [Jin and Stanciulescu, 2016c, Holzapfel et al., 2015b, Gasser et al., 2006b]. For a more realistic representation of the micro-structure, 3-D segmentation tools which can accurately render the fiber morphology is required. At this moment, the quality of the images prevents such analysis which would be beyond the scope of this study.

5. We also assumed the same collagen orientation density distribution for all samples. Nonetheless, it can be seen from the reported data in [Krasny et al., 2017b] that the assumed distribution is within the limits of average orientation density of the measured samples. This is a strong simplification, however; but when it is possible to experimentally measure this distribution, it can easily be introduced in the model.
6. Next, the experimental image stacks corresponded to a depth of 100 μm owing to the quality of the signal at in-depth focal positions. Therefore, morphological information extracted from the image stacks was assumed to be representative of the tissue, which may be questioned.
7. Each fiber in the network was modeled as a chain of segments alternating around a given orientation. This led us to the assumption that all fibers had their ends on the boundaries of the modeled volume. Although this did not compromise the overall stochastic nature of the network, it is worth noting that realistically, fibers which dangle inside the micro-structure could possibly exist.
8. Finally, the material parameters identified for the samples were only based on uniaxial tension loading data. For other loading scenarios, the applicability of these identified parameters has not yet been verified and will be the purpose of future investigations.

To further elucidate the significance of out of plane orientation of collagen on the mechanical response, a sample simulation was conducted. We include a phantom distribution for the polar angle distribution, which has an overall mean in the axial-circumferential plane, the likes of which have been studied briefly in the literature [Holzapfel et al., 2015c, Weisbecker et al., 2015, Gasser et al., 2012b]. From figure 4.17, it could be concluded that the exclusion of polar angle has a noticeable effect. The stretch at which collagen was recruited was observed to be very slightly higher in the case of a 3-D oriented network, while the overall stiffness of the network in the loading direction slightly reduced. In short, as expected, the 3D nature of orientation distributions, compared to 2D, is the cause of a slightly higher magnitude of re-orientation effects in uniaxial tension. Future studies, in particular, experimental one involving the network behavior of collagen, should incorporate the measurement of out of plane orientation distribution if possible.

4.7 Conclusions

The mechanical behavior of collagen micro-structure under uniaxial tensile loading was studied with a discrete random line network model. The micro-structural model incorporated relevant stochastic information of collagen fibers extracted from multi-photon microscopy image stacks. The underlying network kinematics and the global mechanical response were accurately predicted by the model. Reliable constitutive parameters corresponding to collagen and apparent transverse stiffness of the network were estimated by

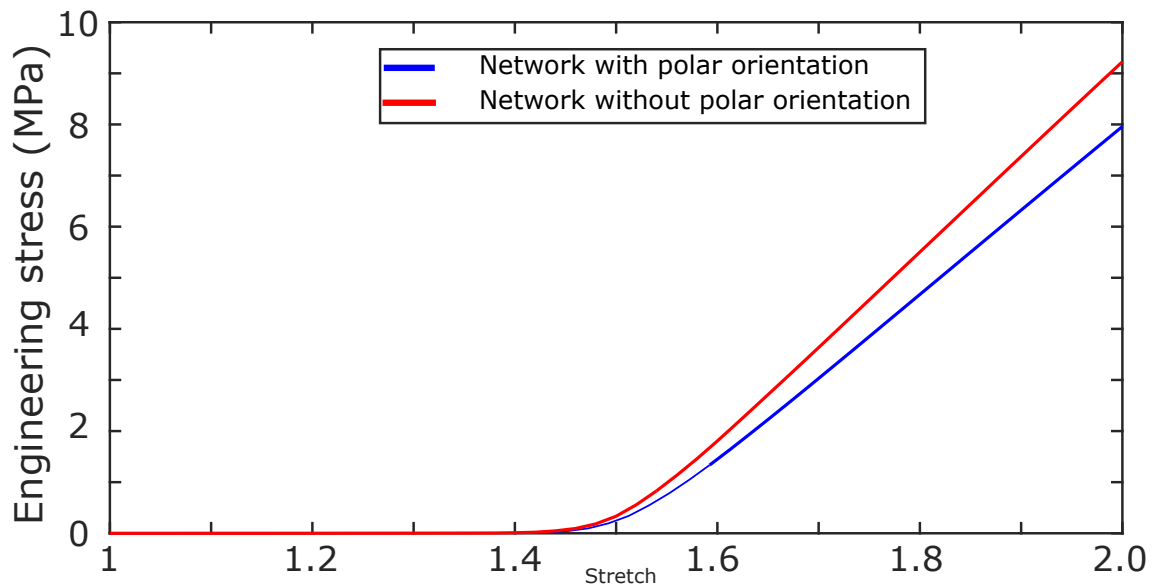


FIGURE 4.17 – Comparison of collagen network behavior with and without the inclusion of polar angle

the model. From this investigation, the model was used to conclude important structure-function relationships that control the mechanical response. The present model, which corresponded to healthy aortas, can be extended to aneurysmal aortas in the future in light of improving our understanding of initiation and propagation of rupture. This model could be ultimately used to develop better safety measures in assessing the risk related to aortic rupture.

Chapter 5

A discrete fiber based damage model for assessing the failure of aortic tissue - applied to human and porcine aortas

Contents of the chapter

5.1	Résumé	120
5.2	Abstract	121
5.3	Introduction	122
5.4	Materials and methods	125
5.4.1	Experiments	125
5.4.1.1	Micro-structural imaging.	125
5.4.1.2	Uniaxial testing	127
5.4.1.3	Bulge-inflation testing	127
5.4.2	Numerical methods.	129
5.4.2.1	Structural model of the tunica adventitia	129
5.4.2.2	Constitutive model for matrix.	129
5.4.2.3	Constitutive model for collagen	130
5.4.2.4	Finite element model	130
5.4.2.5	Parameter estimation	131
5.5	Results	132
5.5.1	Bulge-inflation	132
5.5.2	Uniaxial tension	132
5.5.3	Fiber kinematics.	132

5.6	Discussion	135
5.6.1	Main contributions	135
5.6.2	Collagen rupture strain comparison	138
5.6.3	Correlation between micro-structure and rupture	139
5.6.4	Progressive damage model for collagen fibers	140
5.6.5	Limitations	141
5.6.6	Conclusions.	142

5.1 Résumé

Un anévrisme de l'aorte abdominale est un état pathologique fréquemment observé qui est identifié par un gonflement de l'aorte. Dans la plupart des cas, si l'affection n'est pas traitée, elle peut gonfler davantage jusqu'à ce qu'elle se rompe. La décision d'une intervention chirurgicale pour un anévrisme de l'aorte est généralement associée à une évaluation du risque de rupture. La rupture d'un anévrisme aortique est un événement local qui dépend des caractéristiques mécaniques de la paroi aortique à cet endroit. Par conséquent, les paramètres globaux d'évaluation du risque de rupture, comme le diamètre de la paroi et la croissance de l'anévrisme au fil du temps, ne permettent souvent pas de prévoir le risque de rupture. Bien que le risque de rupture basé sur la contrainte maximale de la paroi évaluée par une analyse biomécanique de la paroi artérielle fournisse des données fiables pour les décisions cliniques, il ne tient pas compte des hétérogénéités locales comme l'épaisseur de paroi, la résistance locale de la paroi, la composition micro-structurale, etc. Cet article étudiera l'hypothèse selon laquelle la microstructure tissulaire à l'échelle des fibres de collagène et d'élastine détermine sa défaillance à des échelles plus longues. Méthodes : Dans ce but, deux protocoles de test différents ont été implémentés. Des échantillons de tissu anévrysmal humain ont été soumis à un test de gonflement par renflement jusqu'à la rupture couplé à une imagerie par microscopie multiphotonique (MPM). Les piles d'images de l'échantillon ont été acquises à différents niveaux de pression. De plus, des échantillons d'aorte porcine ont été testés sous tension uniaxiale jusqu'à la défaillance et leur réponse a été enregistrée. Avant les essais mécaniques, des piles d'images MPM ont été acquises dans quatre zones différentes de l'échantillon. Les piles d'images acquises à l'état libre de charge ont été utilisées pour extraire les informations morphologiques relatives aux fibres de collagène. Ensuite, une approche d'échantillonnage aléatoire inverse a été utilisée pour générer des paramètres pseudo morphologiques pour la reconstruction du réseau. Un modèle de calcul du réseau de collagène signifiant sa nature stochastique a ensuite été développé, incluant à la fois la mécanique avant et après défaillance. Résultats & Conclusion : Le modèle a permis de prédire la réponse mécanique et la défaillance de l'adventice et a démontré que les dommages causés par les fibres peuvent fortement influencer la réponse macroscopique de la défaillance du tissu. Le modèle peut servir d'outil utile pour prédire la défaillance macroscopique de la paroi aortique à partir des variations de la morphologie microscopique.

L'extension du processus de reconstruction numérique pour inclure les dommages au niveau des fibres de collagène a été soumise au Journal of Biomechanics.

5.2 Abstract

An abdominal aortic aneurysm is a frequently observed pathological condition which is identified by a bulge/ swelling of the aorta. In most cases, if the condition is not treated, it might swell further until it ruptures. The decision of surgical intervention for an aortic aneurysm is usually associated with an assessment of risk of its rupture. The rupture of an aortic aneurysm is a local event that depends on the mechanical characteristics of the aortic wall at that location. Consequently, global rupture risk assessment parameters like wall diameter and growth of the aneurysm over time often fail at predicting the risk of rupture. Although the rupture risk based on the peak wall stress evaluated by a biomechanical analysis of the arterial wall provides reliable data for clinical decisions, it does not take into account local heterogeneities like wall thickness, local wall strength, micro-structure composition, etc. This paper will investigate the hypothesis that the tissue micro-structure at the scale of collagen and elastin fibers determines its failure at larger length scales. Methods: To this aim, two different testing protocols have been implemented. Human aneurysmal tissue samples were subjected to bulge-inflation testing until rupture coupled with multiphoton microscopy (MPM) imaging. Image stacks of the sample were acquired at different pressure levels. Additionally, porcine aorta samples were tested under uniaxial tension until failure and their response was recorded. Prior to mechanical testing, MPM image stacks were acquired at four different zones on the sample. The image stacks acquired at the load free state were used to extract morphological information relating to collagen fibers. Then, an inverse random sampling approach was used to generate pseudo morphological parameters for network reconstruction. A computational model of the collagen network signifying its stochastic nature was then developed, including both prefailure and post failure mechanics. Results & Conclusion: The model was able to predict the mechanical response and failure of the adventitia, and demonstrated that fiber based damage can strongly shape the macroscopic failure response of the tissue. The model may serve as a useful tool for predicting macro-scale failure of the aortic wall based on the variations in micro-scale morphology.

The extension of the numerical reconstruction process to include damage at the collagen fiber level was submitted to the Journal of Biomechanics.

5.3 Introduction

An aortic aneurysm is a pathological dilatation of the ascending thoracic aorta, which often grows slowly and usually without symptoms [Humphrey and Holzapfel, 2012b]. Aortic aneurysms are difficult to detect because it is a silent disease. Small and slow-growing aneurysms may never rupture, but large, fast-growing aneurysms may dissect or rupture, leading to the sudden death of the patient [Humphrey and Taylor, 2008b]. Many characteristic changes in aneurysmal aortas can be readily distinguished from healthy tissues. Firstly, evaluation of changes in biomechanical behavior of the aortic wall affected by aneurysms using uniaxial tensile tests showed that the tensile strength is lesser in aneurysmal specimens compared to control specimens [Vorp et al., 2003]. A similar study using planar biaxial testing reported that aneurysmal aortic tissues showed an increase in stiffness and a decrease in extensibility [Vorp et al., 1998]. Micro structure evaluation of aneurysmal tissues in comparison to healthy tissues showed a decreased amount of elastin [Iliopoulos et al., 2009, Lindeman et al., 2010], smooth muscle cell loss, and an increase in collagen content [Tang et al., 2005]. The organization of collagen fibers in the arterial wall has also been shown to be more organized in the circumferential direction [Gasser et al., 2012a]. This shows that aortic aneurysms are a complex phenomena involving several constituents and processes, which is why the existing rupture risk indicators such as the maximum diameter criteria or the growth rate tend to fail [Isselbacher, 2005, Davies et al., 2006, Witzenburg and Barocas, 2016, Pape et al., 2007]. Even with the above knowledge, the prediction of rupture and dissection of aneurysms remains difficult. Furthermore, the above mentioned biomechanical and micro-structural changes in the aneurysmal aortas are highly in-homogeneous, leading to localised abnormalities. Hence, macroscopic criteria such as maximum stress, maximum strain, or minimum thickness even though beneficial, might be controversial in predicting rupture [Cavinato et al., 2019]. A better understanding of failure mechanics of the arterial tissue at the scale of its structural constituents is imperative.

The arterial wall can be identified as composed of three distinct layers in its thickness, each of which are in turn composed of several micro structural constituents such as elastin, collagen, and smooth muscle cells. The distributions, organizations, and interconnections of these constituents give rise to the complex mechanical characteristics of the arterial wall such as heterogeneity, non-linearity, and anisotropy. Due to this complex nature, many loading conditions are required to study the failure of the tissue. *Uniaxial tensile testing* is the easiest and most commonly used method for in-vitro testing of soft tissues. Several researchers performed uniaxial tension tests on excised aneurysmal tissue samples in circumferential, longitudinal, and arbitrary (close to diagonal) directions to assess their failure properties [Krasny et al., 2017a, Khanafer et al., 2011, Azadani et al., 2013, Cavinato et al., 2017]. Majority of these reports concluded that the aneurysmal arterial wall is slightly stiffer in the circumferential direction [Martin et al., 2011, Matsumoto et al., 2009]. Sokolis et al [Sokolis, 2015] performed uniaxial tensile tests on individual arterial wall layers to demonstrate the heterogeneity in failure. They reported the adventitial layer to be the stiffest and strongest of all three layers. *Biaxial tensile testing* of a planar specimen on the other hand is used to directly determine if the tissue properties differ between circumferential and axial directions as it eliminates the consequence of heterogeneous nature of arterial walls. Planar biaxial testing of aneurysmal tissues showed that there is an increase in circumferential stiffness compared to control specimens, indicating an even larger degree of anisotropy [Azadani et al., 2013, Pham et al., 2013]. From planar equibiaxial tests many

studies proposed anisotropy indices based on either the peak stress or peak strain ratio [Avanzini et al., 2014, Choudhury et al., 2009], showing that it is more useful for studying anisotropy than studying failure. Similar to planar biaxial testing, *bulge inflation testing* allows for the investigation of biaxial mechanical behavior, simultaneously allowing the investigation of rupture. Mohan et al [Mohan and Melvin, 1983] conducted quasi-static and dynamic biaxial inflation tests on healthy aortic specimens and concluded that the tissue consistently failed in perpendicular to the long axis. A mean failure strength of 1.14 MPa was reported assuming an isotropic material behavior, along with a mean rupture stretch of 1.44. Marra et al [Marra et al., 2006] reported a slightly higher value of 1.75 MPa for rupture stress challenging the results of Mohan et al, but reported similar observations for rupture stretch and failure direction. Duprey et al [Duprey et al., 2016] tested 31 human aneurysmal specimens using bulge inflation testing and observed dissection-like ruptures, where the medial layer fails whereas the adventitia remains intact; failure stress/ strain showed no correlation with diameter of the aneurysm. Interestingly though, there was a significant decrease in the strength of the tissue as the age increased. The above testing methods focus on principal stress and strain components, although relevant for assessing rupture, they maybe not be relevant for investigation of dissection failure [Witzenburg and Barocas, 2016] where the main mode of failure is transmural shear [van Baardwijk and Roach, 1987]. Some research groups are working in this direction using peel tests and shear lap tests to investigate the delamination strength of arteries. Other experimental methods to assess the failure characteristics of arteries include nanoindentation testing [Hemmasizadeh et al., 2012], 4-D ultrasound techniques, etc. Apart from aneurysms, several other vascular diseases that induce damage in the tissue leading to failure have been recorded experimentally [Oktay et al., 1991, Salunke and Topoleski, 1997].

Structurally motivated continuum models which incorporate the contributions of individual micro-structural constituents have been employed to represent the elastic behavior of arterial walls [Gasser et al., 2006a, Holzapfel et al., 2015a, Agianniotis et al., 2011]. But, the above experimental observations regarding the failure mechanics of the arterial tissue prompted the need for models that account for damage. By combining their existing continuum formulations with continuum damage mechanics theory (CDM), some researchers extended it to capture failure [Shah et al., 2014, Li and Robertson, 2013, Li and Robertson, 2009]. A two layer fiber-reinforced model coupled with anisotropic damage law was introduced by Volokh et al [Volokh, 2007], which was later extended to other constitutive models of arteries (such as Fung and HGO models) [Volokh, 2010]. From the results of these models it was concluded that arterial wall rupture strongly depended on strength of fibers. Rodriguez et al [Rodríguez et al., 2006] proposed a stochastic damage model by assuming that each fiber has a different strain energy density defined by a Beta probability distribution. Alastrue [Alastrué et al., 2007] presented a comparison between a deterministic continuum damage model proposed by Calvo et al [Calvo et al., 2007] and the stochastic damage model proposed by Rodriguez et al [Rodríguez et al., 1994, Rodríguez et al., 2008]. Though both models accurately predict the macroscopic mechanical response, they showed different damage localizations with the continuum model showing large damage localizations at zones of large stress gradients and the stochastic model showing damage localizations at zones of large stretch gradients [Alastrué et al., 2007]. An isotropic, compressible strain energy function was proposed by Marini [Marini et al., 2012a] that includes material damage in the form of strain softening and it agreed well with experimental results, though the damage variable showed slightly poor correlation with rupture. A non-local damage formulation and its applicability to arterial tissue failure

was demonstrated by Waffenschmidt [Waffenschmidt and Tekkaya, 2013, Waffenschmidt et al., 2014]. The model combines an anisotropic, compressible strain energy function with local free energy containing the gradient of non-local damage and was shown to have good agreement with experiments. But, the requirement to solve additional non-local damage variables along with ordinary exponential damage function makes this model computationally expensive. Gasser et al [Gasser, 2011] proposed an elasto-plastic damage model based on the micro-structural architecture of collagen fibrils, with the damage relying on an irreversible sliding of proteoglycan bridges, which in turn induces plastic deformations. Although numerical implementation of this model showed great potential, the evidence of such proteoglycan bridges sliding damage effects and plastic deformation needs further experimental investigation at the microscopic level. For a detailed review of damage models applicable to soft tissues, the reader is directed to: [Holzapfel and Fereidoonzhad, 2017, Robertson et al., 2012, Li, 2016]. While above mentioned continuum damage models have been applied to study aortic aneurysms, other constitutive models which are applicable to fibrous soft tissues are relevant to the current work and will be briefly summarized here. An isotropic damage model with application to cerebral arterial tissue was proposed by Li et al [Li and Robertson, 2013, Li and Robertson, 2009]. It was considered that the damage was accumulated only in elastin fibers with the scalar damage variable derived from experimental threshold for elastin in cerebral arteries. Stochastic damage models have been proposed for collagenous tissues such as tendons and ligaments [Guo and De Vita, 2009, De Vita and Slaughter, 2007, Liao and Belkoff, 1999, Natali et al., 2005]. Liao et al [Liao and Belkoff, 1999] assumed that the fibers in the ligaments are wavy in their stress free state, with the waviness itself assumed to follow a Gaussian probability distribution. Fibers follow a brittle failure once they reach the tensile limit strain, thereby rupturing in the same sequence in which they are recruited. De Vita [De Vita and Slaughter, 2007] introduced a similar stochastic model with a randomly distributed strain threshold instead of a distribution for fiber waviness coupled with strain softening by degrading fiber stiffness beyond its strain threshold. An exponential damage function based on individual fiber stretch was introduced by Natali et al [Natali et al., 2005] coupled with an exponential strain energy function for collagen fibers. The model assumes a gaussian distribution for initial collagen fiber crimp, which needs to be clarified as many studies report a beta or Poisson distribution. Finally, Pena et al [Peña, 2011] assessed the applicability different phenomenological damage functions including exponential, polynomial, and sigmoidal functions in comparison to the non-linear mechanical behavior of muscular vaginal tissue. She concluded that sigmoidal function provides the overall best fit with exponential and polynomial functions providing a better fit in the low strain region.

Stochastic fiber networks such as the ones found in arterial tissue, polymers, carbon nanotubes, and collagen gels have been investigated by directly incorporating their geometry in the model instead of homogenizing their contribution in the strain energy function [D'Amore et al., 2010a, Zhang et al., 2013, Spanos and Esteva, 2009a]. These models enable the investigation of how tissue scale mechanical loading is transferred to the micro-structure thus providing insights to multi-scale processes leading up to damage and failure of the tissue. For this reason, although the above mentioned constitutive models of arterial damage capture the tissues failure response, they are constrained by this ability as the description of micro-structure is limited. To address this limitation, damage can be modeled in numerically reconstructed random fiber models from the scale of the fibers. They have been extensively implemented to study the failure properties of random fiber networks under tensile loading [Hadi et al., 2012, Hadi and Barocas, 2013]. More recently,

this methodology has been extended to study the failure of lamellar unit of the aortic media [Thunes et al., 2018], and the whole arterial wall [Witzenburg and Barocas, 2016]. Although they show good agreement with experimental observations, some limitations should be addressed. For the former, an affine deformation was assumed for the fibers which was shown to not be the case for network densities of such magnitude [Picu, 2011a]. For the latter, the micro-structure organization of collagen fibers was assumed to be a fully random process and not a result of micro-structural investigation which further lead to a non-physiological rupture stretch value for collagen fibers. Nonetheless, they do reinforce the hypothesis that tissue level failure is directly related to failure at the scale of fibrous micro-structure.

In the present work, our main objective is to assess the applicability of a discrete model of collagen fibers including a failure mechanism in predicting tissue level failure. In order to accomplish this goal, collagen fiber network models were numerically generated from collagen fiber architecture experimentally obtained from second harmonic generation (SHG) images. The rest of the article is organized as follows: section 5.4 presents an overview of the experimental and numerical methods utilized, in section 5.5 the results of this analysis are presented followed by discussions, challenges, and limitations in section 5.6, and finally conclusions of the study in section 5.7.

5.4 Materials and methods

5.4.1 Experiments

Two different types of aortic tissue specimens were utilized in this study.

- Healthy porcine aortas ($n = 4$) were procured from a local butchery. The descending thoracic part of the aortas were dissected and the surrounding connective was removed carefully. A cylindrical portion of length 3 cm was then excised and cut open along the longitudinal direction to be used for experimental testing. The medial layer of the aorta was peeled off with caution resulting in adventitial strips. Dog-bone shaped samples (effective length: X mm; width: X mm; thickness: X mm) were cut from the adventitial strips (4 circumferential and 2 longitudinal) and frozen until the day of the experiment. These samples were tested under uniaxial tensile loading.
- Human aneurysmal aortic tissue ($n = 6$) corresponding to the ascending thoracic part were procured from patients undergoing elective surgery to replace the diseased section with a graft. Similar to the porcine aortas, the surrounding connective tissue was removed and the diameter of the aorta was measured at multiple zones using a digital caliper. Following that the aortas were cut open longitudinally and 45 mm square samples with edges parallel to longitudinal and circumferential directions were excised. For human aortic specimens, the collection and experiments followed a protocol approved by the Institutional Review Board of the University Hospital Center of Saint Etienne. These samples were tested under bulge inflation loading, already presented in a previous paper [Cavinato et al., 2019].

5.4.1.1 Micro-structural imaging

Two different multi-photon microscopy setups were used in this study to image the collagen networks.

Porcine samples: Second harmonic generation (SHG) microscopy of collagen fibers was

performed with a confocal microscope consisting of a Biorad (MRC1024) scan head and an Olympus BX50WI upright microscope stand. An 810 nm excitation beam from a mode-locked femtosecond laser delivering up to 3W of power (COHERENT, CHAMALEON VISION II) was focused into the sample using a $20\times$ water immersion objective of $NA = 1$ (XLUMPLFN20XW, Olympus). The samples were scanned in the x-y plane to acquire 512×512 sq μm image window. The z-scan was realized by translation of the motorized objective. The incident laser intensity was varied by using a rotating half-wave plate and a polarizer in front of the microscope such that the average power delivered at the surface ranged from 10–100 mW. The SHG signal was collected in transmission through a 710 nm short pass filter and a 405 nm interference filter by a photo-multiplier tube.

Each sample was scanned through the thickness with a z-spacing of $1 \mu\text{m}$, with the depth of scan varying between 50 – 200 μm , at four different locations along the length of the sample. This allowed to analyze the average micro-structural properties of the respective samples.

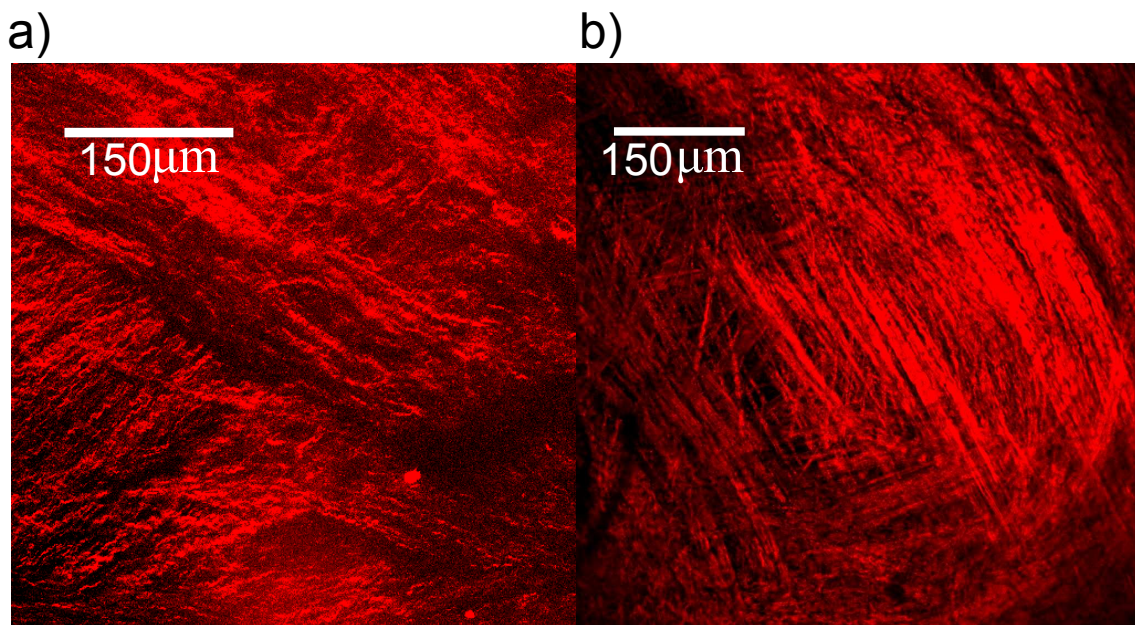


FIGURE 5.1 – Max intensity projection of Multi-photon microscopy image stacks of adventitial collagen of a) healthy porcine sample, b) human aneurysmal sample

Human aneurysmal samples: A LEICA TCS SP2 upright confocal microscope equipped with a water immersion objective (HCX APO L UVI $\times 20$ NA0.5) was used to image human aneurysmal samples. The laser source was a Ti:Sapphire femtosecond laser Chameleon Vision I from COHERENT, Inc. By setting the excitation wavelength 830 nm collagen second harmonic generation (SHG) signal was collected through a 375 – 425 nm band-pass filter. An imaging window of $750 \times 750 \mu\text{m}^2$ was set in the axial-circumferential plane with the depth of scan varying between 100 – 500 μm . Each volume scan had a resolution of 1024×1024 pixels and a z-step of $1 \mu\text{m}$ resulting in an acquisition time of 30 min. SHG image stacks were recorded for each bulge-inflation sample at three pressure levels until the point of rupture: zero pressure, physiological pressure ($\approx 250 \text{ mm} - Hg$), supra-physiological pressure ($\approx 450 \text{ mm} - Hg$). A representative SHG stack of a porcine and a human aneurysmal tissue is presented in figure 5.1.

Sample	Length(mm)	Width(mm)	Thickness(μm)
Circ 1	22.6	7.5	250
Circ 2	24.3	7.5	190
Circ 3	20.5	7.5	204
Circ 4	21.8	7.5	330
Long 1	22.7	7.5	265
Long 1	23.5	7.5	380

TABLE 5.1 – Geometrical parameters of uniaxial samples

5.4.1.2 Uniaxial testing

Uniaxial tensile tests until failure were performed on samples excised from porcine aortas after SHG imaging. On the day of testing the samples were unfrozen by placing them in a saline solution for 15 – 30 minutes. The samples were then mounted onto the uniaxial tensile test apparatus while being submerged in saline solution throughout the test. The length (clamp to clamp) and width of each excised sample were measured with a vernier caliper with a precision of 0.01 mm. The thickness profile of each sample was measured with the help of two high spatial resolution line laser sensors (optoNCDT 1700BL, Micro-Epsilon Messtechnik GmbH & Co. KG, Germany). The average values of length, width and thickness of each sample are presented in table 1. Moreover to prevent the sample from slipping at the clamps during the test, the ends were fixed using sandpaper which maintained the tissue in place during the test. A screw-driven high precision tensile machine (Newport[®], tension-compression stage) with a 22 N capacity load cell and a precision of 0.01 N was used to perform the test. A preconditioning test involving 5 loading and unloading cycles of the sample up to 1.30 stretch was conducted. Following that each sample underwent a quasi-static loading under displacement control until failure at a rate of 2 mm per min and the force-displacement data were recorded. The computed thickness and width of the samples enabled the computation of 1st Piola-Kirchoff stress as $\sigma = \frac{F}{A_0}$ for each sample, where F is the recorded force value and A_0 is the initial cross-section area. The stretch was computed from the actual and reference inter-clamp lengths. With this information the recorded force-displacement data was then converted to 1st Piola-Kirchoff stress versus Green's strain thus generating stress-strain curves for each sample.

5.4.1.3 Bulge-inflation testing

Bulge inflation testing until failure was performed on samples excised from human aneurysmal aortas using a protocol already presented in [Cavinato et al., 2019]. Two circular PVC supports of 30 mm each were used to constrain the samples with the adventitial side facing up. The sample was immersed in PBS throughout the duration of the test. An automatic

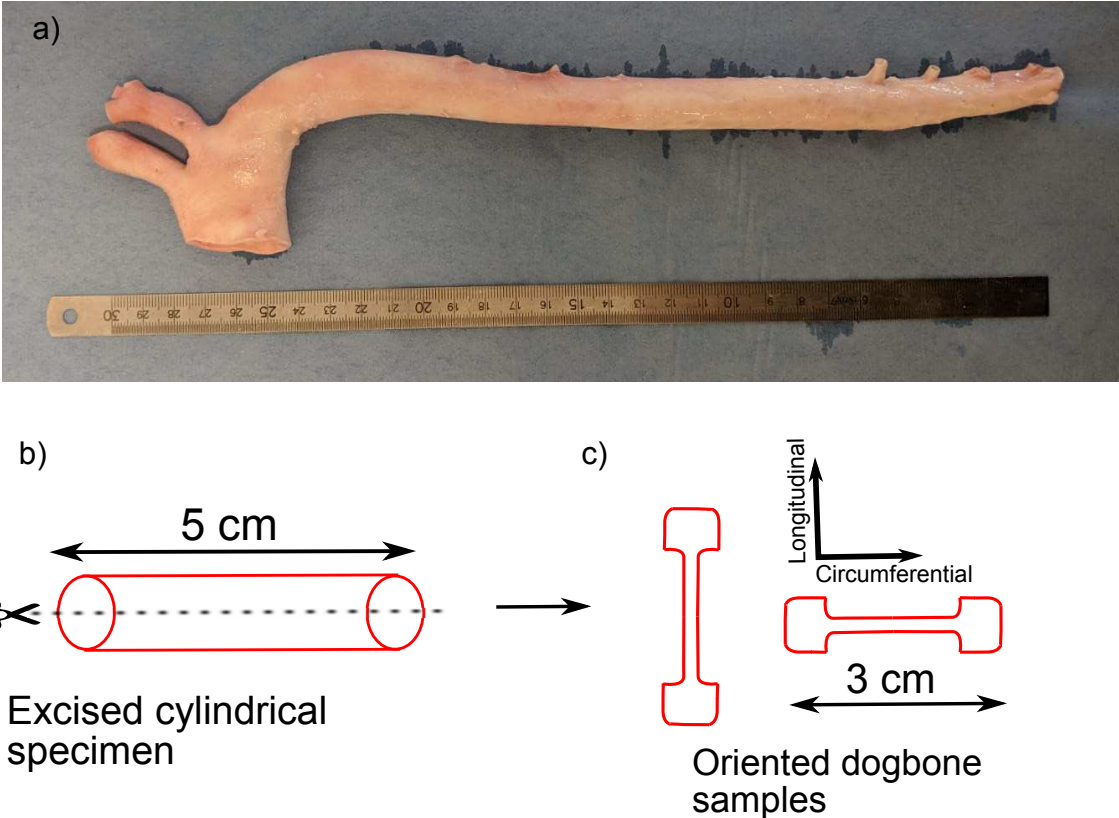


FIGURE 5.2 – Sample preparation. a) Aortic arch of a porcine sample, b) 5 cm cylindrical sections excised from the aorta, c) Schematic representation of cut dog-bone samples for uniaxial testing.

water pumping device (WPI, NE-501 Multi-Phaser) coupled with a program developed in LabVIEW was used to control the water volume injected on the intimal side, which was kept at a constant rate of 2 ml/min. The inflation was stopped by keeping the water volume constant when desired levels of pressure were attained. Further, the pressure values were recorded simultaneously with a pressure transducer (Omega) along with the corresponding radius of the inflated sample. For more detailed information on the experimental protocol, the reader is directed to previously published work [Cavinato et al., 2017].

5.4.2 Numerical methods

5.4.2.1 Structural model of the tunica adventitia

We developed a structural model of the tunica adventitia of each experimentally tested sample by incorporating its collagen network organization. The steps involved in reconstructing the collagen network from micro-structural images are briefly described below:

Morphology estimation: The technique employed to extract relevant morphological parameters from multi-photon image stacks of collagen is similar to that described in [Ayyalasomayajula et al., 2019, Polzer and Gasser, 2015a]. The obtained image stacks were analyzed using an FFT analysis and the resulting orientation (axial-circumferential plane) intensity profile was recorded. The polar (out of plane) angle was assumed to be insignificant and could not be measured on the obtained image stacks. For the case of the porcine samples an average of 4 image stacks was taken as the representative orientation intensity. The resulting intensity of orientations was quantified using a finite mixture of Von-Mises distributions. Following a pore-size analysis of the image stacks, an average fiber diameter of 10 μm was considered for each individual collagen fiber. From a hierarchical standpoint, the network modelled includes collagen fibers, which have typically a radius of 1 – 10 μm [Ushiki, 2002]. The volume fraction of collagen in each image stack was estimated using a semi-automatic segmentation technique in ScanIP[®], a core image processing platform of the commercial software Simpleware[®].

Numerical network reconstruction: A 3-D volume of $500 \times 500 \times t \mu\text{m}^3$ was defined for each sample, with t being the measured sample's average thickness. The collagen fiber network of the adventitia was then reconstructed with each fiber assumed to be a worm like chain with a uniform diameter. Each fiber was defined by a global orientation θ , which was inversely sampled from the quantified orientation distribution, ensured by a goodness of fit test (p-value < 0.05). The fiber is then reconstructed as a sinusoidal wave, whose curvature is determined by the observed crimp of the collagen fibers. The crimp of collagen was not measured on the image stacks used in this study, but was identified in an inverse manner. The length of the fiber was assumed to be larger than the area of interest probed by the microscope and hence each fiber was thought to have its ends intersect the edges of the defined volume. Fibers were added to the network until the desired volume fraction is reached. This numerical network generation schema is similar to the one described in detail in our previous work [Ayyalasomayajula et al., 2019].

5.4.2.2 Constitutive model for matrix

The ground matrix was modeled as a single parameter isotropic, incompressible Neo-Hookean material with the strain energy density $\Psi = \frac{C}{2}(I_1 - 3)$, where C is a material constant and I_1 is the first invariant of the right Cauchy-Green deformation tensor.

5.4.2.3 Constitutive model for collagen

Collagen fibers were modeled as a linearly elastic material with Young's modulus E until the point of critical stretch $\lambda_{critical}$, beyond which the fiber is assumed to be completely damaged. The constitutive law is defined in the equation below and depicted in figure 5.3.

$$\sigma(\lambda) = \begin{cases} E(\lambda - 1) & \text{if } \lambda < \lambda_{critical} \\ 0 & \text{if } \lambda > \lambda_{critical} \end{cases}$$

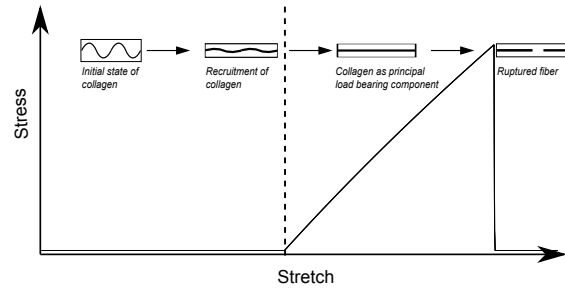


FIGURE 5.3 – Tensile response of a single collagen fiber.

5.4.2.4 Finite element model

A custom Matlab script was used to generate input files of the generated fiber networks to be exported to Abaqus[®] for finite element analysis. The fibers were modeled as 3-D beam elements with negligible but non-zero bending stiffness to aid with the stability of the model. The interaction between matrix and collagen fibers was assumed to be non-existent and the underlying fiber kinematics to be non-affine.

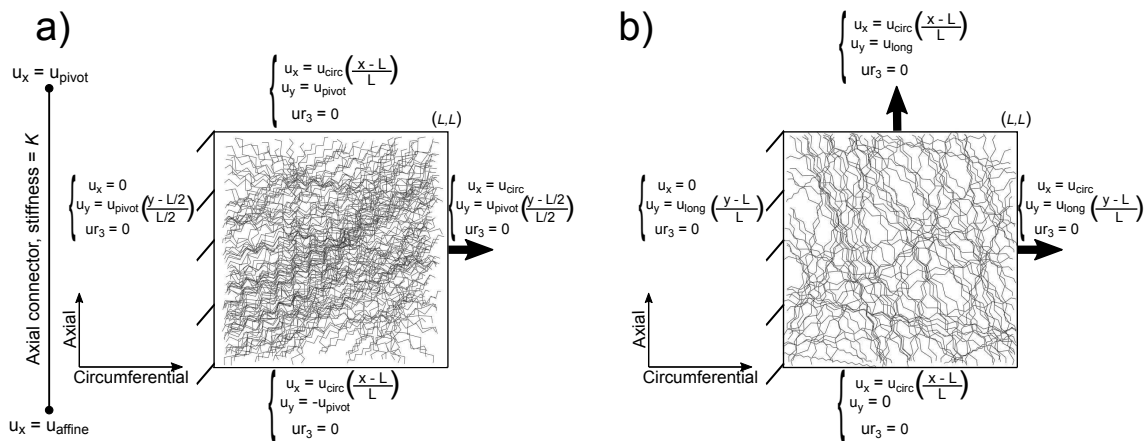


FIGURE 5.4 – Applied boundary conditions for a) uniaxial simulations, b) biaxial simulations

The boundary conditions imposed on the model in order to simulate the uniaxial and biaxial tension are shown in figure 5.4. In all uniaxial simulations, the loading is applied by imposing boundary condition for every node on the domain boundary. The desired axial stretch is achieved by displacing all the nodes on one axially symmetric surface, by a value u_{circ} , while restraining the other end. In the transverse direction, all boundary nodes were kinematically coupled with a free pivot to control their transverse displacement. The

pivot is part of an connector element aligned in transverse direction, whose other node is imposed with a transverse displacement according to the affine kinematics assumption. By varying the stiffness of this connector, the deformation in the transverse direction is controlled [Ayyalasomayajula et al., 2019]. The reaction force at each node on the loaded boundary were summed to obtain the total reaction force, which was then converted to first Piola-Kirchoff stress by dividing with initial the cross-section area.

For the biaxial case, displacement boundary conditions were imposed on two orthogonal surfaces. The amplitudes of imposed displacement in circumferential (u_{circ}) and longitudinal (u_{long}) directions were determined from the bulge-inflation tests in the following manner. First, a geometrically accurate finite element model of each sample was constructed based on stereo-digital image correlation (s-DIC) and thickness measurements [Cavinato et al., 2019]. This model was then compared against the experimental s-DIC displacement to identify the anisotropic hyperelastic material parameters. These experimental data were obtained, for each sample, in a preliminary bulge-inflation test performed in the elastic response domain, combined to s-DIC measurements. The identification procedure and stress/strain state in the region of interest were validated in [Cavinato et al., 2019] and further used in the present work as experimental results of the bulge-inflation test. The stretch values for the discrete network model were taken as the average of the stretch values of all elements in the region of SHG imaging as shown in figure 5.5.

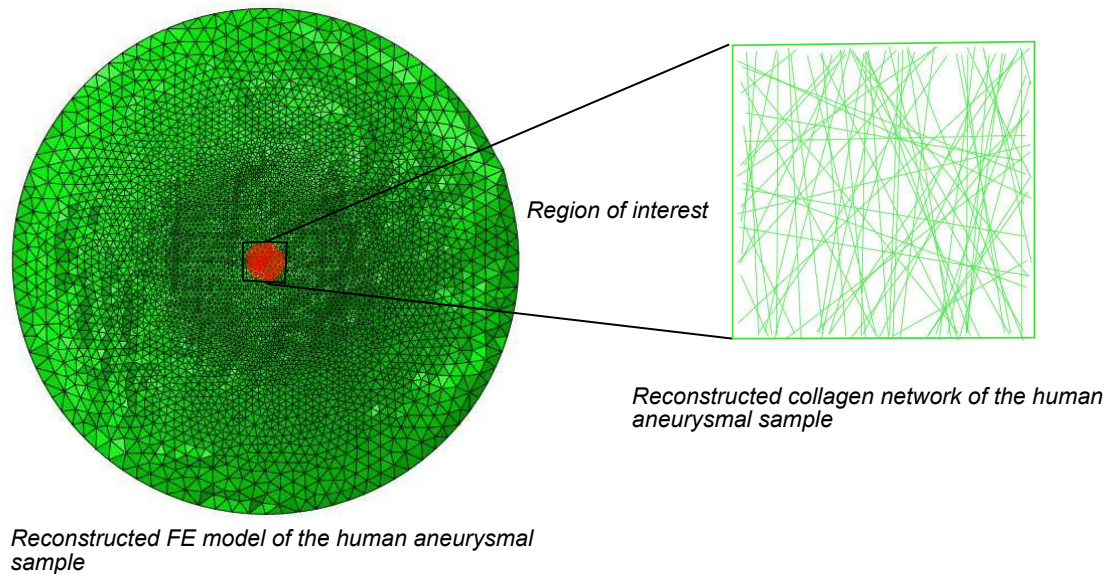


FIGURE 5.5 – Considered window for micro-structural imaging and numerical numerical network reconstruction on the human aneurysmal samples

5.4.2.5 Parameter estimation

Parameters of the model that were unknown at the start of the simulation were identified in an inverse manner. To achieve this a design of experiment approach was used as described in [Ayyalasomayajula et al., 2019] wherein multiple simulations of the reconstructed network were conducted by varying the values of unknown parameters on a regularly gridded parameter space. A multi-dimensional gridded interpolant was built in matlab using the recorded force-displacement responses. As a first step, the Neo-Hookean material parameter was identified on the initial part of the curve. This is due to the assumption that collagen fibers are crimped initially and only contribute to load bearing

beyond a certain stretch (identified on the curve as point with highest rate of change of slope). The parameters for collagen fibers such as elastic modulus and initial crimp were identified through a constrained optimization algorithm in Matlab. By fitting the peak of the elastic stress-stretch response, the tensile critical stretch for individual collagen fibers was identified. The values of identified parameters for each sample are reported as mean \pm 95 % confidence interval. Finally, in order to validate the developed model, the global stress-stretch response was compared to the experimental value for each sample.

5.5 Results

As explained before, experiments were performed on two different specimens: human aneurysmal aortas, and healthy porcine aortas. In the case of human specimens, a bulge-inflation setup was used to pressurize the arterial wall until rupture. In the case of porcine specimens, adventitial strips were prepared and pulled in two different directions, with two samples being tested in the axial direction and four in the circumferential direction. The numerical model aimed at describing all of the different experiments, including both prefailure and failure behavior.

5.5.1 Bulge-inflation

For the case of bulge inflation samples (*B.I.*), the total strain energy was compared between the simulated network model and the region of interest in the reconstructed finite element model. For each experimentally tested sample, the applied pressure was recorded until the point of rupture. Figure 5.6 presents the internal energy for each sample in the region of interest is plotted vs time along with a best fit tissue specific model. The biaxial model results were in good agreement (red dotted line) with and remained within 95 % confidence interval of the experiments. The average coefficient of determination between experiments and simulation had a minimum value of 0.972. Values of the regressed constitutive parameters are presented in Table 2. Figure 5.7 shows the percentage of collagen fibers that ruptured at the point of tissue level rupture (identified as the time of maximum strain energy).

5.5.2 Uniaxial tension

Dog-bone shaped adventitial strips of porcine aortas aligned both circumferentially ($n = 4$) and longitudinally ($n = 2$) were loaded to failure. Figure 5.8 (*a-f*) presents the first Piola-Kirchoff stress (grip force divided by the undeformed cross section area) vs the stretch for each sample along with the simulated best fit tissue specific model curve. The model was capable of reproducing the typical nonlinear response of the tissue along with the ultimate strength of the tissue. The specified geometrical and regressed constitutive model parameters as presented in table 3 allowed the model to match the experimental prefailure and failure results to within 95 % confidence intervals. Figure 5.9 shows the percentage of collagen fibers that ruptured at the point of tissue level rupture (identified as the point of maximum stress).

5.5.3 Fiber kinematics

SHG image stacks were recorded for each bulge-inflation sample at intermediate pressure levels until the point of rupture as stated in section 5.4.1.1. For each sample, orientation

Sample	Neohookean parameter (kPa)	Collagen modulus (MPa)	Critical stretch(μm)
<i>B.I. 1</i>	47.5 ± 6.7	67.3 ± 9.4	1.29
<i>B.I. 2</i>	54.3 ± 3.4	85.1 ± 6.8	1.1275
<i>B.I. 3</i>	37.4 ± 3.78	94.3 ± 11.2	1.2105
<i>B.I. 4</i>	48.11 ± 4.29	48.4 ± 13.9	1.092
<i>B.I. 5</i>	28.67 ± 3.2	79.7 ± 12.3	1.147
<i>B.I. 6</i>	33.2 ± 4.6	68.7 ± 8.7	1.088

TABLE 5.2 – Identified constitutive parameters of human samples tested under bulge-inflation.

Sample	Neohookean parameter (kPa)	Collagen modulus (MPa)	Critical stretch(μm)
Circ 1	28.4 ± 8.7	63.3 ± 5.8	1.187
Circ 2	33.5 ± 4.8	70.5 ± 8.1	1.242
Circ 3	44.6 ± 9.3	72.3 ± 7.1	1.232
Circ 4	64.48 ± 8.4	148.4 ± 6.2	1.216
Long 1	34.67 ± 4.7	64.8 ± 12.3	1.255
Long 2	27.2 ± 5.7	111.7 ± 9.4	1.192

TABLE 5.3 – Identified constitutive parameters of porcine samples under uniaxial tension.

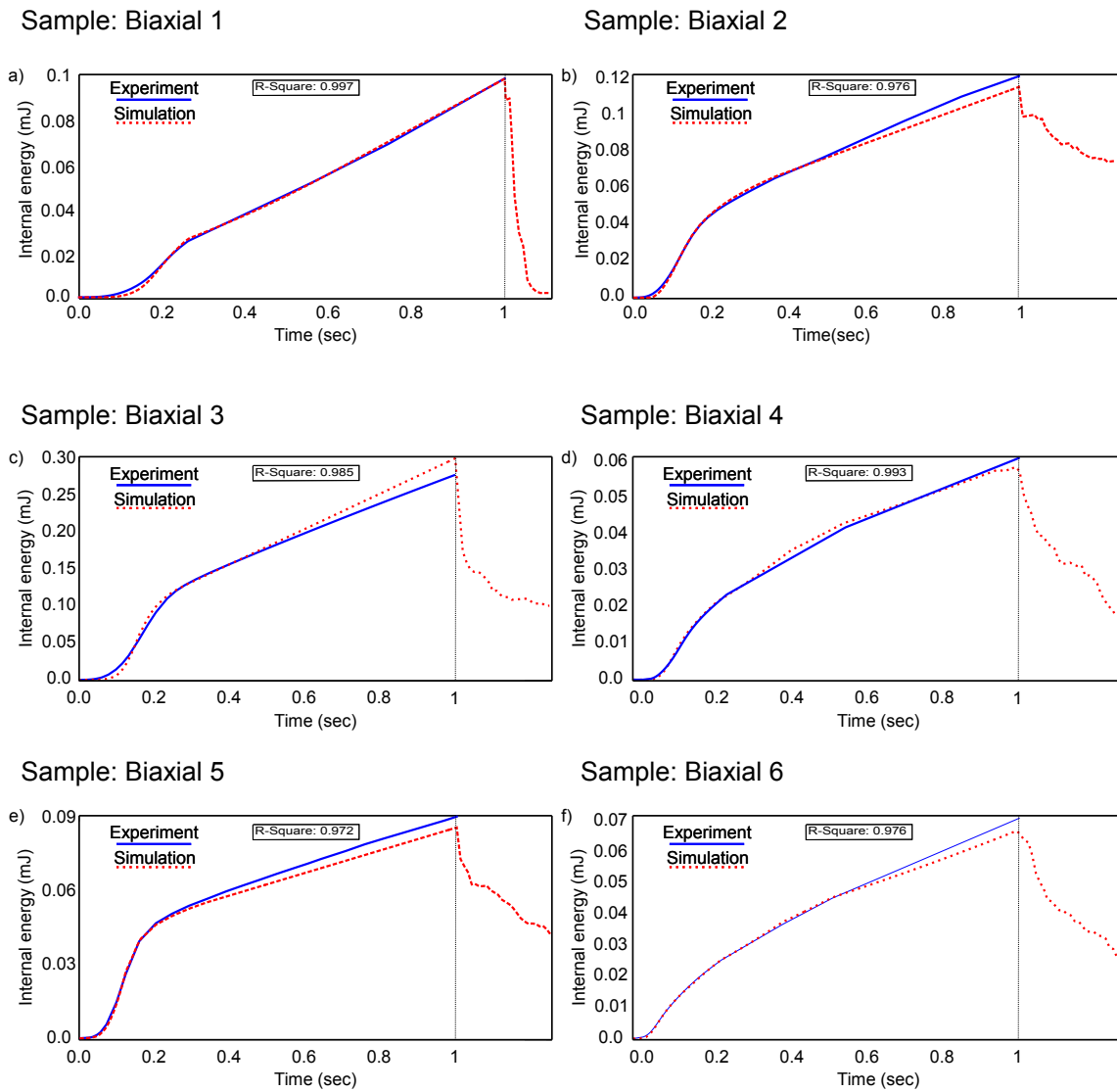


FIGURE 5.6 – Comparison of experimental and simulation responses for human aneurysmal samples.

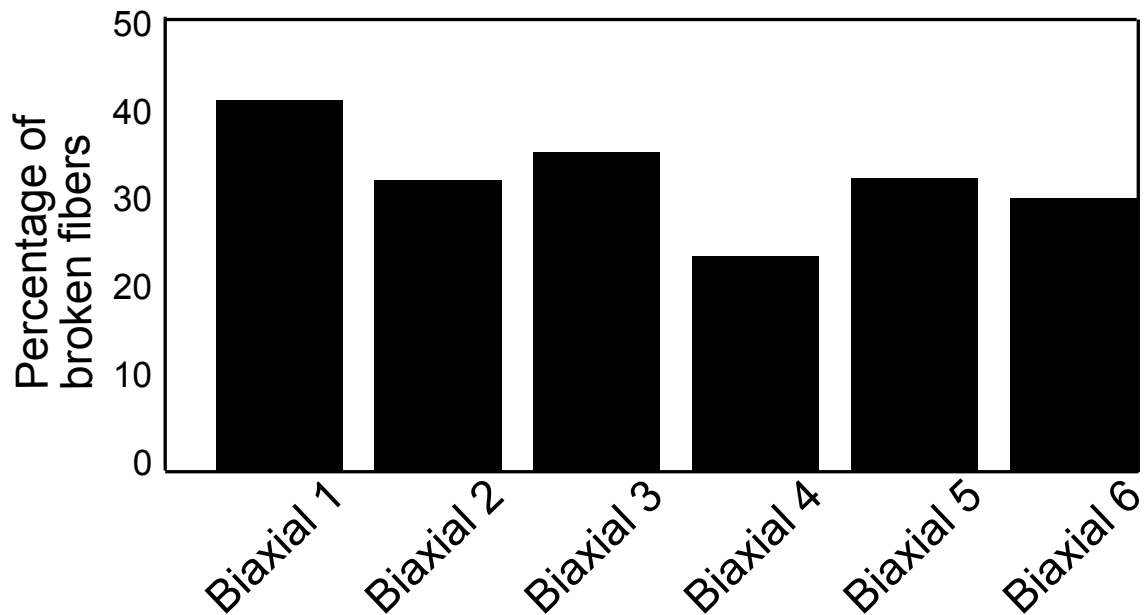


FIGURE 5.7 – Percentage of fibers broken in each human aneurysmal sample at the point of tissue rupture.

distribution of collagen fibers was extracted at a supra-physiological pressure state loading state and compared to the distribution of fiber orientations in the representative model. Figure 5.10 shows the comparison of orientation distribution from experiments and simulations. All samples showed a good agreement with experimental data.

5.6 Discussion

5.6.1 Main contributions

From a biomechanics point of view, aortic aneurysm rupture is considered a local event where the wall stress exceeds the local tissue strength. While it is known that rupture of the tissue occurs at pressure much higher than the physiological rest levels, the exact mechanisms leading up to this event are unclear. Macroscopic characteristics of the tissue such as local strength and thickness have been shown to be not always in correlation with pressure at rupture [Cavinato et al., 2019, Farzaneh et al., 2019, Sokolis et al., 2012]. These findings suggest that the intrinsic difference in micro-structural characteristics from sample to sample and within the sample could be the key determinants in predicting aortic rupture. In this paper we investigate the hypothesis that rupture/damage at the scale of fibrous micro-structure (that of collagen fiber bundles) is responsible for the failure/rupture at the macroscopic level. For this purpose we developed a finite element model of the adventitial micro-structure by explicitly incorporating the morphology of the collagen fiber network. The capability of this modeling method is demonstrated by comparing the simulation results to two experimental testing methods: uniaxial tension and bulge-inflation, with all the identified parameters in an acceptable range of values reported in the literature [Aifantis et al., 2011a, Dutov et al., 2016a, Sherman et al., 2015a, Holzapfel et al., 2000, Chen et al., 2016b].

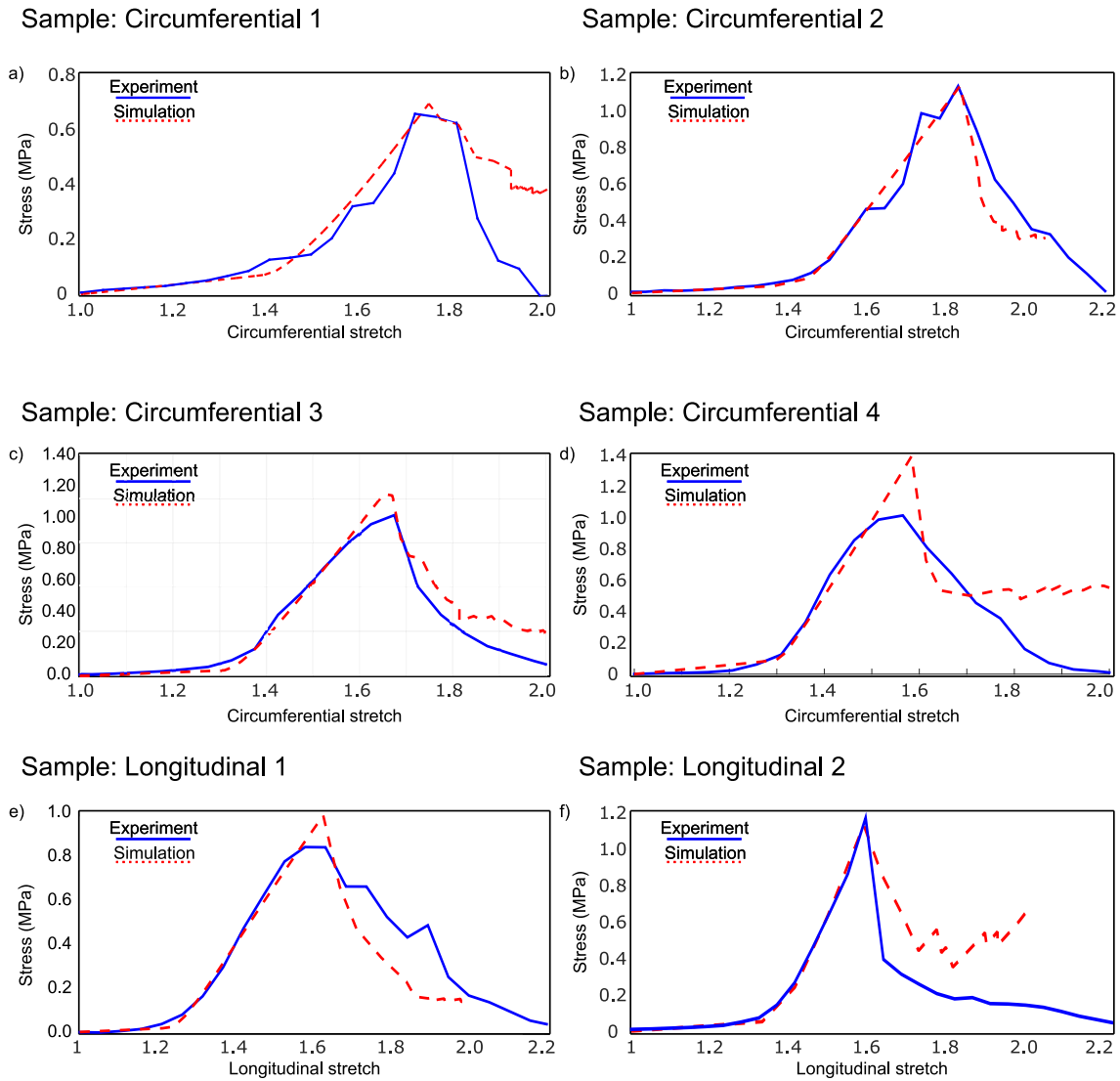


FIGURE 5.8 – Comparison of experimental and simulation stress-stretch responses for healthy porcine samples

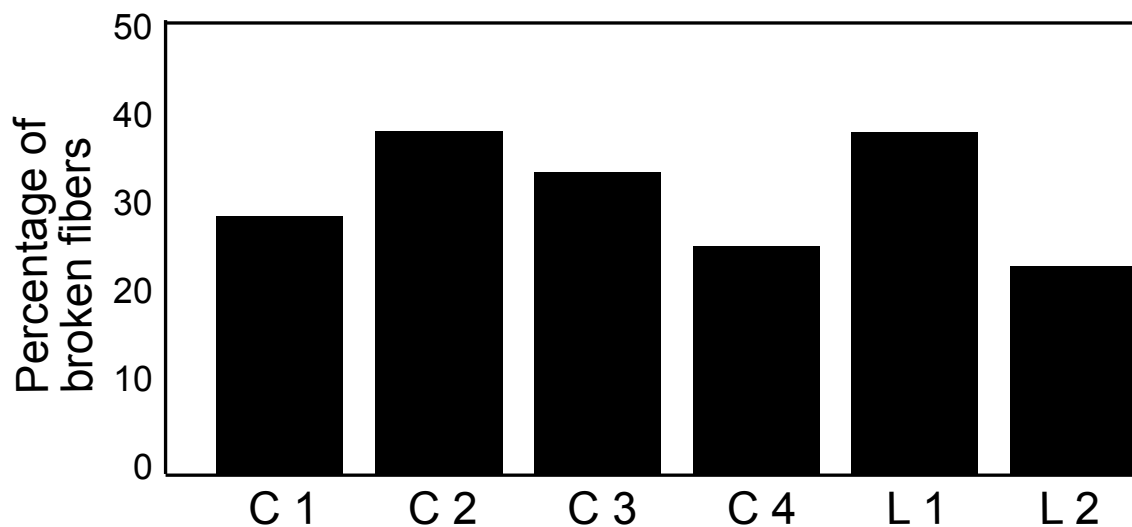


FIGURE 5.9 – Percentage of fibers broken in each healthy porcine sample at the point of tissue rupture.

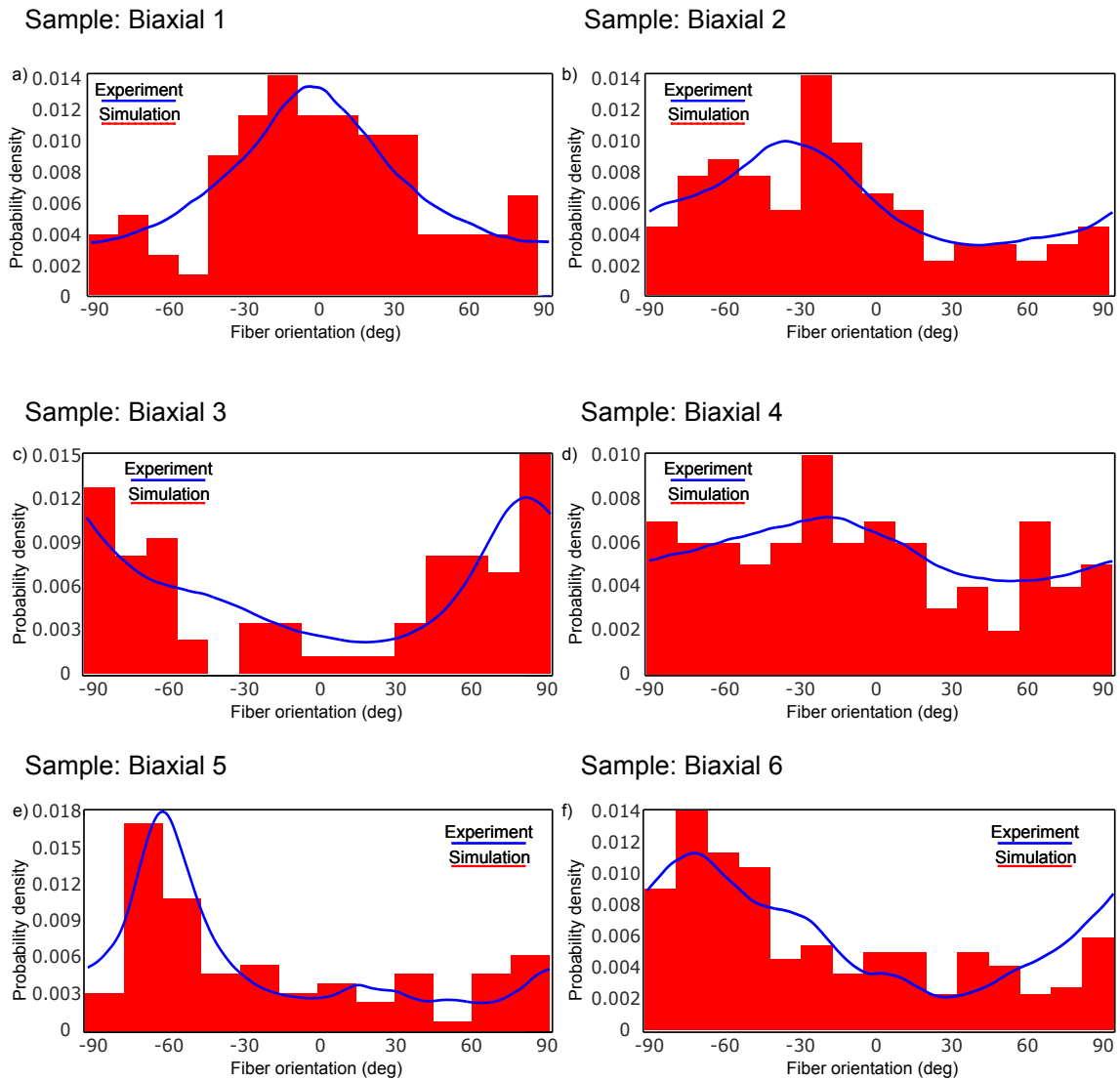


FIGURE 5.10 – Comparison of collagen fiber orientation at supra-physiological pressure state between experiment and simulation. Blue line indicates the orientation distribution obtained from confocal image stacks, red histograms indicate the fiber composition in the reconstructed network at the given load state.

5.6.2 Collagen rupture strain comparison

Collagen is a hierarchical structure and can be seen as composed of these main scales: molecular, fibrillar, fiber, and fiber bundle. Important distinction has to be made while considering the failure properties of collagen as the parameters change with respect to the scale. It was evident from the SHG microscopy images we obtained that, at initial state, fibers tend to form large bundles which slowly separate into fibers as loading increases, which was confirmed by recent observations by our group [Cavinato et al., 2019]. These observations show that collagen fibers are the default structural units in the arterial tissue at physiological pressures, which possibly coalesce into fiber bundles when the loading is removed. For this reason, relevant failure criteria corresponding only to collagen fibers (typical diameters of $1 - 10 \mu\text{m}$) were considered in this study. Also, it should be noted that cohesion between the fibers in a bundle was assumed to be negligible at loads beyond the toe region. The current work utilized the simplest model for collagen fiber failure, that is no damage is accumulated until a critical strain is reached, at which point the fiber is assumed to rupture. Direct comparisons could be made at this point to experimental studies conducted on individual collagen type I fibers.

Miyazaki and Hayashi tested the tensile properties of individual collagen type I fibers (diameters of $1 - 10 \mu\text{m}$) extruded from rabbit patellar tendons [Miyazaki and Hayashi, 1999]. They have reported a failure strain of 0.216 ± 0.03 . A similar study conducted by Gentleman et al on collagen fibers (diameters of $59 - 125 \mu\text{m}$) extruded from rat tail tendons revealed similar findings with a fiber rupture strain of $0.20 - 0.25$ [Gentleman et al., 2003]. A few other experimental findings that have been reported in literature are relevant in this context but are limited by the differences in diameter, cross-linking, and collagen source. This includes the experimental investigation by Shen et al [Shen et al., 2008] on collagen fibrils (diameters of $150 - 470 \text{ nm}$) with an observed yield strain of 0.21 ± 0.13 .

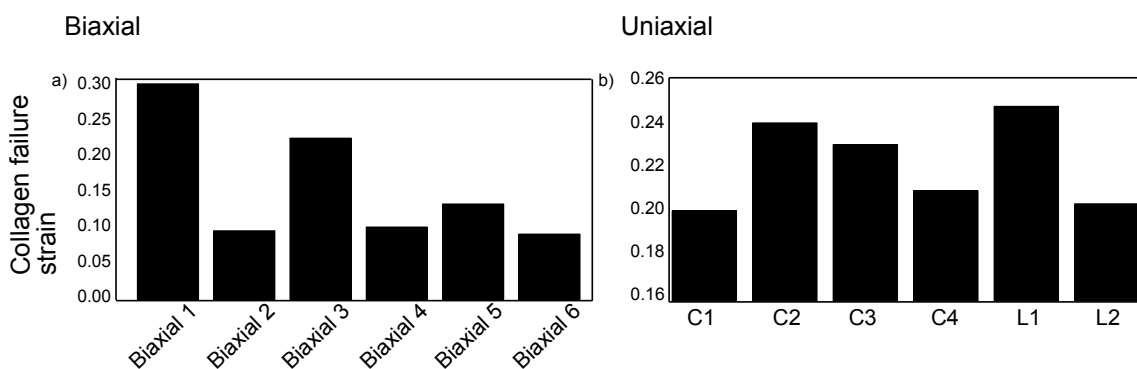


FIGURE 5.11 – Identified values of collagen fiber rupture strain through inverse method for a) bulge-inflation samples, b) uniaxial samples.

Identified collagen rupture strain values showed a high variance in the case of human aneurysmal samples, with a maximum of 0.293 and a minimum of 0.088 as shown in figure 5.11 a. In as many as four samples the identified collagen rupture strain value deviated strongly from those reported in the literature. On the contrary, the porcine samples indicated a very good comparison to experimental findings in terms of identified collagen rupture strain, with a maximum of 0.255 and a minimum of 0.187 as shown in 5.11 b. Although more data is required to reinforce these findings especially as the nature of human samples, being aged and aneurysmatic, may have influence compared to the mentioned

studies on more standardized animal tissues, this might indicate that discrete fiber failure might not be the only mechanism at play causing the rupture at macroscopic level with mechanical sliding between fibers or bundles, or cross-link breakages being possible additional mechanisms. To this effect, further investigation by combining micro-structural imaging and mechanical testing of the tissue (in multiple loading scenarios) is imperative.

5.6.3 Correlation between micro-structure and rupture

Based on the failure mechanism utilized in this work, we investigated the influence of structural parameters such as collagen fiber orientation and waviness on tissue rupture at macro-scale. For this purpose, the orientation distribution is described by a single parameter called the orientation index (OI), which provides a measure of fiber alignment [Pasta et al., 2016].

$$OI = \frac{1}{n} \sum \cos^2(\theta_i) \quad (5.1)$$

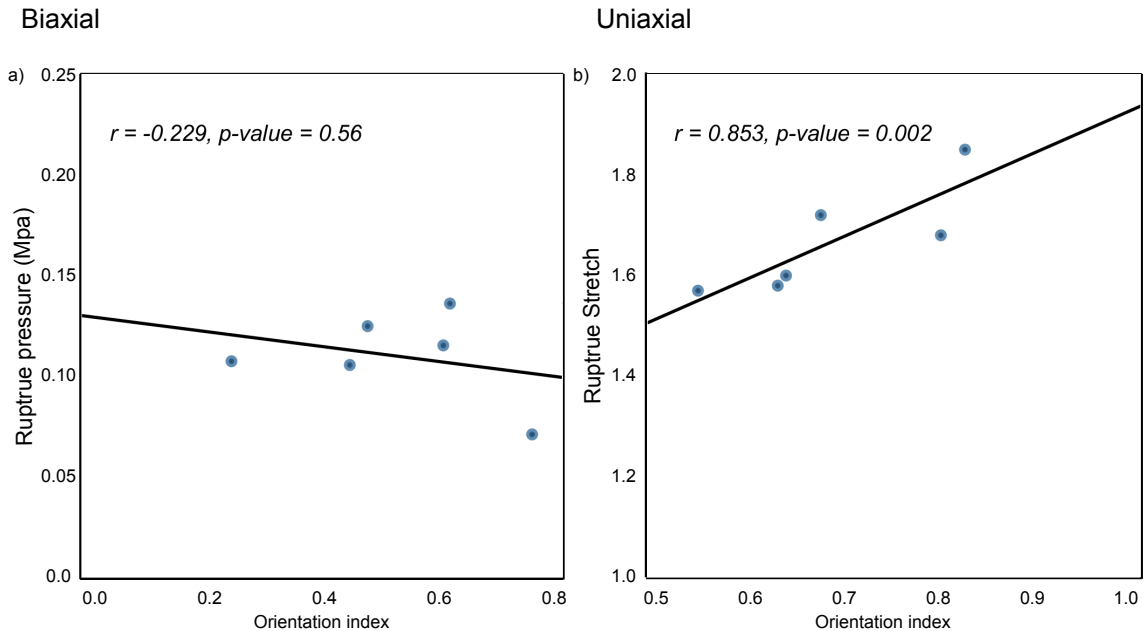


FIGURE 5.12 – Pearson’s correlation between orientation index and recorded tissue strength for a) bulge-inflation samples, b) uniaxial samples

where θ_i is the orientation of a fiber with respect to direction of load, n is the total number of fibers. For bulge-inflation samples, the identified maximum stretch values from s-DIC were different in circumferential and longitudinal directions. The reference direction was assumed to be the one with a higher stretch value. A value of 1 for orientation index indicates that the fibers are perfectly aligned towards a preferred direction (for instance in the case of uniaxial testing, it means that the fibers are predominantly aligned towards the loading direction), whereas a value of 0.5 indicates a random alignment.

Correlation plots for orientation index and tissue strength is presented in figure 5.12. In the case of bulge-inflation tests, the orientation index did not show a significant correlation with rupture pressure, rather a weak negative trend was seen. The Pearson’s coefficient of correlation was observed to be -0.229 with a p-value of 0.56. Although at first sight, this indicates no correlation between the two variables, under equi-biaxial loading conditions (which is likely the case in-vivo for aneurysms) the negative trend might indicate that

rupture occurs in the direction perpendicular to predominant fiber orientation. On the contrary, orientation index showed significant correlation with respect to rupture stretch of the tissue in the case of uniaxial testing. A value of 0.853 for Pearson's correlation coefficient with a p-value of 0.002 was recorded. This, for instance, shows that for a given loading direction the strength of the tissue increases with an increase in fiber alignment with respect to that direction. This is likely the reason why in most cases the strength of the tissue in circumferential direction is higher than that of longitudinal direction [Sommer et al., 2010, Pichamuthu et al., 2013, Smoljkić et al., 2017], suggesting a predominant circumferential fiber alignment. Correlation plots for collagen fiber waviness and tissue

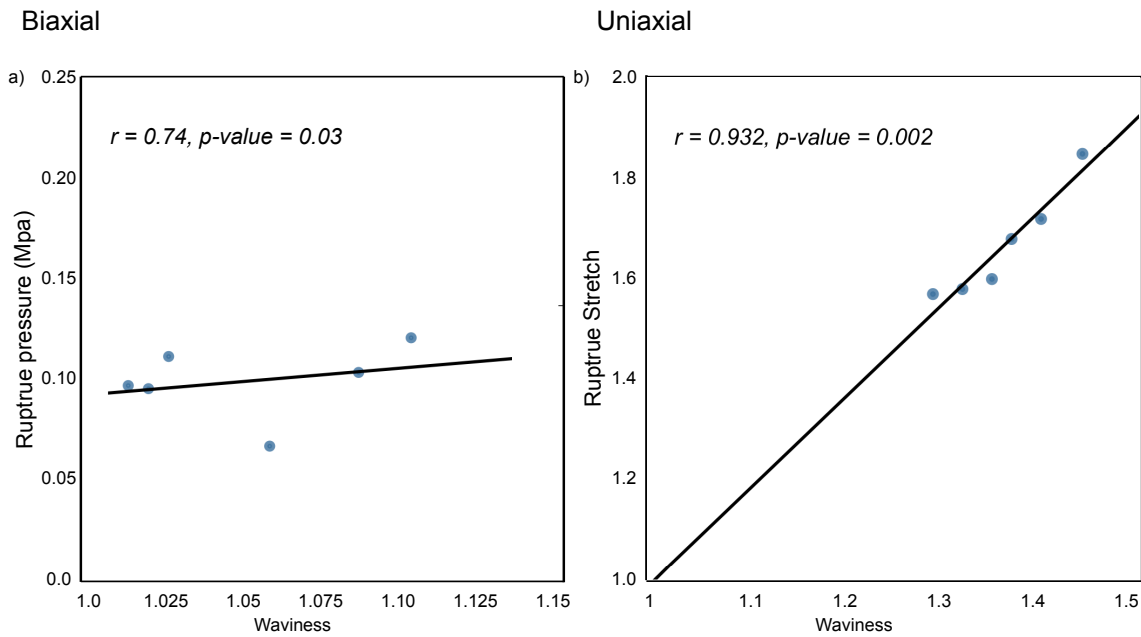


FIGURE 5.13 – Pearson's correlation between collagen fiber waviness and recorded tissue strength for a) bulge-inflation samples, b) uniaxial samples

strength is presented in figure 5.13. The relationship between collagen fiber waviness and tissue strength reveals a positive trend in both bulge-inflation and uniaxial tests. The values of Pearson's correlation coefficient and p-value are 0.74 and 0.03 for bulge-inflation and 0.932 and 0.002 for uniaxial tests. The correlation was observed to be significantly lower in bulge-inflation samples compared to uni-axially tested samples. This shows that as the collagen crimp increases, the strength of the tissue increases. This finding also corroborates the usual hypothesis that aneurysmal tissue has lower failure stretch because the waviness of the network is lower [Pichamuthu et al., 2013, Vorp et al., 2003].

5.6.4 Progressive damage model for collagen fibers

As explained before, the current work employs a brittle failure mechanism for collagen fibers. Even though this type of damage model is relevant and applicable for experimental protocols performed here, it fails to capture irreversible damage accumulation mechanisms (fatigue loading) that may contribute to failure of the tissue. Additionally, it has been suggested empirically that collagen damage at the fiber level is governed by plasticity (leading to a strain softening response) coupled with loss of integrity (leading to material failure) [Marino et al., 2019]. A constitutive model for collagen fiber incorporating the strain softening behavior, similar to that presented in [Marino et al., 2019, Thunes et al., 2018] was implemented. For instance, for a sample network, figure 5.14 shows that there is

a slight change in the prefailure response, but no significant change in the point of rupture (peak stretch).

$$\sigma(\lambda) = \begin{cases} E(\lambda - 1) & \text{if } 0 < \lambda < \lambda_{initiation} \\ Ed(\lambda - 1) & \text{if } \lambda_{initiation} < \lambda < \lambda_{critical} \\ 0 & \text{if } \lambda > \lambda_{critical} \end{cases}$$

where $\lambda_{initiation}$ is the initiation stretch for accumulation of irreversible damage and d is the damage variable.

$$d = 1 - \frac{\lambda_{critical} - \lambda}{\lambda_{critical} - \lambda_{initiation}} \quad (5.2)$$

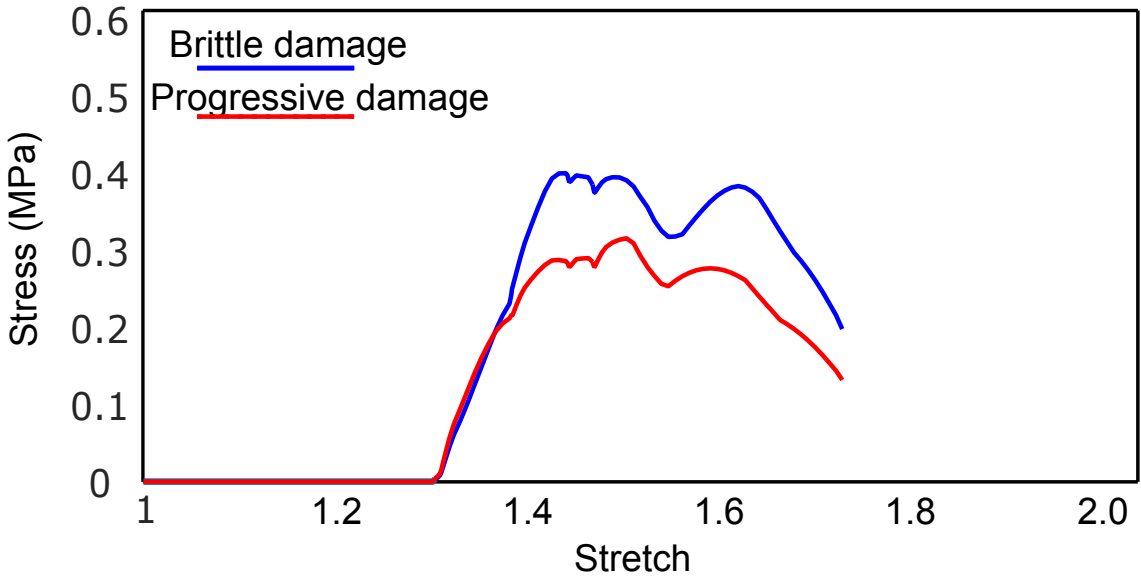


FIGURE 5.14 – Comparison of brittle damage model vs progressive damage on a sample network.

5.6.5 Limitations

The computational model described here has the following limitations.

1. We do not take into account any physical interactions between the ground matrix and the fibers. Additionally, damage is considered only in the collagenous component, which may contribute to the overall tissue strength. However, we do not expect that accounting for damage to the ground matrix will change the major conclusions of the current work.
2. Collagen fiber orientation is derived only in the axial-circumferential plane as extracting the polar orientation from the SHG image stacks was out of scope of the current work. For this reason the out of plane orientation of collagen was assumed to be negligible, which is supported by other studies in the literature [Gasser et al., 2006a, Holzapfel et al., 2015a].
3. One of the primary inputs for this algorithm is the number of fiber segments, which was defined to be a fixed number. This assumption is a temporary compromise, which could be overcome when more reliable information about the fiber length at micro-scale could be conducted.

4. Fiber level damage was considered to be brittle in nature, although it could be easily extended to included irreversible damage.
5. Finally, it is worth noting that the fiber damage model was compared against mechanical testing of arterial tissues in uniaxial and biaxial loading scenarios. More complex experimental testing protocols maybe required to fully characterize the failure mechanisms underlying arterial failure.

5.6.6 Conclusions

In conclusion, we have shown that a discrete fiber network computational model is capable of accurately representing prefailure and failure response of the aortic tissue in two different loading configurations. This model could provide new insights into failure mechanisms involved in aortic aneurysm rupture and is robust enough to incorporate patient specific anatomical models given that patient specific information could be obtained.

Chapter 6

Extension of the methodology from micro-scale to macro-scale

Contents of the chapter

6.1	Résumé du chapitre	143
6.2	Abstract of the chapter	145
6.3	Introduction	146
6.4	Methods	147
6.4.1	Micro-structural imaging	147
6.4.2	Uniaxial testing	148
6.4.3	Multi-scale model	149
6.4.3.1	First approach: direct extension of previous modeling approach 150	
6.4.3.2	Second approach: embedded element approach	150
6.5	Results	153
6.6	Discussion	154
6.7	Conclusion of the chapter	159

6.1 Résumé du chapitre

L'aorte abdominale est une structure hiérarchique complexe dont la mécanique est mal comprise, notamment en cas d'anévrisme. Jusqu'à présent, la quantification du risque de rupture ne tient pas compte de l'information sur les mécanismes microscopiques sous-jacents. Afin d'estimer de façon fiable le risque de rupture, nous avons besoin de modèles

informatiques et d'expériences structurellement précis qui caractérisent la défaillance multidimensionnelle du tissu. Des essais de tension uniaxiale ont été effectués précédemment sur les échantillons d'aorte des orientés dans les directions circonférentielle et longitudinale. Cette étude est une extension des résultats présentés au chapitre 5, où une microstructure moyenne a été considérée pour la modélisation. Afin de tenir compte de l'hétérogénéité locale de l'architecture des fibres de collagène, une imagerie SHG a été réalisée sur les tissus à plusieurs endroits avant les essais mécaniques. Cela a permis de quantifier des informations à l'échelle microscopique, y compris l'organisation des fibres de collagène à l'aide de fonctions de densité de probabilité pertinentes. Deux approches de modélisation différentes sont présentées dans cette étude. Un modèle mécanique multi-échelle a été développé à partir de cette information microstructurale dont les principales composantes sont des fibres de collagène. Simultanément, un modèle d'élément intégré qui tient compte de la cinématique des fibres affines a été développé à Abaqus en utilisant les mêmes informations microstructurelles. Des simulations numériques simulant les expériences de tension uniaxiale ont été réalisées sur les modèles développés. La réponse mécanique globale des deux modèles est en accord avec les données expérimentales, bien qu'elle conduise à des propriétés de matériaux non appariées. Les modèles présentent une description rudimentaire, quoique meilleure qu'auparavant, de la mécanique de la rupture des tissus aortiques, basée sur la représentation des structures. En résumé, cette étude souligne l'importance de l'organisation structurelle des constituants microscopiques et de leur cinématique dans la détermination de la défaillance tissulaire.

6.2 Abstract of the chapter

The abdominal aorta is a complex hierarchical structure whose mechanics are poorly understood especially in the event of aneurysms. So far, the prevalent rupture risk quantification does not consider information of the underlying microscopic mechanisms. In order to reliably estimate the risk of rupture, we need structurally accurate computational models and experiments that characterize the multi-dimensional failure of the tissue. Uniaxial tension tests were performed on the imaged aorta samples oriented in circumferential and longitudinal directions. This study is an extension of the results presented in chapter 5, where an average micro-structure was considered for modeling. In order to account for the local heterogeneity in collagen fiber architecture, SHG imaging was performed on the tissues at several locations prior to mechanical testing. This enabled the quantification of micro-scale information including the organization of collagen fibers using relevant probability density functions. Two different modeling approaches are presented in this study for the sake of comparison. A multi-scale mechanical model was developed using this micro-structural information with collagen fibers as the main components, accounting for non-affine fiber kinematics. Simultaneously, an embedded element model that accounts for affine fiber kinematics was developed in Abaqus using the same micro-structural information. Numerical simulations emulating the uniaxial tension experiments were performed on the developed models. The global mechanical response of both models agreed well with the experimental data, although leading to mismatched material properties. The models present a rudimentary yet better than before representation of structure based description of aortic-tissue failure mechanics. In summary, this study enforces the importance of structural organization of micro-scale constituents and their kinematics in determining tissue failure.

6.3 Introduction

Cardiovascular diseases such as aortic aneurysms are one of the leading causes of death in the western world [Kalita and Schaefer, 2008]. Two distinct phenomena can be identified in characterizing the failure of aneurysmal arteries: dissection and rupture. Aortic dissection, which is relatively uncommon, is associated with a tear in the inner layers of the artery allowing blood flow between the wall layers. Aortic rupture involves a puncture in the arterial wall beyond significant bulging. Aortic aneurysms are treated in two ways: open surgery and endovascular repair (EVAR). Both the mentioned surgical procedures have their own associated risks and are undertaken only if the perceived risk of rupture is greater. For this reason, the clinician needs to reliably evaluate the risk of rupture. Currently, maximal diameter (> 5.5 cm) remains the best parameter to indicate risk of aortic rupture in clinical practice. However, this is a crude parameter as many reported ruptured aneurysms had a diameter less than 5.5 cms [Brown and Powell, 1999]. An individual patient specific assessment of aneurysm rupture risk could reduce the mortality rate associated with aortic aneurysms.

The arterial wall is a complex hierarchical structure made of several constituents at different scales. The identification of a patient-specific rupture risk criterion requires a comprehensive understanding of the organization and interaction of these constituents. The fundamental structural constituents of the arterial wall are elastin and collagen, which occur in the form of fibers at the micro-scale. Elastin is predominantly present in the medial layer of the wall, which is responsible for the structural integrity of the tissue at physiological pressure. On the other hand, collagen is the dominant constituent in the adventitia (outermost layer of the arterial wall), whose organization and strength prevents the arterial wall from over-extension at supra-physiological pressures. The role of fiber architecture in governing the failure of soft tissues has been reported through experimental and computational studies [Anssari-Benam et al., 2012, Keyes et al., 2011, Ritter et al., 2009, Kao et al., 2011]. Hence, characterizing the specific relationship between fiber architecture and failure and macroscopic tissue failure is imperative in determining a patient specific rupture risk assessment.

To better understand the mechanisms underlying aortic rupture, several experimental investigations have been conducted [Duprey et al., 2010, Cavinato et al., 2019, Fillinger et al., 2003, Duprey et al., 2016]. Fillinger et al [Fillinger et al., 2003] analyzed CT scans of abdominal aortic aneurysms. Many of them have reported peak wall stress to be a superior determinant for rupture risk assessment. Contrarily, the results of Romo et al [Romo et al., 2014b] indicated that rupture occurs at a localized strain concentration. In [Duprey et al., 2010], Duprey et al investigated the strength of aneurysmal tissues collected from patients of different age groups. They reported a clear correlation between age and rupture stress, indicating the ambiguity of using a single scalar value of ultimate stress for assessing rupture risk. Furthermore, no proper correlation was observed between the local tissue thickness and mechanical rupture indicators [Cavinato et al., 2019]. These results further strengthen the inference that aortic tissue failure is influenced by the mechanisms occurring at the scale of the fibers.

To address these issues several structural mechanical models have been proposed for depicting the mechanical response of arteries. These models incorporate aspects of tissue

micro-structure such as fiber orientation, fiber crimp, and fiber recruitment either implicitly through strain energy density [Chen et al., 2016b, Gasser et al., 2014, Gasser et al., 2010a, Holzapfel et al., 2000] function or explicitly through directly incorporating the fiber architecture in the modeling process [Jin and Stanciulescu, 2016a, Ayyalasomayajula et al., 2019, Zhang et al., 2013]. In addition, these models have been extended to model tissue failure by using appropriate damage models [Gasser, 2011, Balzani et al., 2012]. Although structural constitutive models are able to predict tissue failure, they are constrained in their ability to provide insights into micro-structural failure mechanisms. Numerically generated fiber networks such as the ones implemented in [Jin and Stanciulescu, 2016a, Thunes et al., 2018] characterize the correlation between micro-structure morphology and tissue’s mechanical response. However, these models are limited as they do not provide a realistic representation of fiber kinematics. Both the models assume an affine transformation for fiber kinematics, which has been shown to be inaccurate [Morin et al., 2018, Cavinato et al., 2020]. Witzenburg et al [Witzenburg and Barocas, 2016] presented a reconstructed realistic multi-scale model for arterial tissue. Their model accurately predicts multi-directional failure properties of arterial tissue. However, the alignment tensor used for collagen fibers was uniform throughout the model and was not based on microscopic investigation. Furthermore, collagen fiber failure was characterized by a stretch value of 1.42, which was inversely identified on collagen-argose gels. Reported experimental values of collagen fiber rupture stretch lie the range of 1.2 – 1.3 [Gentleman et al., 2003, Sherman et al., 2015a]. To the best of author’s knowledge, this is the only study that presents a multi-scale model for arterial tissue with explicit incorporation of fiber architecture.

In the current study we present a multi-scale model of the tunica adventitia, that incorporates the ubiquitous spatial heterogeneity of collagen fiber morphology as observed over a sample. A brittle failure model for collagen fibers was implemented to link micro-scale damage to macro-scale tissue failure. To account for heterogeneous regions in the sample, two methods were proposed ,for the sake of comparison, the first one being a straightforward extension of the previous modeling approach, and the second one requiring the implementation of an embedded finite element approach. The embedded finite element model provides an affine estimate of the fiber mechanics, whereas the proposed model assumes non-affine fiber kinematics. In both sections of the study, the same collagen fiber orientations were used. While the embedded element model uses a recruitment type model [Zulliger et al., 2004] for collagen crimp, it was explicitly included in the non-affine model. We compare the numerical simulation results to experimental data and study the effect of collagen fiber morphology mechanical response of the artery.

6.4 Methods

6.4.1 Micro-structural imaging

Porcine aortic tissues were subjected to confocal microscopy prior to mechanical testing.

A confocal microscope consisting of a Biorad (MRC 1024) scan head and an Olympus BX50WI upright microscope stand was used to perform second harmonic generation (SHG) microscopy. The images were acquired with an excitation wavelength of 810-nm focused onto the sample with a 20x water-immersion objective of NA=1 (XLUMPLFLN20XW, Olympus). A 710-nm short-pass filter (Omega-filters Corp) and a 405-nm interference fil-

ter were used to collect the SHG signal. The resulting images had a resolution of 512×512 pixels corresponding to an image window of $500 \times 500 \mu\text{m}^2$ in the $X - Y$ plane. The scan in the thickness direction was performed using a motorized objective. The depth of the scans varied from sample to sample but remained approximately around $100 \mu\text{m}$. Each sample prepared for uniaxial testing was scanned at four different zones approximately along the center-line, all the four zones being later used in the analysis of each sample. The resulting images of one circumferential sample and one longitudinal sample are shown in figure 6.1a and figure 6.2a respectively.

Each acquired image stack was subjected to an FFT-based method for extracting the

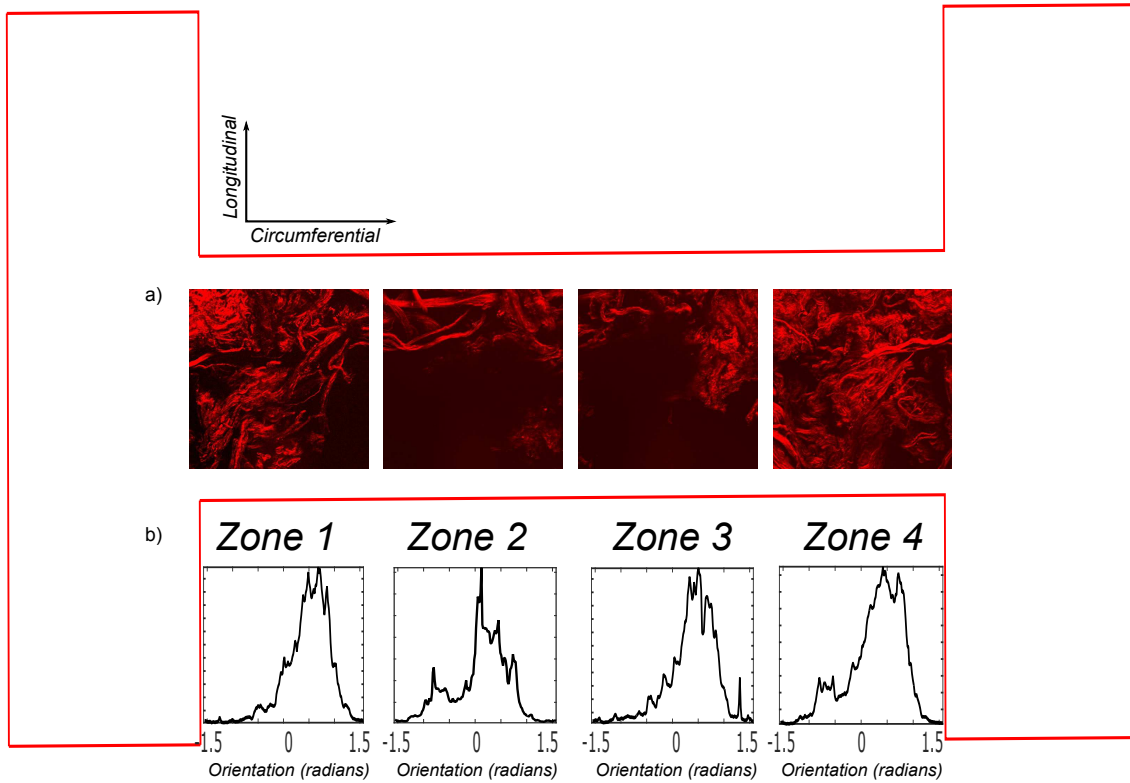


FIGURE 6.1 – Max-intensity projection of SHG image stacks of the circumferential sample acquired at different zones along with their identified orientation distributions.

principle global orientations of collagen fibers. The extracted orientations were then fit to a finite mixture of Von-Mises distributions. The probability distributions for each image stack of the circumferential sample are presented in figure 6.1b, where as figure 6.2b depicts the probability distributions for image stacks acquired on the longitudinal sample. The entire work flow is described in more detail in chapter 3.

6.4.2 Uniaxial testing

Porcine whole aortas ($n = 4$) were procured from a local butchery for mechanical testing. Ensuing dissection of the descending thoracic aorta and careful removal of the connective tissue, cylindrical portions of lengths 3 cms were excised and cut open longitudinally. The medial layer was peeled off carefully and the resulting adventitial strips were used to generate dog-bone shaped samples (effective length $\approx 25 \text{ mm}$; width $\approx 7.5 \text{ mm}$; thickness $\approx 0.2 \text{ mm}$). The prepared samples were frozen until the day of the experiment. The samples were unfrozen by placing them in a saline solution for $15 - 30$ minutes. The samples were

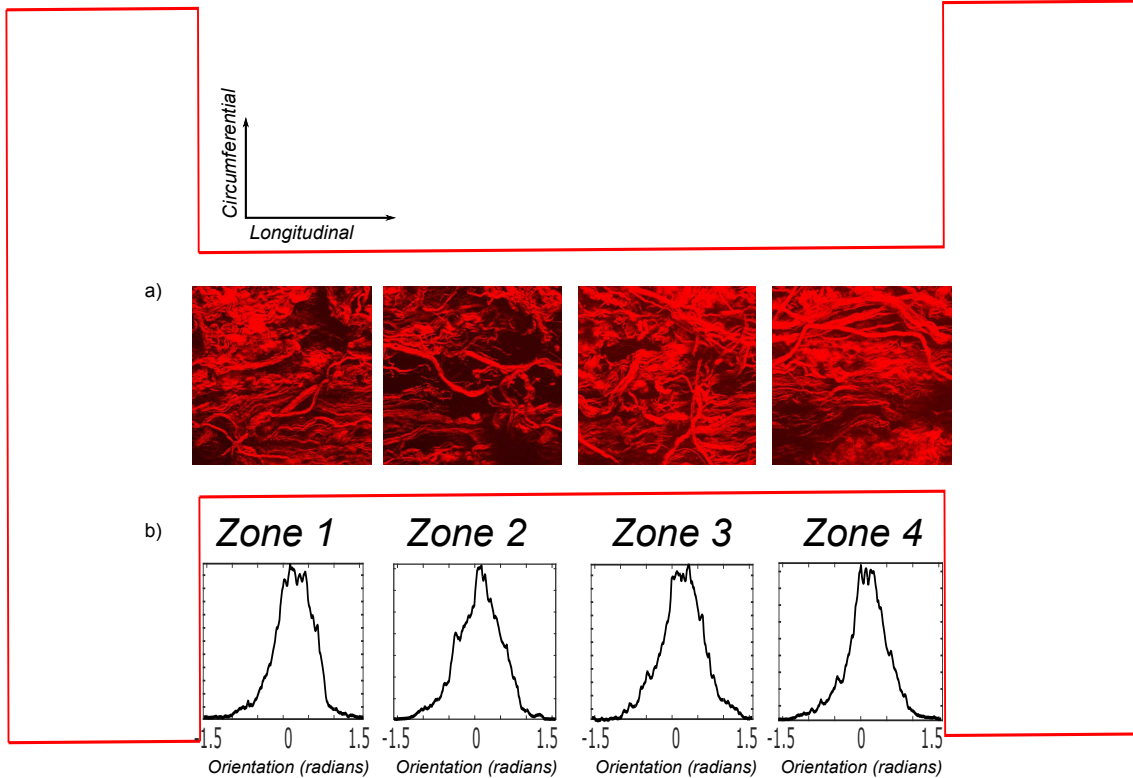


FIGURE 6.2 – Max-intensity projection of SHG image stacks of the longitudinal sample acquired at different zones along with their identified orientation distributions.

mounted onto the uniaxial testing machine, with the ends anchored at the clamps with the help of sand paper. The use of sandpaper prevented any undesirable slipping at the clamps. A screw-driven high precision tensile machine (Newport[®], tension-compression stage) with a 22 N capacity load cell and a precision of 0.01 N was used to perform the test. Following a preconditioning course, the samples were subjected to a quasi-static tensile loading of 2 mm per minute until failure. The force was recorded automatically and the stretch was measured as the ratio between the actual and reference inter-clamp lengths ($\lambda = \frac{l}{l_0}$). The recorded force, measured stretch, and the initial cross-section area produced the 1st Piola-Kirchoff stress ($\sigma = \frac{F}{A_0}$) vs stretch curve for each sample.

6.4.3 Multi-scale model

The collagen morphology information extracted from SHG image stacks of different zones gave rise to the following modeling alternatives. The two methods emulate the same experiment on the tissue-scale, however they differ in terms of underlying fiber kinematics. One model represents a non-affine transformation for fiber kinematics and the other represents affine fiber kinematics. They were tested and compared to the experiment and the micro-scale model presented in chapter 5, where the representative morphology was taken to be the average of the four zones.

6.4.3.1 First approach: direct extension of previous modeling approach

The morphology of collagen fiber network was estimated and quantified for each acquired image stack. The probability distribution functions were used to inverse sample these morphology parameters for numerical reconstruction of the network. The constrained random-walk algorithm presented in chapter 3 was then used to reconstruct the discrete fiber network. A micro-scale structural model was reconstructed for each imaged zone of the uniaxial sample. This process resulted in four individual networks corresponding to a single uniaxially tested sample. The multi-scale mechanical model was then built using the four generated micro-scale models (representative volume element \sim RVE) by linking them in series as shown in figure 6.3. Typically, micro-scale models are on the scale of $500 \mu m$, whereas the domain spans up to $2 cm$. Each micro-scale model was solved independently with a single constraint imposed upon them such that they all undergo the same transverse displacement. The relative axial displacement in each RVE was measured at a desired force level and added up to obtain the total displacement of the model. This enabled the computation of stretch as $\lambda = (1 + \frac{d_1+d_2+d_3+d_4}{l_o})$. For each RVE, an isotropic neo-hookean hyperelastic material was used for the matrix, while the collagen fibers were modelled as linearly elastic with brittle damage at a given critical stretch λ_{crit} . The material parameters were kept homogeneous for all the four networks. The values were previously identified on an averaged RVE as presented in chapter 5.

6.4.3.2 Second approach: embedded element approach

In embedded element method, a composite material model is adopted where the reinforcements and matrix are meshed separately, and then assembled with appropriate constraints. Through this process, the collagen fiber network was assumed to be a reinforcement to the matrix. The identified fiber orientation distribution for each imaged zone was used to regenerate straight fibers. The generated fibers were meshed using truss elements using a custom Matlab[®] script. The diameter of the truss elements was chosen to be $10 \mu m$ similar to the wavy fibers of the multi-scale model. This again resulted in four fiber networks alongside each other. The entire fiber architecture represented by the four generated networks was incorporated into the matrix using the embedded element constraint in Abaqus/Standard. The embedded element constraint is used to specify an element or a group of elements to be enclosed within a host element. The translational degrees of freedom of the embedded nodes are constrained to the interpolated values of the corresponding degrees of freedom of the host element, which explains why this approach intrinsically provides affine fiber kinematics. The shape functions of the host element are used to interpolate these values through out the domain. For instance, the displacements for any point p within the host element (represented here by hexahedral elements) can be computed as:

$$\begin{aligned} d_x &= \sum_{i=1}^8 N_i(p)u_i \\ d_y &= \sum_{i=1}^8 N_i(p)v_i \\ d_z &= \sum_{i=1}^8 N_i(p)w_i \end{aligned} \tag{6.1}$$

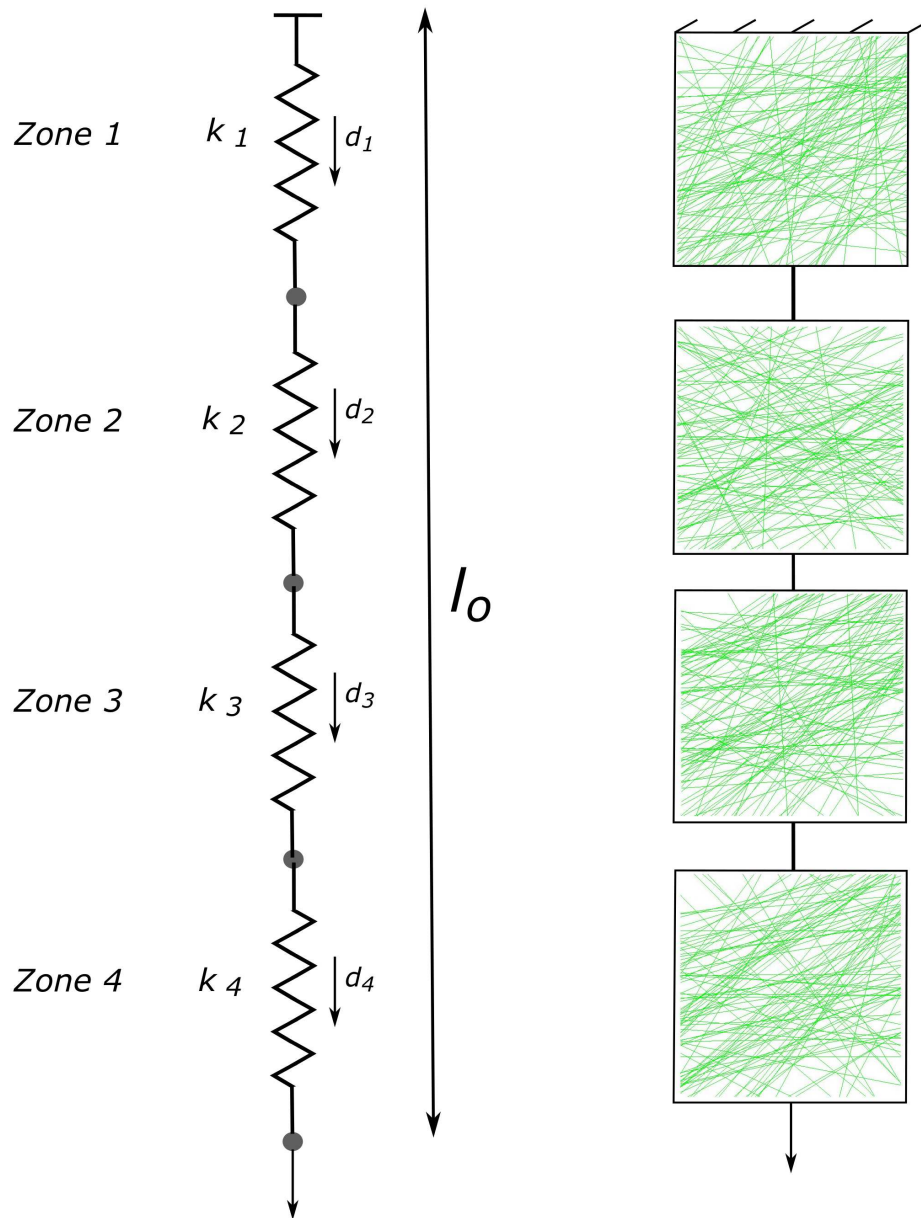


FIGURE 6.3 – A schematic representation of the proposed multi-scale model developed by linking the four individual micro-scale models in series.

where d_x, d_y, d_z are the displacements at the embedded node; N_i are the shape functions of the host element evaluated at the embedded node; u_i, v_i, w_i are the nodal displacements of the host element. The resulting total force on the host element nodes is calculated as $F_{total} = K_{total}dx$ by computing the total stiffness of the system using the equation below:

$$K_{total} = \int_{V(M)} B_M D_M B_M dv + \int_{V(f)} B_M D_f B_M dv \quad (6.2)$$

where B_M is the strain-displacement matrix for the host element, and D_M and D_f are the elasticity matrices for the host and fiber respectively.

The inability of using elements with rotational degrees of freedom as host elements, and

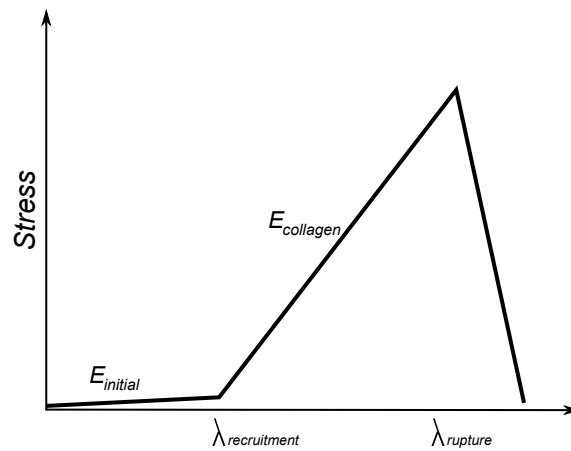


FIGURE 6.4 – Bi-linear elastic model used to represent the behavior of collagen fibers in the embedded element model.

the limitation of unconstrained rotational degrees of freedom on the embedded element led us to model the fibers as straight (uncurled) truss elements. The matrix was modelled as a neohookean solid and collagen fibers were modelled as a bi-linear elastic material with brittle damage as shown in figure 6.4 to represent a recruitment model. The initial low-stiffness region corresponds to the recruitment phase beyond which the stiffness equals the actual tensile modulus of collagen. The tensile modulus was inversely identified with an initial estimate equal to the value identified on the micro-scale model in chapter 5. The stretch value for collagen fiber recruitment was also identified inversely from the global stress-stretch curve. An acceptable starting value was identified from the reported values in literature [Zulliger and Stergiopoulos, 2007b]. The recruitment stretch value can be equated to the waviness parameter as $Waviness = 1 + \lambda_{recruitment}$. To emulate the uniaxial tension experiment, a tensile displacement was applied on one face while simultaneously three orthogonal faces were constrained using symmetric boundary conditions in Abaqus. The reconstructed finite element models for both circumferential and longitudinal samples are shown in figure 6.5. Finally the critical strain for collagen fibers is identified using an inverse method with an initial guess value equal to the one utilized in the micro-scale model. The accepted value was taken as the one that corresponds to the best-fit stress-stretch curve with respect to the experiment.

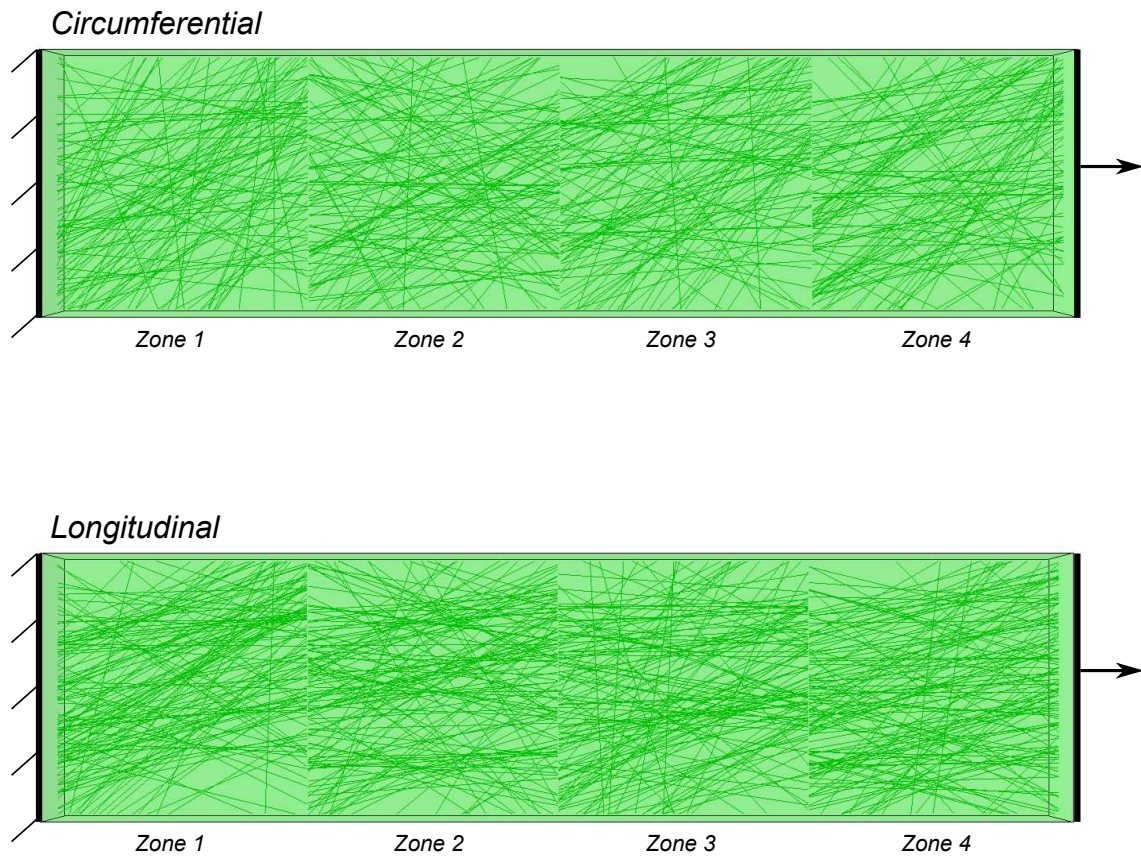


FIGURE 6.5 – A schematic of the embedded element model with collagen fiber networks embedded in to Matrix.

6.5 Results

A comparison of the two methods described above with experimentally recorded stress-stretch curves was made on two samples: one aligned circumferentially, one aligned longitudinally. In figure 6.6, the first Piola-Kirchoff stress, computed as the total reaction force divided by the initial cross-sectional area was plotted against stretch. The blue curve in both figures represents the experimentally recorded result, where as the other three represent the best fit curves for micro-scale approach as presented also in chapter 5, the first approach presented here (which is a direct extension of the micro-scale approach), and the embedded element method. The micro-scale approach uses the average morphology of the four zones, while the other two methods explicitly incorporate each of the four zones' morphology through the modeling process.

The material parameters for collagen modulus for the multi-scale model did not deviate from the value identified on the micro-scale model. However, the embedded element model revealed an increase of up-to 20 %. Identified values of waviness and fiber failure stretch are presented in Table 1. While the value of fitted waviness did not vary much between the micro-scale model and the multi-scale model, the identified waviness was found to be significantly lower for both samples in EEM. This is likely due to the fact that affine transformation, as is the case with EEM induces a slower rate of re-orientation. This leads to lower identified waviness values to be in tune with global recruitment stretch. Further, the disparity was found to be lower in the longitudinal sample, where the fibers were almost aligned to the loading direction, thereby warranting little re-orientation. The deviations in

Sample	Parameter	Micro-scale	Multi-scale	EEM
Circumferential	Waviness	1.364	1.378	1.30
	Collagen failure stretch	1.195	1.213	1.25
Longitudinal	Waviness	1.227	1.23	1.195
	Collagen failure stretch	1.255	1.255	1.28

TABLE 6.1 – Comparison of identified collagen structural and failure parameter for multi-scale and embedded element models.

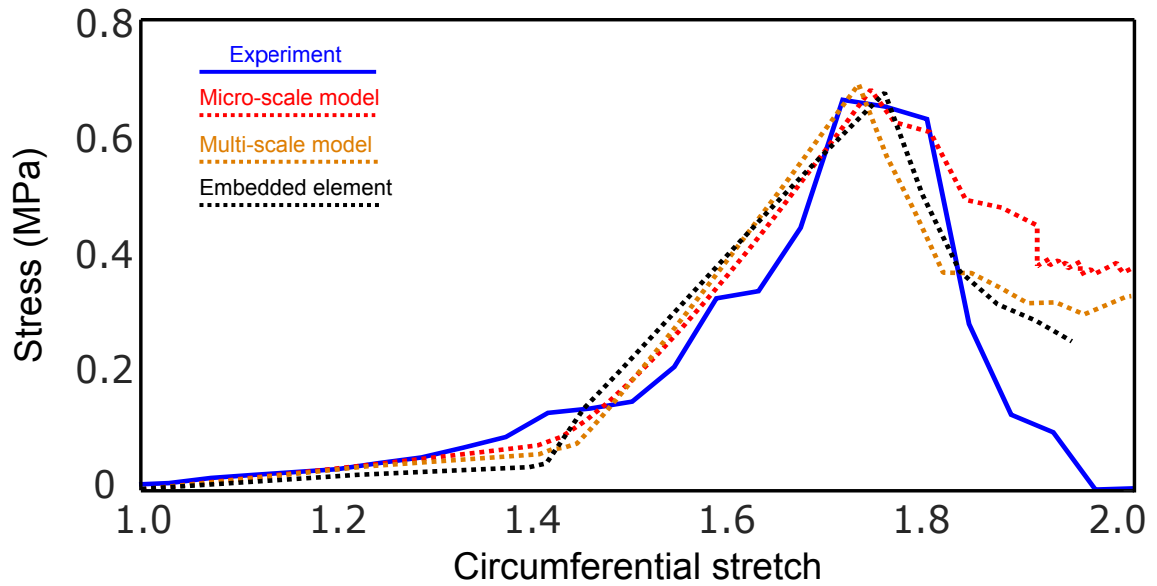
the identified value of waviness between the micro-scale model and the multi-scale model is likely due to the minor changes in the fiber network architecture in different zones. Similarly, the identified values of collagen failure stretch were found to be slightly higher in EEM, where as no significant change was found in multi-scale model. This is a direct consequence of the identified waviness parameter, inducing larger strains in fibers in the EEM model.

6.6 Discussion

In this study we developed a structure based multi-scale model of the tunica adventitia with the help of SHG imaging. The model can serve as a powerful tool for predicting macro-scale failure conditions based on experimentally measured micro-structural fiber architecture. From the results it was demonstrated that a fiber-scale discrete failure model could predict tissue's failure. A major progress in the current study is the potential to accommodate regional structural variations in fiber architecture without too much change in the failure criteria. To compare the proposed model, an embedded element based model was developed in Abaqus. The embedded element model assumes affine kinematics for the fibers. From the comparison to experiments, both models showed potential in predicting tissue-scale mechanics albeit leading to contrasting fiber failure criteria underlining the importance of fiber kinematics, and the importance to handle it as properly as possible.

The material properties utilized in comparing the model's response to experiments were previously recorded in chapter 5 using a micro-structural model. The same values were used in the multi-scale model for collagen's modulus and the neo-hookean material parameter of the matrix. This resulted in a slight difference in the recorded simulation response for the micro-structural and multi-scale models. Although this outcome is encouraging, the limited sample pool suggests to confirm this result on a larger amount of tested samples. In addition, the network architecture in both the circumferential and longitudinal samples did not show marked difference from zone to zone. As more experimental data becomes available, it will become progressively easier to test conclusions such as homogeneity of

Circumferentially aligned sample



Longitudinally aligned sample

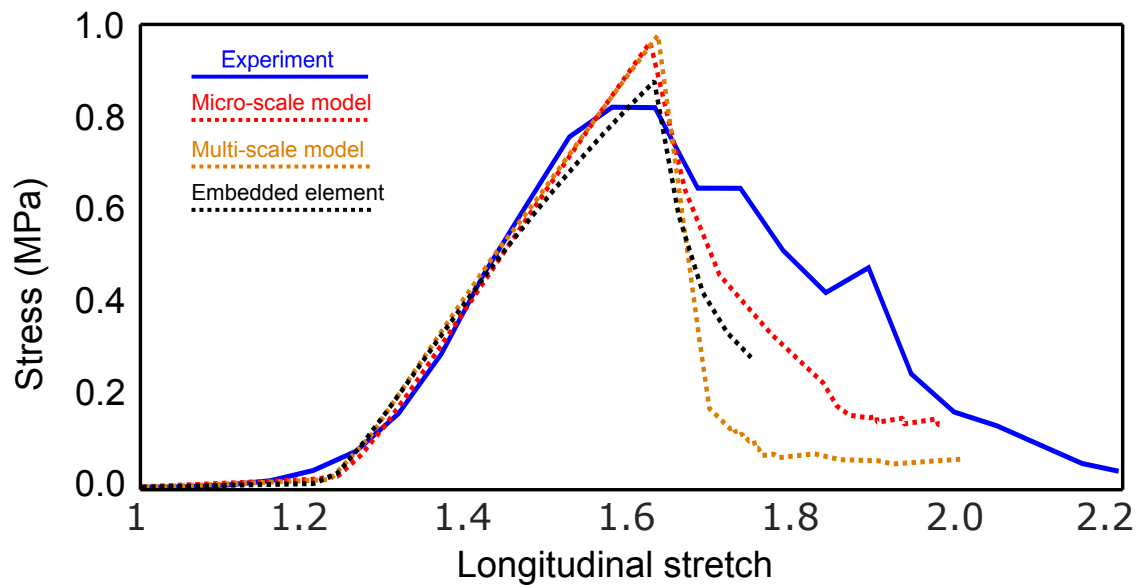


FIGURE 6.6 – Comparison of the stress-stretch curve for micro-scale model (dotted red line), multi-scale model (dotted orange line), embedded element model (dotted black line), against the experiment (solid blue line).

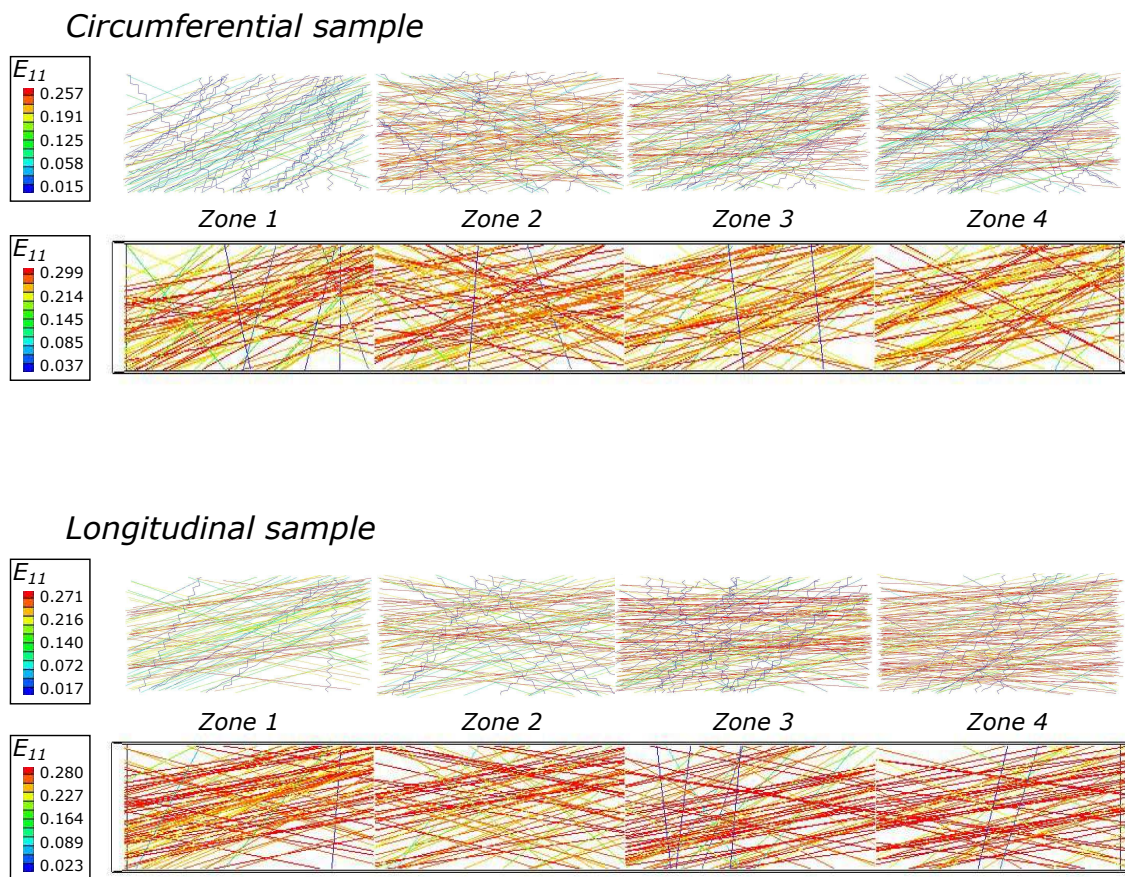


FIGURE 6.7 – A qualitative comparison of the strain distribution in fibers as predicted by multi-scale and embedded element models almost prior to tissue failure.

material properties in the arterial tissue at the mm-scale.

Figure 6.7 shows the axial strain distribution in the fibers just before failure. In both the circumferential and longitudinal samples, it can be seen that the strain in the fibers is slightly higher in the embedded element model. This is justified by the fact that affine-kinematics underestimates the amount of fiber re-orientations. This would mean that for a given axial stretch at the tissue level, the fibers following non-affine kinematics would recruit first as they reorient themselves towards the loading direction quicker. For this reason, the embedded element model predicts a lower waviness value in order to achieve the same fiber recruitment at the tissue scale thereby inducing slightly larger strains. Subsequently as shown in table 1, the fiber failure stretch parameter identified from the embedded element technique is higher than the one identified from non-affine kinematics assumption based multi-scale model. This inspection further adds to the conclusion that the mechanics of the collagen fiber network in arterial tissue is non-affine and should be carefully accounted for in fiber-scale modeling approaches.

Figure 6.8 shows the percentage of broken fibers in each zone in the extended model

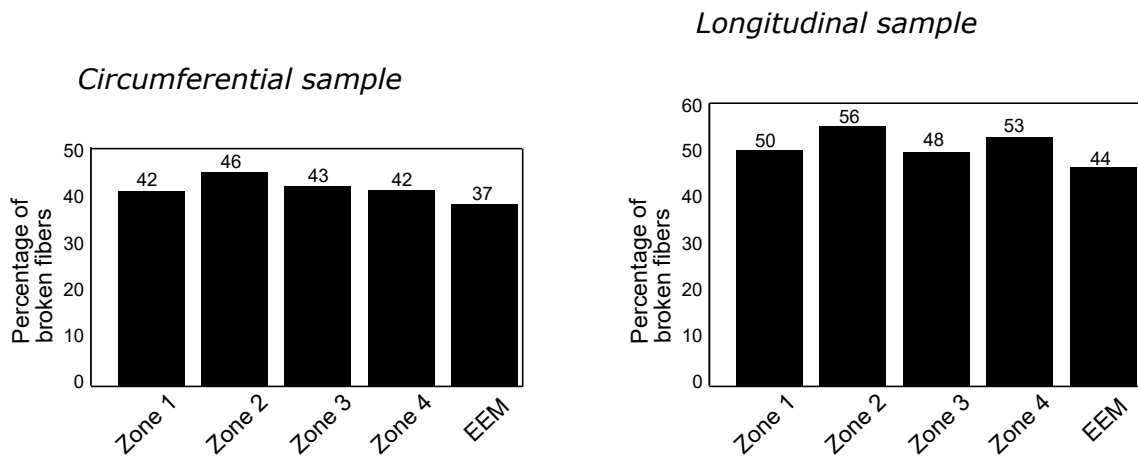


FIGURE 6.8 – Percentage of failed fibers in both models at failure.

and the total percentage of failed fibers in the embedded element model. Figure 6.9 shows the status of the fibers in both networks immediately after failure. The red lines correspond to intact fibers where as blue lines correspond to broken fibers. Both models indicate a similar pattern for micro-structure failure with no apparent distinction. The pattern of failure observed in both models did not show any indication that failure occurs at the mid-point of the sample. This might possibly point towards other co-existing mechanisms for tissue failure apart from sole brittle fiber failure along with fiber-fiber interactions, which are not taken into consideration in the present study.

Despite the good fit with experimental results the model may not yet completely represent the failure mechanisms in arterial tissues. The current model represents a 2 mm length scale of the 2 cm tested tissue sample. It is of course possible to reconstruct a more realistic structural model of the adventitia. This would require further micro-structural investigation or additional assumptions such as a homogeneous collagen fiber architecture within a local zone of the tissue. Further, a recruitment type model was used for fibers in the embedded element model for computational purposes, which could be replaced with a wavy or Fung type model.

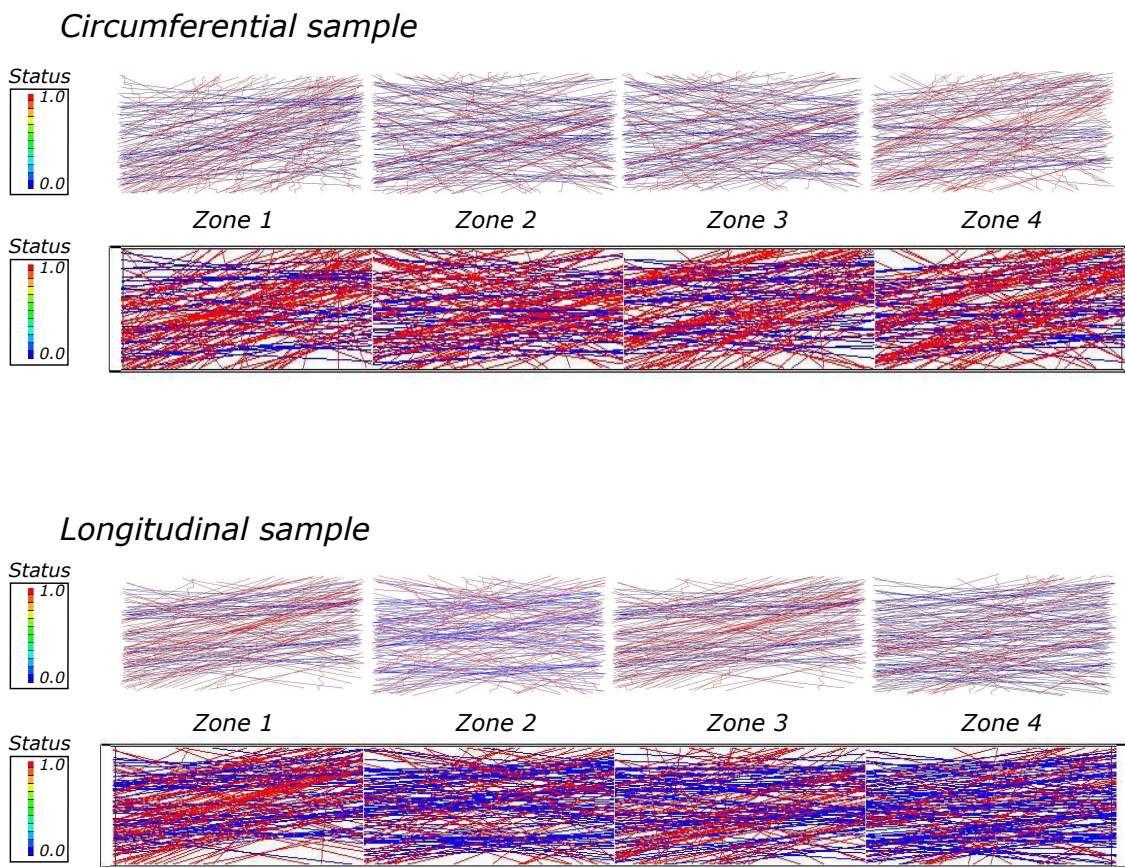


FIGURE 6.9 – An illustration of broken collagen fibers (blue lines) immediately after tissue failure as predicted by the multi-scale and embedded element models.

6.7 Conclusion of the chapter

In this chapter we presented the extension of our structure based micro-scale mechanical model of the tunica adventitia to macro-scale as a first step towards the study of heterogeneity and localization phenomena in adventitial mechanics. This was achieved by combining a thorough investigation of the tissue micro-structure using SHG imaging and the numerical network reconstruction technique provided in chapter 3. Through this analysis we gathered further observations indicating that the underlying fiber kinematics to be non-affine. The model, however limited, demonstrated its ability to accurately predict the tissue's prefailure and failure behavior. This model could provide new insights into failure mechanisms involved in aortic rupture.

Chapter 7

General discussion and conclusions

Contents of the chapter

7.1	Main findings162
7.2	Implications for research in arterial biomechanics163
7.3	Limitations.165
7.4	Future prospects.166

There is a pressing need for a better knowledge of the mechanical behavior of arterial tissues in critical life threatening conditions. The role of micro-structural constituents in determining the tissue's mechanical response is not comprehensively established. In this thesis the mechanical response of arterial tissue and the mechanical state of its micro-structural constituents was investigated via micro-structure based modeling approaches. This chapter presents an overall review of the main results obtained in this thesis and their implications for future research in arterial biomechanics.

7.1 Main findings

- ***Micro-structural imaging:*** After reviewing the state of the art in chapter 1, it was shown that the orientation distribution of collagen fibers is important in determining the mechanical behavior of arterial tissue. A complete 3-D profile of collagen fibers in the adventitial layer using SHG imaging reaffirmed the heterogeneous and anisotropic nature of arterial wall layers. Quantification of the fiber morphology showed that collagen fibers' orientation varied between two adjacent locations in the adventitia. Moreover, it was observed that the fibers tend to have a mean orientation aligned closer towards the circumferential direction. The results were also inconsistent with the assumptions made in the literature that two distinct collagen fiber families can be observed in the adventitia. In some cases, especially in human aneurysmal aortae, a single distinct mean orientation was observed. In other cases, mostly in healthy porcine tissues, two distinct fiber families were quantified but with different volume of fibers in each family. Finally it also revealed the crimped nature of collagen fibers, which explains the highly non-linear stress-stretch response of the tissue beyond physiological load.
- ***Mechanical testing:*** Uniaxial tensile testing of adventitial layers of porcine arteries showed that their mechanical response is highly anisotropic. The results also demonstrated that the circumferential direction has higher tensile strength as compared to the longitudinal direction. The experimental study also showed that the elastic modulus of the tissue in the range of supra-physiological loading is marginally higher in the circumferential direction. These observations are coherent with majority of the reports in the literature. However, some samples did exhibit contrary outcomes, which further suggested local heterogeneity.
- ***Micro-scale mechanical modeling:*** The finite element model based on fiber network morphology extracted from SHG image stacks demonstrated the predictive capability of the model in quantifying the macroscopic mechanical response. The developed model accounts for dominant structural information of collagen fibers such as orientation, crimp, and volume fraction. Chapter 4 presents the first step in implementation of this model where it solely accounts for the elastic response of the tissue. The model demonstrated an excellent comparison to experimental data, implying the applicability of micro-scale mechanical models in analyzing macro-scale mechanical response. A parametric study explained the relation between micro-structure and the tissue's macroscopic mechanical behavior. The analysis showed that elastic modulus

of collagen bears a high influence on the tissue's elastic modulus in the high-strain region (see figure 4.9), indicating that the high variability in collagen fiber stiffness (≈ 60 MPa to 450 MPa as reported in literature [Sherman et al., 2015a, Gentleman et al., 2003, Miyazaki and Hayashi, 1999]) could be one the reason for varying tissue strength. Structural parameters such as collagen crimp and orientation distribution also indicated a significant influence on the macroscopic mechanical response. The model allowed for the evaluation of two important parameters that characterize the nature of fiber kinematics: gradual uncrimping and reorientation of fibers towards the loading direction. Finally, this study enabled the quantification of the affine nature of fiber kinematics. The results showed that collagen fibers undergo higher reorientation than predicted by affine transformation, signifying the non-affine nature of their underlying kinematics.

- **Damage modeling:** An extension of the developed micro-scale model of the adventitia to model tissue damage was presented in chapter 5. Damage at the micro-scale under supra-physiological tension is represented by brittle failure of collagen fibers as motivated from the observations made in literature [Gentleman et al., 2003]. The comparison of the proposed model's response to experimental observations showed that a fiber-based damage model could precisely predict macroscopic tissue failure. The model reproduced two different experiments; bulge inflation testing conducted on human aneurysmal tissues and uniaxial tensile testing of porcine arteries. The determined collagen failure criteria indicated that aneurysmal tissues may have alterations resulting in abnormal collagen fiber failure stretch values. On the other hand, collagen fiber failure stretch determined for porcine samples agreed well with literature reported values. This showed the pertinence of a fiber failure mechanism in shaping tissue's failure.
- **Multi-scale modeling:** The local heterogeneity in collagen fiber morphology was represented via a micro-structurally based multi-scale model. The model was able to predict the tissue's mechanical response with same material parameters identified on the micro-scale model (representing the spatially averaged micro-structure). This showed that material properties of collagen possibly remain homogeneous throughout the tissue. This proposed methodology could contribute to novel insights into the failure mechanisms responsible for aortic rupture.

7.2 Implications for research in arterial biomechanics

The implications arising from the results are multi-fold leading to the following conclusions and questions.

- **Structure-function relationship:** Recent experiments on aortic tissue have revealed that the strength of the tissue is correlated to collagen content [Schrieffl et al., 2015, Weisbecker et al., 2013]. The effect of aging on the tensile strength of the aneurysmal sinus tissue was demonstrated by [Iliopoulos et al., 2013], who concluded that preferential alignment of collagen in circumferential direction lends it more strength. Pichamuthu et al [Pichamuthu et al., 2013] demonstrated that both circumferential and longitudinal tensile strengths are higher in Bicuspid aortic valve

(BAV) patients compared to Tricuspid aortic valve (TAV) patients. Phillippi et al [Phillippi et al., 2014] reported collagen fiber micro-structure in the aortic media ECM is uniquely distinct between aneurysmal BAV and TAV tissue. These prior works circumstantially demonstrate how collagen fiber organization directly influences tissue strength in the human aorta. Our present study advances prior structure-function theories for tissue mechanics by identifying the micro-structural mechanisms in healthy and diseased tissue under in-plane loading conditions. Our work suggests that differences in collagen fiber orientation and crimp among other considerations can explain the differences in their uniaxial aortic tissue strength. This is also in line with experimental observations made in our group [Cavinato, 2020], who found that aneurysmal and aged presented structural changes, like waviness at no load, which could affect their response at loads close to rupture. Furthermore, it shows that the recruitment of collagen into load bearing is controlled by both gradual reorientation and uncrimping processes.

- **Non-affine fiber kinematics:** Collagen fibers reorganize themselves according to the applied load. Majority of the investigations concluded that the re-orientation of collagen fibers follows non-affine transformation [Chandran, 2005, Krasny et al., 2017a, Morin et al., 2018]. Most of the micro-structure based mechanical models assume an affine approximation in their theories. It is equivalent to assuming that each fiber is tied to the underlying homogeneous continuum. However, in reality this was demonstrated to not be the case, although exact characterization of this behavior is still not available. Nonetheless, the results of our model demonstrated that non-affine kinematics accurately predict the tissue's macro-scale mechanical behavior. Although affine assumption leads to acceptable results for networks of high densities, for a reliable performance on any fiber network subjected to more complex deformations, non-affine assumption needs to be taken into account [Picu, 2011a]. The non-affine nature of fiber deformation is demonstrated in figure 4.12, which shows that non-affinity increases with applied loading in accordance with literature [Mauri et al., 2016].
- **Micro-scale mechanical state:** Quantifying the statistics of micro-scale mechanical state in composite materials is a challenging task and is widely acknowledged [Chamis, 1987, Aboudi, 1988, Sriramula and Chryssanthopoulos, 2009]. This is because of the complexity of experimental setup, instrumentation constraints, and the number of variables required for obtaining a statistically significant result. Our model, with the help of appropriate assumptions and micro-structure based information helps us quantify this information as presented in figures 4.13 and 4.14. Such quantified information on collagen fiber's stress and strain at loads close to rupture help us identify possible micro-scale rupture mechanisms to further devise quantitative rupture criteria.
- **Collagen fiber damage:** The tensile tests conducted on extracted individual collagen fibers suggest that fibers tend to fail with little to none plastic deformations [Miyazaki and Hayashi, 1999, Gentleman et al., 2003]. Owing to these observations, a brittle failure model has been implemented for collagen fibers in this thesis. A discussion of the model's macroscopic failure properties with respect to reported failure hypotheses in the literature could be of interest for further studies. Constitutive parameters of the model were estimated from quasi-static uniaxial testing of adventitial strips of

porcine arteries, which demonstrated that the model's behavior captures salient mechanical features of vascular tissue. Clearly, the proposed constitutive model was able to predict the macroscopic tissue failure, however testing a sufficiently large number of tissue samples under appropriate conditions is required to draw sound conclusions regarding the failure mechanisms of the abdominal aortic aneurysm (AAA) wall and the reliability of the proposed constitutive description. Other microscopic damage mechanisms such as cross-link failure at the collagen fibril level [Gasser, 2011, Scott, 2003] and inter-strand delamination at the molecular level [Marino et al., 2019] have gained traction. Perhaps irreversible plastic deformations are a precursor to collagen fiber failure, which in-turn trigger tissue failure. These phenomena could be incorporated in our model using a progressive damage model as shown in figure 5.14. Although plastic deformations and damage of vascular tissue have been observed during macroscopic mechanical testing, knowledge of their micro-scale mechanisms is meager. Hence, a greater extent of experimental investigations are required for calibrating such a model. Moreover, very little is known at the moment about vascular collagen fibers, due to which the study performed in the thesis was motivated from observations of collagen from ligaments and tendons instead.

- Open ended questions: The conclusions derived from the results of this thesis pose the following questions.
 - How does the model benefit from a more realistic representation of the micro-structure, such as the result of a direct segmentation (as discussed in chapter 3) ?
 - How to reduce the uncertainty propagation from micro-scale mechanical characteristics such as collagen elastic modulus to macro-scale mechanical behavior?
 - What is the significance of fiber-fiber interactions and how to include fiber cross-links in the model? This includes the characterization of type of cross-links and their strength.
 - How does the model benefit from including the micro-structure of the medial layer? One short hand interpretation would be to characterize dissection type failure, which is known to initiate in the inner layers of the arterial wall.
 - How to link fibrous micro-structure based rupture criteria to clinical assessment of rupture risk quantification and treatment?

7.3 Limitations

The study presented in this thesis is not without limitations, which are presented here:

- The entire thesis was dedicated in investigating the micro-scale mechanics of the adventitia, as the mechanics of other layers were not considered. The reason for this choice was as follows: the medial layer is primarily made up of elastin and a few collagen fibers aligned neatly towards the circumferential direction. In contrast, the adventitial layer is almost exclusively made up of collagen fibers organized randomly.

In addition, collagen fibers have higher tensile strength as compared to elastin fibers making the adventitia a protective sheath, preventing the arterial wall from over-extension at supra-physiological pressures.

- The collagen fibers' orientation was considered only in the longitudinal-circumferential plane. Although the reports in the literature indicate that the out of plane orientation is insignificant, it is nonetheless present. Further, all the samples subjected to micro-structural imaging were stored at -20° C. Yet, possible induced changes in micro-structure due to the storage choice were not accounted for.
- The SHG image stacks acquired on the tissues did not encompass the entire thickness of the adventitia, limited by the quality of the signal. Hence, the acquired image stack was assumed to be representative of the micro-structure at the imaged location.
- The developed numerical model does not capture any fiber-matrix or fiber-fiber interactions. However, this assumption was shown to be valid for flexible fiber networks of high-densities. This led to the supposition of an additive law for the total stress.
- In predicting the tissue's macroscopic failure, a brittle damage model was used for the fibers. This is a simplistic assumption as experimental evidence demonstrates more complex irreversible damage mechanisms, possibly originating at the fibril or molecular level.

7.4 Future prospects

- The 3-D orientation profile of the fibers could be readily incorporated into the model, which is predicated on more sophisticated imaging techniques.
- The assumption of neglecting fiber-fiber interactions induces homogeneous stress-strain state for the whole fiber. The complexity of the model could be enhanced by introducing cross-links between the fibers. The density of cross-links and their behavior characterization requires additional micro-structural investigation.
- In this study, only uniaxial tension and bulge-inflation testing protocols have been explored in connection to micro-structural imaging. In order to fully characterize the failure behavior of arterial tissue, additional mechanical testing protocols could be imagined, such as: shear lap testing, tension inflation testing, and peel testing.
- The straightforward and quick nature of multi-photon microscopy could be exploited to acquire a more detailed profile of the tissue's micro-structure, which in-turn could be fed into the multi-scale model. This would enable the construction of a more realistic micro-scale based mechanical model of the tissue.

- The damage model presented in the study could be extended to represent more complex mechanisms such as plastic deformations which induce irreversible damage.
- A robust machine learning tool could be devised to detect the risk of tissue failure based on complex data sets of collagen fiber architecture. Such a tool could provide a reliable assessment of risk of rupture based on tissue's morphology for possible future clinical applications.
- It is important to consider the nature of the tissue in characterizing its failure properties. Therefore a larger study involving the mechanical testing and micro-scale analysis of tissues acquired from patients of different age groups and patients with different genetic disorders would help in assessing the correlation of these parameters with rupture.
- Incremental improvement of processing of SHG image stacks: this is an ongoing PhD thesis undertaken by Zeineb Nejim, where the goal is to develop image processing algorithms to improve the acquired images and then to reconstruct synthetic images having the same characteristics as the micro-structures in the sense of obtaining a "clone" image that exhibits all the original characteristics.

Conclusion générale

Il est urgent de mieux connaître le comportement mécanique des tissus artériels dans des conditions critiques mettant la vie en danger. Le rôle des constituants microstructuraux dans la détermination de la réponse mécanique des tissus n'est pas bien établi. Dans cette thèse, la réponse mécanique du tissu artériel et l'état mécanique de ses constituants microstructuraux ont été étudiés par des approches de modélisation basées sur la microstructure.

Principaux résultats

- **Imagerie micro-structurale:** Après avoir passé en revue l'état de l'art au chapitre 1, il a été démontré que la distribution d'orientation des fibres de collagène est importante pour déterminer le comportement mécanique du tissu artériel. Un profil 3D complet des fibres de collagène dans la couche adventitielle à l'aide de l'imagerie SHG a confirmé la nature hétérogène et anisotrope des couches de la paroi artérielle. La quantification de la morphologie des fibres a montré que l'orientation des fibres de collagène variait entre deux endroits adjacents de l'adventice. De plus, on a observé que les fibres ont tendance à avoir une orientation moyenne alignée plus près de la direction circonférentielle. Les résultats ne concordaient généralement pas avec les hypothèses formulées dans la documentation selon lesquelles deux familles distinctes de fibres de collagène peuvent être observées dans l'adventice. Dans certains cas, en particulier dans les anévrismes aortiques humains, une seule orientation moyenne distincte a été observée. Dans d'autres cas, surtout dans les tissus porcins sains, deux familles de fibres distinctes ont été quantifiées, mais avec un volume de fibres différent dans chaque famille. Enfin, il a également révélé la nature ondulée des fibres de collagène, ce qui explique la réponse très non-linéaire du tissu au stress et à l'étirement au-delà de la charge physiologique.
- **Essais mécaniques:** Des essais de traction uniaxiale sur des couches adventitielles d'artères porcines ont montré que leur réponse mécanique est très anisotrope. Les résultats ont également démontré que la direction circonférentielle est plus résistante à la traction que la direction longitudinale. L'étude expérimentale a également montré que le module d'élasticité du tissu dans la gamme des charges supra-physiologiques est légèrement plus élevé dans la direction circonférentielle. Ces observations sont cohérentes avec la majorité des rapports de la littérature. Cependant, certains échantillons présentaient des résultats contraires, ce qui soulignait davantage l'hétérogénéité locale.

- **Modélisation mécanique à l'échelle microscopique:** Le modèle éléments finis basé sur la morphologie du réseau de fibres extrait des piles d'images SHG a démontré la capacité prédictive du modèle à quantifier la réponse mécanique macroscopique. Le modèle développé tient compte des informations structurelles dominantes sur les fibres de collagène telles que l'orientation, l'ondulation et la fraction volumique. Le chapitre 4 présente la première étape de la mise en œuvre de ce modèle où il ne tient compte que de la réponse élastique du tissu. Une étude paramétrique a expliqué la relation entre la microstructure et le comportement mécanique macroscopique du tissu. Le modèle a permis d'évaluer deux paramètres importants qui caractérisent la nature de la cinématique des fibres : la désondulation progressive et la réorientation des fibres dans le sens de la charge. Enfin, cette étude a permis de quantifier la nature affine de la cinématique des fibres. Les résultats ont montré que les fibres de collagène subissent une réorientation plus élevée que prévue par la transformation affine, ce qui révèle la nature non affine de leur cinématique sous-jacente.
- **Modélisation de l'endommagement:** Une extension du modèle micro-échelle développé de l'adventice pour modéliser les lésions tissulaires a été présentée au chapitre 5. La comparaison de la réponse du modèle aux observations expérimentales a montré qu'un modèle basé sur l'endommagement des fibres pouvait prédire avec précision la défaillance macroscopique des tissus. Le modèle reproduit deux expériences différentes : l'essai de gonflement sur des tissus anévrysmals humains et l'essai de traction uniaxiale sur des artères porcines. Les critères de défaillance du collagène déterminés indiquaient que les tissus anévrysmaux pouvaient présenter des altérations entraînant des valeurs anormales d'allongement à rupture des fibres de collagène en cas de défaillance. D'autre part, l'allongement à rupture des fibres de collagène déterminé pour les échantillons porcins correspond bien aux valeurs rapportées dans la littérature. Cela a montré la pertinence d'un mécanisme de défaillance des fibres pour modéliser la défaillance des tissus
- **Modélisation multi-échelles:** L'hétérogénéité locale de la morphologie des fibres de collagène a été représentée par un modèle multi-échelle basé sur la microstructure. Le modèle a été en mesure de prédire la réponse mécanique du tissu à l'aide des mêmes paramètres matériels que ceux identifiés sur le modèle à micro-échelle (représentant la microstructure moyenne de l'échantillon). Ceci a montré que les propriétés matérielles du collagène peuvent rester homogènes à travers les tissus. La méthodologie proposée pourrait contribuer à mieux comprendre les mécanismes de défaillance responsables de la rupture de l'aorte.

Limites

L'étude présentée dans cette thèse n'est pas sans limites, qui sont présentées ici :

- Toute la thèse a été consacrée à l'étude de la micro-mécanique de l'adventice, car la mécanique des autres couches n'a pas été prise en compte. La raison de ce choix était la suivante : la couche médiane est principalement constituée d'élastine et de quelques fibres de collagène bien alignées dans le sens circonférentiel. En revanche,

la couche adventitielle est presque exclusivement constituée de fibres de collagène organisées au hasard. En outre, les fibres de collagène ont une résistance à la traction supérieure à celle des fibres d'élastine, ce qui fait de l'adventice une gaine protectrice, empêchant la paroi artérielle de s'étirer à des pressions supra-physiologiques.

- L'orientation des fibres de collagène n'a été prise en compte que dans le plan longitudinal-circconférentiel. Bien que les rapports de la littérature indiquent que l'orientation hors plan est insignifiante, elle est néanmoins présente. De plus, tous les échantillons soumis à l'imagerie microstructurale ont été entreposés à -20°C . Pourtant, les éventuels changements induits dans la microstructure dus au choix de stockage n'ont pas été pris en compte.
- Les piles d'images SHG acquises sur les tissus n'englobaient pas toute l'épaisseur de l'adventice, limitée par la qualité du signal. Par conséquent, on a supposé que la pile d'images acquise était représentative de la microstructure à l'emplacement de l'image.
- Le modèle numérique développé ne reproduit pas les interactions fibre-matrice ou fibre-fibre. Toutefois, cette hypothèse s'est avérée valable pour les réseaux de fibres flexibles à haute densité. Cela a conduit à l'hypothèse d'une loi additive pour la contrainte locale.
- En prédisant la défaillance macroscopique du tissu, on a utilisé un modèle d'endommagement fragile pour les fibres. Il s'agit d'une hypothèse simpliste, car les données expérimentales démontrent des mécanismes de dommages irréversibles plus complexes, qui peuvent avoir leur origine au niveau des fibrilles ou au niveau moléculaire.

Perspectives d'avenir

- Le profil d'orientation 3D des fibres pourrait être facilement incorporé dans le modèle, sur la base d'informations obtenues par des techniques d'imagerie plus sophistiquées.
- L'hypothèse de négliger les interactions fibre-fibre induit un état de contrainte-déformation homogène pour l'ensemble de la fibre. La complexité du modèle pourrait être augmentée par l'introduction de liaisons entre les fibres. La densité des liaisons et leur caractérisation nécessitent une étude microstructurale supplémentaire.
- Dans cette étude, seuls les protocoles d'essais de tension uniaxiale et de gonflement ont été explorés dans le cadre de l'imagerie microstructurale. Afin de caractériser pleinement le comportement de défaillance du tissu artériel, on pourrait imaginer d'autres protocoles d'essais mécaniques, tels que les essais de cisaillement, les essais de gonflement sous tension et les essais de pelage.
- La nature simple et rapide de la microscopie multiphotonique pourrait être exploitée pour acquérir un profil plus détaillé de la microstructure du tissu, qui à son tour

pourrait être introduit dans le modèle multi-échelle. Cela permet la construction d'un modèle mécanique à micro-échelle plus réaliste du tissu.

- Le modèle d'endommagement présenté dans l'étude pourrait être étendu pour représenter des mécanismes plus complexes tels que les déformations plastiques qui induisent des dommages irréversibles.
- Un outil robuste d'apprentissage machine pourrait être conçu pour détecter le risque de défaillance des tissus à partir d'ensembles de données complexes sur l'architecture des fibres de collagène. Un tel outil pourrait fournir une évaluation fiable du risque de rupture en fonction de la morphologie des tissus.
- Il est important de considérer la nature du tissu pour caractériser ses propriétés de rupture. Par conséquent, une large étude incluant les essais mécaniques et l'analyse microscopique des tissus acquis de patients de groupes d'âge différents et présentant différents troubles génétiques devrait aider à établir la corrélation de ces paramètres avec la rupture
- Improvisation incrémentale du traitement des piles d'images SHG : il s'agit d'une thèse de doctorat en cours de Zeineb Nejim, dont le but est de développer des algorithmes de traitement d'images pour améliorer les images acquises et ensuite reconstruire des images synthétiques ayant les mêmes caractéristiques que les microstructures dans le sens d'obtenir une image "clone" qui présente toutes les caractéristiques originales.

Appendix A

The general experimental approach of combining SHG imaging with mechanical testing was used to build structurally based mechanical models as described in chapter 3. Prior to using that undertaking, uniaxial testing of porcine aortas was conducted in order to provide quantification of the elastic moduli of arterial tissue at different levels of loading. Furthermore, the failure properties for each loading direction (circumferential and longitudinal) were noted. This appendix mainly aims at sharing these experimental data as they are still rare in the literature.

Methods

Porcine whole aortas ($n = 11$) procured from a local butchery were used in this study. The descending portion of the aorta was excised and cylindrical portions of length 3 *cms* were cut. The cylindrical portions were cut open longitudinally and the resulting rectangular strips were used to extract dog-bone shaped samples for uniaxial testing. The medial layer of the samples was carefully peeled off and the resulting adventitial strips were frozen until the day of the experiment. For each porcine aorta one sample aligned with circumferential and one aligned with longitudinal direction were prepared for mechanical testing. A thickness measurement protocol was performed on the samples as described in section 2.5 to extract the thickness profile of each sample. A TA ElectroForce tensile machine was used to conduct the uniaxial tensile tests. The dog-bone samples were mounted on to the device and clamped at the ends using sand paper in order to prevent slippage. The initial position was chosen so as to not induce any stretch. The samples were elongated either until failure or until the limit of the tensile machine. The stretch was measured as the ratio of actual inter-clamp distance and initial inter-clamp distance: $\lambda = \frac{l}{l_0}$. The first Piola-Kirchoff stress versus stretch was recorded and plotted for each sample.

Results

The resulting stress-stretch curves of the aortae 1 – 6 are presented in figures A.1 and aortae 7 – 11 are presented in A.2.

The results presented here demonstrated that the aorta indeed is highly anisotropic. In as many as 8 specimens, the circumferential samples had a higher tensile strength than longitudinal samples. The cohort averaged ultimate tensile strength for circumferentially aligned samples was 0.95 MPa, and the cohort averaged ultimate tensile strength for longitudinally aligned samples was 0.81 MPa. The statistical averages of physiological modulus, maximum tensile modulus (MEM), ultimate tensile strength (UTS), and ultimate stretch for the cohort are presented in figure A.3 ($a - d$).

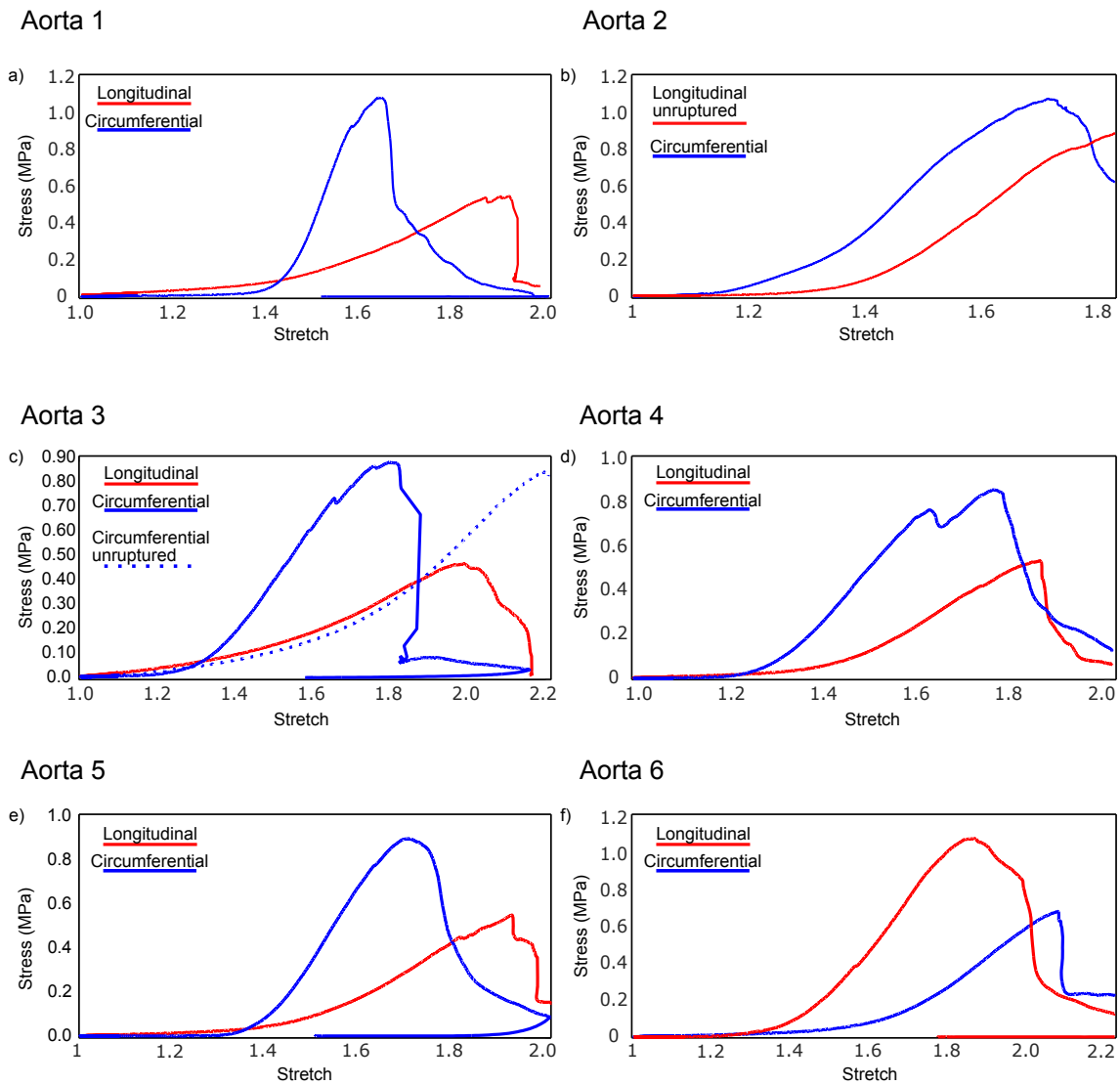


FIGURE 1 – Experimentally recorded stress-stretch curves for the porcine specimens 1 through 6.

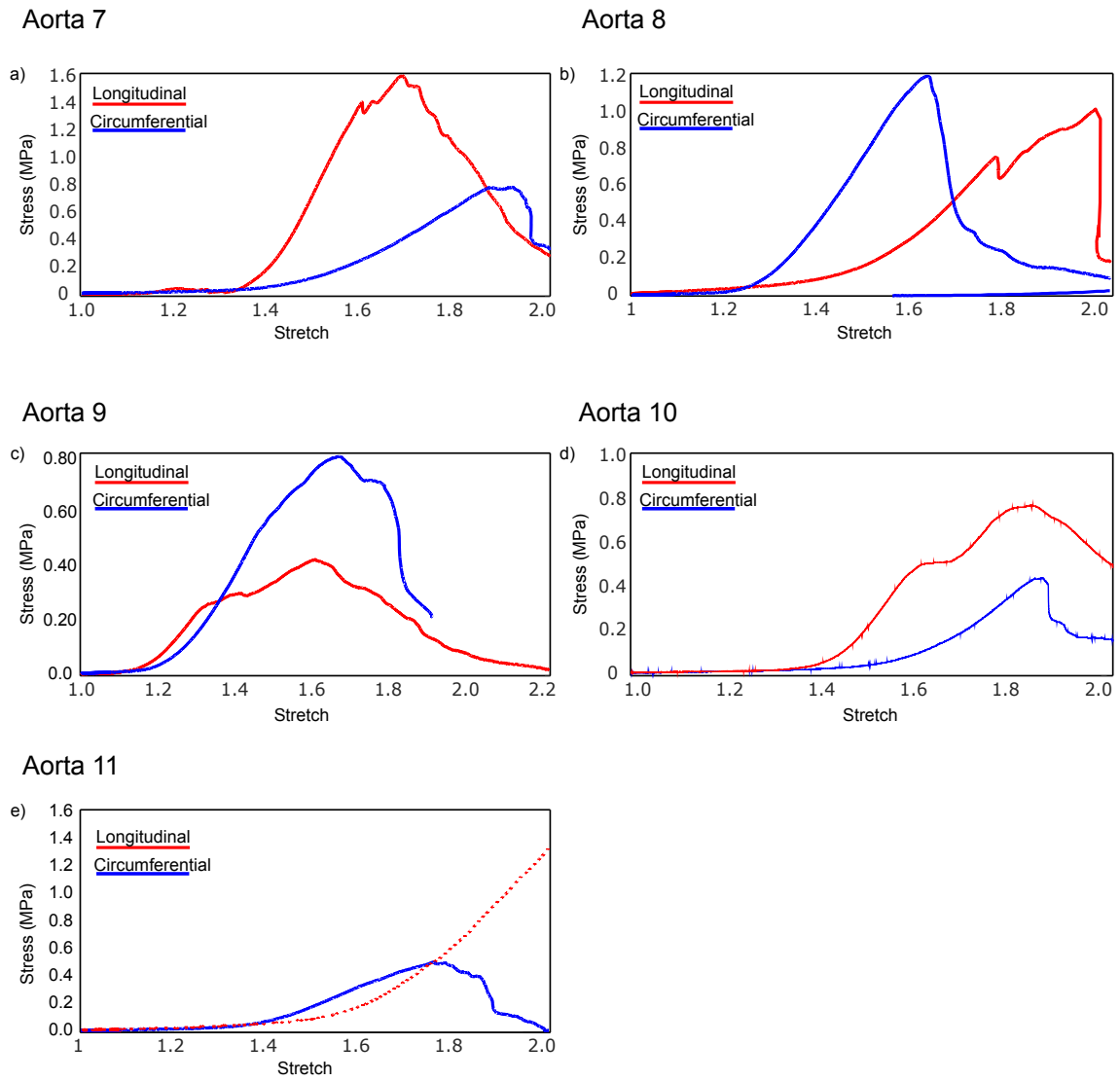


FIGURE 2 – Experimentally recorded stress-stretch curves for the porcine specimens 7 through 11.

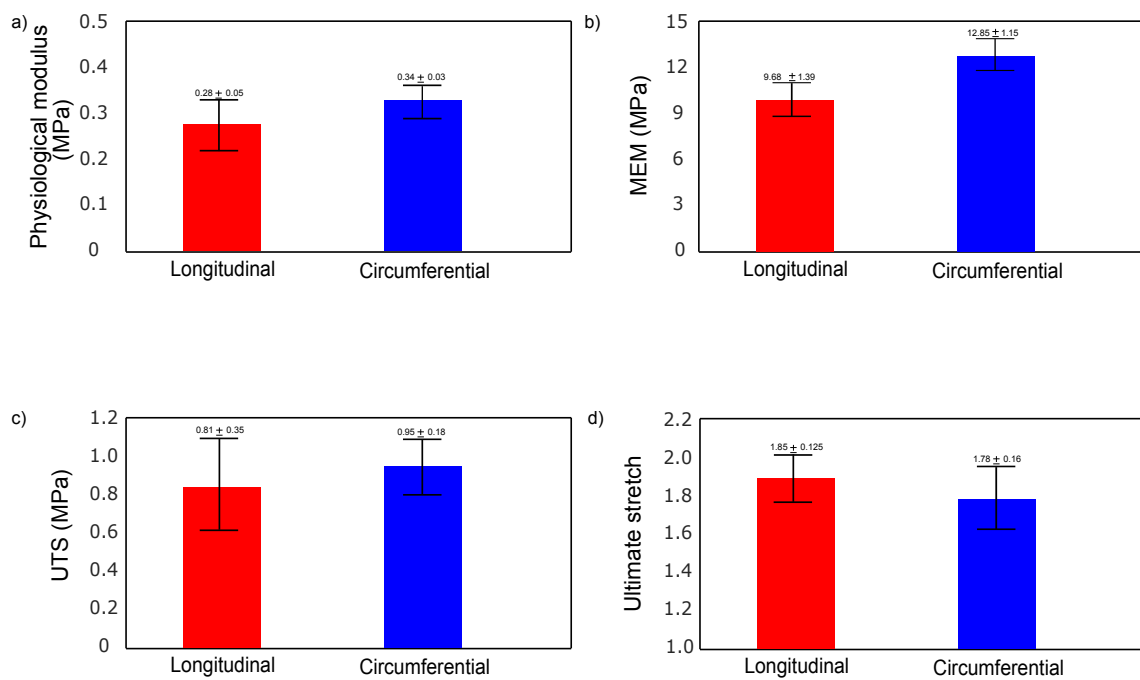


FIGURE 3 – Descriptive statistics of the porcine specimens presented as *mean ± standard deviation*.

Bibliography

- [Aboudi, 1988] Aboudi, J. (1988). Micromechanical analysis of the strength of unidirectional fiber composites. *Composites science and technology*, 33(2):79–96.
- [Adham et al., 1996] Adham, M., Gournier, J.-P., Favre, J.-P., De La Roche, E., Ducerf, C., Baulieux, J., Barral, X., and Pouyet, M. (1996). Mechanical characteristics of fresh and frozen human descending thoracic aorta. *Journal of Surgical Research*, 64(1):32–34.
- [Agianniotis et al., 2011] Agianniotis, A., Rezakhaniha, R., and Stergiopoulos, N. (2011). A structural constitutive model considering angular dispersion and waviness of collagen fibres of rabbit facial veins. *Biomedical engineering online*, 10(1):18.
- [Aifantis et al., 2011a] Aifantis, K. E., Shrivastava, S., and Odegard, G. M. (2011a). Transverse mechanical properties of collagen fibers from nanoindentation. *J Mater Sci: Mater Med*, 22(6):1375–1381.
- [Aifantis et al., 2011b] Aifantis, K. E., Shrivastava, S., and Odegard, G. M. (2011b). Transverse mechanical properties of collagen fibers from nanoindentation. *Journal of Materials Science: Materials in Medicine*, 22(6):1375–1381.
- [Al-Kofahi et al., 2002] Al-Kofahi, K. A., Lasek, S., Szarowski, D. H., Pace, C. J., Nagy, G., Turner, J. N., and Roysam, B. (2002). Rapid automated three-dimensional tracing of neurons from confocal image stacks. *IEEE Transactions on information technology in biomedicine*, 6(2):171–187.
- [Aladin et al., 2010] Aladin, D. M., Cheung, K. M., Ngan, A. H., Chan, D., Leung, V. Y., Lim, C. T., Luk, K. D., and Lu, W. W. (2010). Nanostructure of collagen fibrils in human nucleus pulposus and its correlation with macroscale tissue mechanics. *Journal of Orthopaedic Research*, 28(4):497–502.
- [Alastrué et al., 2009] Alastrué, V., Martínez, M., Menzel, A., and Doblaré, M. (2009). On the use of non-linear transformations for the evaluation of anisotropic rotationally symmetric directional integrals. Application to the stress analysis in fibred soft tissues. *International Journal for Numerical Methods in Engineering*, 79(4):474–504.
- [Alastrué et al., 2007] Alastrué, V., Rodríguez, J., Calvo, B., and Doblaré, M. (2007). Structural damage models for fibrous biological soft tissues. *International Journal of Solids and Structures*, 44(18-19):5894–5911.
- [Alastrué et al., 2010] Alastrué, V., Sáez, P., Martínez, M., and Doblaré, M. (2010). On the use of the Bingham statistical distribution in microsphere-based constitutive models for arterial tissue. *Mechanics Research Communications*, 37(8):700–706.

- [Alford, 2007] Alford, P. W. (2007). *Growth and Remodeling in a Thick-Walled Artery Model*, volume 69.
- [Alford et al., 2008] Alford, P. W., Humphrey, J. D., and Taber, L. A. (2008). Growth and remodeling in a thick-walled artery model: Effects of spatial variations in wall constituents. *Biomechanics and Modeling in Mechanobiology*, 7(4):245–262.
- [Altendorf et al., 2012] Altendorf, H., Decencière, E., Jeulin, D., Peixoto, P. D. S., DENISET-BESSEAU, A., Angelini, E., Mosser, G., and SCHANNE-KLEIN, M.-C. (2012). Imaging and 3D morphological analysis of collagen fibrils. *Journal of microscopy*, 247(2):161–175.
- [Ambrosi et al., 2011] Ambrosi, D., Ateshian, G. A., Arruda, E. M., Cowin, S., Dumais, J., Goriely, A., Holzapfel, G. A., Humphrey, J. D., Kemkemer, R., and Kuhl, E. (2011). Perspectives on biological growth and remodeling. *Journal of the Mechanics and Physics of Solids*, 59(4):863–883.
- [Amoroso et al., 2011] Amoroso, N. J., D’Amore, A., Hong, Y., Wagner, W. R., and Sacks, M. S. (2011). Elastomeric electrospun polyurethane scaffolds: The interrelationship between fabrication conditions, fiber topology, and mechanical properties. *Advanced Materials*, 23(1):106–111.
- [Anssari-Benam et al., 2012] Anssari-Benam, A., Gupta, H. S., and Screen, H. R. (2012). Strain transfer through the aortic valve. *Journal of biomechanical engineering*, 134(6):061003.
- [Antoniou et al., 2011] Antoniou, G. A., Antoniou, A. I., Antoniou, S. A., and Lazarides, M. K. (2011). A historical perspective of medical terminology of aortic aneurysm. *Journal of Vascular Surgery*, 54(5):1527–1528.
- [Armentano et al., 1995] Armentano, R. L., Barra, J. G., Levenson, J., Simon, A., and Pichel, R. H. (1995). Arterial wall mechanics in conscious dogs: Assessment of viscous, inertial, and elastic moduli to characterize aortic wall behavior. *Circulation Research*, 76(3):468–478.
- [Ateshian et al., 2009] Ateshian, G. A., Rajan, V., Chahine, N. O., Canal, C. E., and Hung, C. T. (2009). Modeling the matrix of articular cartilage using a continuous fiber angular distribution predicts many observed phenomena. *Journal of biomechanical engineering*, 131(6):061003.
- [Atlantic,] Atlantic, M. I. Peripheral Artery Disease Treatment NJ or PAD - a serious problem that Causes Leg Pain and Nonhealing wounds.
- [Avanzini et al., 2014] Avanzini, A., Battini, D., Bagozzi, L., and Bisleri, G. (2014). Biomechanical evaluation of ascending aortic aneurysms. *BioMed research international*, 2014.
- [Ayyalasomayajula et al., 2019] Ayyalasomayajula, V., Pierrat, B., and Badel, P. (2019). A computational model for understanding the micro-mechanics of collagen fiber network in the tunica adventitia. *Biomechanics and modeling in mechanobiology*, pages 1–22.
- [Azadani et al., 2013] Azadani, A. N., Chitsaz, S., Mannion, A., Mookhoek, A., Wisneski, A., Guccione, J. M., Hope, M. D., Ge, L., and Tseng, E. E. (2013). Biomechanical properties of human ascending thoracic aortic aneurysms. *The Annals of thoracic surgery*, 96(1):50–58.

- [Balzani et al., 2012] Balzani, D., Brinkhues, S., and Holzapfel, G. A. (2012). Constitutive framework for the modeling of damage in collagenous soft tissues with application to arterial walls. *Computer Methods in Applied Mechanics and Engineering*, 213-216:139–151.
- [Bank, 1999] Bank, A. (1999). Intravascular ultrasound studies of arterial elastic mechanics. *Pathologie-biologie*, 47(7):731–737.
- [Bayan et al., 2009] Bayan, C., Levitt, J. M., Miller, E., Kaplan, D., and Georgakoudi, I. (2009). Fully automated, quantitative, noninvasive assessment of collagen fiber content and organization in thick collagen gels. *Journal of applied physics*, 105(10):102042.
- [Benmansour and Cohen, 2011] Benmansour, F. and Cohen, L. D. (2011). Tubular structure segmentation based on minimal path method and anisotropic enhancement. *International Journal of Computer Vision*, 92(2):192–210.
- [Bergel, 1961] Bergel, D. (1961). The static elastic properties of the arterial wall. *The Journal of physiology*, 156(3):445–457.
- [Bergel, 1960] Bergel, D. H. (1960). The visco-elastic properties of the arterial wall.
- [Berillis, 2013] Berillis, P. (2013). The role of collagen in the aorta’s structure. *The open circulation and vascular journal*, 6(1).
- [Beskos and Jenkins, 1975] Beskos, D. and Jenkins, J. (1975). A mechanical model for mammalian tendon. *Journal of Applied Mechanics*, 42(4):755–758.
- [Bevan et al., 2018] Bevan, T., Merabet, N., Hornsby, J., Watton, P. N., and Thompson, M. S. (2018). A biomechanical model for fibril recruitment: Evaluation in tendons and arteries. *Journal of Biomechanics*, 74:192–196.
- [Bianchi et al., 2016] Bianchi, D., Marino, M., and Vairo, G. (2016). An integrated computational approach for aortic mechanics including geometric, histological and chemico-physical data. *Journal of biomechanics*, 49(12):2331–2340.
- [Bircher et al., 2017] Bircher, K., Ehret, A. E., and Mazza, E. (2017). Microstructure based prediction of the deformation behavior of soft collagenous membranes. 13(30):5107–5116.
- [Blanchard et al., 2000] Blanchard, J. F., Armenian, H. K., and Friesen, P. P. (2000). Risk factors for abdominal aortic aneurysm: Results of a case-control study. *American journal of epidemiology*, 151(6):575–583.
- [Boddy et al., 2008] Boddy, A. M., Lenk, G. M., Lillvis, J. H., Nischan, J., Kyo, Y., and Kuivaniemi, H. (2008). Basic research studies to understand aneurysm disease. *Drug news & perspectives*, 21(3):142–148.
- [Boulesteix et al., 2006] Boulesteix, T., Pena, A.-M., Pagès, N., Godeau, G., Sauviat, M.-P., Beaurepaire, E., and Schanne-Klein, M.-C. (2006). Micrometer scale ex vivo multiphoton imaging of unstained arterial wall structure. *Cytometry Part A: The Journal of the International Society for Analytical Cytology*, 69(1):20–26.

- [Boyer et al., 2013] Boyer, G., Molimard, J., Tkaya, M. B., Zahouani, H., Pericoi, M., and Avril, S. (2013). Assessment of the in-plane biomechanical properties of human skin using a finite element model updating approach combined with an optical full-field measurement on a new tensile device. *Journal of the mechanical behavior of biomedical materials*, 27:273–282.
- [Bredfeldt et al., 2014] Bredfeldt, J. S., Liu, Y., Pehlke, C. A., Conklin, M. W., Szulcowski, J. M., Inman, D. R., Keely, P. J., Nowak, R. D., Mackie, T. R., and Eliceiri, K. W. (2014). Computational segmentation of collagen fibers from second-harmonic generation images of breast cancer. *Journal of biomedical optics*, 19(1):016007.
- [Brossollet and Vito, 1996] Brossollet, L. and Vito, R. (1996). A new approach to mechanical testing and modeling of biological tissues, with application to blood vessels. *Journal of biomechanical engineering*, 118(4):433–439.
- [Brown et al., 2003] Brown, E., McKee, T., Pluen, A., Seed, B., Boucher, Y., and Jain, R. K. (2003). Dynamic imaging of collagen and its modulation in tumors in vivo using second-harmonic generation. *Nature medicine*, 9(6):796.
- [Brown and Powell, 1999] Brown, L. C. and Powell, J. T. (1999). Risk factors for aneurysm rupture in patients kept under ultrasound surveillance. *Annals of surgery*, 230(3):289.
- [Buehler, 2006] Buehler, M. J. (2006). Atomistic and continuum modeling of mechanical properties of collagen: Elasticity, fracture, and self-assembly. *Journal of Materials Research*, 21(8):1947–1961.
- [Buehler, 2008] Buehler, M. J. (2008). Nanomechanics of collagen fibrils under varying cross-link densities: Atomistic and continuum studies. *Journal of the mechanical behavior of biomedical materials*, 1(1):59–67.
- [Bulder et al., 2019] Bulder, R., Bastiaannet, E., Hamming, J., and Lindeman, J. (2019). Meta-analysis of long-term survival after elective endovascular or open repair of abdominal aortic aneurysm. *British Journal of Surgery*, 106(5):523–533.
- [Burton, 1954] Burton, A. C. (1954). Relation of structure to function of the tissues of the wall of blood vessels. *Physiological reviews*, 34(4):619–642.
- [Cacho et al., 2007] Cacho, F., Elbischger, P., Rodriguez, J., Doblaré, M., and Holzapfel, G. A. (2007). A constitutive model for fibrous tissues considering collagen fiber crimp. *International Journal of Non-Linear Mechanics*, 42(2):391–402.
- [Calvo et al., 2007] Calvo, B., Peña, E., Martinez, M., and Doblaré, M. (2007). An uncoupled directional damage model for fibred biological soft tissues. Formulation and computational aspects. *International journal for numerical methods in engineering*, 69(10):2036–2057.
- [Cameron, 1999] Cameron, J. (1999). Estimation of arterial mechanics in clinical practice and as a research technique. *Clinical and experimental pharmacology and physiology*, 26(4):285–294.
- [Čanić et al., 2006] Čanić, S., Tambača, J., Guidoboni, G., Mikelić, A., Hartley, C. J., and Rosenstrauch, D. (2006). Modeling viscoelastic behavior of arterial walls and their interaction with pulsatile blood flow. *SIAM Journal on Applied Mathematics*, 67(1):164–193.

-
- [Carew et al., 1968] Carew, T. E., Vaishnav, R. N., and Patel, D. J. (1968). Compressibility of the arterial wall. *Circulation research*, 23(1):61–68.
- [Carlisle et al., 2010a] Carlisle, C., Coulais, C., and Guthold, M. (2010a). The mechanical stress–strain properties of single electrospun collagen type I nanofibers. *Acta Biomaterialia*, 6(8):2997–3003.
- [Carlisle et al., 2010b] Carlisle, C., Coulais, C., and Guthold, M. (2010b). The mechanical stress–strain properties of single electrospun collagen type I nanofibers. *Acta Biomaterialia*, 6(8):2997–3003.
- [Cavinato, 2020] Cavinato, C. (2020). Characterization of deformation and rupture micro-mechanisms in aortic aneurysm wall (unpublished doctoral thesis). *Ecole des Mines de Saint Etienne*.
- [Cavinato et al., 2020] Cavinato, C., Badel, P., Krasny, W., Avril, S., and Morin, C. (2020). Experimental Characterization of Adventitial Collagen Fiber Kinematics Using Second-Harmonic Generation Imaging Microscopy: Similarities and Differences Across Arteries, Species and Testing Conditions. In *Multi-Scale Extracellular Matrix Mechanics and Mechanobiology*, pages 123–164. Springer.
- [Cavinato et al., 2017] Cavinato, C., Helfenstein-Didier, C., Olivier, T., Du Roscoat, S. R., Laroche, N., and Badel, P. (2017). Biaxial loading of arterial tissues with 3D in situ observations of adventitia fibrous microstructure: A method coupling multi-photon confocal microscopy and bulge inflation test. *Journal of the mechanical behavior of biomedical materials*, 74:488–498.
- [Cavinato et al., 2019] Cavinato, C., Molimard, J., Curt, N., Campisi, S., Orgéas, L., and Badel, P. (2019). Does the knowledge of the local thickness of human ascending thoracic aneurysm walls improve their mechanical analysis? *Frontiers in bioengineering and biotechnology*, 7:169.
- [Chamis, 1987] Chamis, C. C. (1987). Simplified composite micromechanics for predicting microstresses. *Journal of reinforced plastics and composites*, 6(3):268–289.
- [Chandran, 2005] Chandran, P. L. (2005). Affine Versus Non-Affine Fibril Kinematics in Collagen Networks: Theoretical Studies of Network Behavior. *Journal of Biomechanical Engineering*, 128(2):259.
- [Chandran and Barocas, 2006] Chandran, P. L. and Barocas, V. H. (2006). Deterministic material-based averaging theory model of collagen gel micromechanics.
- [Chaudhry et al., 1997] Chaudhry, H., Bukiet, B., Davis, A., Ritter, A., and Findley, T. (1997). Residual stresses in oscillating thoracic arteries reduce circumferential stresses and stress gradients. *Journal of biomechanics*, 30(1):57–62.
- [Chen et al., 2016a] Chen, H., Guo, X., Luo, T., and Kassab, G. S. (2016a). A validated 3D microstructure-based constitutive model of coronary artery adventitia. *Journal of Applied Physiology*, 121(1):333–342.
- [Chen et al., 2016b] Chen, H., Guo, X., Luo, T., and Kassab, G. S. (2016b). A validated 3D microstructure-based constitutive model of coronary artery adventitia. *Journal of Applied Physiology*, 121(1):333–342.
-

- [Chen and Kassab, 2016] Chen, H. and Kassab, G. S. (2016). Microstructure-based biomechanics of coronary arteries in health and disease. *Journal of Biomechanics*, 49(12):2548–2559.
- [Chen et al., 2011] Chen, H., Liu, Y., Slipchenko, M. N., Zhao, X., Cheng, J.-X., and Kassab, G. S. (2011). The Layered Structure of Coronary Adventitia under Mechanical Load. *Biophysical Journal*, 101(11):2555–2562.
- [Choudhury et al., 2009] Choudhury, N., Bouchot, O., Rouleau, L., Tremblay, D., Cartier, R., Butany, J., Mongrain, R., and Leask, R. L. (2009). Local mechanical and structural properties of healthy and diseased human ascending aorta tissue. *Cardiovascular Pathology*, 18(2):83–91.
- [Chow and Zhang, 2011a] Chow, M.-J. and Zhang, Y. (2011a). Changes in the mechanical and biochemical properties of aortic tissue due to cold storage. *Journal of Surgical Research*, 171(2):434–442.
- [Chow and Zhang, 2011b] Chow, M.-J. and Zhang, Y. (2011b). Changes in the Mechanical and Biochemical Properties of Aortic Tissue due to Cold Storage. *Journal of Surgical Research*, 171(2):434–442.
- [Chuong and Fung, 1983a] Chuong, C. and Fung, Y. (1983a). Three-dimensional stress distribution in arteries. *Journal of biomechanical engineering*, 105(3):268–274.
- [Chuong and Fung, 1983b] Chuong, C. J. and Fung, Y. C. (1983b). Three-Dimensional Stress Distribution in Arteries. *Journal of Biomechanical Engineering*, 105(3):268.
- [Chuong and Fung, 1986] Chuong, C.-J. and Fung, Y.-C. (1986). Residual stress in arteries. In *Frontiers in Biomechanics*, pages 117–129. Springer.
- [Clark and Glagov, 1979] Clark, J. and Glagov, S. (1979). Structural integration of the arterial wall. I. Relationships and attachments of medial smooth muscle cells in normally distended and hyperdistended aortas. *Laboratory investigation; a journal of technical methods and pathology*, 40(5):587–602.
- [Clark and Glagov, 1985] Clark, J. M. and Glagov, S. (1985). Transmural organization of the arterial media. The lamellar unit revisited. *Arteriosclerosis: An Official Journal of the American Heart Association, Inc.*, 5(1):19–34.
- [Cleveland,] Cleveland, h. Aorta: Aortic aneurysm.
- [Cohen et al., 1994] Cohen, A., Roysam, B., and Turner, J. (1994). Automated tracing and volume measurements of neurons from 3-D confocal fluorescence microscopy data. *Journal of microscopy*, 173(2):103–114.
- [Cohen and Kimmel, 1997] Cohen, L. D. and Kimmel, R. (1997). Global minimum for active contour models: A minimal path approach. *International journal of computer vision*, 24(1):57–78.
- [Collin et al., 1988] Collin, J., Walton, J., Araujo, L., and Lindsell, D. (1988). Oxford screening programme for abdominal aortic aneurysm in men aged 65 to 74 years. *The Lancet*, 332(8611):613–615.

-
- [Comninou and Yannas, 1976] Comninou, M. and Yannas, I. V. (1976). Dependence of stress-strain nonlinearity of connective tissues on the geometry of collagen fibres. *Journal of Biomechanics*, 9(7):427–433.
- [Cortes et al., 2010a] Cortes, D. H., Lake, S. P., Kadlowec, J. A., Soslowky, L. J., and Elliott, D. M. (2010a). Characterizing the mechanical contribution of fiber angular distribution in connective tissue: Comparison of two modeling approaches. *Biomechanics and modeling in mechanobiology*, 9(5):651–658.
- [Cortes et al., 2010b] Cortes, D. H., Lake, S. P., Kadlowec, J. A., Soslowky, L. J., and Elliott, D. M. (2010b). Characterizing the mechanical contribution of fiber angular distribution in connective tissue: Comparison of two modeling approaches. *Biomechanics and Modeling in Mechanobiology*, 9(5):651–658.
- [Courtney et al., 2006] Courtney, T., Sacks, M. S., Stankus, J., Guan, J., and Wagner, W. R. (2006). Design and analysis of tissue engineering scaffolds that mimic soft tissue mechanical anisotropy. *Biomaterials*, 27(19):3631–3638.
- [Cox, 1975] Cox, R. (1975). Anisotropic properties of the canine carotid artery in vitro. *Journal of biomechanics*, 8(5):293–300.
- [Cox, 1978] Cox, R. H. (1978). Passive mechanics and connective tissue composition of canine arteries. *American Journal of Physiology-Heart and Circulatory Physiology*, 234(5):H533–H541.
- [Currey, 2006] Currey, J. D. (2006). *Bones: Structure and Mechanics*. Princeton university press.
- [Cusack and Miller, 1979] Cusack, S. and Miller, A. (1979). Determination of the elastic constants of collagen by Brillouin light scattering. *Journal of molecular biology*, 135(1):39–51.
- [Cyron et al., 2016] Cyron, C., Aydin, R., and Humphrey, J. (2016). A homogenized constrained mixture (and mechanical analog) model for growth and remodeling of soft tissue. *Biomechanics and modeling in mechanobiology*, 15(6):1389–1403.
- [Cyron and Humphrey, 2017] Cyron, C. and Humphrey, J. (2017). Growth and remodeling of load-bearing biological soft tissues. *Meccanica*, 52(3):645–664.
- [Daly, 1969] Daly, C. (1969). The role of elastin in the mechanical behavior of human skin. *Proc. 8th Inr. Confi Med. Biol. Engr*, pages 18–27.
- [D’Amore et al., 2010a] D’Amore, A., Stella, J. A., Wagner, W. R., and Sacks, M. S. (2010a). Characterization of the complete fiber network topology of planar fibrous tissues and scaffolds. *Biomaterials*, 31(20):5345–5354.
- [D’Amore et al., 2010b] D’Amore, A., Stella, J. A., Wagner, W. R., and Sacks, M. S. (2010b). Characterization of the complete fiber network topology of planar fibrous tissues and scaffolds. *Biomaterials*, 31(20):5345–5354.
- [Darling et al., 1977] Darling, R., Messina, C., Brewster, D., and Ottinger, L. (1977). Autopsy study of unoperated abdominal aortic aneurysms. The case for early resection. *Circulation*, 56(3 Suppl):II161–4.
-

- [Davies et al., 2006] Davies, R. R., Gallo, A., Coady, M. A., Tellides, G., Botta, D. M., Burke, B., Coe, M. P., Kopf, G. S., and Elefteriades, J. A. (2006). Novel measurement of relative aortic size predicts rupture of thoracic aortic aneurysms. *The Annals of thoracic surgery*, 81(1):169–177.
- [Davis, 1993] Davis, E. C. (1993). Endothelial cell connecting filaments anchor endothelial cells to the subjacent elastic lamina in the developing aortic intima of the mouse. *Cell and tissue research*, 272(2):211–219.
- [Davis et al., 2016] Davis, F. M., Luo, Y., Avril, S., Duprey, A., and Lu, J. (2016). Local mechanical properties of human ascending thoracic aneurysms. *Journal of the mechanical behavior of biomedical materials*, 61:235–249.
- [De Putter et al., 2007] De Putter, S., Wolters, B., Rutten, M., Breeuwer, M., Gerritsen, F., and Van de Vosse, F. (2007). Patient-specific initial wall stress in abdominal aortic aneurysms with a backward incremental method. *Journal of biomechanics*, 40(5):1081–1090.
- [De Vita and Slaughter, 2007] De Vita, R. and Slaughter, W. S. (2007). A constitutive law for the failure behavior of medial collateral ligaments. *Biomechanics and modeling in mechanobiology*, 6(3):189–197.
- [Deng et al., 1994] Deng, S., Tomioka, J., Debes, J., and Fung, Y. (1994). New experiments on shear modulus of elasticity of arteries. *American Journal of Physiology-Heart and Circulatory Physiology*, 266(1):H1–H10.
- [DeRubertis et al., 2007] DeRubertis, B. G., Trocciola, S. M., Ryer, E. J., Pieracci, F. M., McKinsey, J. F., Faries, P. L., and Kent, K. C. (2007). Abdominal aortic aneurysm in women: Prevalence, risk factors, and implications for screening. *Journal of vascular surgery*, 46(4):630–635.
- [Di Martino et al., 2006] Di Martino, E. S., Bohra, A., Geest, J. P. V., Gupta, N., Makaroun, M. S., and Vorp, D. A. (2006). Biomechanical properties of ruptured versus electively repaired abdominal aortic aneurysm wall tissue. *Journal of Vascular Surgery*, 43(3):570–576.
- [Diamant et al., 1972] Diamant, J., Keller, A., Baer, E., Litt, M., and Arridge, R. (1972). Collagen; ultrastructure and its relation to mechanical properties as a function of ageing. *Proc. R. Soc. Lond. B*, 180(1060):293–315.
- [Dickey et al., 1998] Dickey, J., Hewlett, B., Dumas, G., and Bednar, D. (1998). Measuring collagen fiber orientation: A two-dimensional quantitative macroscopic technique.
- [Díez, 2007] Díez, J. (2007). Arterial stiffness and extracellular matrix. In *Atherosclerosis, Large Arteries and Cardiovascular Risk*, volume 44, pages 76–95. Karger Publishers.
- [Dijkstra, 1959] Dijkstra, E. (1959). Dijkstra’s algorithm. *Dutch scientist Dr. Edsger Dijkstra network algorithm*: http://en.wikipedia.org/wiki/Dijkstra's_algorithm.
- [Dixon et al., 2003] Dixon, S. A., Heikes, R. G., and Vito, R. P. (2003). Constitutive modeling of porcine coronary arteries using designed experiments. *Journal of biomechanical engineering*, 125(2):274–279.

- [Dobrin, 2011] Dobrin, P. B. (2011). Vascular mechanics. *Comprehensive Physiology*, pages 65–102.
- [Draney et al., 2002] Draney, M. T., Herfkens, R. J., Hughes, T. J., Pelc, N. J., Wedding, K. L., Zarins, C. K., and Taylor, C. A. (2002). Quantification of vessel wall cyclic strain using cine phase contrast magnetic resonance imaging. *Annals of biomedical engineering*, 30(8):1033–1045.
- [Driessen et al., 2005] Driessen, N. J., Bouten, C. V., and Baaijens, F. P. (2005). A structural constitutive model for collagenous cardiovascular tissues incorporating the angular fiber distribution. *Journal of biomechanical engineering*, 127(3):494–503.
- [Duprey et al., 2010] Duprey, A., Khanafer, K., Schlicht, M., Avril, S., Williams, D., and Berguer, R. (2010). In Vitro Characterisation of Physiological and Maximum Elastic Modulus of Ascending Thoracic Aortic Aneurysms Using Uniaxial Tensile Testing. *European Journal of Vascular and Endovascular Surgery*, 39(6):700–707.
- [Duprey et al., 2016] Duprey, A., Trabelsi, O., Vola, M., Favre, J.-P., and Avril, S. (2016). Biaxial rupture properties of ascending thoracic aortic aneurysms. *Acta Biomaterialia*, 42:273–285.
- [Dutov et al., 2016a] Dutov, P., Antipova, O., Varma, S., Orgel, J. P., and Schieber, J. D. (2016a). Measurement of elastic modulus of collagen type I single fiber. *PLoS one*, 11(1):e0145711.
- [Dutov et al., 2016b] Dutov, P., Antipova, O., Varma, S., Orgel, J. P. R. O., and Schieber, J. D. (2016b). Measurement of Elastic Modulus of Collagen Type I Single Fiber. *PLoS ONE*, 11(1):e0145711.
- [Dutov et al., 2016c] Dutov, P., Antipova, O., Varma, S., Orgel, J. P. R. O., and Schieber, J. D. (2016c). Measurement of Elastic Modulus of Collagen Type I Single Fiber. *PLOS ONE*, 11(1):e0145711.
- [Ebenstein et al., 2009] Ebenstein, D. M., Coughlin, D., Chapman, J., Li, C., and Pruitt, L. A. (2009). Nanomechanical properties of calcification, fibrous tissue, and hematoma from atherosclerotic plaques. *Journal of Biomedical Materials Research Part A: An Official Journal of The Society for Biomaterials, The Japanese Society for Biomaterials, and The Australian Society for Biomaterials and the Korean Society for Biomaterials*, 91(4):1028–1037.
- [Engelmayer and Sacks, 2006] Engelmayer, G. C. and Sacks, M. S. (2006). A structural model for the flexural mechanics of nonwoven tissue engineering scaffolds. *Journal of biomechanical engineering*, 128(4):610–622.
- [Engelmayer Jr et al., 2008] Engelmayer Jr, G. C., Cheng, M., Bettinger, C. J., Borenstein, J. T., Langer, R., and Freed, L. E. (2008). Accordion-like honeycombs for tissue engineering of cardiac anisotropy. *Nature materials*, 7(12):1003.
- [Entman et al., 2019] Entman, M. L., Michael, F. O., and Jacob, S. W. (2019). Human cardiovascular system. *Encyclopædia Britannica*.
- [Eppell et al., 2005] Eppell, S., Smith, B., Kahn, H., and Ballarini, R. (2005). Nano measurements with micro-devices: Mechanical properties of hydrated collagen fibrils. *Journal of the Royal Society Interface*, 3(6):117–121.

- [Erhart et al., 2014] Erhart, P., Grond-Ginsbach, C., Hakimi, M., Lasitschka, F., Dihlmann, S., Böckler, D., and Hyhlik-Dürr, A. (2014). Finite Element Analysis of Abdominal Aortic Aneurysms: Predicted Rupture Risk Correlates With Aortic Wall Histology in Individual Patients. *Journal of Endovascular Therapy*, 21(4):556–564.
- [Erhart et al., 2015] Erhart, P., Hyhlik-Dürr, A., Geisbüsch, P., Kotelis, D., Müller-Eschner, M., Gasser, T. C., von Tengg-Kobligk, H., and Böckler, D. (2015). Finite element analysis in asymptomatic, symptomatic, and ruptured abdominal aortic aneurysms: In search of new rupture risk predictors. *European Journal of Vascular and Endovascular Surgery*, 49(3):239–245.
- [Eriksson et al., 2014] Eriksson, T., Watton, P., Luo, X., and Ventikos, Y. (2014). Modelling volumetric growth in a thick walled fibre reinforced artery. *Journal of the Mechanics and Physics of Solids*, 73:134–150.
- [Falzon et al., 2008] Falzon, G., Pearson, S., and Murison, R. (2008). Analysis of collagen fibre shape changes in breast cancer. *Physics in Medicine & Biology*, 53(23):6641.
- [Farand et al., 2007] Farand, P., Garon, A., and Plante, G. E. (2007). Structure of large arteries: Orientation of elastin in rabbit aortic internal elastic lamina and in the elastic lamellae of aortic media. *Microvascular research*, 73(2):95–99.
- [Farzaneh et al., 2019] Farzaneh, S., Trabelsi, O., Chavent, B., and Avril, S. (2019). Identifying local arterial stiffness to assess the risk of rupture of ascending thoracic aortic aneurysms. *Annals of biomedical engineering*, 47(4):1038–1050.
- [Federico and Gasser, 2010] Federico, S. and Gasser, T. C. (2010). Nonlinear elasticity of biological tissues with statistical fibre orientation. *Journal of the Royal Society Interface*, 7(47):955–966.
- [Fillinger et al., 2003] Fillinger, M. F., Marra, S. P., Raghavan, M. L., and Kennedy, F. E. (2003). Prediction of rupture risk in abdominal aortic aneurysm during observation: Wall stress versus diameter. *Journal of vascular surgery*, 37(4):724–732.
- [Fillinger et al., 2002] Fillinger, M. F., Raghavan, M., Marra, S. P., Cronenwett, J. L., and Kennedy, F. E. (2002). In vivo analysis of mechanical wall stress and abdominal aortic aneurysm rupture risk. *Journal of Vascular Surgery*, 36(3):589–597.
- [Fitzsimmons and Shanahan, 2002] Fitzsimmons, C. M. and Shanahan, C. M. (2002). Vascular extracellular matrix. In *Pan Vascular Medicine*, pages 217–231. Springer.
- [Fonck et al., 2007] Fonck, E., Prod’hom, G., Roy, S., Augsburger, L., Rufenacht, D., and Stergiopoulos, N. (2007). Effect of elastin degradation on carotid wall mechanics as assessed by a constituent-based biomechanical model. *American Journal of Physiology-Heart and Circulatory Physiology*, 292(6):H2754–H2763.
- [Fowler et al.,] Fowler, S., Roush, R., and Wise, J. Concepts of Biology. page 621.
- [Fratzl, 2008] Fratzl, P. (2008). Collagen: Structure and mechanics, an introduction. In *Collagen*, pages 1–13. Springer.
- [Fratzl et al., 1998] Fratzl, P., Misof, K., Zizak, I., Rapp, G., Amenitsch, H., and Bernstorff, S. (1998). Fibrillar structure and mechanical properties of collagen. *Journal of structural biology*, 122(1-2):119–122.

- [Fred, 2004] Fred, H. L. (2004). Drawbacks and limitations of computed tomography: Views from a medical educator. *Texas Heart Institute Journal*, 31(4):345.
- [Freed and Doehring, 2005] Freed, A. D. and Doehring, T. C. (2005). Elastic model for crimped collagen fibrils. *Journal of biomechanical engineering*, 127(4):587–593.
- [Fung, 1967] Fung, Y. (1967). Elasticity of soft tissues in simple elongation. *American Journal of Physiology-Legacy Content*, 213(6):1532–1544.
- [Fung et al., 1979] Fung, Y., Fronek, K., and Patitucci, P. (1979). Pseudoelasticity of arteries and the choice of its mathematical expression. *American Journal of Physiology-Heart and Circulatory Physiology*, 237(5):H620–H631.
- [Fung, 1984] Fung, Y.-C. (1984). Biodynamics. *Circulation*, 64.
- [Fung, 2013] Fung, Y.-c. (2013). *Biomechanics: Mechanical Properties of Living Tissues*. Springer Science & Business Media.
- [Fung, 1973] Fung, Y.-C. B. (1973). Biorheology of soft tissues. *Biorheology*, 10(2):139–155.
- [García-Herrera et al., 2012] García-Herrera, C. M., Atienza, J., Rojo, F., Claes, E., Guinea, G., Celentano, D. J., García-Montero, C., and Burgos, R. (2012). Mechanical behaviour and rupture of normal and pathological human ascending aortic wall. *Medical & biological engineering & computing*, 50(6):559–566.
- [Garimella and Kraft, 2017] Garimella, H. T. and Kraft, R. H. (2017). A new computational approach for modeling diffusion tractography in the brain. *Neural regeneration research*, 12(1):23.
- [Gasser et al., 2010a] Gasser, T., Auer, M., Labruto, F., Swedenborg, J., and Roy, J. (2010a). Biomechanical Rupture Risk Assessment of Abdominal Aortic Aneurysms: Model Complexity versus Predictability of Finite Element Simulations. *European Journal of Vascular and Endovascular Surgery*, 40(2):176–185.
- [Gasser et al., 2010b] Gasser, T., Auer, M., Labruto, F., Swedenborg, J., and Roy, J. (2010b). Biomechanical Rupture Risk Assessment of Abdominal Aortic Aneurysms: Model Complexity versus Predictability of Finite Element Simulations. *European Journal of Vascular and Endovascular Surgery*, 40(2):176–185.
- [Gasser, 2011] Gasser, T. C. (2011). An irreversible constitutive model for fibrous soft biological tissue: A 3-D microfiber approach with demonstrative application to abdominal aortic aneurysms. *Acta Biomaterialia*, 7(6):2457–2466.
- [Gasser, 2016] Gasser, T. C. (2016). Biomechanical rupture risk assessment. *Aorta*, 4(02):42–60.
- [Gasser et al., 2012a] Gasser, T. C., Gallinetti, S., Xing, X., Forsell, C., Swedenborg, J., and Roy, J. (2012a). Spatial orientation of collagen fibers in the abdominal aortic aneurysm’s wall and its relation to wall mechanics. *Acta biomaterialia*, 8(8):3091–3103.
- [Gasser et al., 2012b] Gasser, T. C., Gallinetti, S., Xing, X., Forsell, C., Swedenborg, J., and Roy, J. (2012b). Spatial orientation of collagen fibers in the abdominal aortic aneurysm’s wall and its relation to wall mechanics. *Acta Biomaterialia*, 8(8):3091–3103.

- [Gasser and Holzapfel, 2002] Gasser, T. C. and Holzapfel, G. A. (2002). A rate-independent elastoplastic constitutive model for biological fiber-reinforced composites at finite strains: Continuum basis, algorithmic formulation and finite element implementation. *Computational Mechanics*, 29(4-5):340–360.
- [Gasser et al., 2014] Gasser, T. C., Nchimi, A., Swedenborg, J., Roy, J., Sakalihasan, N., Böckler, D., and Hyhlik-Dürr, A. (2014). A novel strategy to translate the biomechanical rupture risk of abdominal aortic aneurysms to their equivalent diameter risk: Method and retrospective validation. *European Journal of Vascular and Endovascular Surgery*, 47(3):288–295.
- [Gasser et al., 2006a] Gasser, T. C., Ogden, R. W., and Holzapfel, G. A. (2006a). Hyperelastic modelling of arterial layers with distributed collagen fibre orientations. *J. R. Soc. Interface*, 3(6):15–35.
- [Gasser et al., 2006b] Gasser, T. C., Ogden, R. W., and Holzapfel, G. A. (2006b). Hyperelastic modelling of arterial layers with distributed collagen fibre orientations. *Journal of The Royal Society Interface*, 3(6):15–35.
- [Gatto, 2008] Gatto, R. (2008). Some computational aspects of the generalized von Mises distribution. *Statistics and computing*, 18(3):321–331.
- [Gautieri et al., 2009] Gautieri, A., Buehler, M. J., and Redaelli, A. (2009). Deformation rate controls elasticity and unfolding pathway of single tropocollagen molecules. *Journal of the Mechanical Behavior of Biomedical Materials*, 2(2):130–137.
- [Gautieri et al., 2010] Gautieri, A., Russo, A., Vesentini, S., Redaelli, A., and Buehler, M. J. (2010). Coarse-grained model of collagen molecules using an extended MARTINI force field. *Journal of Chemical Theory and Computation*, 6(4):1210–1218.
- [Gautieri et al., 2011] Gautieri, A., Vesentini, S., Redaelli, A., and Buehler, M. J. (2011). Hierarchical Structure and Nanomechanics of Collagen Microfibrils from the Atomistic Scale Up. *Nano Lett.*, 11(2):757–766.
- [Geest et al., 2008] Geest, J. P. V., Schmidt, D. E., Sacks, M. S., and Vorp, D. A. (2008). The effects of anisotropy on the stress analyses of patient-specific abdominal aortic aneurysms. *Annals of biomedical engineering*, 36(6):921–932.
- [Geest et al., 2006] Geest, J. P. V., Wang, D. H., Wisniewski, S. R., Makaroun, M. S., and Vorp, D. A. (2006). Towards a noninvasive method for determination of patient-specific wall strength distribution in abdominal aortic aneurysms. *Annals of biomedical engineering*, 34(7):1098–1106.
- [Gentleman et al., 2003] Gentleman, E., Lay, A. N., Dickerson, D. A., Nauman, E. A., Livesay, G. A., and Dee, K. C. (2003). Mechanical characterization of collagen fibers and scaffolds for tissue engineering. *Biomaterials*, 24(21):3805–3813.
- [Gerrity and Cliff, 1972] Gerrity, R. and Cliff, W. (1972). The aortic tunica intima in young and aging rats. *Experimental and molecular pathology*, 16(3):382–402.
- [Girerd et al., 1992] Girerd, X. J., Acar, C., Mourad, J.-J., Boutouyrie, P., Safar, M. E., and Laurent, S. (1992). Incompressibility of the human arterial wall: An in vitro ultrasound study. *Journal of hypertension. Supplement: official journal of the International Society of Hypertension*, 10(6):S111–4.

-
- [Gizzi et al., 2014] Gizzi, A., Vasta, M., and Pandolfi, A. (2014). Modeling collagen recruitment in hyperelastic bio-material models with statistical distribution of the fiber orientation. *International Journal of Engineering Science*, 78:48–60.
- [Golledge and Norman, 2010] Golledge, J. and Norman, P. E. (2010). Atherosclerosis and abdominal aortic aneurysm: Cause, response, or common risk factors?
- [Grant, 1967] Grant, R. (1967). Content and distribution of aortic collagen, elastin and carbohydrate in different species. *Journal of atherosclerosis research*, 7(4):463–472.
- [Greenhalgh and The, 2004] Greenhalgh, R. and The, E. (2004). Comparison of endovascular aneurysm repair with open repair in patients with abdominal aortic aneurysm (EVAR trial 1), 30-day operative mortality results: Randomised controlled trial. *The Lancet*, 364(9437):843–848.
- [Greenhalgh and Powell, 2008] Greenhalgh, R. M. and Powell, J. T. (2008). Endovascular repair of abdominal aortic aneurysm. *New England Journal of Medicine*, 358(5):494–501.
- [Grytz and Meschke, 2009] Grytz, R. and Meschke, G. (2009). Constitutive modeling of crimped collagen fibrils in soft tissues. *Journal of the mechanical behavior of biomedical materials*, 2(5):522–533.
- [Guido and Tranquillo, 1993] Guido, S. and Tranquillo, R. T. (1993). A methodology for the systematic and quantitative study of cell contact guidance in oriented collagen gels. Correlation of fibroblast orientation and gel birefringence. *Journal of cell science*, 105(2):317–331.
- [Guinea et al., 2005] Guinea, G. V., Atienza, J. M., Elices, M., Aragoncillo, P., and Hayashi, K. (2005). Thermomechanical behavior of human carotid arteries in the passive state. *American Journal of Physiology-Heart and Circulatory Physiology*, 288(6):H2940–H2945.
- [Guo and De Vita, 2009] Guo, Z. and De Vita, R. (2009). Probabilistic constitutive law for damage in ligaments. *Medical engineering & physics*, 31(9):1104–1109.
- [Gupta et al., 2004] Gupta, H., Messmer, P., Roschger, P., Bernstorff, S., Klaushofer, K., and Fratzl, P. (2004). Synchrotron diffraction study of deformation mechanisms in mineralized tendon. *Physical review letters*, 93(15):158101.
- [Gupta et al., 2006] Gupta, H. S., Seto, J., Wagermaier, W., Zaslansky, P., Boesecke, P., and Fratzl, P. (2006). Cooperative deformation of mineral and collagen in bone at the nanoscale. *Proceedings of the National Academy of Sciences*, 103(47):17741–17746.
- [Gupta et al., 2005] Gupta, H. S., Wagermaier, W., Zickler, G. A., Raz-Ben Aroush, D., Funari, S. S., Roschger, P., Wagner, H. D., and Fratzl, P. (2005). Nanoscale deformation mechanisms in bone. *Nano letters*, 5(10):2108–2111.
- [Hadi and Barocas, 2013] Hadi, M. F. and Barocas, V. H. (2013). Microscale fiber network alignment affects macroscale failure behavior in simulated collagen tissue analogs. *Journal of biomechanical engineering*, 135(2):021026.
- [Hadi et al., 2012] Hadi, M. F., Sander, E. A., and Barocas, V. H. (2012). Multiscale model predicts tissue-level failure from collagen fiber-level damage. *Journal of biomechanical engineering*, 134(9):091005.
-

- [Hansen et al., 2002] Hansen, K. A., Weiss, J. A., and Barton, J. K. (2002). Recruitment of tendon crimp with applied tensile strain. *Journal of biomechanical engineering*, 124(1):72–77.
- [HARKNESS and HARKNESS, 1959] HARKNESS, M. L. R. and HARKNESS, R. D. (1959). Effect of Enzymes on Mechanical Properties of Tissues. *Nature*, 183(4678):1821–1822.
- [Haschek et al.,] Haschek, W. M., Rousseaux, C. G., and Wallig, M. A. Cardiovascular and Skeletal Muscle Systems. *Structure and function*, page 58.
- [Haut, 1986] Haut, R. C. (1986). The influence of specimen length on the tensile failure properties of tendon collagen. *Journal of biomechanics*, 19(11):951–955.
- [He and Roach, 1994] He, C. M. and Roach, M. R. (1994). The composition and mechanical properties of abdominal aortic aneurysms. *Journal of Vascular Surgery*, 20(1):6–13.
- [He et al., 2003] He, W., Hamilton, T. A., Cohen, A. R., Holmes, T. J., Pace, C., Szarowski, D. H., Turner, J. N., and Roysam, B. (2003). Automated three-dimensional tracing of neurons in confocal and brightfield images. *Microscopy and microanalysis*, 9(4):296–310.
- [Head et al., 2003] Head, D., Levine, A., and MacKintosh, F. (2003). Distinct regimes of elastic response and deformation modes of cross-linked cytoskeletal and semiflexible polymer networks. *Physical Review E*, 68(6):061907.
- [Hemmasizadeh et al., 2012] Hemmasizadeh, A., Autieri, M., and Darvish, K. (2012). Multilayer material properties of aorta determined from nanoindentation tests. *Journal of the mechanical behavior of biomedical materials*, 15:199–207.
- [Heng et al., 2008] Heng, M. S., Fagan, M. J., Collier, J. W., Desai, G., McCollum, P. T., and Chetter, I. C. (2008). Peak wall stress measurement in elective and acute abdominal aortic aneurysms. *Journal of vascular surgery*, 47(1):17–22.
- [Heussinger et al., 2007] Heussinger, C., Schaefer, B., and Frey, E. (2007). Nonaffine rubber elasticity for stiff polymer networks. *Physical Review E*, 76(3):031906.
- [Hewett et al., 1994] Hewett, D., Lynch, J., Child, A., and Sykes, B. (1994). A new missense mutation of fibrillin in a patient with Marfan syndrome. *Journal of medical genetics*, 31(4):338–339.
- [Hill et al., 2012a] Hill, M. R., Duan, X., Gibson, G. A., Watkins, S., and Robertson, A. M. (2012a). A theoretical and non-destructive experimental approach for direct inclusion of measured collagen orientation and recruitment into mechanical models of the artery wall. *Journal of biomechanics*, 45(5):762–771.
- [Hill et al., 2012b] Hill, M. R., Duan, X., Gibson, G. A., Watkins, S., and Robertson, A. M. (2012b). A theoretical and non-destructive experimental approach for direct inclusion of measured collagen orientation and recruitment into mechanical models of the artery wall. *Journal of Biomechanics*, 45(5):762–771.
- [Hofmann et al., 1984] Hofmann, H., Voss, T., Kühn, K., and Engel, J. (1984). Localization of flexible sites in thread-like molecules from electron micrographs: Comparison

- of interstitial, basement membrane and intima collagens. *Journal of molecular biology*, 172(3):325–343.
- [Holzapfel, 2001] Holzapfel, G. A. (2001). Biomechanics of soft tissue. *The handbook of materials behavior models*, 3:1049–1063.
- [Holzapfel and Fereidoonzhad, 2017] Holzapfel, G. A. and Fereidoonzhad, B. (2017). Modeling of Damage in Soft Biological Tissues. In *Biomechanics of Living Organs*, pages 101–123. Elsevier.
- [Holzapfel et al., 2000] Holzapfel, G. A., Gasser, T. C., and Ogden, R. W. (2000). A new constitutive framework for arterial wall mechanics and a comparative study of material models. *Journal of elasticity and the physical science of solids*, 61(1-3):1–48.
- [Holzapfel et al., 2002] Holzapfel, G. A., Gasser, T. C., and Stadler, M. (2002). A structural model for the viscoelastic behavior of arterial walls: Continuum formulation and finite element analysis. *European Journal of Mechanics-A/Solids*, 21(3):441–463.
- [Holzapfel et al., 2015a] Holzapfel, G. A., Niestrawska, J. A., Ogden, R. W., Reinisch, A. J., and Schriefl, A. J. (2015a). Modelling non-symmetric collagen fibre dispersion in arterial walls. *Journal of the Royal Society Interface*, 12(106):20150188.
- [Holzapfel et al., 2015b] Holzapfel, G. A., Niestrawska, J. A., Ogden, R. W., Reinisch, A. J., and Schriefl, A. J. (2015b). Modelling non-symmetric collagen fibre dispersion in arterial walls. *Journal of The Royal Society Interface*, 12(106):20150188–20150188.
- [Holzapfel et al., 2015c] Holzapfel, G. A., Niestrawska, J. A., Ogden, R. W., Reinisch, A. J., and Schriefl, A. J. (2015c). Modelling non-symmetric collagen fibre dispersion in arterial walls. *Journal of The Royal Society Interface*, 12(106):20150188–20150188.
- [Holzapfel and Ogden, 2015] Holzapfel, G. A. and Ogden, R. W. (2015). On the tension–compression switch in soft fibrous solids. *European Journal of Mechanics-A/Solids*, 49:561–569.
- [Holzapfel and Ogden, 2017] Holzapfel, G. A. and Ogden, R. W. (2017). Comparison of two model frameworks for fiber dispersion in the elasticity of soft biological tissues. *European Journal of Mechanics-A/Solids*, 66:193–200.
- [Holzapfel et al., 2014a] Holzapfel, G. A., Unterberger, M. J., and Ogden, R. W. (2014a). An affine continuum mechanical model for cross-linked F-actin networks with compliant linker proteins. *Journal of the mechanical behavior of biomedical materials*, 38:78–90.
- [Holzapfel et al., 2014b] Holzapfel, G. A., Unterberger, M. J., and Ogden, R. W. (2014b). An affine continuum mechanical model for cross-linked F-actin networks with compliant linker proteins. *Journal of the Mechanical Behavior of Biomedical Materials*, 38:78–90.
- [Holzapfel and Weizsäcker, 1998] Holzapfel, G. A. and Weizsäcker, H. W. (1998). Biomechanical behavior of the arterial wall and its numerical characterization. *Computers in biology and medicine*, 28(4):377–392.
- [Holzapfel and Weizsäcker, 1998] Holzapfel, G. A. and Weizsäcker, H. W. (1998). Biomechanical behavior of the arterial wall and its numerical characterization. *Computers in Biology and Medicine*, 28(4):377–392.

- [Hopkins,] Hopkins, J. Johns Hopkins Medicine.
- [Hornik and Grün, 2014] Hornik, K. and Grün, B. (2014). movMF: An R package for fitting mixtures of von Mises-Fisher distributions. *Journal of Statistical Software*, 58(10):1–31.
- [Hua and Mower, 2001] Hua, J. and Mower, W. R. (2001). Simple geometric characteristics fail to reliably predict abdominal aortic aneurysm wall stresses. *Journal of vascular surgery*, 34(2):308–315.
- [Humphrey, 2003] Humphrey, J. (2003). Continuum thermomechanics and the clinical treatment of disease and injury. *Appl. Mech. Rev.*, 56(2):231–260.
- [Humphrey et al., 2009] Humphrey, J., Eberth, J., Dye, W., and Gleason, R. (2009). Fundamental role of axial stress in compensatory adaptations by arteries. *Journal of biomechanics*, 42(1):1–8.
- [Humphrey and Epstein, 2002] Humphrey, J. and Epstein, M. (2002). Cardiovascular solid mechanics: Cells, tissues, and organs.
- [Humphrey and Holzapfel, 2012a] Humphrey, J. and Holzapfel, G. (2012a). Mechanics, mechanobiology, and modeling of human abdominal aorta and aneurysms. *Journal of Biomechanics*, 45(5):805–814.
- [Humphrey and Holzapfel, 2012b] Humphrey, J. and Holzapfel, G. (2012b). Mechanics, mechanobiology, and modeling of human abdominal aorta and aneurysms. *Journal of Biomechanics*, 45(5):805–814.
- [Humphrey and Rajagopal, 2002] Humphrey, J. and Rajagopal, K. (2002). A constrained mixture model for growth and remodeling of soft tissues. *Mathematical models and methods in applied sciences*, 12(03):407–430.
- [Humphrey and Taylor, 2008a] Humphrey, J. and Taylor, C. (2008a). Intracranial and Abdominal Aortic Aneurysms: Similarities, Differences, and Need for a New Class of Computational Models. *Annual Review of Biomedical Engineering*, 10(1):221–246.
- [Humphrey and Taylor, 2008b] Humphrey, J. and Taylor, C. (2008b). Intracranial and abdominal aortic aneurysms: Similarities, differences, and need for a new class of computational models. *Annu. Rev. Biomed. Eng.*, 10:221–246.
- [Humphrey, 1995] Humphrey, J. D. (1995). Mechanics of the arterial wall: Review and directions. *Critical ReviewsTM in Biomedical Engineering*, 23(1-2).
- [Humphrey, 1999] Humphrey, J. D. (1999). An Evaluation of Pseudoelastic Descriptors Used in Arterial Mechanics. *Journal of Biomechanical Engineering*, 121(2):259.
- [Humphrey, 2002] Humphrey, J. D. (2002). *Cardiovascular Solid Mechanics*. Springer New York, New York, NY.
- [Humphrey, 2002] Humphrey, J. (2002). The normal arterial wall. In *Cardiovascular Solid Mechanics*. Springer, New York, NY.
- [Hurschler et al., 1997] Hurschler, C., Loitz-Ramage, B., and Vanderby, R. (1997). A structurally based stress-stretch relationship for tendon and ligament. *Journal of biomechanical engineering*, 119(4):392–399.

- [Iliopoulos et al., 2013] Iliopoulos, D. C., Kritharis, E. P., Boussias, S., Demis, A., Iliopoulos, C. D., and Sokolis, D. P. (2013). Biomechanical properties and histological structure of sinus of Valsalva aneurysms in relation to age and region. *Journal of biomechanics*, 46(5):931–940.
- [Iliopoulos et al., 2009] Iliopoulos, D. C., Kritharis, E. P., Giagini, A. T., Papadodima, S. A., and Sokolis, D. P. (2009). Ascending thoracic aortic aneurysms are associated with compositional remodeling and vessel stiffening but not weakening in age-matched subjects. *The Journal of thoracic and cardiovascular surgery*, 137(1):101–109.
- [Isselbacher, 2005] Isselbacher, E. M. (2005). Thoracic and abdominal aortic aneurysms. *Circulation*, 111(6):816–828.
- [Itani et al., 2002] Itani, Y., Watanabe, S., Masuda, Y., Hanamura, K., Asakura, K., Sone, S., Sunami, Y., and Miyamoto, T. (2002). Measurement of aortic diameters and detection of asymptomatic aortic aneurysms in a mass screening program using a mobile helical computed tomography unit. *Heart and Vessels*, 16(2):42–45.
- [Jayyosi et al., 2016] Jayyosi, C., Coret, M., and Bruyère-Garnier, K. (2016). Characterizing liver capsule microstructure via in situ bulge test coupled with multiphoton imaging. *Journal of the mechanical behavior of biomedical materials*, 54:229–243.
- [Jin and Stanciulescu, 2016a] Jin, T. and Stanciulescu, I. (2016a). Computational modeling of the arterial wall based on layer-specific histological data. *Biomechanics and modeling in mechanobiology*, 15(6):1479–1494.
- [Jin and Stanciulescu, 2016b] Jin, T. and Stanciulescu, I. (2016b). Computational modeling of the arterial wall based on layer-specific histological data. *Biomechanics and Modeling in Mechanobiology*, 15(6):1479–1494.
- [Jin and Stanciulescu, 2016c] Jin, T. and Stanciulescu, I. (2016c). Computational modeling of the arterial wall based on layer-specific histological data. *Biomechanics and Modeling in Mechanobiology*, 15(6):1479–1494.
- [Johnson and Tarbell, 2001] Johnson, M. and Tarbell, J. M. (2001). A biphasic, anisotropic model of the aortic wall. *Journal of biomechanical engineering*, 123(1):52–57.
- [Johnston et al., 1991] Johnston, K. W., Rutherford, R. B., Tilson, M. D., Shah, D. M., Hollier, L., and Stanley, J. C. (1991). Suggested standards for reporting on arterial aneurysms. *Journal of vascular surgery*, 13(3):452–458.
- [Kalita and Schaefer, 2008] Kalita, P. and Schaefer, R. (2008). Mechanical models of artery walls. *Archives of Computational Methods in Engineering*, 15(1):1–36.
- [Kang et al., 1995] Kang, T., Resar, J., and Humphrey, J. (1995). Heat-induced changes in the mechanical behavior of passive coronary arteries. *Journal of biomechanical engineering*, 117(1):86–93.
- [Kannus, 2000] Kannus, P. (2000). Structure of the tendon connective tissue. *Scandinavian journal of medicine & science in sports*, 10(6):312–320.
- [Kao et al., 2011] Kao, P. H., Lammers, S. R., Tian, L., Hunter, K., Stenmark, K. R., Shandas, R., and Qi, H. J. (2011). A microstructurally driven model for pulmonary artery tissue. *Journal of biomechanical engineering*, 133(5):051002.

- [Karimi et al., 2013] Karimi, A., Navidbakhsh, M., Shojaei, A., and Faghihi, S. (2013). Measurement of the uniaxial mechanical properties of healthy and atherosclerotic human coronary arteries. *Materials Science and Engineering: C*, 33(5):2550–2554.
- [Kastelic et al., 1980] Kastelic, J., Palley, I., and Baer, E. (1980). A structural mechanical model for tendon crimping. *Journal of biomechanics*, 13(10):887–893.
- [Kato et al., 1989a] Kato, Y., Christiansen, D. L., Hahn, R. A., Shieh, S.-J., Goldstein, J. D., and Silver, F. H. (1989a). Mechanical properties of collagen fibres: A comparison of reconstituted and rat tail tendon fibres. *Biomaterials*, 10(1):38–42.
- [Kato et al., 1989b] Kato, Y., Christiansen, D. L., Hahn, R. A., Shieh, S.-J., Goldstein, J. D., and Silver, F. H. (1989b). Mechanical properties of collagen fibres: A comparison of reconstituted and rat tail tendon fibres. *Biomaterials*, 10(1):38–42.
- [Kazi et al., 2003] Kazi, M., Thyberg, J., Religa, P., Roy, J., Eriksson, P., Hedin, U., and Swedenborg, J. (2003). Influence of intraluminal thrombus on structural and cellular composition of abdominal aortic aneurysm wall. *Journal of vascular surgery*, 38(6):1283–1292.
- [Kelley and Ashurst, 2019] Kelley, J. and Ashurst, J. (2019). Anatomy, Thorax, Aortic Arch.
- [Kenyon, 1979] Kenyon, D. E. (1979). A mathematical model of water flux through aortic tissue. *Bulletin of mathematical biology*, 41(1):79–90.
- [Keyes et al., 2011] Keyes, J. T., Haskett, D. G., Utzinger, U., Azhar, M., and Vande Geest, J. P. (2011). Adaptation of a planar microbiaxial optomechanical device for the tubular biaxial microstructural and macroscopic characterization of small vascular tissues. *Journal of biomechanical engineering*, 133(7).
- [Khanafar et al., 2011] Khanafar, K., Duprey, A., Zainal, M., Schlicht, M., Williams, D., and Berguer, R. (2011). Determination of the elastic modulus of ascending thoracic aortic aneurysm at different ranges of pressure using uniaxial tensile testing. *The Journal of Thoracic and Cardiovascular Surgery*, 142(3):682–686.
- [Koch et al., 2014] Koch, R. G., Tsamis, A., D’Amore, A., Wagner, W. R., Watkins, S. C., Gleason, T. G., and Vorp, D. A. (2014). A custom image-based analysis tool for quantifying elastin and collagen micro-architecture in the wall of the human aorta from multi-photon microscopy. *Journal of biomechanics*, 47(5):935–943.
- [Krasny et al., 2017a] Krasny, W., Morin, C., Magoaric, H., and Avril, S. (2017a). A comprehensive study of layer-specific morphological changes in the microstructure of carotid arteries under uniaxial load. *Acta biomaterialia*, 57:342–351.
- [Krasny et al., 2017b] Krasny, W., Morin, C., Magoaric, H., and Avril, S. (2017b). A comprehensive study of layer-specific morphological changes in the microstructure of carotid arteries under uniaxial load. *Acta Biomaterialia*, 57:342–351.
- [Krauss et al., 2012a] Krauss, P., Metzner, C., Lange, J., Lang, N., and Fabry, B. (2012a). Parameter-free binarization and skeletonization of fiber networks from confocal image stacks. *PLoS One*, 7(5):e36575.

- [Krauss et al., 2012b] Krauss, P., Metzner, C., Lange, J., Lang, N., and Fabry, B. (2012b). Parameter-Free Binarization and Skeletonization of Fiber Networks from Confocal Image Stacks. *PLoS ONE*, 7(5):e36575.
- [Krishnan et al., 2015] Krishnan, K., Ge, L., Haraldsson, H., Hope, M. D., Saloner, D. A., Guccione, J. M., and Tseng, E. E. (2015). Ascending thoracic aortic aneurysm wall stress analysis using patient-specific finite element modeling of in vivo magnetic resonance imaging. *Interactive cardiovascular and thoracic surgery*, 21(4):471–480.
- [Kuivaniemi et al., 2012] Kuivaniemi, H., Tromp, G., Carey, D. J., and Elmore, J. R. (2012). The molecular biology and genetics of aneurysms. In *Molecular and Translational Vascular Medicine*, pages 3–33. Springer.
- [Labrosse, 2007] Labrosse, M. R. (2007). Structure and mechanics of the artery. *Vascular mechanics and pathology. 1st ed. New York: Springer*, pages 45–81.
- [Lake et al., 2012a] Lake, S. P., Hadi, M. F., Lai, V. K., and Barocas, V. H. (2012a). Mechanics of a fiber network within a non-fibrillar matrix: Model and comparison with collagen-agarose co-gels. *Annals of biomedical engineering*, 40(10):2111–2121.
- [Lake et al., 2012b] Lake, S. P., Hadi, M. F., Lai, V. K., and Barocas, V. H. (2012b). Mechanics of a Fiber Network Within a Non-Fibrillar Matrix: Model and Comparison with Collagen-Agarose Co-gels. *Annals of Biomedical Engineering*, 40(10):2111–2121.
- [Lanir, 1979] Lanir, Y. (1979). A structural theory for the homogeneous biaxial stress-strain relationships in flat collagenous tissues. *Journal of biomechanics*, 12(6):423–436.
- [Lanir, 1983a] Lanir, Y. (1983a). Constitutive equations for fibrous connective tissues. *Journal of biomechanics*, 16(1):1–12.
- [Lanir, 1983b] Lanir, Y. (1983b). Constitutive equations for fibrous connective tissues. *Journal of biomechanics*, 16(1):1–12.
- [Länne et al., 1992] Länne, T., Sonesson, B., Bergqvist, D., Bengtsson, H., and Gustafsson, D. (1992). Diameter and compliance in the male human abdominal aorta: Influence of age and aortic aneurysm. *European journal of vascular surgery*, 6(2):178–184.
- [Larsson et al., 2011] Larsson, E., Labruto, F., Gasser, T. C., Swedenborg, J., and Hultgren, R. (2011). Analysis of aortic wall stress and rupture risk in patients with abdominal aortic aneurysm with a gender perspective. *Journal of vascular surgery*, 54(2):295–299.
- [Law et al., 1989] Law, J., Parsons, J., Silver, F., and Weiss, A. (1989). An evaluation of purified reconstituted type 1 collagen fibers. *Journal of biomedical materials research*, 23(9):961–977.
- [Lederle et al., 2012] Lederle, F. A., Freischlag, J. A., Kyriakides, T. C., Matsumura, J. S., Padberg Jr, F. T., Kohler, T. R., Kougiyas, P., Jean-Claude, J. M., Cikrit, D. F., and Swanson, K. M. (2012). Long-term comparison of endovascular and open repair of abdominal aortic aneurysm. *New England Journal of Medicine*, 367(21):1988–1997.
- [Lederle et al., 2009] Lederle, F. A., Freischlag, J. A., Kyriakides, T. C., Padberg, F. T., Matsumura, J. S., Kohler, T. R., Lin, P. H., Jean-Claude, J. M., Cikrit, D. F., and Swanson, K. M. (2009). Outcomes following endovascular vs open repair of abdominal aortic aneurysm: A randomized trial. *Jama*, 302(14):1535–1542.

- [Leonhardt et al., 1993] Leonhardt, H., Kahle, W., and Platzer, W. (1993). Color Atlas/Text of Human Anatomy, Vol. 2.
- [Levy and Tedgui, 1999] Levy, B. I. and Tedgui, A., editors (1999). *Biology of the Arterial Wall*. Number 1 in Basic Science for the Cardiologist. Kluwer Acad. Publ, Dordrecht. OCLC: 246332960.
- [Levy and Tedgui, 2007] Levy, B. I. and Tedgui, A. (2007). *Biology of the Arterial Wall*, volume 1. Springer Science & Business Media.
- [Li and Robertson, 2009] Li, D. and Robertson, A. M. (2009). A structural multi-mechanism damage model for cerebral arterial tissue. *Journal of biomechanical engineering*, 131(10):101013.
- [Li and Robertson, 2013] Li, D. and Robertson, A. M. (2013). Finite Element Modeling of Cerebral Angioplasty Using a Multi-Mechanism Structural Damage Model. In *ASME 2009 Summer Bioengineering Conference*, pages 1145–1146. American Society of Mechanical Engineers Digital Collection.
- [Li, 2016] Li, W. (2016). Damage models for soft tissues: A survey. *Journal of Medical and Biological Engineering*, 36(3):285–307.
- [Liao and Belkoff, 1999] Liao, H. and Belkoff, S. M. (1999). A failure model for ligaments. *Journal of biomechanics*, 32(2):183–188.
- [Lindeman et al., 2010] Lindeman, J. H., Ashcroft, B. A., Beenakker, J.-W. M., van Es, M., Koekkoek, N. B., Prins, F. A., Tielemans, J. F., Abdul-Hussien, H., Bank, R. A., and Oosterkamp, T. H. (2010). Distinct defects in collagen microarchitecture underlie vessel-wall failure in advanced abdominal aneurysms and aneurysms in Marfan syndrome. *Proceedings of the National Academy of Sciences*, 107(2):862–865.
- [Liu and Fung, 1988] Liu, S. and Fung, Y. (1988). Zero-stress states of arteries. *Journal of biomechanical engineering*, 110(1):82–84.
- [Liu et al., 2017] Liu, Y., Keikhosravi, A., Mehta, G. S., Drifka, C. R., and Eliceiri, K. W. (2017). Methods for quantifying fibrillar collagen alignment. In *Fibrosis*, pages 429–451. Springer.
- [Lorenzo and Caffarena, 2005] Lorenzo, A. C. and Caffarena, E. R. (2005). Elastic properties, Young’s modulus determination and structural stability of the tropocollagen molecule: A computational study by steered molecular dynamics. *Journal of biomechanics*, 38(7):1527–1533.
- [Lucero and Kagan, 2006] Lucero, H. . and Kagan, H. (2006). Lysyl oxidase: An oxidative enzyme and effector of cell function. *Cellular and Molecular Life Sciences CMLS*, 63(19-20):2304–2316.
- [Maier et al., 2010] Maier, A., Gee, M., Reeps, C., Pongratz, J., Eckstein, H.-H., and Wall, W. (2010). A comparison of diameter, wall stress, and rupture potential index for abdominal aortic aneurysm rupture risk prediction. *Annals of biomedical engineering*, 38(10):3124–3134.

- [Marini et al., 2012a] Marini, G., Maier, A., Reeps, C., Eckstein, H.-H., Wall, W. A., and Gee, M. W. (2012a). A continuum description of the damage process in the arterial wall of abdominal aortic aneurysms. *International Journal for Numerical Methods in Biomedical Engineering*, 28(1):87–99.
- [Marini et al., 2012b] Marini, G., Maier, A., Reeps, C., Eckstein, H.-H., Wall, W. A., and Gee, M. W. (2012b). A continuum description of the damage process in the arterial wall of abdominal aortic aneurysms: A CONTINUUM DAMAGE MODEL FOR AAA WALL. *International Journal for Numerical Methods in Biomedical Engineering*, 28(1):87–99.
- [Marino et al., 2019] Marino, M., Converse, M. I., Monson, K. L., and Wriggers, P. (2019). Molecular-level collagen damage explains softening and failure of arterial tissues: A quantitative interpretation of CHP data with a novel elasto-damage model. *Journal of the mechanical behavior of biomedical materials*, 97:254–271.
- [Marino and Vairo, 2014] Marino, M. and Vairo, G. (2014). Influence of inter-molecular interactions on the elasto-damage mechanics of collagen fibrils: A bottom-up approach towards macroscopic tissue modeling. *Journal of the Mechanics and Physics of Solids*, 73:38–54.
- [Marra et al., 2006] Marra, S. P., Kennedy, F. E., Kinkaid, J. N., and Fillinger, M. F. (2006). Elastic and rupture properties of porcine aortic tissue measured using inflation testing. *Cardiovascular Engineering*, 6(4):123–131.
- [Martin et al., 2011] Martin, C., Pham, T., and Sun, W. (2011). Significant differences in the material properties between aged human and porcine aortic tissues. *European Journal of Cardio-Thoracic Surgery*, 40(1):28–34.
- [Matsumoto et al., 2009] Matsumoto, T., Fukui, T., Tanaka, T., Ikuta, N., Ohashi, T., Kumagai, K., Akimoto, H., Tabayashi, K., and Sato, M. (2009). Biaxial tensile properties of thoracic aortic aneurysm tissues. *Journal of Biomechanical Science and Engineering*, 4(4):518–529.
- [Mauri et al., 2016] Mauri, A., Hopf, R., Ehret, A. E., Picu, C. R., and Mazza, E. (2016). A discrete network model to represent the deformation behavior of human amnion. *Journal of the Mechanical Behavior of Biomedical Materials*, 58:45–56.
- [MBBS et al., 2011] MBBS, S. A., MBBS, A. Q., Sharma, V., and Sharma, A. (2011). Abdominal aortic aneurysm: A comprehensive review. 16(1):5.
- [Meijering et al., 2003] Meijering, E. H., Jacob, M., Sarria, J.-C. F., and Unser, M. (2003). A Novel Approach to Neurite Tracing in Fluorescence Microscopy Images. In *SIP*, pages 491–495.
- [Melnik et al., 2015] Melnik, A. V., Da Rocha, H. B., and Goriely, A. (2015). On the modeling of fiber dispersion in fiber-reinforced elastic materials. *International Journal of Non-Linear Mechanics*, 75:92–106.
- [Menashi et al., 1987] Menashi, S., Campa, J. S., Greenhalgh, R. M., and Powell, J. T. (1987). Collagen in abdominal aortic aneurysm: Typing, content, and degradation. *Journal of vascular surgery*, 6(6):578–582.

- [Menzel and Kuhl, 2012] Menzel, A. and Kuhl, E. (2012). Frontiers in growth and remodeling. *Mechanics research communications*, 42:1–14.
- [Metafratzi et al., 2002] Metafratzi, Z. M., Efremidis, S. C., Skopelitou, A. S., and De Roos, A. (2002). The clinical significance of aortic compliance and its assessment with magnetic resonance imaging. *Journal of Cardiovascular Magnetic Resonance*, 4(4):481–491.
- [Miller and Gay, 1982] Miller, E. J. and Gay, S. (1982). [1] Collagen: An overview. In *Methods in Enzymology*, volume 82, pages 3–32. Elsevier.
- [Ming-Che et al., 1994] Ming-Che, W., Pins, G. D., and Silver, F. H. (1994). Collagen fibres with improved strength for the repair of soft tissue injuries. *Biomaterials*, 15(7):507–512.
- [Miyazaki and Hayashi, 1999] Miyazaki, H. and Hayashi, K. (1999). Tensile tests of collagen fibers obtained from the rabbit patellar tendon. *Biomedical Microdevices*, 2(2):151–157.
- [Mohan and Melvin, 1982] Mohan, D. and Melvin, J. W. (1982). Failure properties of passive human aortic tissue. I—Uniaxial tension tests. *Journal of Biomechanics*, 15(11):887–902.
- [Mohan and Melvin, 1983] Mohan, D. and Melvin, J. W. (1983). Failure properties of passive human aortic tissue. II—Biaxial tension tests. *Journal of Biomechanics*, 16(1):31–44.
- [Molnar et al., 2003] Molnar, J., Fong, K., He, Q., Hayashi, K., Kim, Y., Fong, S., Fogelgren, B., Szauter, K. M., Mink, M., and Csiszar, K. (2003). Structural and functional diversity of lysyl oxidase and the LOX-like proteins. *Biochimica et biophysica acta (BBA)-proteins and proteomics*, 1647(1-2):220–224.
- [Morein et al., 1978] Morein, G., Goldgefter, L., Kobylansky, E., Goldschmidt-Nathan, M., and Nathan, H. (1978). Changes in the mechanical properties of rat tail tendon during postnatal ontogenesis. *Anatomy and embryology*, 154(1):121–124.
- [Morgan, 1960] Morgan, F. (1960). Mechanical properties of raw collagen fibers. *J Soc Leather Trade’s Chemists*, 44:2–23.
- [Morin et al., 2018] Morin, C., Avril, S., and Hellmich, C. (2018). Non-affine fiber kinematics in arterial mechanics: A continuum micromechanical investigation. *ZAMM-Journal of Applied Mathematics and Mechanics/Zeitschrift für Angewandte Mathematik und Mechanik*, 98(12):2101–2121.
- [Morris and Wood, 2000] Morris, P. and Wood, W. (2000). Oxford textbook of surgery: Acute abdomen.
- [Mousavi and Avril, 2017] Mousavi, S. J. and Avril, S. (2017). Patient-specific stress analyses in the ascending thoracic aorta using a finite-element implementation of the constrained mixture theory. *Biomechanics and modeling in mechanobiology*, 16(5):1765–1777.
- [Moutos et al., 2007] Moutos, F. T., Freed, L. E., and Guilak, F. (2007). A biomimetic three-dimensional woven composite scaffold for functional tissue engineering of cartilage. *Nature materials*, 6(2):162.

- [Natali et al., 2005] Natali, A., Pavan, P., Carniel, E., Lucisano, M., and Tagliavero, G. (2005). Anisotropic elasto-damage constitutive model for the biomechanical analysis of tendons. *Medical engineering & physics*, 27(3):209–214.
- [Natsis et al., 2009] Natsis, K. I., Tsitouridis, I. A., Didagelos, M. V., Fillipidis, A. A., Vlasis, K. G., and Tsikaras, P. D. (2009). Anatomical variations in the branches of the human aortic arch in 633 angiographies: Clinical significance and literature review. *Surg Radiol Anat*, 31(5):319–323.
- [Nestler et al., 1983] Nestler, F. H. M., Hvidt, S., Ferry, J. D., and Veis, A. (1983). Flexibility of collagen determined from dilute solution viscoelastic measurements. *Biopolymers: Original Research on Biomolecules*, 22(7):1747–1758.
- [Netter and Colacino, 1989] Netter, F. H. and Colacino, S. (1989). *Atlas of Human Anatomy*. Ciba-Geigy Corporation.
- [Newton et al., 1995] Newton, R., Haffagee, J., and Ho, M. (1995). Polarized light microscopy of weakly birefringent biological specimens. *Journal of microscopy*, 180(2):127–130.
- [Nicholls et al., 1998] Nicholls, S. C., Gardner, J. B., Meissner, M. H., and Johansen, K. H. (1998). Rupture in small abdominal aortic aneurysms. *Journal of vascular surgery*, 28(5):884–888.
- [Nienaber et al., 2016] Nienaber, C. A., Clough, R. E., Sakalihasan, N., Suzuki, T., Gibbs, R., Mussa, F., Jenkins, M. P., Thompson, M. M., Evangelista, A., and Yeh, J. S. (2016). Aortic dissection. *Nature Reviews Disease Primers*, 2:16053.
- [Niestrawska et al., 2016] Niestrawska, J. A., Viertler, C., Regitnig, P., Cohnert, T. U., Sommer, G., and Holzapfel, G. A. (2016). Microstructure and mechanics of healthy and aneurysmatic abdominal aortas: Experimental analysis and modelling. *Journal of The Royal Society Interface*, 13(124):20160620.
- [Nordon et al., 2011] Nordon, I. M., Hinchliffe, R. J., Loftus, I. M., and Thompson, M. M. (2011). Pathophysiology and epidemiology of abdominal aortic aneurysms. *Nature reviews cardiology*, 8(2):92.
- [O’Connell et al., 2008] O’Connell, M. K., Murthy, S., Phan, S., Xu, C., Buchanan, J., Spilker, R., Dalman, R. L., Zarins, C. K., Denk, W., and Taylor, C. A. (2008). The three-dimensional micro- and nanostructure of the aortic medial lamellar unit measured using 3D confocal and electron microscopy imaging. *Matrix Biology*, 27(3):171–181.
- [Oka et al., 2001] Oka, N., Aomi, S., Tomioka, H., Endo, M., and Koyanagi, H. (2001). Surgical treatment of multiple aneurysms in a patient with Ehlers-Danlos syndrome. *The Journal of thoracic and cardiovascular surgery*, 121(6):1210–1211.
- [Okamoto et al., 2002] Okamoto, R. J., Wagenseil, J. E., DeLong, W. R., Peterson, S. J., Kouchoukos, N. T., and Sundt, T. M. (2002). Mechanical properties of dilated human ascending aorta. *Annals of Biomedical Engineering*, 30(5):624–635.
- [Okamoto et al., 2003] Okamoto, R. J., Xu, H., Kouchoukos, N. T., Moon, M. R., and Sundt III, T. M. (2003). The influence of mechanical properties on wall stress and distensibility of the dilated ascending aorta. *The Journal of thoracic and cardiovascular surgery*, 126(3):842–850.

- [Oktay et al., 1991] Oktay, H., Kang, T., Humphrey, J., and Bishop, G. (1991). Changes in the mechanical behavior of arteries following balloon angioplasty. ASME 1991 Biomechanics Symposium, AMD-Vol. 120. *American Society of Mechanical Engineers*, 120.
- [O’Leary et al., 2014] O’Leary, S. A., Doyle, B. J., and McGloughlin, T. M. (2014). The impact of long term freezing on the mechanical properties of porcine aortic tissue. *Journal of the mechanical behavior of biomedical materials*, 37:165–173.
- [O’Leary et al., 2015] O’Leary, S. A., Mulvihill, J. J., Barrett, H. E., Kavanagh, E. G., Walsh, M. T., McGloughlin, T. M., and Doyle, B. J. (2015). Determining the influence of calcification on the failure properties of abdominal aortic aneurysm (AAA) tissue. *Journal of the mechanical behavior of biomedical materials*, 42:154–167.
- [Orgel et al., 2006] Orgel, J. P., Irving, T. C., Miller, A., and Wess, T. J. (2006). Microfibrillar structure of type I collagen in situ. *Proceedings of the National Academy of Sciences*, 103(24):9001–9005.
- [Ottani et al., 2001] Ottani, V., Raspanti, M., and Ruggeri, A. (2001). Collagen structure and functional implications. *Micron*, 32(3):251–260.
- [Oxlund and Andreassen,] Oxlund, H. and Andreassen, T. T. The roles of hyaluronic acid, collagen and elastin in the mechanical properties of connective tissues. page 10.
- [Pape et al., 2007] Pape, L. A., Tsai, T. T., Isselbacher, E. M., Oh, J. K., O’Gara, P. T., Evangelista, A., Fattori, R., Meinhardt, G., Trimarchi, S., and Bossone, E. (2007). CLINICAL PERSPECTIVE. *Circulation*, 116(10):1120–1127.
- [Participants, 1998] Participants, T. U. S. A. T. (1998). Mortality results for randomised controlled trial of early elective surgery or ultrasonographic surveillance for small abdominal aortic aneurysms. *The Lancet*, 352(9141):1649–1655.
- [Pasta et al., 2017] Pasta, S., Agnese, V., Di Giuseppe, M., Gentile, G., Raffa, G. M., Bellavia, D., and Pilato, M. (2017). In vivo strain analysis of dilated ascending thoracic aorta by ECG-gated CT angiographic imaging. *Annals of biomedical engineering*, 45(12):2911–2920.
- [Pasta et al., 2016] Pasta, S., Phillippi, J. A., Tsamis, A., D’Amore, A., Raffa, G. M., Pilato, M., Scardulla, C., Watkins, S. C., Wagner, W. R., and Gleason, T. G. (2016). Constitutive modeling of ascending thoracic aortic aneurysms using microstructural parameters. *Medical engineering & physics*, 38(2):121–130.
- [Patel et al., 1969] Patel, D. J., Fry, D. L., and Janicki, J. S. (1969). The elastic symmetry of arterial segments in dogs. *Circulation research*, 24(1):1–8.
- [Patel and Vaishnav, 1972] Patel, D. J. and Vaishnav, R. N. (1972). The rheology of large blood vessels. *Cardiovascular fluid dynamics*, 2(11):2–65.
- [Pehlke et al., 2014] Pehlke, C., Bredfeldt, J., Doot, J., Sung, K., Provenzano, P., and Riching, K. (2014). Quantification of collagen architecture using the curvelet transform. *Integrative Biology, in Review*.
- [Peña, 2011] Peña, E. (2011). Damage functions of the internal variables for soft biological fibred tissues. *Mechanics Research Communications*, 38(8):610–615.

- [Peng et al., 2010] Peng, H., Ruan, Z., Atasoy, D., and Sternson, S. (2010). Automatic reconstruction of 3D neuron structures using a graph-augmented deformable model. *Bioinformatics*, 26(12):i38–i46.
- [Perejda et al., 1985] Perejda, A. J., Abraham, P., Carnes, W. H., Coulson, W. F., and Uitto, J. (1985). Marfan’s syndrome: Structural, biochemical, and mechanical studies of the aortic media. *The Journal of laboratory and clinical medicine*, 106(4):369–375.
- [Pham et al., 2013] Pham, T., Martin, C., Elefteriades, J., and Sun, W. (2013). Biomechanical characterization of ascending aortic aneurysm with concomitant bicuspid aortic valve and bovine aortic arch. *Acta biomaterialia*, 9(8):7927–7936.
- [Phillippi et al., 2014] Phillippi, J. A., Green, B. R., Eskay, M. A., Kotlarczyk, M. P., Hill, M. R., Robertson, A. M., Watkins, S. C., Vorp, D. A., and Gleason, T. G. (2014). Mechanism of aortic medial matrix remodeling is distinct in patients with bicuspid aortic valve. *The Journal of thoracic and cardiovascular surgery*, 147(3):1056–1064.
- [Pichamuthu et al., 2013] Pichamuthu, J. E., Phillippi, J. A., Cleary, D. A., Chew, D. W., Hempel, J., Vorp, D. A., and Gleason, T. G. (2013). Differential tensile strength and collagen composition in ascending aortic aneurysms by aortic valve phenotype. *The Annals of thoracic surgery*, 96(6):2147–2154.
- [Picu, 2011a] Picu, R. (2011a). Mechanics of random fiber networks—a review. *Soft Matter*, 7(15):6768–6785.
- [Picu, 2011b] Picu, R. C. (2011b). Mechanics of random fiber networks—a review. *Soft Matter*, 7(15):6768.
- [Pierce et al., 2015] Pierce, D. M., Maier, F., Weisbecker, H., Viertler, C., Verbrugge, P., Famaey, N., Fourneau, I., Herijgers, P., and Holzapfel, G. A. (2015). Human thoracic and abdominal aortic aneurysmal tissues: Damage experiments, statistical analysis and constitutive modeling. *Journal of the mechanical behavior of biomedical materials*, 41:92–107.
- [Pins et al., 1997] Pins, G. D., Christiansen, D. L., Patel, R., and Silver, F. H. (1997). Self-assembly of collagen fibers. Influence of fibrillar alignment and decorin on mechanical properties. *Biophysical journal*, 73(4):2164–2172.
- [Polzer and Gasser, 2015a] Polzer, S. and Gasser, T. C. (2015a). Biomechanical rupture risk assessment of abdominal aortic aneurysms based on a novel probabilistic rupture risk index. *J. R. Soc. Interface*, 12(113):20150852.
- [Polzer and Gasser, 2015b] Polzer, S. and Gasser, T. C. (2015b). Biomechanical rupture risk assessment of abdominal aortic aneurysms based on a novel probabilistic rupture risk index. *Journal of The Royal Society Interface*, 12(113):20150852.
- [Polzer et al., 2013] Polzer, S., Gasser, T. C., Forsell, C., and Tichy, M. (2013). Automatic Identification and Validation of Planar Collagen Organization in the Aorta Wall with Application to Abdominal Aortic Aneurysm. *Microscopy and Microanalysis*, 19(06):1395–1404.

- [Raghavan et al., 2011] Raghavan, M. L., Hanaoka, M. M., Kratzberg, J. A., de Lourdes Higuchi, M., and Da Silva, E. S. (2011). Biomechanical failure properties and microstructural content of ruptured and unruptured abdominal aortic aneurysms. *Journal of biomechanics*, 44(13):2501–2507.
- [Raghavan et al., 2006] Raghavan, M. L., Kratzberg, J., de Tolosa, E. M. C., Hanaoka, M. M., Walker, P., and da Silva, E. S. (2006). Regional distribution of wall thickness and failure properties of human abdominal aortic aneurysm. *Journal of biomechanics*, 39(16):3010–3016.
- [Raghavan et al., 2000] Raghavan, M. L., Vorp, D. A., Federle, M. P., Makaroun, M. S., and Webster, M. W. (2000). Wall stress distribution on three-dimensionally reconstructed models of human abdominal aortic aneurysm. *Journal of vascular surgery*, 31(4):760–769.
- [Raghavan et al., 1996] Raghavan, M. L., Webster, M. W., and Vorp, D. A. (1996). Ex vivo biomechanical behavior of abdominal aortic aneurysm: Assessment using a new mathematical model. *Annals of biomedical engineering*, 24(5):573–582.
- [Rajagopal and Srinivasa, 1998] Rajagopal, K. and Srinivasa, A. (1998). Mechanics of the inelastic behavior of materials—Part 1, theoretical underpinnings. *International Journal of Plasticity*, 14(10-11):945–967.
- [Rezakhaniha and Agianniotis, 2012] Rezakhaniha, R. and Agianniotis (2012). Experimental investigation of collagen waviness and orientation in the arterial adventitia using confocal laser scanning microscopy. *Biomechanics and modeling in mechanobiology*, 11(3-4):461–473.
- [Rezakhaniha et al., 2012] Rezakhaniha, R., Agianniotis, A., Schrauwen, J. T. C., Griffa, A., Sage, D., Bouten, C. V. C., van de Vosse, F. N., Unser, M., and Stergiopoulos, N. (2012). Experimental investigation of collagen waviness and orientation in the arterial adventitia using confocal laser scanning microscopy. *Biomechanics and Modeling in Mechanobiology*, 11(3-4):461–473.
- [Risau and Flamme, 1995] Risau, W. and Flamme, I. (1995). Vasculogenesis. *Annual review of cell and developmental biology*, 11(1):73–91.
- [Ritter et al., 2009] Ritter, M. C., Jesudason, R., Majumdar, A., Stamenović, D., Buczek-Thomas, J. A., Stone, P. J., Nugent, M. A., and Suki, B. (2009). A zipper network model of the failure mechanics of extracellular matrices. *Proceedings of the National Academy of Sciences*, 106(4):1081–1086.
- [Roach and Burton, 1957] Roach, M. R. and Burton, A. C. (1957). The reason for the shape of the distensibility curves of arteries. *Canadian journal of biochemistry and physiology*, 35(8):681–690.
- [Robert et al., 2017] Robert, M., Juillièrè, Y., Gabet, A., Kownator, S., and Olié, V. (2017). Time trends in hospital admissions and mortality due to abdominal aortic aneurysms in France, 2002–2013. *International Journal of Cardiology*, 234:28–32.
- [Robertson et al., 2012] Robertson, A. M., Hill, M. R., and Li, D. (2012). Structurally motivated damage models for arterial walls. Theory and application. In *Modeling of Physiological Flows*, pages 143–185. Springer.

-
- [Rodríguez et al., 1994] Rodríguez, E. K., Hoger, A., and McCulloch, A. D. (1994). Stress-dependent finite growth in soft elastic tissues. *Journal of biomechanics*, 27(4):455–467.
- [Rodríguez et al., 2006] Rodríguez, J. F., Cacho, F., Bea, J. A., and Doblaré, M. (2006). A stochastic-structurally based three dimensional finite-strain damage model for fibrous soft tissue. *Journal of the Mechanics and Physics of Solids*, 54(4):864–886.
- [Rodríguez et al., 2008] Rodríguez, J. F., Ruiz, C., Doblaré, M., and Holzapfel, G. A. (2008). Mechanical stresses in abdominal aortic aneurysms: Influence of diameter, asymmetry, and material anisotropy. *Journal of biomechanical engineering*, 130(2):021023.
- [Romo et al., 2014a] Romo, A., Badel, P., Duprey, A., Favre, J.-P., and Avril, S. (2014a). In vitro analysis of localized aneurysm rupture. *Journal of Biomechanics*, 47(3):607–616.
- [Romo et al., 2014b] Romo, A., Badel, P., Duprey, A., Favre, J.-P., and Avril, S. (2014b). In vitro analysis of localized aneurysm rupture. *Journal of Biomechanics*, 47(3):607–616.
- [Roy, 1881] Roy, C. S. (1881). The elastic properties of the arterial wall. *The Journal of physiology*, 3(2):125–159.
- [Sacks, 2003] Sacks, M. S. (2003). Incorporation of experimentally-derived fiber orientation into a structural constitutive model for planar collagenous tissues. *Journal of biomechanical engineering*, 125(2):280–287.
- [Salunke and Topoleski, 1997] Salunke, N. and Topoleski, L. (1997). Biomechanics of atherosclerotic plaque. *Critical Reviews in Biomedical Engineering*, 25(3):243–285.
- [Sasaki and Odajima, 1996] Sasaki, N. and Odajima, S. (1996). Elongation mechanism of collagen fibrils and force-strain relations of tendon at each level of structural hierarchy. *Journal of biomechanics*, 29(9):1131–1136.
- [Scarr, 2011] Scarr, G. (2011). Helical tensegrity as a structural mechanism in human anatomy. *International Journal of Osteopathic Medicine*, 14(1):24–32.
- [Schrieffl et al., 2012a] Schrieffl, A. J., Reinisch, A. J., Sankaran, S., Pierce, D. M., and Holzapfel, G. A. (2012a). Quantitative assessment of collagen fibre orientations from two-dimensional images of soft biological tissues. *Journal of The Royal Society Interface*, 9(76):3081–3093.
- [Schrieffl et al., 2012b] Schrieffl, A. J., Reinisch, A. J., Sankaran, S., Pierce, D. M., and Holzapfel, G. A. (2012b). Quantitative assessment of collagen fibre orientations from two-dimensional images of soft biological tissues. *Journal of The Royal Society Interface*, 9(76):3081–3093.
- [Schrieffl et al., 2015] Schrieffl, A. J., Schmidt, T., Balzani, D., Sommer, G., and Holzapfel, G. A. (2015). Selective enzymatic removal of elastin and collagen from human abdominal aortas: Uniaxial mechanical response and constitutive modeling. *Acta biomaterialia*, 17:125–136.
- [Schrieffl et al., 2011] Schrieffl, A. J., Zeindlinger, G., Pierce, D. M., Regitnig, P., and Holzapfel, G. A. (2011). Determination of the layer-specific distributed collagen fibre orientations in human thoracic and abdominal aortas and common iliac arteries. *Journal of the Royal Society Interface*, 9(71):1275–1286.
-

- [Schulze-Bauer et al., 2002] Schulze-Bauer, C. A. J., Regitnig, P., and Holzapfel, G. A. (2002). Mechanics of the human femoral adventitia including the high-pressure response. *American Journal of Physiology-Heart and Circulatory Physiology*, 282(6):H2427–H2440.
- [Scott, 2003] Scott, J. (2003). Elasticity in extracellular matrix ‘shape modules’ of tendon, cartilage, etc. A sliding proteoglycan-filament model. *The Journal of physiology*, 553(2):335–343.
- [Selimovic et al., 2014] Selimovic, A., Ventikos, Y., and Watton, P. N. (2014). Modelling the evolution of cerebral aneurysms: Biomechanics, mechanobiology and multiscale modelling. *Procedia IUTAM*, 10:396–409.
- [Shah et al., 2014] Shah, S. B., Witzenburg, C., Hadi, M. F., Wagner, H. P., Goodrich, J. M., Alford, P. W., and Barocas, V. H. (2014). Prefailure and failure mechanics of the porcine ascending thoracic aorta: Experiments and a multiscale model. *Journal of biomechanical engineering*, 136(2):021028.
- [Shen et al., 2008] Shen, Z. L., Dodge, M. R., Kahn, H., Ballarini, R., and Eppell, S. J. (2008). Stress-strain experiments on individual collagen fibrils. *Biophysical journal*, 95(8):3956–3963.
- [Sherman et al., 2015a] Sherman, V. R., Yang, W., and Meyers, M. A. (2015a). The materials science of collagen. *Journal of the Mechanical Behavior of Biomedical Materials*, 52:22–50.
- [Sherman et al., 2015b] Sherman, V. R., Yang, W., and Meyers, M. A. (2015b). The materials science of collagen. *Journal of the Mechanical Behavior of Biomedical Materials*, 52:22–50.
- [Sigrist et al., 2017] Sigrist, R. M., Liau, J., El Kaffas, A., Chammas, M. C., and Willmann, J. K. (2017). Ultrasound elastography: Review of techniques and clinical applications. *Theranostics*, 7(5):1303.
- [Simon et al., 1998] Simon, B., Kaufmann, M., McAfee, M., Baldwin, A., and Wilson, L. (1998). Identification and determination of material properties for porohyperelastic analysis of large arteries. *Journal of biomechanical engineering*, 120(2):188–194.
- [Smith et al., 1981] Smith, J. H., Canham, P. B., and Starkey, J. (1981). Orientation of collagen in the tunica adventitia of the human cerebral artery measured with polarized light and the universal stage. *Journal of Ultrastructure Research*, 77(2):133–145.
- [Smith et al., 1986] Smith, L. C., Benson, D. M., Gotto Jr, A. M., and Bryan, J. (1986). Digital imaging fluorescence microscopy. In *Methods in Enzymology*, volume 129, pages 857–873. Elsevier.
- [Smoljkić et al., 2017] Smoljkić, M., Fehervary, H., Van den Bergh, P., Jorge-Peñas, A., Kluyskens, L., Dymarkowski, S., Verbrugge, P., Meuris, B., Vander Sloten, J., and Famaey, N. (2017). Biomechanical characterization of ascending aortic aneurysms. *Biomechanics and modeling in mechanobiology*, 16(2):705–720.
- [Sokolis, 2015] Sokolis, D. P. (2015). Effects of aneurysm on the directional, regional, and layer distribution of residual strains in ascending thoracic aorta. *Journal of the mechanical behavior of biomedical materials*, 46:229–243.

- [Sokolis et al., 2012] Sokolis, D. P., Kritharis, E. P., Giagini, A. T., Lampropoulos, K. M., Papadodima, S. A., and Iliopoulos, D. C. (2012). Biomechanical response of ascending thoracic aortic aneurysms: Association with structural remodelling. *Computer methods in biomechanics and biomedical engineering*, 15(3):231–248.
- [Solitchka,] Solitchka. Collagen.
- [Sommer et al., 2010] Sommer, G., Regitnig, P., Költringer, L., and Holzapfel, G. A. (2010). Biaxial mechanical properties of intact and layer-dissected human carotid arteries at physiological and suprphysiological loadings. *American Journal of Physiology-Heart and Circulatory Physiology*, 298(3):H898–H912.
- [Spanos and Esteva, 2009a] Spanos, P. and Esteva, M. (2009a). Effect of stochastic nanotube waviness on the elastic and thermal properties of nanocomposites by fiber embedment in finite elements. *Journal of Computational and Theoretical Nanoscience*, 6(10):2317–2333.
- [Spanos and Esteva, 2009b] Spanos, P. D. and Esteva, M. (2009b). Effect of Stochastic Nanotube Waviness on the Elastic and Thermal Properties of Nanocomposites by Fiber Embedment in Finite Elements. *Journal of Computational and Theoretical Nanoscience*, 6(10):2317–2333.
- [Speelman et al., 2007] Speelman, L., Bohra, A., Bosboom, E. M. H., Schurink, G. W. H., van de Vosse, F. N., Makaroun, M. S., and Vorp, D. A. (2007). Effects of wall calcifications in patient-specific wall stress analyses of abdominal aortic aneurysms. *Journal of biomechanical engineering*, 129(1):105–109.
- [Sriramula and Chryssanthopoulos, 2009] Sriramula, S. and Chryssanthopoulos, M. K. (2009). Quantification of uncertainty modelling in stochastic analysis of FRP composites. *Composites Part A: Applied Science and Manufacturing*, 40(11):1673–1684.
- [Stålhand et al., 2004] Stålhand, J., Klarbring, A., and Karlsson, M. (2004). Towards in vivo aorta material identification and stress estimation. *Biomechanics and modeling in mechanobiology*, 2(3):169–186.
- [Stamatakis, 1953] Stamatakis, I. (1953). Dictionary of the New Greek Language. *Athens: Dimitrakou Publ*, page 1160.
- [Starck et al., 2002] Starck, J.-L., Candès, E. J., and Donoho, D. L. (2002). The curvelet transform for image denoising. *IEEE Transactions on image processing*, 11(6):670–684.
- [Stehbens, 1958] Stehbens, W. E. (1958). HISTORY OF ANEURYSMS. *Med. Hist.*, 2(4):274–280.
- [Stein et al., 2008] Stein, A. M., Vader, D. A., Jawerth, L. M., Weitz, D. A., and Sander, L. M. (2008). An algorithm for extracting the network geometry of three-dimensional collagen gels. *Journal of microscopy*, 232(3):463–475.
- [Steinberg and Stein, 1966] Steinberg, I. and Stein, H. L. (1966). Arteriosclerotic abdominal aneurysms: Report of 200 consecutive cases diagnosed by intravenous aortography. *Jama*, 195(12):1025–1029.

- [Stemper et al., 2007a] Stemper, B. D., Yoganandan, N., Stineman, M. R., Gennarelli, T. A., Baisden, J. L., and Pintar, F. A. (2007a). Mechanics of fresh, refrigerated, and frozen arterial tissue. *Journal of Surgical Research*, 139(2):236–242.
- [Stemper et al., 2007b] Stemper, B. D., Yoganandan, N., Stineman, M. R., Gennarelli, T. A., Baisden, J. L., and Pintar, F. A. (2007b). Mechanics of Fresh, Refrigerated, and Frozen Arterial Tissue. *Journal of Surgical Research*, 139(2):236–242.
- [Stenbaek et al., 2000] Stenbaek, J., Kalin, B., and Swedenborg, J. (2000). Growth of thrombus may be a better predictor of rupture than diameter in patients with abdominal aortic aneurysms. *European Journal of Vascular and Endovascular Surgery*, 20(5):466–469.
- [Stenmark et al., 2006] Stenmark, K. R., Davie, N., Frid, M., Gerasimovskaya, E., and Das, M. (2006). Role of the Adventitia in Pulmonary Vascular Remodeling. *Physiology*, 21(2):134–145.
- [Sterpetti et al., 1987] Sterpetti, A. V., Schultz, R. D., Feldhaus, R. J., Cheng, S. E., and Peetz Jr, D. J. (1987). Factors influencing enlargement rate of small abdominal aortic aneurysms. *Journal of Surgical Research*, 43(3):211–219.
- [Stouffer et al., 1985] Stouffer, D., Butler, D., and Hosny, D. (1985). The relationship between crimp pattern and mechanical response of human patellar tendon-bone units. *Journal of biomechanical engineering*, 107(2):158–165.
- [Sugimoto et al., 2017] Sugimoto, M., Koyama, A., Niimi, K., Kodama, A., Banno, H., and Komori, K. (2017). Long-term comparison of endovascular and open repair of abdominal aortic aneurysms: Retrospective analysis of matched cohorts with propensity score. *Annals of vascular surgery*, 43:96–103.
- [Suri et al., 1996] Suri, C., Jones, P. F., Patan, S., Bartunkova, S., Maisonpierre, P. C., Davis, S., Sato, T. N., and Yancopoulos, G. D. (1996). Requisite role of angiopoietin-1, a ligand for the TIE2 receptor, during embryonic angiogenesis. *Cell*, 87(7):1171–1180.
- [Sweat et al., 1964] Sweat, F., Puchtler, H., and Rosenthal, S. I. (1964). Sirius red F3BA as a stain for connective tissue. *Archives of pathology*, 78:69–72.
- [Sweeting et al., 2012] Sweeting, M., Thompson, S., Brown, L., Powell, J., and RESCAN collaborators (2012). Meta-analysis of individual patient data to examine factors affecting growth and rupture of small abdominal aortic aneurysms. *British Journal of Surgery*, 99(5):655–665.
- [Takamizawa and Hayashi, 1987] Takamizawa, K. and Hayashi, K. (1987). Strain energy density function and uniform strain hypothesis for arterial mechanics. *Journal of biomechanics*, 20(1):7–17.
- [Takamizawa and Hayashi, 1988] Takamizawa, K. and Hayashi, K. (1988). Uniform strain hypothesis and thin-walled theory in arterial mechanics. *Biorheology*, 25(3):555–565.
- [Tang et al., 2005] Tang, P. C., Coady, M. A., Lovoulos, C., Dardik, A., Aslan, M., Elefteriades, J. A., and Tellides, G. (2005). Hyperplastic cellular remodeling of the media in ascending thoracic aortic aneurysms. *Circulation*, 112(8):1098–1105.

- [Thunes et al., 2018] Thunes, J. R., Phillippi, J. A., Gleason, T. G., Vorp, D. A., and Maiti, S. (2018). Structural modeling reveals microstructure-strength relationship for human ascending thoracic aorta. *Journal of biomechanics*, 71:84–93.
- [Tseders and Purinya, 1976] Tseders, d. d. and Purinya, B. A. (1976). The mechanical properties of human blood vessels relative to their location. *Polymer Mechanics*, 11(2):271–275.
- [Ushiki, 2002] Ushiki, T. (2002). Collagen fibers, reticular fibers and elastic fibers. A comprehensive understanding from a morphological viewpoint. *Archives of histology and cytology*, 65(2):109–126.
- [Vaishnav and Vossoughi, 1983] Vaishnav, R. N. and Vossoughi, J. (1983). Estimation of residual strains in aortic segments. In *Biomedical Engineering II*, pages 330–333. Elsevier.
- [Vaishnav et al., 1972] Vaishnav, R. N., Young, J. T., Janicki, J. S., and Patel, D. J. (1972). Nonlinear anisotropic elastic properties of the canine aorta. *Biophysical Journal*, 12(8):1008–1027.
- [Vaishnav et al., 1973] Vaishnav, R. N., Young, J. T., and Patel, D. J. (1973). Distribution of Stresses and of Strain-Energy Density through the Wall Thickness in a Canine Aortic Segment. *Circulation Research*, 32(5):577–583.
- [Valenta, 1993] Valenta, J. (1993). Clinical aspects of biomedicine. *Biomechanics*, 2:142–179.
- [Vallabhaneni et al., 2004] Vallabhaneni, S. R., Gilling-Smith, G. L., How, T. V., Carter, S. D., Brennan, J. A., and Harris, P. L. (2004). Heterogeneity of tensile strength and matrix metalloproteinase activity in the wall of abdominal aortic aneurysms. *Journal of Endovascular Therapy*, 11(4):494–502.
- [van Baardwijk and Roach, 1987] van Baardwijk, C. and Roach, M. R. (1987). Factors in the propagation of aortic dissections in canine thoracic aortas. *Journal of biomechanics*, 20(1):67–73.
- [Van der Rest and Garrone, 1991] Van der Rest, M. and Garrone, R. (1991). Collagen family of proteins. *The FASEB journal*, 5(13):2814–2823.
- [Van Dyke and Hoger, 2002] Van Dyke, T. J. and Hoger, A. (2002). A new method for predicting the opening angle for soft tissues. *Journal of biomechanical engineering*, 124(4):347–354.
- [Vande Geest et al., 2006] Vande Geest, J. P., Sacks, M. S., and Vorp, D. A. (2006). The effects of aneurysm on the biaxial mechanical behavior of human abdominal aorta. *Journal of Biomechanics*, 39(7):1324–1334.
- [Vasilkoski and Stepanyants, 2009] Vasilkoski, Z. and Stepanyants, A. (2009). Detection of the optimal neuron traces in confocal microscopy images. *Journal of neuroscience methods*, 178(1):197–204.
- [Venkatasubramaniam et al., 2004] Venkatasubramaniam, A., Fagan, M., Mehta, T., Mylankal, K., Ray, B., Kuhan, G., Chetter, I., and McCollum, P. (2004). A comparative

- study of aortic wall stress using finite element analysis for ruptured and non-ruptured abdominal aortic aneurysms. *European Journal of Vascular and Endovascular Surgery*, 28(2):168–176.
- [Venkatasubramanian et al., 2006a] Venkatasubramanian, R. T., Grassl, E. D., Barocas, V. H., Lafontaine, D., and Bischof, J. C. (2006a). Effects of freezing and cryopreservation on the mechanical properties of arteries. *Annals of Biomedical Engineering*, 34(5):823–832.
- [Venkatasubramanian et al., 2006b] Venkatasubramanian, R. T., Grassl, E. D., Barocas, V. H., Lafontaine, D., and Bischof, J. C. (2006b). Effects of Freezing and Cryopreservation on the Mechanical Properties of Arteries. *Annals of Biomedical Engineering*, 34(5):823–832.
- [Veress et al., 2000] Veress, A., Vince, D., Anderson, P. M., Cornhill, J., Herderick, E., Klingensmith, J., Kuban, B., Greenberg, N., and Thomas, J. (2000). Vascular mechanics of the coronary artery. *Zeitschrift für Kardiologie*, 89(2):S092–S100.
- [Vesentini et al., 2005] Vesentini, S., Fitié, C. F., Montevecchi, F. M., and Redaelli, A. (2005). Molecular assessment of the elastic properties of collagen-like homotrimer sequences. *Biomechanics and modeling in mechanobiology*, 3(4):224–234.
- [Viidik et al.,] Viidik, A., Danielsen, C. C., and Oxlund, H. FOURTH INTERNATIONAL CONGRESS OF BIORHEOLOGY SYMPOSIUM ON MECHANICAL PROPERTIES OF LIVING TISSUES. 19:15.
- [Virchow, 1910] Virchow, H. (1910). *Mikroskopische Anatomie Der Äusseren Augenhaut Und Des Lidapparates, von Dr. Hans Virchow,...* W. Engelmann.
- [Vito and Dixon, 2003] Vito, R. P. and Dixon, S. A. (2003). Blood vessel constitutive models—1995–2002. *Annual review of biomedical engineering*, 5(1):413–439.
- [Vlachopoulos et al., 2011] Vlachopoulos, C., O’Rourke, M., and Nichols, W. W. (2011). *McDonald’s Blood Flow in Arteries: Theoretical, Experimental and Clinical Principles*. CRC press.
- [Volokh, 2007] Volokh, K. (2007). Hyperelasticity with softening for modeling materials failure. *Journal of the Mechanics and Physics of Solids*, 55(10):2237–2264.
- [Volokh, 2010] Volokh, K. (2010). Comparison of biomechanical failure criteria for abdominal aortic aneurysm. *Journal of biomechanics*, 43(10):2032–2034.
- [Von Maltzahn et al., 1981] Von Maltzahn, W.-W., Besdo, D., and Wiemer, W. (1981). Elastic properties of arteries: A nonlinear two-layer cylindrical model. *Journal of Biomechanics*, 14(6):389–397.
- [von Maltzahn et al., 1984] von Maltzahn, W. W., Warriyar, R. G., and Keitzer, W. F. (1984). Experimental measurements of elastic properties of media and adventitia of bovine carotid arteries. *Journal of biomechanics*, 17(11):839–847.
- [Vorp et al., 1998] Vorp, D. A., Raghavan, M., and Webster, M. W. (1998). Mechanical wall stress in abdominal aortic aneurysm: Influence of diameter and asymmetry. *Journal of vascular surgery*, 27(4):632–639.

- [Vorp et al., 1995] Vorp, D. A., Rajagopal, K., Smolinski, P. J., and Borovetz, H. S. (1995). Identification of elastic properties of homogeneous, orthotropic vascular segments in distension. *Journal of biomechanics*, 28(5):501–512.
- [Vorp et al., 2003] Vorp, D. A., Schiro, B. J., Ehrlich, M. P., Juvonen, T. S., Ergin, M., and Griffith, B. P. (2003). Effect of aneurysm on the tensile strength and biomechanical behavior of the ascending thoracic aorta. *The Annals of Thoracic Surgery*, 75(4):1210–1214.
- [Vuorio and De Crombrughe, 1990] Vuorio, E. and De Crombrughe, B. (1990). The family of collagen genes. *Annual review of biochemistry*, 59(1):837–872.
- [Waffenschmidt et al., 2014] Waffenschmidt, T., Polindara, C., Menzel, A., and Blanco, S. (2014). A gradient-enhanced large-deformation continuum damage model for fibre-reinforced materials. *Computer Methods in Applied Mechanics and Engineering*, 268:801–842.
- [Waffenschmidt and Tekkaya, 2013] Waffenschmidt, T. and Tekkaya, I. E. (2013). Modelling and simulation of adaptation and degradation in anisotropic biological tissues.
- [Wagenseil and Mecham, 2009a] Wagenseil, J. E. and Mecham, R. P. (2009a). Vascular Extracellular Matrix and Arterial Mechanics. *Physiological Reviews*, 89(3):957–989.
- [Wagenseil and Mecham, 2009b] Wagenseil, J. E. and Mecham, R. P. (2009b). Vascular Extracellular Matrix and Arterial Mechanics. 89(3):957–989.
- [Wainwright et al., 1982] Wainwright, S. A., Biggs, W., and Currey, J. D. (1982). *Mechanical Design in Organisms*. Princeton University Press.
- [Wang et al., 2000] Wang, C., Berhan, L., and Sastry, A. (2000). Structure, mechanics and failure of stochastic fibrous networks: Part I—Microscale considerations. *Journal of Engineering Materials and Technology*, 122(4):450–459.
- [Wanhainen et al., 2008] Wanhainen, A., Themudo, R., Ahlström, H., Lind, L., and Johansson, L. (2008). Thoracic and abdominal aortic dimension in 70-year-old men and women—a population-based whole-body magnetic resonance imaging (MRI) study. *Journal of vascular surgery*, 47(3):504–512.
- [Watton et al., 2004] Watton, P., Hill, N., and Heil, M. (2004). A mathematical model for the growth of the abdominal aortic aneurysm. *Biomechanics and modeling in mechanobiology*, 3(2):98–113.
- [Watton et al., 2011] Watton, P., Selimovic, A., Raberger, N. B., Huang, P., Holzapfel, G., and Ventikos, Y. (2011). Modelling evolution and the evolving mechanical environment of saccular cerebral aneurysms. *Biomechanics and modeling in mechanobiology*, 10(1):109–132.
- [Weisbecker et al., 2012] Weisbecker, H., Pierce, D. M., Regitnig, P., and Holzapfel, G. A. (2012). Layer-specific damage experiments and modeling of human thoracic and abdominal aortas with non-atherosclerotic intimal thickening. *Journal of the mechanical behavior of biomedical materials*, 12:93–106.

- [Weisbecker et al., 2015] Weisbecker, H., Unterberger, M. J., and Holzapfel, G. A. (2015). Constitutive modelling of arteries considering fibre recruitment and three-dimensional fibre distribution. *Journal of The Royal Society Interface*, 12(105):20150111–20150111.
- [Weisbecker et al., 2013] Weisbecker, H., Viertler, C., Pierce, D. M., and Holzapfel, G. A. (2013). The role of elastin and collagen in the softening behavior of the human thoracic aortic media. *Journal of biomechanics*, 46(11):1859–1865.
- [Weizsacker and Pinto, 1988] Weizsacker, H. W. and Pinto, J. G. (1988). Isotropy and anisotropy of the arterial wall. *Journal of biomechanics*, 21(6):477–487.
- [Wenger et al., 2007] Wenger, M. P., Bozec, L., Horton, M. A., and Mesquida, P. (2007). Mechanical properties of collagen fibrils. *Biophysical journal*, 93(4):1255–1263.
- [Wertheim, 1847] Wertheim, G. (1847). *Mémoire Sur l'élasticité et La Cohésion Des Principaux Tissus Du Corps Humain*.
- [Wilhelm and Frey, 2003] Wilhelm, J. and Frey, E. (2003). Elasticity of stiff polymer networks. *Physical review letters*, 91(10):108103.
- [Williams et al., 2005] Williams, R. M., Zipfel, W. R., and Webb, W. W. (2005). Interpreting second-harmonic generation images of collagen I fibrils. *Biophysical journal*, 88(2):1377–1386.
- [Wilson et al., 2003] Wilson, K. A., Lee, A. J., Hoskins, P. R., Fowkes, F. G. R., Ruckley, C. V., and Bradbury, A. W. (2003). The relationship between aortic wall distensibility and rupture of infrarenal abdominal aortic aneurysm. *Journal of vascular surgery*, 37(1):112–117.
- [Witzenburg and Barocas, 2016] Witzenburg, C. M. and Barocas, V. H. (2016). A non-linear anisotropic inverse method for computational dissection of inhomogeneous planar tissues. *Computer methods in biomechanics and biomedical engineering*, 19(15):1630–1646.
- [Wolinsky and Glagov, 1967a] Wolinsky, H. and Glagov, S. (1967a). A lamellar unit of aortic medial structure and function in mammals. *Circulation research*, 20(1):99–111.
- [Wolinsky and Glagov, 1967b] Wolinsky, H. and Glagov, S. (1967b). A Lamellar Unit of Aortic Medial Structure and Function in Mammals. *Circulation Research*, 20(1):99–111.
- [Wong et al., 1993] Wong, M., Edelstein, J., Wollman, J., and Bond, M. G. (1993). Ultrasonic-pathological comparison of the human arterial wall. Verification of intima-media thickness. *Arteriosclerosis and thrombosis: a journal of vascular biology*, 13(4):482–486.
- [Wu et al., 2003] Wu, J., Rajwa, B., Filmer, D., Hoffmann, C., Yuan, B., Chiang, C., Sturgis, J., and Robinson, J. (2003). Automated quantification and reconstruction of collagen matrix from 3D confocal datasets. *Journal of microscopy*, 210(2):158–165.
- [Wulandana and Robertson, 2005] Wulandana, R. and Robertson, A. (2005). An inelastic multi-mechanism constitutive equation for cerebral arterial tissue. *Biomechanics and Modeling in Mechanobiology*, 4(4):235–248.

- [Xiong et al., 2006] Xiong, G., Zhou, X., and Ji, L. (2006). Automated segmentation of Drosophila RNAi fluorescence cellular images using deformable models. *IEEE Transactions on Circuits and Systems I: Regular Papers*, 53(11):2415–2424.
- [Xuan et al., 2018] Xuan, Y., Wang, Z., Liu, R., Haraldsson, H., Hope, M. D., Saloner, D. A., Guccione, J. M., Ge, L., and Tseng, E. (2018). Wall stress on ascending thoracic aortic aneurysms with bicuspid compared with tricuspid aortic valve. *The Journal of thoracic and cardiovascular surgery*, 156(2):492–500.
- [Yamamoto et al., 1999] Yamamoto, E., Hayashi, K., and Yamamoto, N. (1999). Mechanical properties of collagen fascicles from the rabbit patellar tendon. *Journal of biomechanical engineering*, 121(1):124–131.
- [Yang et al., 2008a] Yang, L., Fitié, C. F., van der Werf, K. O., Bennink, M. L., Dijkstra, P. J., and Feijen, J. (2008a). Mechanical properties of single electrospun collagen type I fibers. *Biomaterials*, 29(8):955–962.
- [Yang et al., 2008b] Yang, L., Van der Werf, K. O., Fitié, C. F., Bennink, M. L., Dijkstra, P. J., and Feijen, J. (2008b). Mechanical properties of native and cross-linked type I collagen fibrils. *Biophysical journal*, 94(6):2204–2211.
- [Zemanek and Michal,] Zemanek, M. and Michal. BIAXIAL TENSION TESTS WITH SOFT TISSUES OF ARTERIAL WALL. *Engineering MECHANICS*, page 9.
- [Zemanek,] Zemanek, Miroslav, M. BIAXIAL TENSION TESTS WITH SOFT TISSUES OF ARTERIAL WALL. *Engineering MECHANICS*, page 9.
- [Zhang et al., 2012] Zhang, L., Lake, S. P., Lai, V. K., Picu, C. R., Barocas, V. H., and Shephard, M. S. (2012). A Coupled Fiber-Matrix Model Demonstrates Highly Inhomogeneous Microstructural Interactions in Soft Tissues Under Tensile Load. *Journal of Biomechanical Engineering*, 135(1):011008.
- [Zhang et al., 2013] Zhang, L., Lake, S. P., Lai, V. K., Picu, C. R., Barocas, V. H., and Shephard, M. S. (2013). A coupled fiber-matrix model demonstrates highly inhomogeneous microstructural interactions in soft tissues under tensile load. *Journal of biomechanical engineering*, 135(1):011008.
- [Zoumi et al., 2002] Zoumi, A., Yeh, A., and Tromberg, B. J. (2002). Imaging cells and extracellular matrix in vivo by using second-harmonic generation and two-photon excited fluorescence. *Proceedings of the National Academy of Sciences*, 99(17):11014–11019.
- [Zulliger et al., 2004] Zulliger, M. A., Fridez, P., Hayashi, K., and Stergiopoulos, N. (2004). A strain energy function for arteries accounting for wall composition and structure. *Journal of biomechanics*, 37(7):989–1000.
- [Zulliger and Stergiopoulos, 2007a] Zulliger, M. A. and Stergiopoulos, N. (2007a). Structural strain energy function applied to the ageing of the human aorta. *Journal of Biomechanics*, 40(14):3061–3069.
- [Zulliger and Stergiopoulos, 2007b] Zulliger, M. A. and Stergiopoulos, N. (2007b). Structural strain energy function applied to the ageing of the human aorta. *Journal of biomechanics*, 40(14):3061–3069.

NNT: Communiqué le jour de la soutenance

Author: Venkat AYYALASOMAYAJULA

Title: 3-D reconstruction of micro-scale mechanical state of the abdominal aortic aneurysm wall

Speciality: Mechanics and Engineering

Keywords: Aortic aneurysm, Rupture, Finite elements, collagen.

Abstract

The aortic wall is a complex hierarchical structure comprised of a non-uniform organization of its micro-structural constituents. The mechanical response of the tissue to external stimuli is heavily predicated on the arrangement and content of these constituents.

The following doctoral thesis is aimed at investigating the hypothesis: the mechanical phenomena occurring at the level of the fibrous micro-structure is responsible for the macroscopic mechanical response of the tissue close to failure. For this purpose mechanical testing of arterial tissues was accomplished in conjunction with multi-photon microscopy imaging. The mechanical testing served as an assessment of the tissue's macroscopic mechanical behavior, whereas the micro-structural imaging allowed for the quantification of the tissue's morphology. Through the combined knowledge of these two developments, structure based micro-scale mechanical models were constructed. The micro-scale model enabled the analysis of mechanical state of the fibers at various tissue level load. The investigation concentrated on establishing the relationship between morphology of collagen fiber network in the outermost layer of the aortic wall, the adventitia, and its macroscopic mechanical response. Furthermore, possible fiber scale damage mechanisms that contribute to tissue's macroscopic failure have been analyzed. The resulting contribution consists of quantification of fiber's mechanical state, and an assessment of their kinematics at loads beyond the physiological range.

NNT: Communiqué le jour de la soutenance

Auteur: Venkat Ayyalasomayajula

Titre: Reconstruction 3D de l'état mécanique microscopique de la paroi de l'anévrisme de l'aorte abdominale

Spécialité: Mécanique et ingénierie

Mots-Clefs: Anévrisme aortique, rupture, éléments finis, collagène.

Résumé

La paroi aortique est une structure hiérarchique complexe composée d'une organisation non uniforme de ses constituants microstructuraux. La réponse mécanique des tissus aux stimuli externes dépend fortement de la disposition et du contenu de ces constituants.

La thèse de doctorat suivante vise à étudier l'hypothèse : les phénomènes mécaniques se produisant au niveau de la microstructure fibreuse sont responsables de la réponse mécanique macroscopique du tissu proche de la rupture. À cette fin, des essais mécaniques des tissus artériels ont été réalisés en conjonction avec l'imagerie par microscopie multiphotonique. Les essais mécaniques ont servi à évaluer le comportement mécanique macroscopique du tissu, tandis que l'imagerie microstructurale a permis de quantifier la morphologie du tissu. Grâce à la connaissance combinée de ces deux développements, des modèles mécaniques à micro-échelle basés sur la structure ont été construits. Le modèle à micro-échelle a permis l'analyse de l'état mécanique des fibres à différentes charges au niveau des tissus. L'étude s'est concentrée sur l'établissement de la relation entre la morphologie du réseau de fibres de collagène dans la couche la plus externe de la paroi aortique, l'adventice, et sa réponse mécanique macroscopique. En outre, les mécanismes possibles de détérioration des fibres qui contribuent à la rupture macroscopique des tissus ont été analysés. La contribution qui en résulte consiste à quantifier l'état mécanique des fibres et à évaluer leur cinématique à des charges dépassant la plage physiologique.